AD-A120 044 INFRARED INFORMATION AND ANALYSIS CENTER ANN ARBOR MI F/G 17/5
IRIA STATE-OF-THE-ART REPORT: OPTICAL-MECHANICAL, ACTIVE/PASSIV--ETC(U)
MAY 82 C T DUE, L M PETERSON N00014-77-C-0125
UNCLASSIFIED IRIA-153200-2-T-1 SBI-AD-E750 695 NL

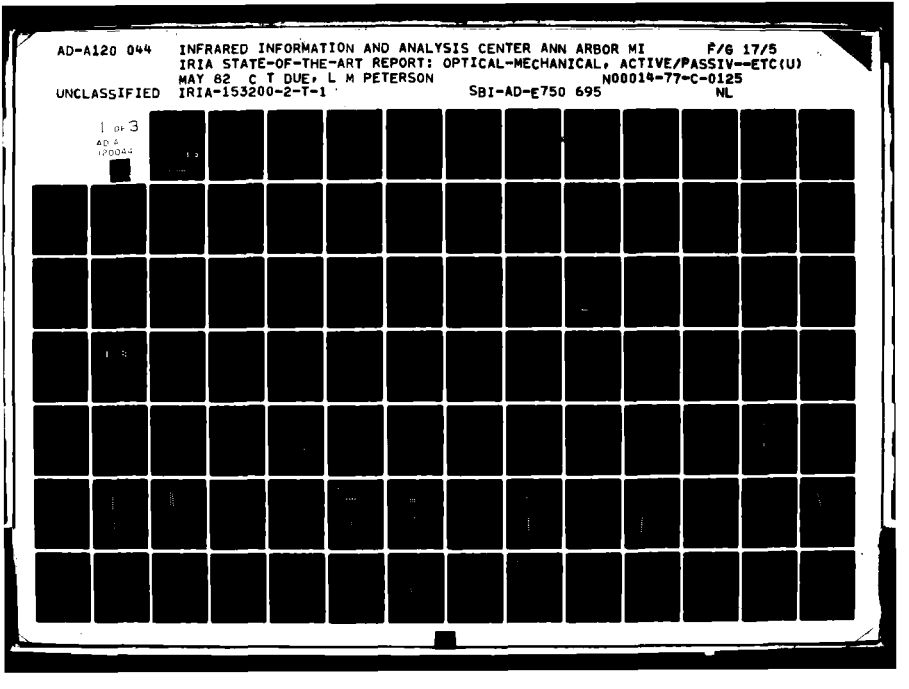

153200-2-T

An IRIA State-of-the-Art Report

OPTICAL-MECHANICAL, ACTIVE/PASSIVE IMAGING SYSTEMS — VOLUME I

CHRISTOPHER T. DUE, LAUREN M. PETERSON
Infrared Information and Analysis Center
A DTIC-Sponsored DoD Information Analysis Center

MAY 1982

Office of Naval Research
Department of the Navy
Arlington, Virginia 22217
Contract Nos. N00014-77-C-0125, N00014-80-C-0510,
and N00014-81-C-0425

ENVIRONMENTAL
RESEARCH INSTITUTE OF MICHIGAN
BOX 8618 • ANN ARBOR • MICHIGAN 48107

NOTICES

Sponsorship. This state-of-the-art report was prepared by the Infrared Information and Analysis (IRIA) Center as part of its services to the infrared community, under Contracts N00014-77-C-0125, N00014-80-C-0510 and N00014-81-C-0425 with the Office of Naval Research, funded by the Defense Technical Information Center.

ENVIRONMENTAL
RESEARCH INSTITUTE OF MICHIGAN
P O BOX 8618 • ANN ARBOR • MICHIGAN • 48107
INFRARED INFORMATION AND ANALYSIS CENTER
PHONE (313) 994 1200
EXT 214

AD-A120 006

27 September 1982

Defense Technical Information Center
ATTN: DTIC-TC
Cameron Station
Alexandria, VA 22314

Gentlemen:

Enclosed for announcement by DTIC are two copies of the:

IRIA-IRIS State-of-the-Art Report: Optical-Mechanical, Active/ Passive Imaging Systems (U), Volume I
Unclassified, May 1982

As a Department of Defense Information and Analysis Center, we are recovering partial costs of our publications through user charges. Thus, the TAB entry should read:

Availability: IRIA Center
Environmental Research Institute of Michigan
P. O. Box 8618
Ann Arbor, MI 48107.

(NO COPIES FURNISHED BY DTIC OR NTIS)

Thank you for your assistance in this matter.

Sincerely,

Mildred F. Denecke

Mildred F. Denecke
Manager, Infrared Information
and Analysis Center

MFD:rmc
Encls. (2)

UNCLASSIFIED

SECURITY CLASSIFICATION OF THIS PAGE (When Data Entered)

REPORT DOCUMENTATION PAGE		READ INSTRUCTIONS BEFORE COMPLETING FORM
1. REPORT NUMBER 153200-2-T(I)	2. GOVT ACCESSION NO AD-A120044	3. RECIPIENT'S CATALOG NUMBER
4. TITLE (and Subtitle) IRIA State-of-the-Art Report: Optical-Mechanical, Active/Passive Imaging Systems, Volume I		5. TYPE OF REPORT & PERIOD COVERED Technical 6. PERFORMING ORG. REPORT NUMBER 153200-2-T(I)
7. AUTHOR(s) Christopher T. Due Lauren M. Peterson		8. CONTRACT OR GRANT NUMBER(s) N00014-77-C-0125 N00014-80-C-0510 N00014-81-C-0425
9. PERFORMING ORGANIZATION NAME AND ADDRESS Environmental Research Institute of Michigan Infrared Information and Analysis Center P. O. Box 8618, Ann Arbor, MI 48107		10. PROGRAM ELEMENT, PROJECT, TASK AREA & WORK UNIT NUMBERS
11. CONTROLLING OFFICE NAME AND ADDRESS Office of Naval Research, Code 760 Department of the Navy Arlington, VA 22217		12. REPORT DATE May 1982 13. NUMBER OF PAGES 246
14. MONITORING AGENCY NAME AND ADDRESS (if different from Controlling Office) Office of Naval Research, Code 412 Department of the Navy Arlington, VA 22217		15. SECURITY CLASS (of this report) Unclassified 15a. DECLASSIFICATION/DOWNGRADING SCHEDULE N/A

16. DISTRIBUTION STATEMENT (of this Report)

Approved for public release; distribution unlimited.

17. DISTRIBUTION STATEMENT (of the abstract entered in Block 20, if different from Report)

18. SUPPLEMENTARY NOTES

Available only from the Infrared Information and Analysis (IRIA) Center, ERIM, P. O. Box 8618, Ann Arbor, MI 48107

19. KEY WORDS (Continue on reverse side if necessary and identify by block number)

FLIR Systems	Line Scanning	Optical Equipment	Scanners
Infrared Equipment	Multispectral	Optical Scanning	
Infrared Scanning	Night Vision Device	Reviews	
Lasers	Optical Detectors	State of the Art	

20. ABSTRACT (Continue on reverse side if necessary and identify by block number)

This first volume of a two part report on the state-of-the-art of optical-mechanical, active/passive imaging systems presents a tutorial treatment of such systems. Included are design and characterizing parameters relating to the radiation available for imaging, the intervening atmosphere, optical and mechanical components, scanning processes, detectors, and associated electronics. The second volume presents a survey of systems developed during the 1970's.

DD FORM 1 JAN 73 1473 EDITION OF 1 NOV 65 IS OBSOLETE

UNCLASSIFIED

SECURITY CLASSIFICATION OF THIS PAGE (When Data Entered)

PREFACE

The Infrared Information and Analysis (IRIA) Center is a Defense Technical Information Center (DTIC)-funded Department of Defense Information Analysis Center operated by the Environmental Research Institute of Michigan (ERIM) under contract to the Office of Naval Research. Its mission is to collect, analyze, and disseminate to authorized recipients information concerning infrared and electro-optical research and development. To this end, the IRIA Center prepares, publishes, and distributes IRIA Annotated Bibliographies, the Infrared Newsletter, IRIA Data Compilations, and IRIA State-of-the-Art Reports. The Center serves as a national reference library in military infrared technology, offering assistance and advice to visitors having the appropriate clearances and need-to-know. Special bibliographies and searches can be prepared upon authorized request.

FOREWORD

This report presents in two volumes the state-of-the-art of optical-mechanical, active/passive imaging systems. Volume I is in two major sections. Section one, by Christopher T. Due, treats passive imaging systems in a tutorial overview of parameters needed to design and characterize such devices. These parameters relate to the emitted and reflected, naturally-occurring radiation from the scene, the intervening atmosphere, the optical and mechanical components of the systems, and the detectors and associated electronics. An attempt has been made to make this section self-sufficient at a basic level. Section two, by Lauren M. Peterson, contains an overall treatment of active, optical-mechanical imaging systems. It has also been written to be self-sufficient for a fundamental understanding of these devices.

Volume II, by Christopher T. Due, contains detailed descriptions of systems produced in the 1970s. Almost exclusively, the text format for each system or group of systems, follows the sequence: General Information; Optics and Scan Mechanism; Detectors and Cooling; Calibration (if present); Electronics, Display, and Data Processing; and Bibliography. Included in each General Information section is a table of sensor data. Part of each Optics and Scan Mechanism section is an illustration of the system(s) under discussion.

Since the terms, symbols, and units used to describe these systems have varied with individual, time, and application, those used here are listed in the glossary of terms in the Appendix to this report. The units used are those prescribed by the International System of Units (SI). Where measurements were made in other units, the original measurements and units are included in parentheses.

G. J. Zissis
Director, Infrared Information
and Analysis Center

ACKNOWLEDGMENTS

The author wishes to acknowledge the contributions of: Dr. George J. Zissis, who provided technical direction and critically reviewed the manuscript of the report; Gary Gatien, who helped to organize the manuscript and acted as copy editor for the entire report; Kirk Gianolla and other Art Department Staff who prepared the illustrations; Jimmie C. Ladd and Carl Miller, in the Infrared and Optics Division, who assisted in the data collection and organization of the material; those in government and industry who supplied and reviewed much of the material contained in this report; and Rose Coleman for typing the many drafts and final copy of the report.

TABLE OF CONTENTS

SECTION 2.0
ACTIVE OPTICAL-MECHANICAL IMAGING SENSORS

LIST OF ILLUSTRATIONS

SECTION 1.0

LIST OF TABLES

SECTION 1.0
PASSIVE OPTICAL-MECHANICAL IMAGING SENSORS

1.1 BACKGROUND

Optical-mechanical imaging systems operating passively rely on naturally emitted radiation or reflected sunlight, in contrast to active imaging systems in which an artifical source is used to illuminate the scene. The chief advantages this type of instrument offers over vidicons, orthicons, image intensifier/converters, film, etc., are the ability to produce imagery in the far infrared and the ability to provide high sensitivity over a narrow wavelength region.

The components in an optical-mechanical imaging system can be functionally divided into five groups as illustrated in Figure 1-1:

(1) The collecting optics, an optical system to image the object or scene onto a field stop or detector which defines a narrow solid angular region of space from which the system collects radiation,

(2) Scanning optics, mechanically driven to systematically sweep or scan the narrow field of view across the scene,

(3) Detector(s), to transform the radiation passing the field stop into an electrical signal,

(4) Electronics, to amplify and process the signal,

(5) Display system, to construct a visible image of the scene as sensed by the detector.

Note that the scene, atmosphere and observer are included in Figure 1-1. This is because the scene characteristics, atmosphere and the useability of the output image to an observer affect the performance of the system.

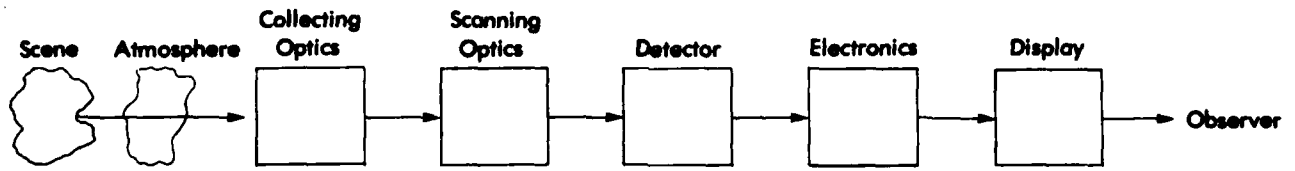

FIGURE 1-1. ELEMENTS OF AN OPTICAL-MECHANICAL IMAGING SYSTEM

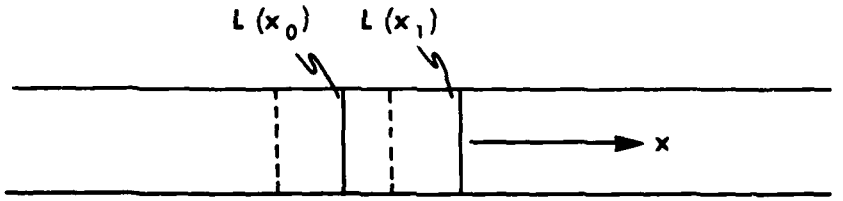

FIGURE 1-2. SWEEP OF THE IFOV ALONG A SCAN LINE

In many systems the above five groups are intertwined along with many auxiliary components. The collecting optics may be mechanically driven to provide scanning. The detector may be packaged in a dewar and cryogenically cooled in far infrared applications. The electronics may involve computer processing. The detector may actually be an array of sensitive elements.

The development of these systems resulted, to a large degree, from the use of infrared technology in military applications. (For a brief history of infrared technology, see Reference [1-1], pp.40-41.) Prior to World War II, use of infrared technology was limited. This was partly because many present applications were not envisioned at the time. More importantly, optical materials, filters, sources, detectors and other technology were not sufficiently advanced to permit useful scanning devices. At the end of the war, there were less than a dozen military scanners in existence within the U.S. -- mostly nonimage-forming. With few exceptions, these devices used reflective optical systems, similar detectors (thermistor bolometers), and oscillating collecting mirrors as the chief method of scanning.

During World War II, Germany placed considerable emphasis on military infrared technology. Because of this, many techniques and components were available in the post-war period. While the period up to 1950 did not produce a large number of systems, it served to create interest in the application of this technology as well as producing improved detector materials, a wider variety of optical components, and other related technical advances.

From 1950 to 1960 a number of infrared scanners were built and tested. Included among these devices were search systems, tracking systems, and

---

[1-1] R. G. Reeves, A. Anson and D. Landen, Manual of Remote Sensing, American Society of Photogrammetry, Falls Church, VA, Volume I, 1975.

mapping/imaging systems. A number of scanning techniques were developed due to the variety of instruments using optical-mechanical scanning. (See References [1-1], Chapter 8, and [1-2], Chapters 9 and 10.)

During the next decade, real-time (30 frames/sec) frame scanning in the far infrared became possible due to the advent of suitable detector materials. The short time constant of these new detector types made it possible to scan the full frame in a fraction of a second and yet provide adequate sensivity to the 8 - 12 μm spectral region to make a practical system. These frame-scanning systems are now called FLIRs -- an acronym for forward-looking infrared. Also during the 60's, satellite-borne scanning systems for meteorological and earth resource survey purposes became possible because of the space program. Through the use of thermal reconnaissance strip mappers, the visible and near-infrared regions were added to these systems.

Optical-mechanical scanning is accomplished by the movement of optical elements (such as mirrors, prisms, or complete fore-optics). A variety of scan patterns can be generated, but for imaging systems the scan pattern must sample all portions of the scene to be imaged. Imaging scanners may internally generate both dimensions of scanning required for an image, or they may rely on the motion of the vehicle or platform carrying the system to generate one dimension of scan. Scanning systems generating one dimension of scan are often used in aircraft and orbital satellites. They produce a continuous strip of imagery and are known as strip mappers. Scanning systems which generate both dimensions of scan are known as frame or raster scanners, as well as FLIRs.

[1-2] W. L. Wolfe and G. J. Zissis, The Infrared Handbook, Office of Naval Research, Arlington, VA, 1978. Available from: Order Department, Environmental Research Institute of Michigan, Ann Arbor, MI.

1.2 SCENE CHARACTERISTICS

Optical-mechanically scanning imaging devices operating passively rely solely on naturally emitted or reflected optical radiation from the scene to provide a visible image for interpretation. In this type of device the image is generated by systematically sampling the radiation from each portion of the scene. At any given instant in time these devices "see" only a narrow solid angular portion of the scene. The radiation collected is then converted into a corresponding electrical signal by the detector. This narrow field of view or "instantaneous" field of view (IFOV) is then systematically swept across the total scene to be covered, dissecting the scene to be imaged.

The movement of an IFOV with a square cross section along a scan line is depicted in Figure 1-2. The variation in radiation received by the detector as the IFOV sweeps the scene may be due to changes in reflectance, incident radiation, emissivity and temperature of the scene objects encountered. Also, the objects encountered may not fill the IFOV, and as a result, radiation may be received from multiple objects.

For an observer to interpret the image of an object of interest, the cross section of the IFOV at the object must be considerably smaller than the size of the object. In this situation the IFOV is completely filled. The irradiance at the entrance of the sensor from that portion of the object's surface is

$$E_o = \tau_a \omega L \qquad \left(W\ cm^{-2}\right) \tag{1-1}$$

where ω = solid angle of the IFOV (sr)

τ_a = transmittance of the atmosphere over the path to the sensor

L = combined reflected and emitted radiance ($W\ cm^{-2}\ sr^{-1}$) from the object at the object's surface in the direction of the sensor

Since the changes in the irradiance at the sensor's entrance aperture as the scene is scanned produce the relative contrast in the image

presented to the observer, the changes in scene radiance, L, due to changes in reflectance, ρ, incident radiant flux, Φ_i, emissivity, ε, and temperature, T, are of interest. Using the chain rule for partial derivatives, one can express this as

$$dL = \left(\frac{\partial L}{\partial \rho}\right) d\rho + \left(\frac{\partial L}{\partial \Phi_i}\right) d\Phi_i + \left(\frac{\partial L}{\partial \varepsilon}\right) d\varepsilon + \left(\frac{\partial L}{\partial T}\right) dT \qquad (1\text{-}2)$$

In a terrestrial application, the radiation from the scene would be composed of thermally emitted radiation at earth temperatures (about 300 K) and reflected sunlight during daylight hours. For systems operating in shorter wavelength, near infrared bands, the changes in scene radiance may be due to both reflectance and emission changes. However, in systems which operate in the visible atmospheric window*, the changes in radiance are primarily due to changes in the reflectance of the scene illuminated by sunlight. While for systems operating in the 3 to 5 and 8 to 14 μm atmospheric windows, such as thermal strip mappers, the changes in radiance are primarily due to the changes in emission from the scene. Because of this, system analysis is often accomplished by considering reflected or emitted radiation only.

1.2.1 Surface Characteristics

The amount of flux received by a sensor from an emitting or reflecting surface may vary as a function of the orientation of the surface. For surfaces which are specular, the distribution of emitted or reflected flux is directional. A mirror is a perfectly specular reflector.

For perfectly diffusely reflecting or emitting surfaces, the flux per unit solid angle is proportional to the cosine of the angle between the sensor line of sight and the normal to the surface. This is known as

*See the discussion in Section 1.3.

Lambert's cosine law. (See References [1-2], Chapter 1, and [1-3], p. 29.) Since the projected area of the surface also varies with the cosine of this angle, the radiance of the surface as seen by the sensor is independent of the viewing angle. For a diffusely emitting surface emitting into a hemisphere, the radiance seen by the sensor is

$$L = \frac{\varepsilon M}{\pi} \qquad \left(W\ cm^{-2}\ sr^{-1}\right) \tag{1-3}$$

where εM is the total radiant exitance ($W\ cm^{-2}$) and ε the emissivity of the surface.

1.2.2 Thermal Radiation

If there is no significant contribution from reflected radiation, such as sunlight, the scanner IFOV only receives radiation from thermally emitting objects, and Equation (1-2) becomes

$$dL = \left(\frac{\partial L}{\partial \varepsilon}\right) d\varepsilon + \left(\frac{\partial L}{\partial T}\right) dT \tag{1-4}$$

Frequently, analysis is accomplished by treating the contributions due to changes in ε as equivalent changes in temperature allowing the analysis to be done by use of the Planck blackbody function. (See References [1-1], Volume I, Chapters 3, 4, 7, and 8, and [1-2,1-3, and 1-19].) This is done by setting $d\varepsilon = 0$ and $\varepsilon(\lambda) = 1$:

$$dL = \left(\frac{\partial L}{\partial T}\right) dT \tag{1-5}$$

Planck's law can be written as

$$M_\lambda(\lambda)d\lambda = c_1\ \lambda^{-5} \left(e^{c_2/\lambda T} - 1\right)^{-1} \quad d\lambda \tag{1-6}$$

[1-3] R. D. Hudson, Jr., Infrared Systems Engineering, John Wiley and Sons, New York, NY, 1969.

where $c_1 = 2\pi hc^2 = 3.74 \times 10^4$ (W cm^{-2} μm^4)
$c_2 = hc/k_B = 1.44 \times 10^4$ (μm K)

Since it is assumed that the object to be imaged emits as a blackbody, i.e., $\varepsilon(\lambda) = 1$, the spectral radiance from the surface is

$$L_\lambda(\lambda,T) = \frac{M_\lambda(\lambda,T)}{\pi} \tag{1-7}$$

$$= \frac{c_1}{\pi} \lambda^{-5} \left(e^{c_2/\lambda T} - 1\right)^{-1} \qquad \left(\text{W cm}^{-2}\ \text{sr}^{-1}\ \mu\text{m}^{-1}\right)$$

It can be shown that

$$\frac{d\, L_\lambda(\lambda,T)}{dT} = \frac{c_2}{\lambda T} \frac{e^{c_2/\lambda T}}{\left(e^{c_2/\lambda T^2} - 1\right)} L_\lambda(\lambda,T) \tag{1-8}$$

Plots of these two functions for three blackbody temperatures are shown in Figures 1-3 and 1-4.

To obtain the total change in radiance per unit temperature, one must integrate Equation (1-8) over the spectral response of the sensor. A useful approximation by Sanderson (Reference [1-4], Chapter 5) is to neglect the term

$$\frac{e^{c_2/\lambda T}}{e^{c_2/\lambda T} - 1} \tag{1-9}$$

which has less than 1% error for $T < 3100$ μm K.

The change in radiance due to temperature may also be calculated by power series expansion. Refering to Equation (1-1), one can state the

[1-4] J. A. Sanderson, "Emission, Transmission, and Detection of Infrared," A. S. Locke (ed.), Guidance, Princeton, NJ, 1955.

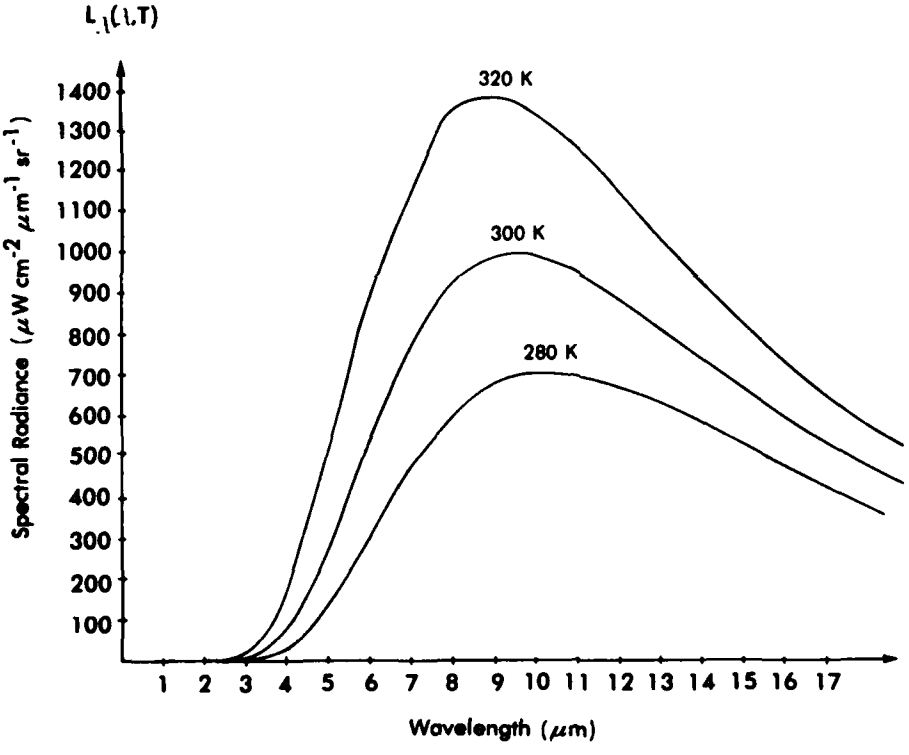

FIGURE 1-3. SPECTRAL RADIANCE OF A BLACKBODY

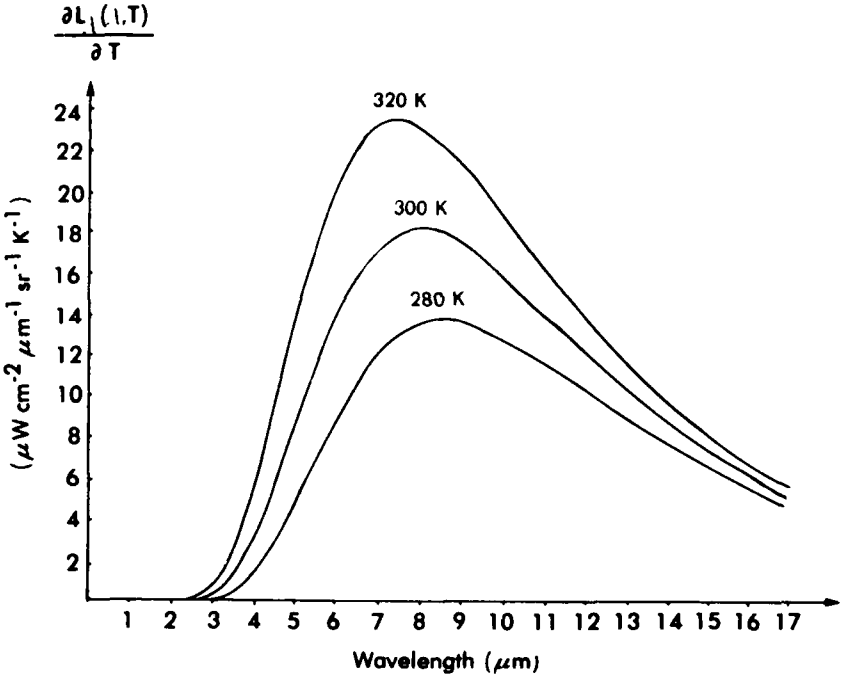

FIGURE 1-4. FIRST PARTIAL DERIVATIVE OF SPECTRAL RADIANCE OF A BLACKBODY WITH RESPECT TO TEMPERATURE

change in irradiance at the sensor due to a unit change in scene temperature as

$$\delta E_{0,\lambda}(\lambda) = \tau_a(\lambda)\ \omega\ \delta L_\lambda(\lambda) = \omega\ \tau_a(\lambda)\ \frac{\partial L_\lambda(\lambda,T)}{\partial T} \qquad (1\text{-}10)$$

for $\delta T = 1^{o}C$

Although analysis is often accomplished by the above method, the radiance received by a sensor often fluctuates with emissivity. Thus it is interesting to note the change in radiance with respect to a corresponding change in emissivity. If one assumes a diffusely emitting surface, then

$$L_\lambda(\lambda,T) = \frac{\varepsilon(\lambda)\ M_\lambda(\lambda,T)}{\pi} \qquad (1\text{-}11)$$

and

$$\frac{\partial L_\lambda(\lambda,T)}{\partial \varepsilon} = \frac{M_\lambda(\lambda,T)}{\pi} \qquad (1\text{-}12)$$

1.2.3 Reflected Sunlight

For imaging systems operating in the visible and near infrared atmospheric windows, the change in scene radiance as the IFOV sweeps the scene is primarily due to change in reflectance along the scan line. This is because the input from the sun is relatively constant and system sensitivity to thermal radiation is low. An example of this is in the visible and near-IR bands of a multispsectral scanner (MSS). These scanners provide registered images of the same scene in several wavelength regions. In this situation

$$\delta L = \left(\frac{\partial L}{\partial \rho}\right) \delta\rho \qquad (1\text{-}13)$$

A useful way to treat reflectance in this situation is by use of the bidirectional reflectance distribution function (BRDF). (See Reference [1-5], p.3.) See Figure 1-5. In general, the reflectance is a function of the angles of incidence and reflection, the solid angle subtended by the receiver and the area of the surface:

$$d\Phi_r = \rho(\phi_i, \theta_i;\ \phi_r, \theta_r;\ \Omega_r; A_s)\, d\Phi_i \tag{1-14}$$

where $d\Phi_r = L_r\, dA_s \cos\theta_r\, d\Omega_r$

$d\Phi_i = E_i\, dA_s$

The BRDF is defined as:

$$f_r\left(\theta_i, \phi_i; \theta_r, \phi_r\right) = \frac{dL\left(\theta_r, \phi_r, \Omega_r\right)}{dE\left(\theta_i, \phi_i\right)} \qquad \left(sr^{-1}\right) \tag{1-15}$$

For a perfectly diffuse (Lambertian) reflector, the reflected radiance has no dependence on angle:

$$L = \left(\frac{\rho}{\pi}\right) E_{incident} \tag{1-16}$$

where ρ/π is the Lambertian BRDF and $E_{incident}$ is the irradiance incident upon the object. Under this condition, the change in radiance at the sensor due to changes in reflectance as the IFOV of the device traverses the scene is:

[1-5] F. E. Nicodemus, J. C. Richmond, J. J. Hsia, I. W. Ginsberg, and T. Limperis, "Geometrical Considerations and Nomenclature for Reflectance," NBS Monograph 160, National Bureau of Standards, Washington, DC, October 1977.

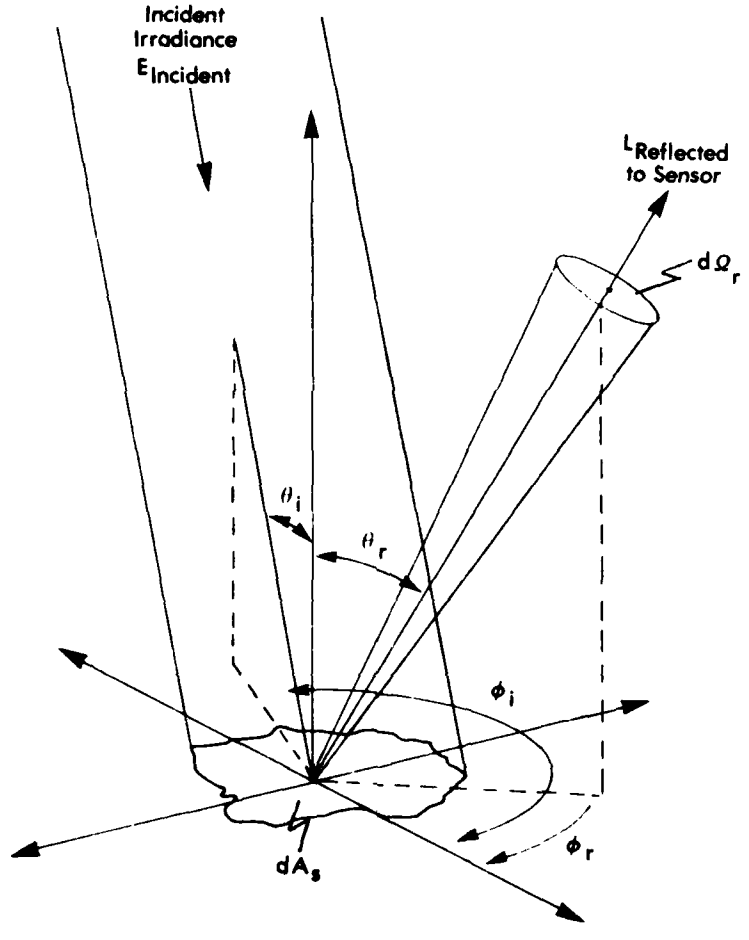

FIGURE 1-5. BIDIRECTIONAL REFLECTANCE DISTRIBUTION FUNCTION (BRDF) GEOMETRY

$$\frac{\partial L_\lambda(\lambda)}{\partial \rho} = \frac{\partial}{\partial \rho}\left[\frac{\rho(\lambda)}{\pi} E_\lambda(\lambda)_{\text{incident}}\right] \qquad (1\text{-}17)$$

$$= \frac{E_\lambda(\lambda)_{\text{incident}}}{\pi}$$

and the change in irradiance at the sensor is:

$$\delta E_{0,\lambda}(\lambda) = \tau_a(\lambda)\ \omega\ \delta L_\lambda(\lambda) \qquad (1\text{-}18)$$

$$= \frac{\omega\ \tau_a(\lambda)}{\pi} E_\lambda(\lambda)_{\text{incident}}$$

In this discussion, no mention was made of atmospheric attenuation between the source (i.e., the sun) and the surface (terrain). Imaging systems operating in reflective spectral regions typically reference the incident radiation present at the sensor (for convenience). Thus the τ_a in Equation (1-18) includes the transmittance of the sunlight to the terrain as well as from the terrain. This will be covered further in Section 1.3.

Figure 1-6 shows the extraterrestrial solar irradiance and the irradiance at the earth's surface. Figure 1-7 shows the irradiance at the earths surface for various slant paths. (Reference [1-2], Chapter 3.)

1.3 ATMOSPHERIC EFFECTS

The process by which radiation is attenuated as it passes through the atmosphere is known as extinction. (See Reference [1-2], Chapters 4 and 5.) The extinction of radiation traversing the atmosphere is proportional to the initial radiance, to the density of the atmosphere and to the distance traversed so that

$$dL_\lambda(\lambda,s) = -k(\lambda,s)L_\lambda(\lambda,s)\rho(s)ds \qquad (1\text{-}19)$$

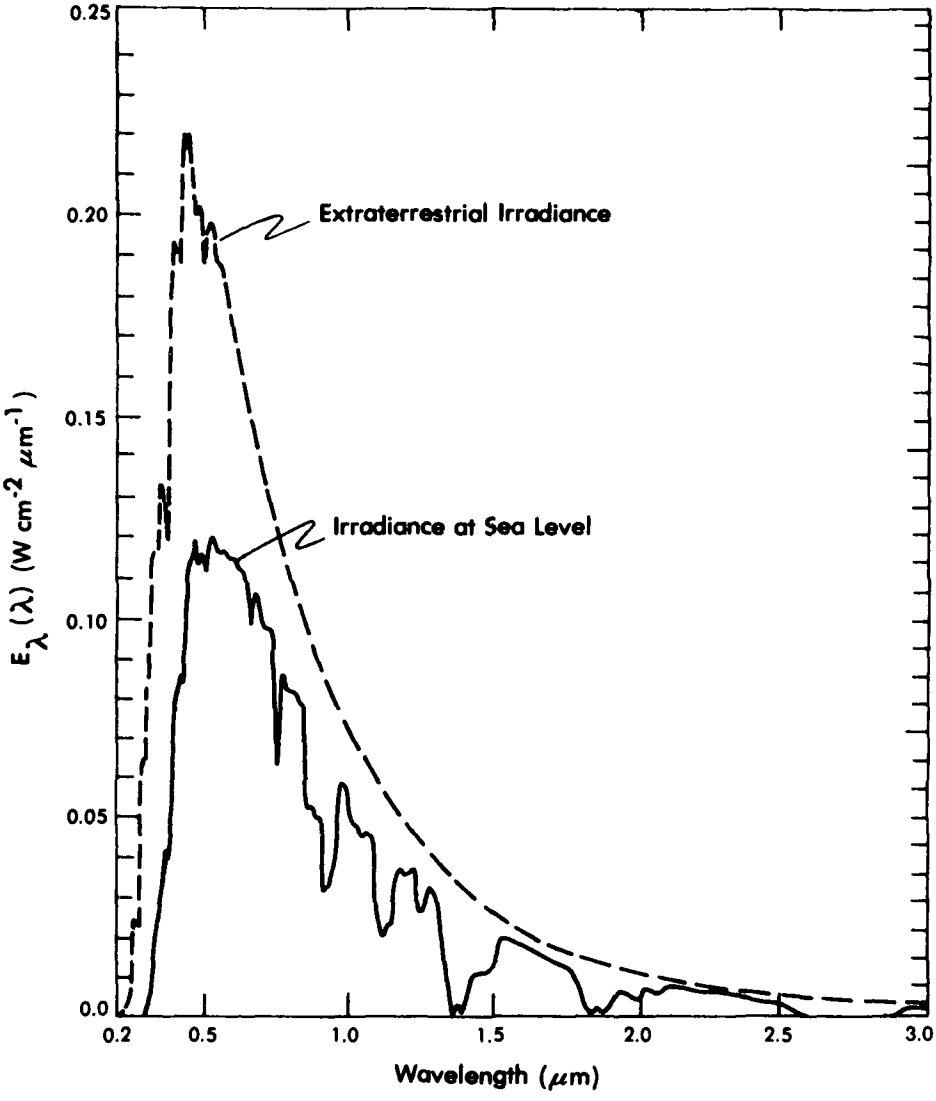

FIGURE 1-6. SPECTRAL IRRADIANCE FOR DIRECT SOLAR RADIATION PERPENDICULAR TO THE SUN'S RAYS FOR AN AIR MASS, M, OF 1.5 (Reference [1-6], p. 523)

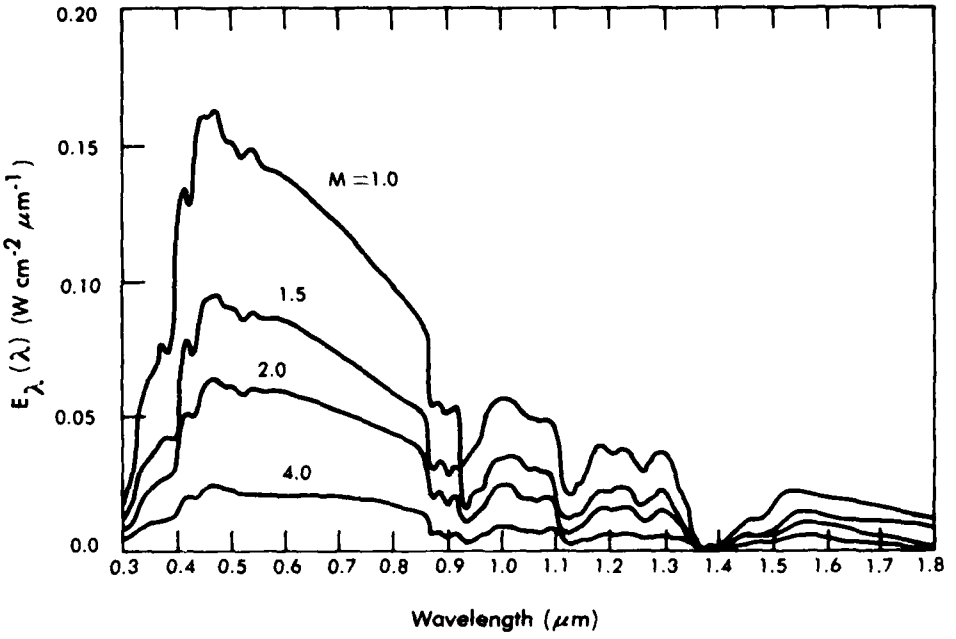

FIGURE 1-7. SPECTRAL IRRADIANCE OF TOTAL SOLAR RADIATION INCIDENT AT SEA LEVEL ON A HORIZONTAL SURFACE FOR VARIOUS SLANT PATHS CORRESPONDING TO AIR MASSES OF M = 1.0, 1.5, 2.0 AND 4.0 (Reference [1-6], p. 523)

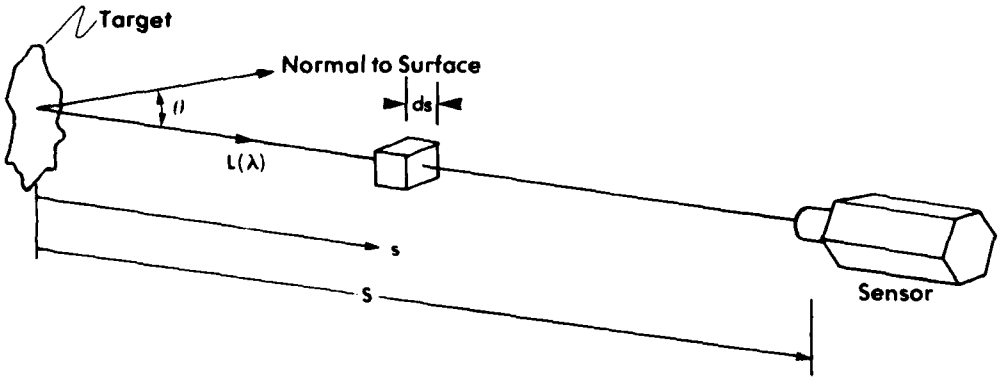

FIGURE 1-8. EXTINCTION OF RADIATION ALONG A PATH TO THE SENSOR

where $L\lambda(\lambda,s)$ = the spectral radiance at a point, s
$\rho(s)$ = the density of the atmosphere at point s
$k(\lambda,s)$ = the spectral mass extinction coefficient. (See Figure 1-8.)

Two different processes contribute to atmospheric extinction. In general,

$$k(\lambda,s) = k_a(\lambda,s) + k_s(\lambda,s) \tag{1-20}$$

where $k_a(\lambda,s)$ is the mass absorption coefficient and accounts for absorption of radiation by gaseous molecules in the atmosphere, and $k_s(\lambda,s)$ is the mass scattering coefficient and accounts for scattering of radiation by haze, fog and gaseous molecules.

Since the interest here is in the transmission of target radiance along the line of sight of a sensor, it is necessary to find the ratio of radiance at the sensor, $L(\lambda,S)$, to the radiance at the target, $L(\lambda,0)$:

$$\tau_a(\lambda) = \frac{L(\lambda,S)}{L(\lambda,0)} \tag{1-21}$$

Rewriting Equation (1-19) gives

$$\int_{L_\lambda(\lambda,0)}^{L_\lambda(\lambda,S)} \frac{dL_\lambda(\lambda,s)}{L_\lambda(\lambda,s)} = \int_0^S -k(\lambda,s)\rho(s)ds \tag{1-22}$$

or

$$\tau_a(\lambda) = \frac{L_\lambda(\lambda,S)}{L_\lambda(\lambda,0)} = e^{-\int_0^S k(\lambda,s)\rho(s)ds} \tag{1-23}$$

The exponent in Equation (1-23) is known as the optical depth. The above can be simplified by assuming that k and ρ are uniform over the path for a given wavelength:

$$\sigma(\lambda) = \alpha(\lambda) + \delta(\lambda) = k(\lambda)\rho S \qquad (1\text{-}24)$$

where $\sigma(\lambda)$ = the spectral extinction coefficient
$\alpha(\lambda)$ = the spectral absorption coefficient
$\delta(\lambda)$ = the spectral scattering coefficient

The above is relatively true for calm atmospheres and horizontal paths. However, for vertical or slant paths the density of the atmosphere varies considerably with altitude. Analysis of transmission along these paths is often accomplished by assuming the atmosphere is composed of statified layers of constant density.

The transmission of the atmosphere over a 1000 ft horizontal path at sea level is shown in Figure 1-9. The curve can be characterized by regions of high transmittance with intervening regions of high absorption and/or scattering. Regions of high transmission are called atmospheric windows. In the infrared portions of the spectrum, absorption processes are more dominant than scattering processes. The major absorbing molecules are identified above their respective absorption bands in the figure.

In the visible and near infrared regions of the spectrum, scattering effects are of more concern. These effects can be seen in the form of haze, fog, and other scattering molecules. However, when the particles within these aerosols grow to sizes near the wavelengths of the band being used by a sensor, heavy scattering will occur. As such, clouds and heavy fog will affect the performance of far-infrared imaging systems.

The above discussion neglects self-emission of radiation by the atmosphere. However, this is not normally a consideration in that a well designed imaging system will not respond to radiation at those corresponding wavelengths. An exception to this is found in meteorological scanners where spectral bands passing are selected to

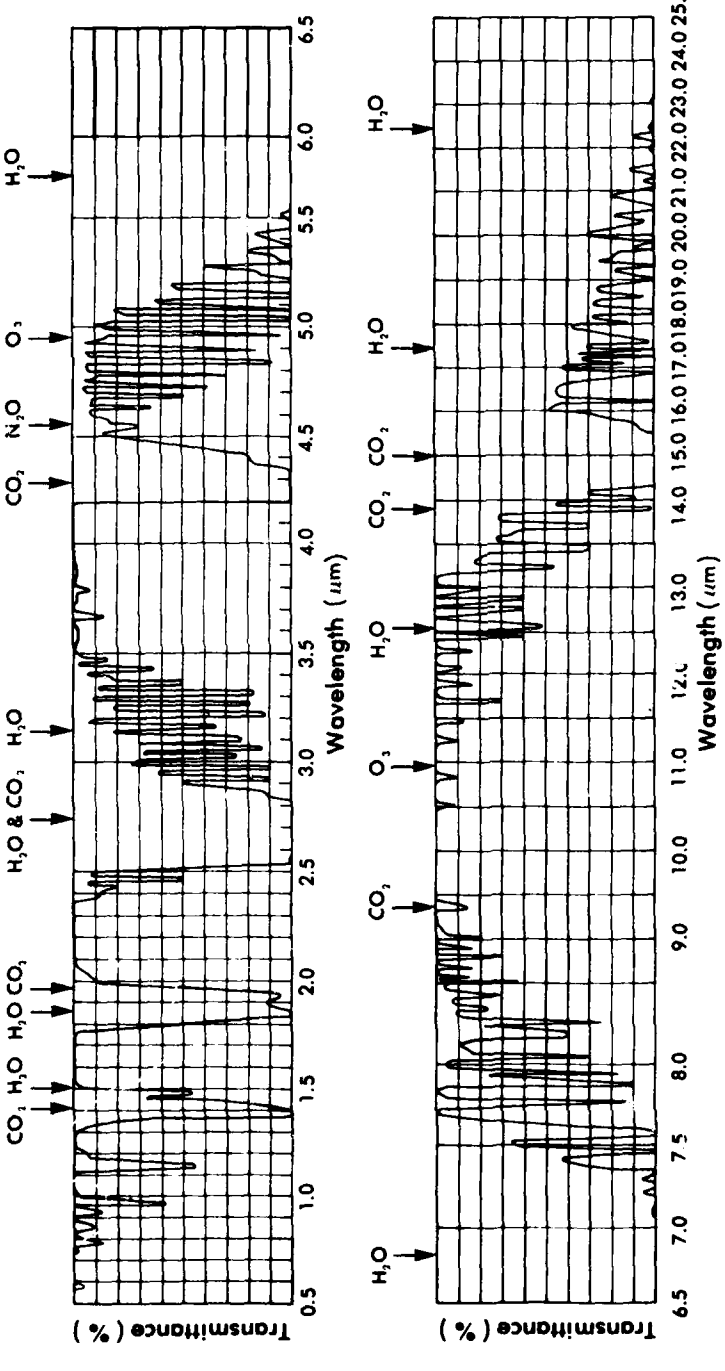

FIGURE 1-9. TRANSMITTANCE OF THE ATMOSPHERE OVER A 1000 ft PATH AT SEA LEVEL CONTAINING 5.7 mm OF PRECIPITABLE WATER AT 79° F [1-7]

correspond to atmospheric absorption bands. Here the atmosphere itself is of interest.

As can be seen from Figure 1-9, the three major absorbing molecules are water vapor, carbon dioxide and ozone. The concentration of ozone is dependent on altitude, latitude, and season. On the average, the ozone in the atmosphere is concentrated in a layer centered at about 80,000 ft. The concentration of this layer drops to about 10% of its peak value at 30,000 ft. Absorption of ozone for systems operating below this altitude is usually negligible compared with other losses. For systems operating from a satellite, this layer is of more concern as the sensor must look through it.

Carbon dioxide, which is distributed fairly uniformly through the atmosphere, is a strong absorber in certain bands of the infrared spectrum. In the 3 to 5 μm atmospheric window, carbon dioxide causes considerable attenuation. However, the losses from carbon dioxide are often less significant than losses due to absorption by water.

Water vapor, which is the most dominant absorber, is also the most variable constituent of the atmosphere. The density of water vapor in the atmosphere may vary from a few tenths of a gram per cubic meter to as much as 30 grams per cubic meter. The interelation between absolute humidity, relative humidity and air temperature is shown in Figure 1-10. As in the figure, absolute humidity is often expressed in cm of precipitable water per unit length. This is convenient for calculating transmittance over long paths as it expresses the volume of water contained over the path per square centimeter. To complicate matters, the concentration of water vapor in the atmosphere varies as a function of altitude, with the greatest concentration occurring at sea level.

There are many models used to calculate atmospheric transmission. Probably the Aggregate and LOWTRAN models are the most generally useful for a wide variety of applications. Although the Aggregate is more

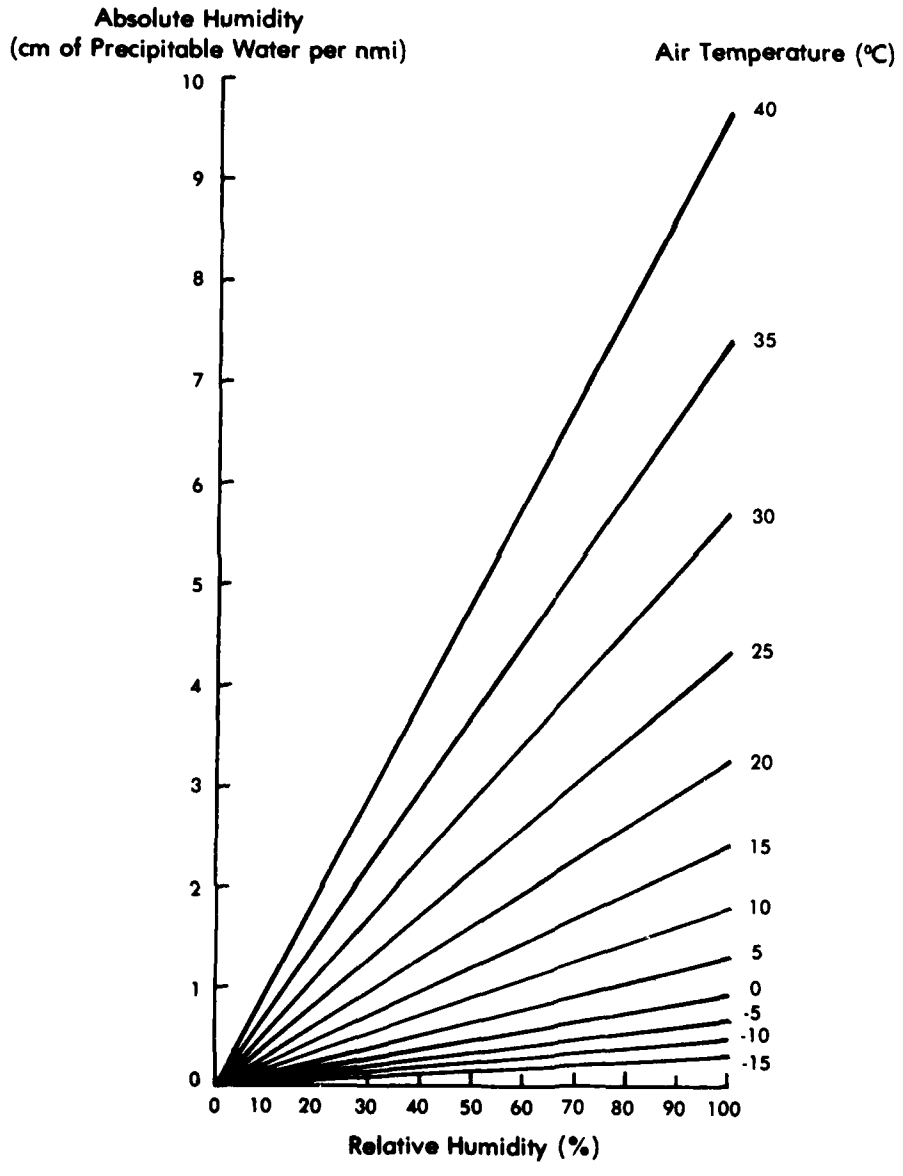

FIGURE 1-10. INTERRELATION OF ABSOLUTE HUMIDITY, RELATIVE HUMIDITY AND AIR TEMPERATURE

accurate than the empirically derived LOWTRAN model, the LOWTRAN model is simpler to use and is currently the most popular of the models. (See Reference [1-2], Chapter 5.)

1.3.1 *Transmission of Thermal Radiation*

As in Section 1.1, the concern here is with the change in irradiance available to a sensor to detect a unit change in temperature of a scene object. The irradiance change available to the sensor per unit temperature change is

$$\delta E_{0,\lambda}(\lambda) = \omega\, \tau_a(\lambda)\, \frac{\partial L_\lambda(\lambda,T)}{\partial T} \tag{1-25}$$

If one assumes an average scene temperature of 300 K and that the emissivity of the scene is unity, then the quantity

$$\frac{\partial L_\lambda(\lambda,T)}{\partial T}$$

can be obtained from Figure 1-4. If, in addition, one assumes that the transmittance over the path to the sensor can be described by the curve illustrated in Figure 1-9, then the quantity

$$\tau_a(\lambda)\, \frac{\partial L(\lambda,T)}{\partial T}$$

can be obtained by multiplication of the two graphs. The result is shown in Figure 1-11.

1.4 OPTICAL SYSTEMS

The optical system chosen for an imaging sensor depends to a large degree on the intended application of the system. Various fields of view, resolution and sensitivity requirements can be achieved by a number of means. For a meaningful output image, two dimensions of scan motion are required. Scan motion may be accomplished by angular displacement of the

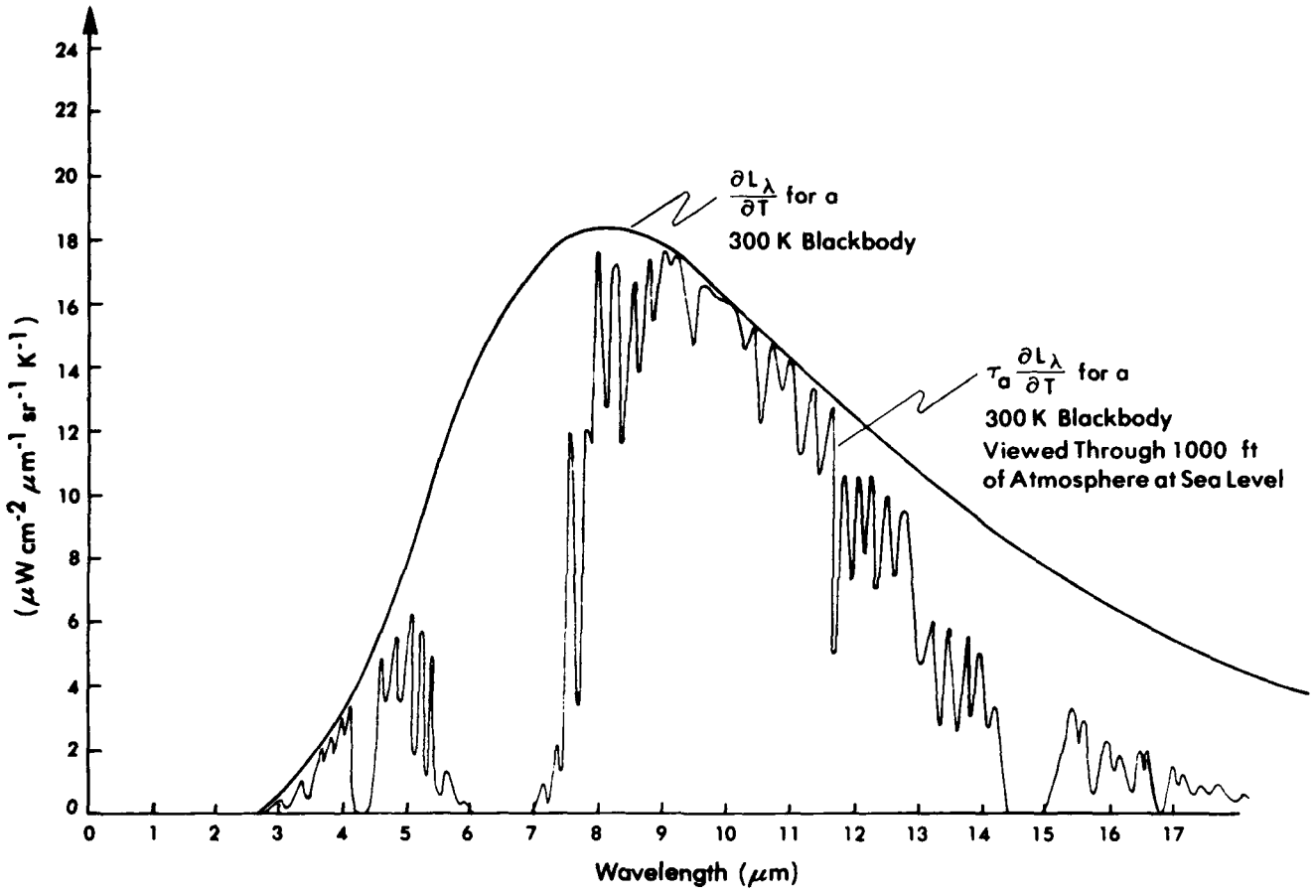

FIGURE 1-11. FIRST PARTIAL DERIVATIVE OF TARGET SPECTRAL RADIANCE WITH RESPECT TO TEMPERATURE AS VIEWED THROUGH 1000 ft OF ATMOSPHERE CONTAINING 5.7 mm OF PRECIPITABLE WATER AT 79° F

IFOV or by linear displacement of the IFOV caused by motion of the imaging system with respect to the object(s) being imaged.

Systems which are used for imaging terrain and mapping meteorological conditions are often carried by aircraft and non-geosynchronous spacecraft. As such, the imaging systems designed for such applications frequently use the linear motion of the vehicle to provide one dimension of the scan motion required. The other dimension of scan motion is provided by angular displacement of the IFOV perpendicular to the velocity vector of the vehicle. (See Figure 1-12.) The angular width of the region imaged by such a system is known as its field of view (FOV) or swathwidth. Because of the continuous strip of imagery obtained from this type of system, they are often referred to as "strip mappers". (Most strip mappers generate straight scan lines perpendicular to the vehicle motion. These are known as "line scanners".) It is interesting to note that these systems have also been used in a side-looking mode in ground vehicles. (See Reference [1-8], p.10.)

Systems operating from a stationary point must provide two dimensions of scan motion. Because this type of system frames a certain angular region of space, they are known as "frame scanners". (See Figure 1-13.) The angular region imaged by these systems is their FOV. This type of system has been used extensively in far-infrared thermal imaging.

The mechanical scanning rate required to produce contiguous scanning in a strip mapper, or a high frame rate in a FLIR, can be reduced by use of an array of detectors to simultaneously sweep a number of scan lines. (See Figure 1-14.) Systems using this technique require good off-axis performance of the collecting optics. In practice, a staggered array is often used to allow for physical separation of the sensitive detector elements.

[1-8] Daedalus Staff, "Daedalus Scanner Applications Worldwide 1980," *Daedalus Enterprises, Inc., Ann Arbor, MI, 1980.*

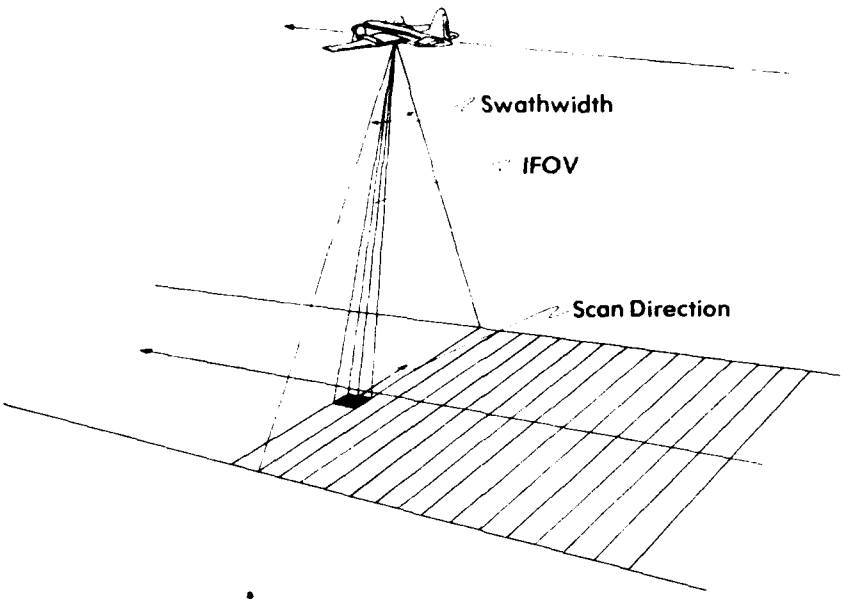

FIGURE 1-12. STRIP MAPPING SCANNER (LINE SCAN EXAMPLE)

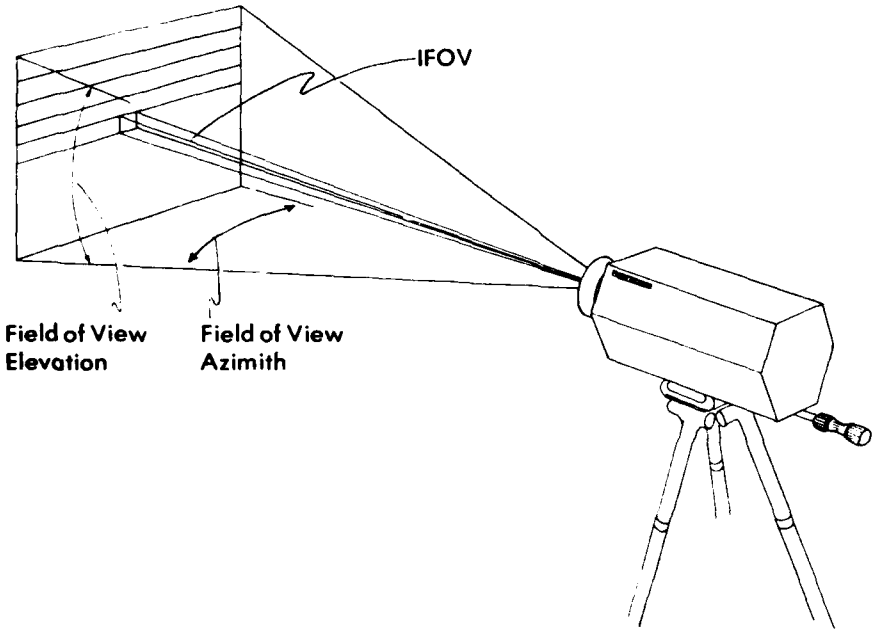

FIGURE 1-13. FRAME SCANNING SYSTEM

Before considering the various scanning optical systems, a discussion of the limitations of the collecting optical systems is necessary.

1.4.1 Collecting Optics

The collecting optics can consist of reflective elements or refractive elements, or a combination of both. An all-refractive system provides better volume efficiency than does a reflective due to the obscuration of the aperture by secondary elements in a reflective system. For most FLIR applications a window is required to protect the system from the environment. If a refractive objective is employed, it can serve as the window whereas with reflective optics a separate window would be needed.

The performance of reflective optics is relatively independent of wavelength and the same optical system can be used over broad spectral bands or in multispectral applications. In addition to the lack of chromatic aberrations, there is also no need to correct for changes in refractive index with temperature.

Reflective optical systems are frequently used in strip mapping systems. Such systems are often flown at high altitudes where fairly good spatial resolution is required to map terrain in sufficient detail. The diffraction-limited angular resolution of an optical system is inversely proportional to aperture diameter. Thus, a large diameter optical system may be required and a reflective system used to reduce cost. Optics, material costs and fabrication difficulties are generally less than for refractive optics, particularly for large elements.

Additionally, many strip mapping systems are multispectral. If a reflective optical system is used, the collecting optics can be common for a group of spectral channels without the chromatic aberrations or transmittance problems associated with refractive optics.

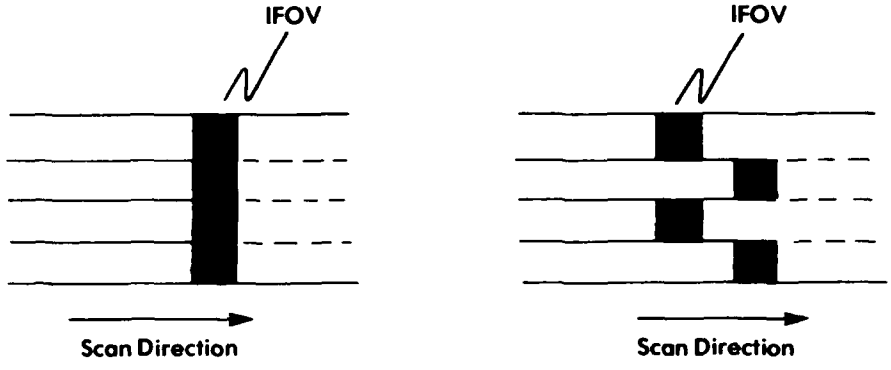

(a) 4-Element Line Array)

(b) 4-Element Staggered Array

FIGURE 1-14. DETECTOR ARRAYS

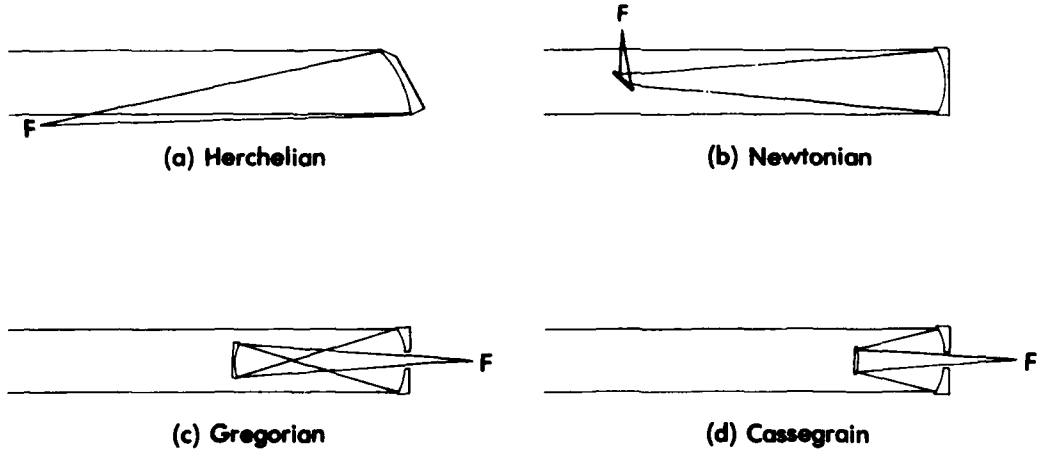

(a) Herchelian

(b) Newtonian

(c) Gregorian

(d) Cassegrain

FIGURE 1-15. CLASSICAL MIRROR SYSTEMS

Reflective Optics

The image plane of a spherical or parabolic mirror lies in the path of incoming radiation. Since this often places the detector in an inconvenient position where it obstructs incoming radiation, secondary mirror systems are frequently used.

Some classical mirror systems are shown in Figure 1-15. Each is shown with equivalent effective focal lengths and primary mirror diameters. The fraction of the aperture area blocked by secondary elements and their supports is called obscuration. The simplest system is the Herchelian because it contains one element and has no obscuration. This type of telescope is rarely used in imaging systems because of its comparatively long length and off-axis mirror. The Newtonian telescope also has a comparatively long length and, like the Herchelian, is difficult to make rigid. The Gregorian and Cassegrain systems have essentially identical performance excluding the greater obscuration and length in the Gregorian. Thus, the Cassegrain is the more preferred system in its various forms.

The classical Cassegrain consists of a parabolic primary and a hyperbolic secondary. (See Reference [1-2], Chapter 9.) The off-axis image of this system is quite comatic and is unsuitable for use with large arrays of detectors. A popular variation of the Cassegrain consists of an aspheric primary mirror and a spherical secondary and has roughly the same performance as the Cassegrain. This is the Dall-Kirkham and is much easier to fabricate because of the spherical secondary. If an aspheric primary and secondary are used, coma may be eliminated. This variation of the Cassegrain is the Richey-Chrétien system and is useful when off-axis performance is required. The aberrations of these systems can be found in Reference [1-2], Chapter 8.

Catadioptric Objectives

When it is necessary to obtain good image quality over a wide field of view, a catadioptric system, a system combining a primary mirror with a correcting lens, can be used. Three systems of this type are shown in Figure 1-16.

The spherical aberration of a spherical mirror can be corrected by a refracting layer applied to the surface as in the Mangin mirror. This is accomplished at the penalty of potentially serious chromatic aberration.

The spherical aberration of a spherical mirror can also be corrected by a thick meniscus lens as in the Bowers-Maksutov system. The radii of all the system elements are concentric and the stop is placed at the common center of curvature. The resulting system has zero coma and astigmatism.

One other way of correcting the spherical aberration in a spherical mirror is to use an aspheric corrector plate located at the aperture stop at the mirror's center of curvature. In the resulting system, coma and astigmatism are essentially zero. This is known as the Schmidt system and is an excellent system for covering a wide field of view. The aberrations for these systems are listed in Reference [1-2], Chapter 9.

Refracting Objectives

In practice, the design of refractive objectives is accomplished by using computer modeling and optimization. This can be done by calculating the ray trace followed by a number of rays through the various surfaces in a system, and in turn optimizing the curvature of each surface and minimizing the number of elements.

This optimization is often accomplished assuming spherical surfaces for ease of fabrication. Aspheric designs have been used in the past, but these required elaborate grinding processes. Since the advent of

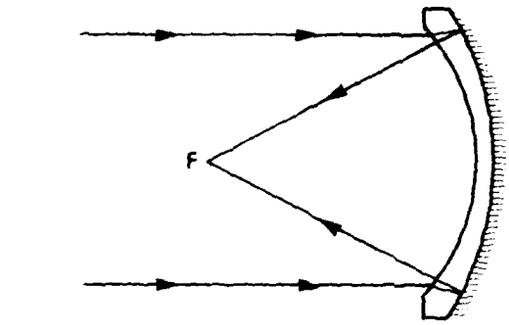

(a) Mangin Mirror [1-9]

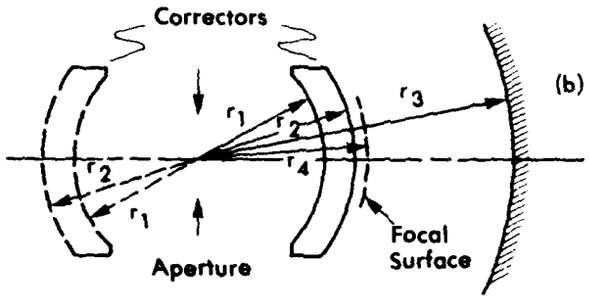

(b) Bowers-Maksutov System [1-10]

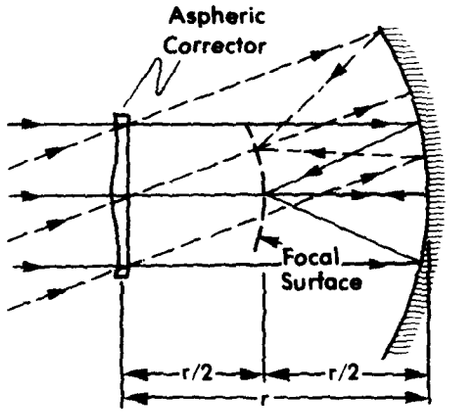

(c) Schmidt System [1-2]

FIGURE 1-16. CATADIOPTRIC OBJECTIVES (Reference [1-2], p. 9-24)

automated tooling of aspheric surfaces, aspheric designs have become more common.

Because of the above, larger numbers of diffraction-limited, wide-field refractive objectives have been built in recent times. In addition to this, designs have been such that many refracting objectives have low chromatic aberration over relatively wide spectral bands and exhibit a fair degree of compensation for refractive index changes with temperature.

A number of materials used for refracting systems are listed in Figure 1-17 along with their transmission regions. (See Reference [1-2], Chapter 7.)

Afocal Systems

Afocal systems are often used in scanning systems which require spectral separation of different channels or to reduce the size of the scanning optics. The Galilean telescope, which has a positive focal length objective and a negative secondary (or eyepiece), is shown in Figure 1-18. This forms a compact telescope where the final image is erect.

An astronomical telescope is a telescope where both elements have positive focal lengths. Here the image is inverted. The image can be erected by placing an inverting element such as a positive lens between the objective and eyepiece. However, in a scanning system the image can often be erected elsewhere in the system. The angular magnification* of an afocal system can be written

$$m_a = -\frac{f_o}{f_i} \qquad (1\text{-}26)$$

*In this report, the sign convention of Jenkins and White (Reference [1-11]) is used.

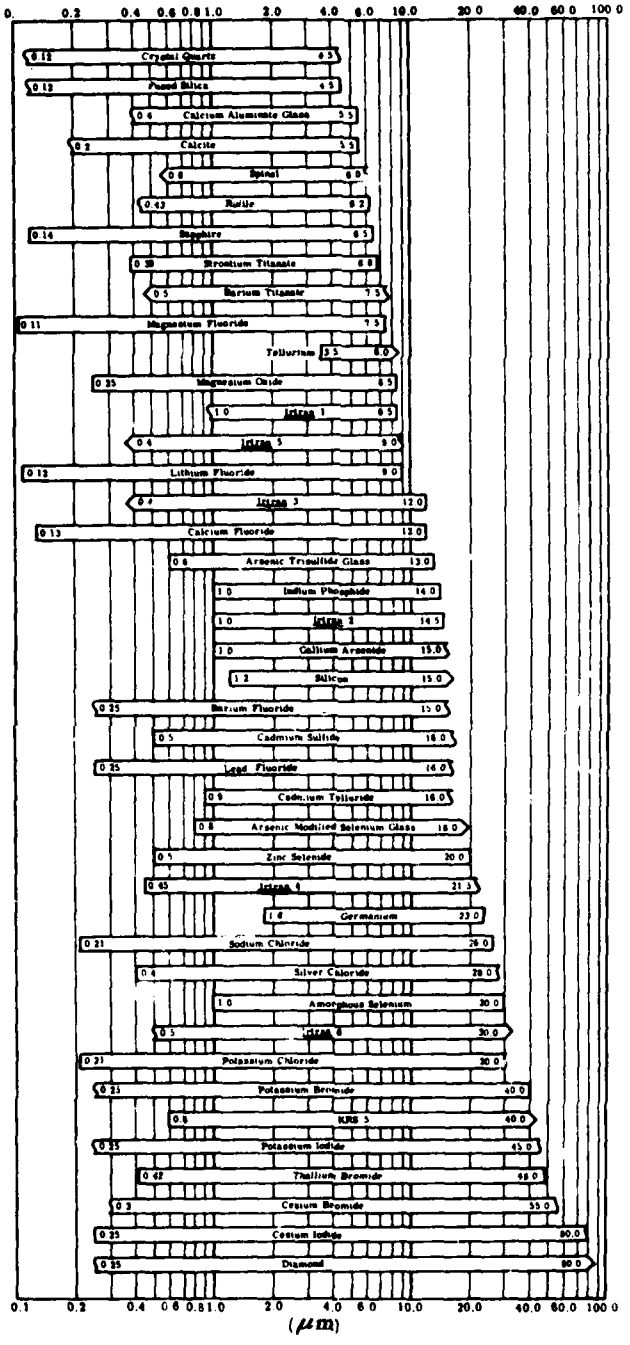

FIGURE 1-17. TRANSMISSION REGIONS OF OPTICAL MATERIALS (2 mm THICKNESS). The cutoff is defined as 10% external transmittance. Irtran® 6 is no longer manufactured by Kodak. Irtran® is a registered trademark of the Eastman Kodak Co. (Reference [1-2], p. 7-17).

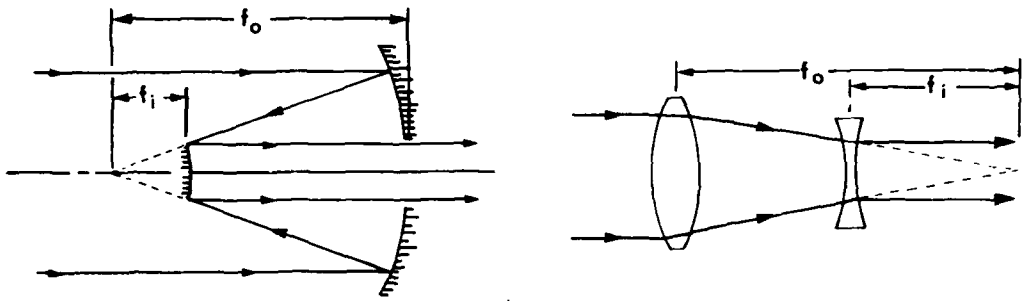

(a) Galilean Telescopes

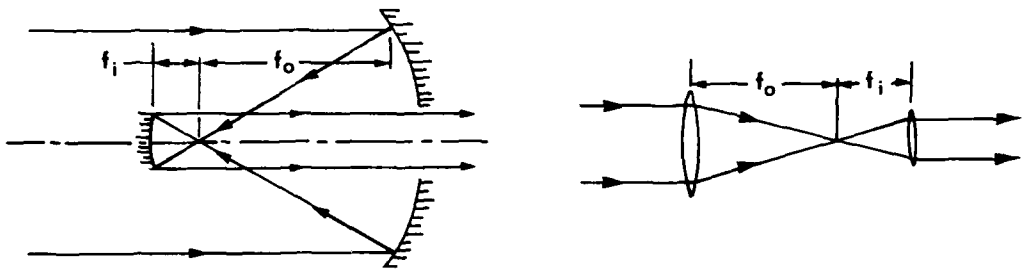

(b) Astronomical Telescopes

FIGURE 1-18. AFOCAL SYSTEMS (Reference [1-2], p. 9-7)

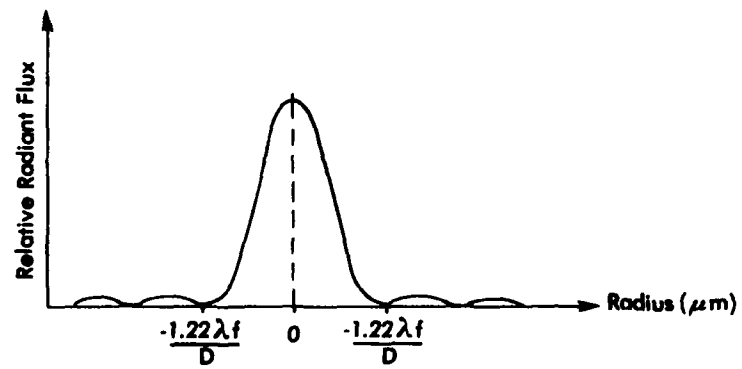

FIGURE 1-19. DISTRIBUTION OF RADIANT FLUX IN THE DIFFRACTION IMAGE OF A POINT SOURCE

where f_i is the focal length of the eyepiece and f_o is the focal length of the objective.

1.4.2 Diffraction Limited Optics

In the past, detector materials were such that it was necessary to use relatively large detector elements to provide adequate sensitivity. This was often achieved at the expense of resolution because of limitations on the optical system external diameter. Resolution was governed by geometrical optics and was taken to be the ratio of the detector dimension to the effective focal length of the optical system and was expressed in milliradians. Detector subtense and IFOV are often considered to mean the same thing.

As advances in detector technology permitted the fabrication of smaller detector elements with higher sensitivity, diffraction became a more significant limit to system resolution. Many current systems are limited, about equally, by wave optics and geometric optics effects. There are other effects which limit the performance of a scanning system such as detector high-frequency roll-off.

Point Resolution Criteria

Diffraction is observed in the interaction of radiation wavefronts with a finite optical aperture. The image of a point source formed by diffraction-limited circular optics appears as a bright circular disk surrounded by concentric rings of diminishing flux density. The central disk, which contains 84% of the radiant flux, is called the Airy disk. (See Reference [1-11].) The distribution of radiant flux is shown in Figure 1-19. The diameter of the Airy disk is

$$d = \frac{2.44\ \lambda\ f}{D} \qquad (\mu m) \qquad (1\text{-}27)$$

where d = the diameter of the disk (μm)
λ = the wavelength of the radiation from the point source (μm)
f = the effective focal length of the optical system (cm)
D = the diameter of the circular optical aperture (cm)

The Rayleigh criterion is that two adjacent, equal-intensity point sources can be considered resolved if the first dark ring in one point diffraction image coincides with the maximum of the other point diffraction image. This is a somewhat arbitrary but useful criterion for the resolution of an optical system. The separation of the two point images is equal to the radius of the first dark ring:

$$\text{Separation} = \frac{1.22\ \lambda\ f}{D} \qquad (\mu m) \qquad (1\text{-}28)$$

The Sparrow criterion is that two adjacent point sources (not necessarily equal) can be considered resolved if the combined diffraction pattern has no minimum between the two point images. This occurs when

$$\text{Separation} = \frac{\lambda f}{D} \qquad (\mu m) \qquad (1\text{-}29)$$

Image Quality Criteria

The term "diffraction limited" is generally associated with the Rayleigh quarter-wave criterion. This criterion states that if the optical path difference for a wavefront passing through an optical system varies no more than one-quarter wavelength peak-to-peak over the aperture of the system, then the image produced will be sensibly perfect. One-quarter wavelength peak-to-peak of third-order spherical aberration

equals about 0.075 wavelengths rms wavefront error. (See Reference [1-12], p.197.)

The effects of wavefront deformation on the diffraction pattern of a point source is to shift some of the energy from the central disk into the ring pattern. This is a detectable change, but in practice is difficult to measure. A system with less than one-quarter wavelength of peak-to-peak wavefront error is excellent for most purposes.

Another criterion for image quality is the Strehl definition. The Strehl definition is the ratio of the radiant flux at the peak of an aberrated point-image (point spread function) to the radiant flux at the center of a diffraction-limited point-image. A Strehl ratio of 0.8 is equal to the Rayleigh quarter-wave limit, but has broader applications. The Strehl definition can be evaluated by

$$\text{Strehl Definition} = \left[\frac{1}{A}\iint e^{i\Delta\phi}dA\right]^2 \qquad (1\text{-}30)$$

where integration is over the pupil area A, and $\Delta\phi$ is the phase difference of the wavefront at the aperture.

The optical transfer function (OTF) is a more complete expression for resolution performance than Rayleigh, Strehl or other single measure. The performance of any linear system can be described by an impulse (or transfer) function. (See Reference [1-13], p.1.) The response of an optical system can be written as the convolution of the spatial

---

[1-12] R. R. Shannon and J. C. Wyant, Applied Optics and Optical Engineering, Academic Press, New York, NY, Volume VIII, 1980.

[1-13] J. W. Goodman, Introduction to Fourier Optics, McGraw-Hill, New York, NY, 1968.

distribution of the scene viewed by an optical system with the point spread function:

$$i(x,y) = h(x,y)^{*}\, o(x,y) \tag{1-31}$$

where i = the spatial distribution in the image plane
o = the spatial distribution in the object plane
h = the point spread function of the optical system

It can also be written in the spatial frequency spectrum of the object and image plane using the Fourier Transform of the above equation:

$$I(f_x,f_y) = H(f_x,f_y)\, O(f_x,f_y) \tag{1-32}$$

In general, the optical transfer function can be written in Cartesian and polar form as follows:

$$H(f_x,f_y) = Re[H] + jIm[H] = |H|e^{j\phi} \tag{1-33}$$

where $H(f_x,f_y)$ = the complex OTF
Re[H] = the real part of the complex OTF
Im[H] = the imaginary part of the complex OTF
H = the modulation transfer function (MTF) which is the absolute magnitude of the OTF
ϕ = the phase transfer function (PTF)

Modulation is the measure of what one commonly calls contrast. Modulation of radiance can be defined as follows:

$$\text{Modulation} = \frac{L_{max} - L_{min}}{L_{max} + L_{min}} \tag{1-34}$$

The modulation transfer is the ratio of modulation of radiance in the image plane to that in the object plane:

$$\text{Modulation Transfer} = \frac{\dfrac{L_{max} - L_{min}}{L_{max} + L_{min}}}{\dfrac{L_{max} - L_{min}}{L_{max} + L_{min}}} \tag{1-35}$$

The MTF may vary differently in one direction of the field of view than it does in the other. This is especially true for optical systems for scanners where better MTF may be needed in one direction than in the other.

MTF varies not only with field angle, but with aberrations, focus and location of glare stops and baffles. It will always vary with wavelength, aperture size and geometry because of the diffraction limit.

In general, an optical system is incapable of transmitting spatial frequencies higher than a cutoff frequency, f_c, where

$$f_c = \frac{1}{\lambda\left(\frac{f}{no.}\right)} \qquad \left(\text{cycles } \mu m^{-1}\right) \tag{1-36}$$

This is identical with the Sparrow resolution criterion. For many applications, it is more useful to express this limit in angular frequency.

The computation of the OTF can be accomplished by autoconvolution of the system pupil transmission function. For a diffraction limited system, the MTF is the normalized area common to the pupil and the pupil displaced laterally by an amount proportional to the frequency. The maximum pupil dimension is f_c, the cut-off frequency. Goodman examines these calculations and gives a number of examples. (See Reference [1-13], pp.113-120.)

For a uniformly transmitting circular optical-system without aberations, the MTF for a sine wave target can be given by:

$$MTF\left(f_r\right) = \frac{2}{\pi}\left\{\cos^{-1}\left(\lambda\ f_r\left(\frac{f}{no.}\right)\right) - \lambda f_r\left(\frac{f}{no.}\right)\sin\left[\cos^{-1}\left(\lambda\ f_r\left(\frac{f}{no.}\right)\right)\right]\right\} \tag{1-37}$$

This is plotted in Figure 1-20 along with the MTF for a square wave target. If the frequency of the square wave target is taken as the

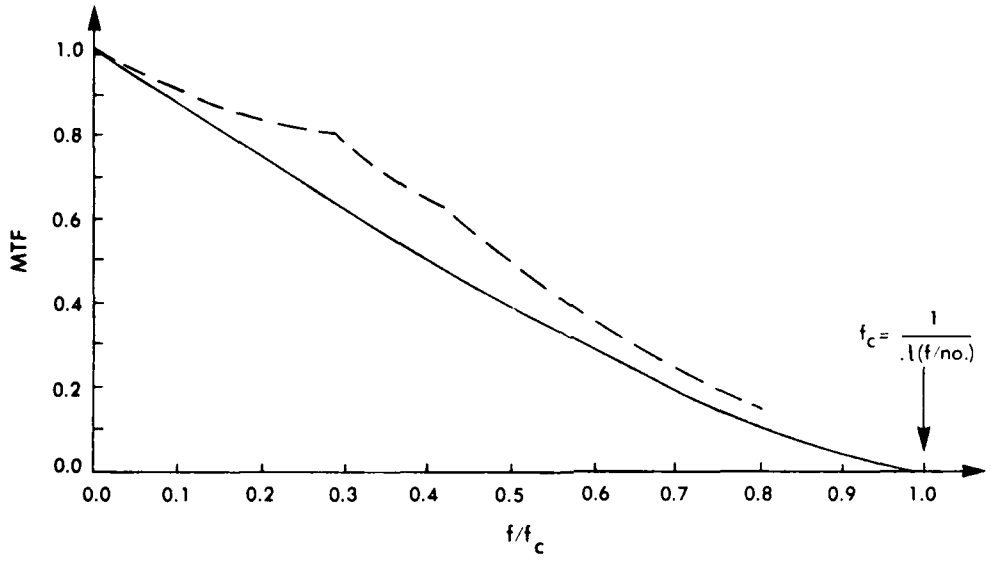

FIGURE 1-20. MODULATION TRANSFER FUNCTION (MTF) OF A DIFFRACTION LIMITED CIRCULAR OPTICAL SYSTEM. Note that the spatial frequency is given in terms of the limiting resolution frequency f_c. The dashed line is the MTF for a square wave target; the solid line is for a sine-wave target (Reference [1-2], p. 8-33).

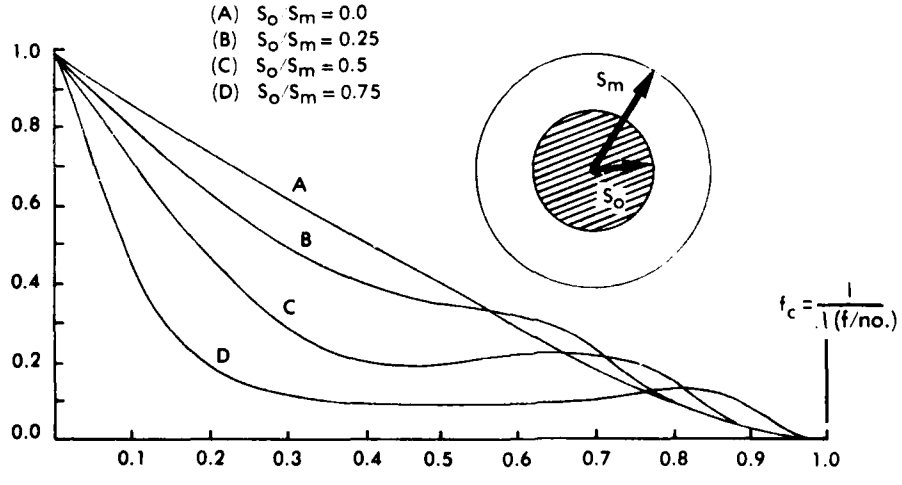

FIGURE 1-21. THE EFFECT OF A CENTRAL OBSCURATION ON THE MTF OF A DIFFRACTION LIMITED OPTICAL SYSTEM (Reference [1-2], p. 8-34)

reciprocal of the center-line bar spacing, the MTF is higher than that indicated for the sine wave target. This is because the frequency content of a bar target is heavily concentrated in frequencies lower than the basic frequency of the bar target.

The MTF of a reflective optical system varies as a function of obscuration. As the obscuration of the system increases, the MTF is reduced at lower frequencies and slightly increased at high frequencies. This is shown in Figure 1-21.

1.4.3 Scan Patterns and Mechanisms

The scan mechanism and optics chosen for a system depend on the scan pattern, resolution, and a number of other requirements imposed by a particular application. There are a number of factors governing the choice between refractive scanning optics and reflective optics, and the choice of location of the scanning optics with respect to the collecting optics. This section reviews some of these considerations as well as presents some techniques used and their relative advantages.

Scanning Optics Location

For systems with small collecting apertures, it may be feasible to place scanning optics of reasonable size in front of the collecting optics. This permits a simple system where the IFOV is swept through the scene as if the entire system were moving. This is called object plane scanning and is illustrated in Figure 1-22. As resolution and scanning rates are increased, however, it may not be feasible to place scanning optics in that location.

Strip-mapping systems frequently use object plane scanning in spite of typically large collecting optic diameters because high scanning rates are not needed. There is difficulty, however, in building large scanning

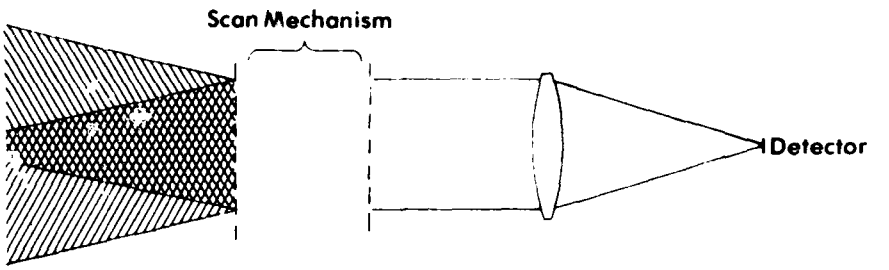

FIGURE 1-22. OBJECT PLANE SCANNING

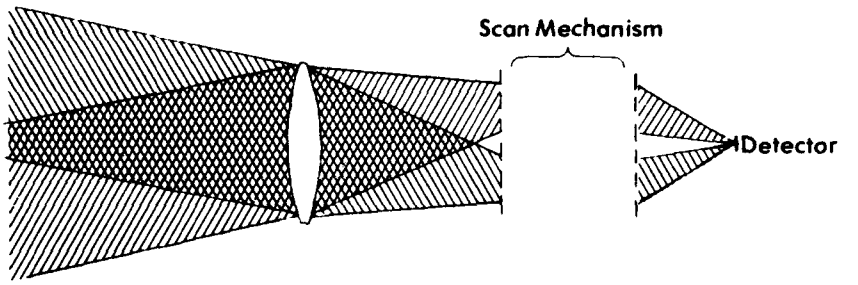

FIGURE 1-23. IMAGE PLANE SCANNING

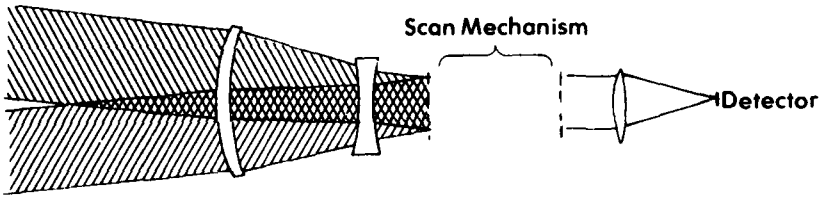

FIGURE 1-24. COLLIMATED BEAM SCANNING

mirrors or other mechanisms with sufficient rigidity to withstand mechanical distortion.

FLIRs, on the other hand, often require frame times less than 1/20 second. If the required collecting optics are large, the correspondingly large scanning optics for object-plane scanning may lead to unacceptable increases in system power, weight and size. One alternative is to place the scan mechanism after the collecting optics where the radiation has converged sufficiently to allow a reasonably sized scan mechanism (Figure 1-23). In this situation, the detectors are effectively scanned through the image produced by the collecting optics. Image plane scanning exibits some disadvantages. Since the scene is viewed off the optical axis, image quality may degrade as aberrations are greatest off-axis. Additionally, loss of focus may occur as a function of scan mechanism position.

Another alternative is to use a low resolution system, with corresponding low scan mechanism size, and fit the system with an afocal telescope of whatever angular magnification is needed to achieve a desired resolution. This allows the scan mechanism to operate in a relatively small diameter collimated beam. (See Figure 1-24.) Two disadvantages are that more optical elements are required than would otherwise be needed and that, for a large field of view, large elements are required for the afocal. For FLIRs, this method has proven to be quite useful in that it allows for simple modification of a basic or "standardized" system to meet a wide variety of requirements.

One other image plane scanning technique is to rotate or translate the detector itself in a fixed image made by a stationary optical system. This has proven to be difficult due to electrical contact stability and adjustment difficulties. However, electronic scanning (e.g., IRCCDs) offer significant potential in such designs.

Strip Mappers

A general illustration for a linescanner is shown in Figure 1-25. If the IFOV in the direction of flight is α(rad) for each detector element, and C is the number of equivalent elements in the array along the flight path, then the length of the detector array image directly beneath the aircraft is αhC where h is the altitude of the aircraft. To assure that there are no gaps or overlap between successive scans the aircraft must move αhC along its path. The velocity of the aircraft must be

$$v = f_s \, \alpha hC \tag{1-38}$$

where f_s is the number of scan cycles per second. The scan rate, $\dot{\theta}$, necessary for contiguous scanning is

$$\dot{\theta} = \frac{\theta f_s}{\eta_s} = \frac{\theta}{\eta_s \alpha C} \left(\frac{v}{h}\right) \tag{1-39}$$

where θ is the swathwidth (rad), and η_s is the scan efficiency -- the fraction of time in a scan cycle the IFOV is scanning across the swath. The time when the IFOV is not viewing the swath is referred to as dead time. The quantity (v/h) is an important parameter in that it describes the angular rate at which the ground passes beneath the aircraft. If the velocity of the aircraft varies, then the scan rate must be changed to compensate. This is often accomplished by some form of (v/h) sensor and servo loop control of the scan motor speed.

Given a constant angular scan rate $\dot{\theta}$, and that the IFOV of each detector element subtends an angle β(rad) in the direction of scan, then the amount of time the detector views any given point on the ground is

$$\tau_d = \frac{\beta}{\dot{\theta}} = \frac{\alpha\beta C \eta_s}{\theta V} \tag{1-40}$$

where V is the (v/h) ratio. This is called the detector dwell time. Since the solid angle of the IFOV of each detector, ω, is equal to $\alpha\beta$, the

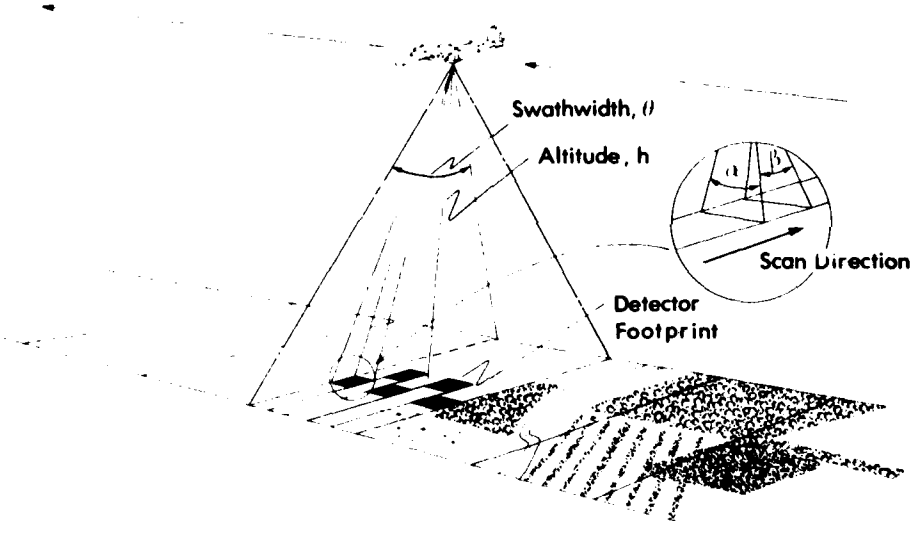

FIGURE 1-25. LINE SCANNER GEOMETRY

dwell time is

$$\tau_d = \frac{\omega C \eta_s}{\theta V} \tag{1-41}$$

The scan patterns generated by strip-mapping systems can be divided geometrically into two basic groups: those that produce scan lines directly perpendicular to the aircraft flight path (line scanning), and those that use a circular scan which is translated by the motion of the aircraft (Palmer or translated circular scan). In addition to this, a number of array patterns can be used. The parameters discussed above are based on the scan rate or frequency. As such, they apply to each of these situations.

Conceptually, the simplest scan mechanism is the rotating 45 deg mirror. (See Figure 1-26*.) The line of sight of the collecting optics is aligned with the aircraft velocity vector and is redirected 90 deg by the scan mirror which oriented 45 deg from the optic axis. The scan mirror axis of rotation is also aligned with the aircraft velocity vector as depicted in the figure. This produces a line scan pattern. Since the scan mirror rotates 2π radians per scan cycle, the scan efficiency is

$$\eta_s = \frac{\theta}{2\pi} \tag{1-42}$$

where θ is the swathwidth in radians. A less obvious aspect of this type of system is that the orientation of the subtense of a square detector or field stop changes with scan angle. Because of this, this type of scanner is usually limited to single-element detector applications. Also, since swathwidths are typically less than $\pi/2$, the scan efficiency is less than 25%. In some applications, this is an advantage in that calibration

*Perspective line drawings are used to illustrate the optical layout of the systems described in this report. For the most part, the ray trace lines used in the figures show the envelope of a radiation bundle passing the system aperture that focuses to a single on-axis point in the detector plane.

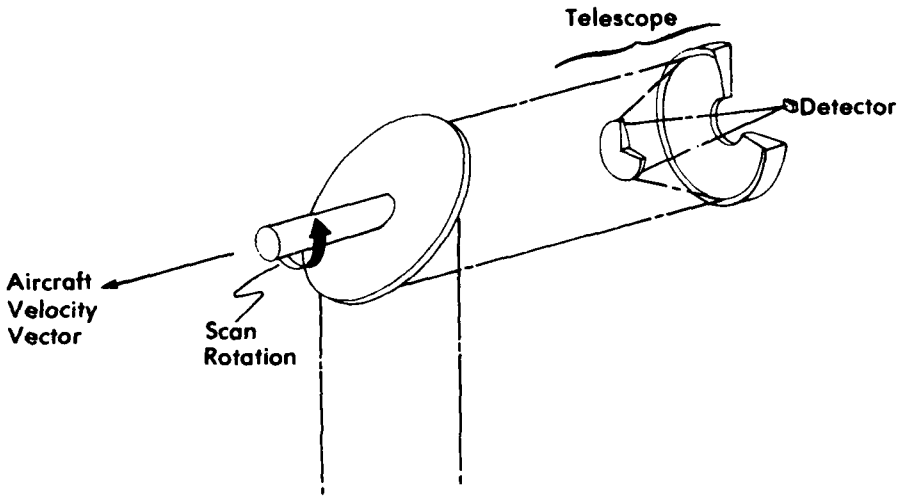

FIGURE 1-26. ROTATING 45 deg MIRROR SCANNER

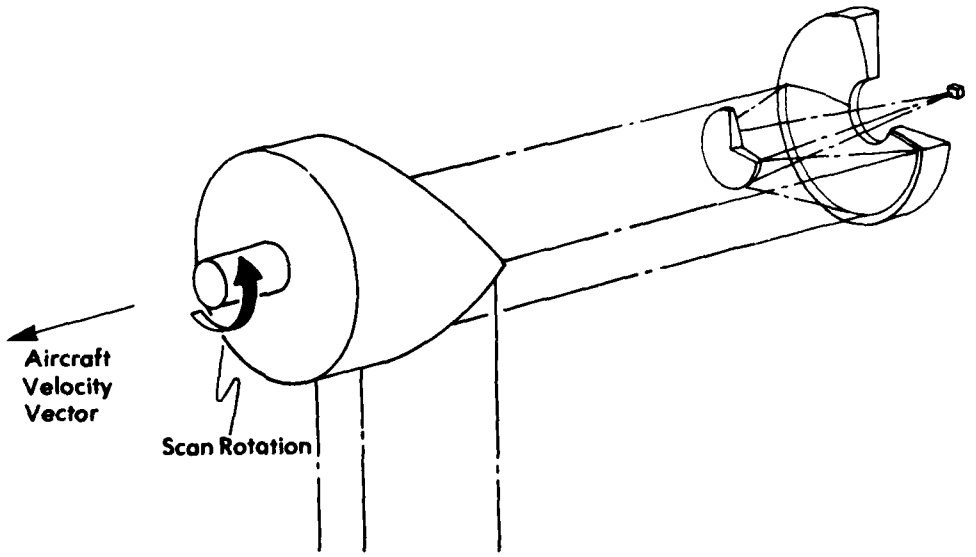

FIGURE 1-27. AXE-BLADE SCANNER

sources can be easily mounted in portions of the sensor housing viewed by the scanner as it looks away from the terrain.

The above scanner requires a relatively fast rotation rate of the scan mirror, which must be balanced for smooth rotation.

These problems can be alleviated by the use of an axe-blade scanner design as illustrated in Figure 1-27. This provides two FOV scans per scan mirror revolution and a scan efficiency of

$$\eta_s = \frac{\theta}{\pi} \tag{1-43}$$

Two disadvantages of this system are that it is still usually limited to single-element detector applications, and that, to maintain the same aperture as the 45 deg scan mirror system, it must have a scan mirror of at least twice the dimensions of the 45 deg scan mirror.

One solution to the problems mentioned above is to use a mirror oriented 45 deg to the optical axis of the telescope and to oscillate it along an axis through the mirror in the direction of the aircraft velocity vector as pictured in Figure 1-28. If the scan pattern of this scanning system does not extend far beyond the intended swathwidth, then the scan efficiency will be nearly 100%. Some of the sensors based on this design utilize a sinusoidal oscillation of the mirror. By using a wide scan pattern, and only using quasi-linear portions of the motion, contiguous scanning can be obtained. Another method is to torque the mirror in one direction and to allow it to deflect off of a bumper. Active scanning occurs during the linear motion after deflection, after which the mirror is again torqued onto the bumper to complete the scan cycle. Dead time is adjusted to provide contiguous scanning.

Another scanning system which can be used with detector arrays is the so-called Kennedy scanner. This system has a multifaceted mirror which is rotated along an axis aligned with the velocity vector as illustrated in

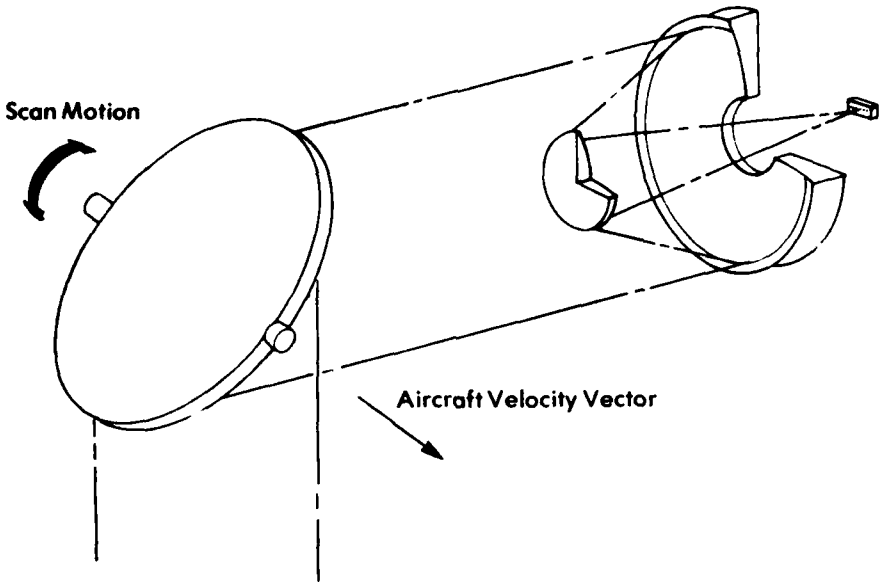

FIGURE 1-28. OSCILLATING MIRROR SCANNER

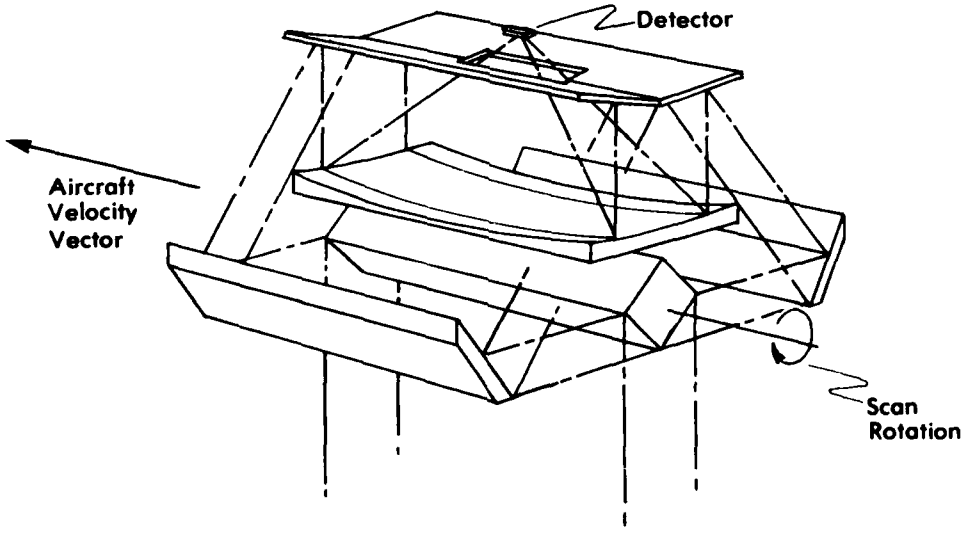

FIGURE 1-29. KENNEDY SCANNER

Figure 1-29 for a four-faceted mirror. Because of the symmetry of the scan mirror about the axis of rotation, and the usual dimensions of the mirror, high scan rates can be obtained without the large mechanical stress on the scan mirror that is associated with the oscillating mirror system. Additionally, there are many scan cycles per scan mirror revolution yielding a scan efficiency of

$$\eta_s = \frac{M\theta}{2\pi} \tag{1-44}$$

where m is the number of facets on the scan mirror. Variations of this design have been built with scan mirrors with three, four, five and six facets.

A difficulty with line scanners is that the dimensions and shape of the ground footprint of the IFOV (i.e., projected image of the field stop) vary with scan angle. As the scan angle increases, so does the footprint. This results in a bow-tie-shaped scan line and overlapping scans at the edges of the swath. An alternative is to use a scanner which uses a translated circular (Palmer) scan. Because the distance to the terrain is constant, the IFOV footprint is constant. Additionally, because the range is constant, variations in atmospheric effects are minimized. Typically, only the fore-portion of the scan is used. However, the aft-scan can also be used to obtain a stereo image of the terrain. One way of implementing this type of scan pattern is illustrated in Figure 1-30. A disadvantage of this type of system is that the imagery collected is more difficult to display than that of the previously discussed systems.

While image plane scanning is rarely used in strip mapping systems for producing primary scanning, this type of scan mechanism is sometimes used to compensate for the drift of the IFOV along the flight path during a single scan line. It is also used to compensate for nonlinear motion in oscillating mirror scanning systems. This is known as image motion compensation or correction (IMC).

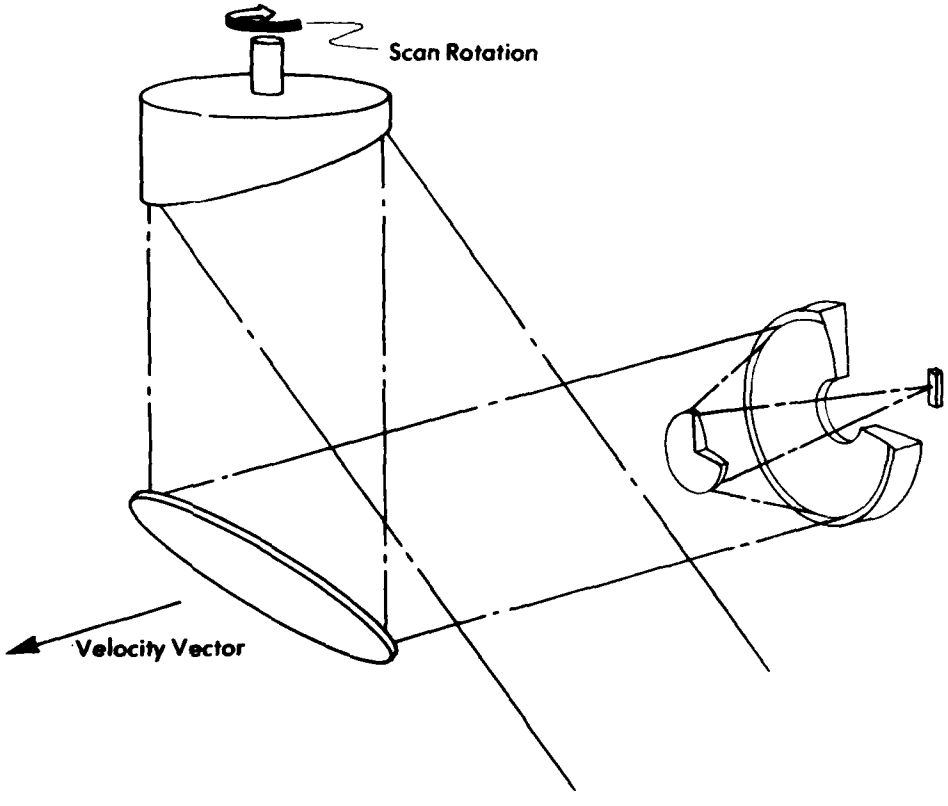

FIGURE 1-30. TRANSLATED CIRCULAR SCANNERS

Frame Scanning Systems

The simplest form of frame scanning is the familiar raster scan used in TV systems. This is illus rated in Figure 1-31. If the frame rates used are TV compatible (i.e., 30 frames per second), the relatively common CRT display systems can be used. The angular scanning rate required of the scan mechanism is

$$\theta = F \frac{\Omega}{\omega} \frac{\beta}{\eta_s} = F \frac{\Omega}{\eta_s \alpha} \tag{1-45}$$

where F = the frame rate

η_s = the scan efficiency

Ω = the solid angle subtended by the field of view

With a single element detector, the mechanical rate required of the scan mechanism may be difficult to achieve. To reduce the mechanical scanning rate, one can use an array of C elements arranged perpendicular to the scan direction as illustrated in Figure 1-32. This reduces the mechanical scan rate to

$$\dot{\theta} = F \frac{\Omega}{\eta_s C \alpha} \tag{1-46}$$

The dwell time of each detector can be given by

$$\tau_d = \frac{\beta}{\dot{\theta}} = \frac{\eta_s C \omega}{\Omega F} \tag{1-47}$$

For TV compatibility when scanning with an array, one must electronically multiplex the detector outputs perpendicular to the direction of scan. However, it is often rather difficult to synchronize the multiplexing operation with the mechanical scan motion. Although some frame-scanning systems do not require TV compatibility, there is always a tradeoff between the mechanical scanning rate and the number of detectors.

There is a wide variety of scan patterns and mechanisms used with frame-scanning systems. The examples cited above involve unidirectional

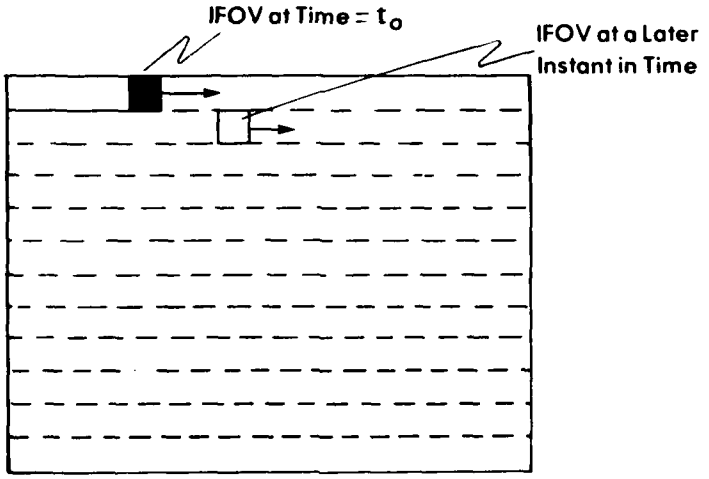

FIGURE 1-31. RASTER SCAN

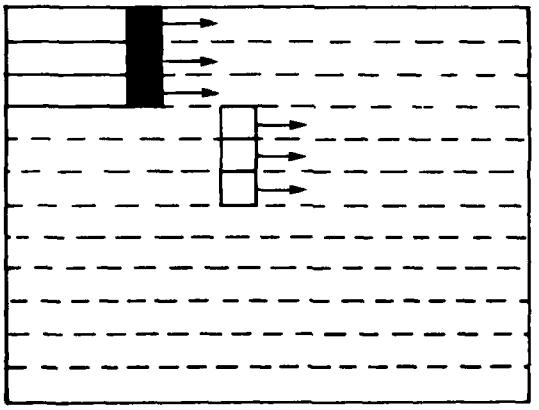

FIGURE 1-32. FRAME SCANNING WITH AN ARRAY OF DETECTORS

scanning in that active scanning is performed in one direction only. One commonly used means of producing this type of scan is illustrated in Figure 1-33. The azimuth scan lines are swept out by the rotating multifaceted mirror. Vertical scan motion is produced by the planar mirror. The vertical scan is often accomplished by rotating the planar mirror at a constant velocity to separate the scans and then quickly retracing the mirror to begin a new frame.

Since placing the detectors in a row (as was illustrated in Figure 1-32) has practical difficulties, one often uses a staggered array. Another alternative is interlaced scan lines produced by an array as illustrated in Figures 1-34 and 1-35. The interlace ratio (2:1 and 4:1 in the figures) is the ratio of the number of azimuth scan cycles required per frame. In this situation the azimuth scan frequency is called the field rate. If a large staggered array is used as illustrated in Figure 1-36, then the need to interlace is eliminated and the frame and field rates are identical.

The type of scan mechanism discussed above exhibits some disadvantages. One of these is that the scan efficiency is low because of the time required for each new facet to come into position. Also, because of the relatively high rotation rates typically used for the azimuth scan, there may be a need to evacuate the scan cavity. One other disadvantage is the distortion caused by the motion of the elevation scan mirror during an azimuth scan cycle. This results in tilted scan lines.

Another unidirectional scan mechanism design is illustrated in Figure 1-37. This type of mechanism improves the scan efficiency and eliminates the rough elevation scan mirror motion. The use of refracting elements in this design can result in chromatic aberrations. An alternative is to use the multifaceted scan mirror ring design illustrated in Figure 1-38. The angle of each mirror facet is adjusted so as to interlace the scan lines.

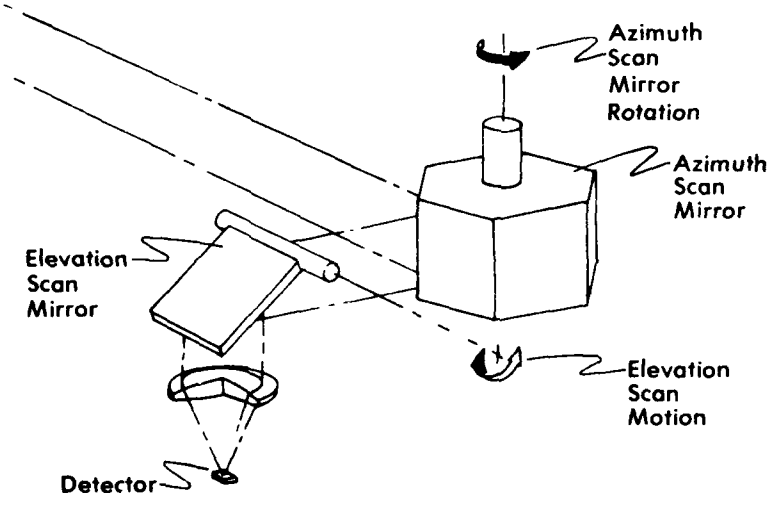

FIGURE 1-33. UNIDIRECTIONAL SCANNER ("SERIAL SCANNER")

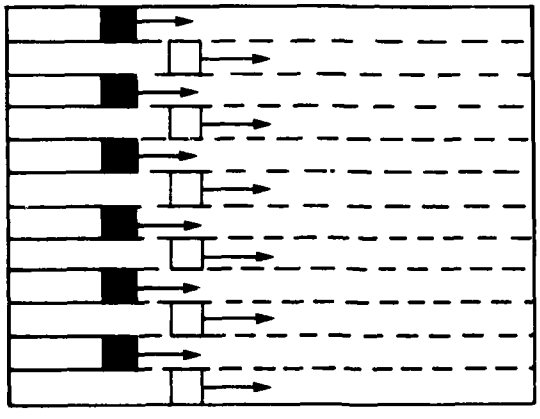

FIGURE 1-34. 2:1 INTERLACE SCANNING

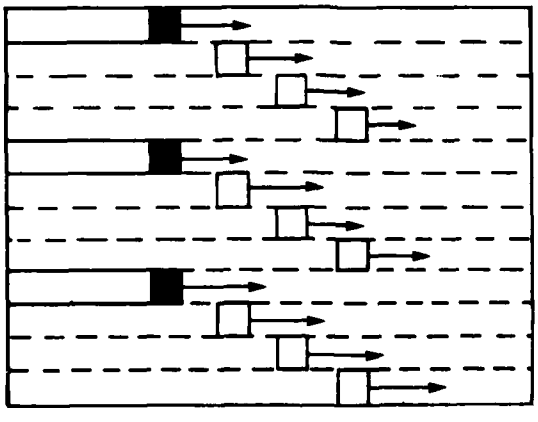

FIGURE 1-35. 4:1 INTERLACE SCANNING

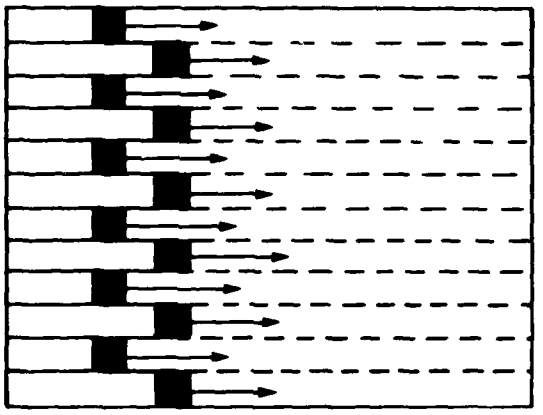

FIGURE 1-36. FRAME SCANNING WITH A STAGGERED ARRAY

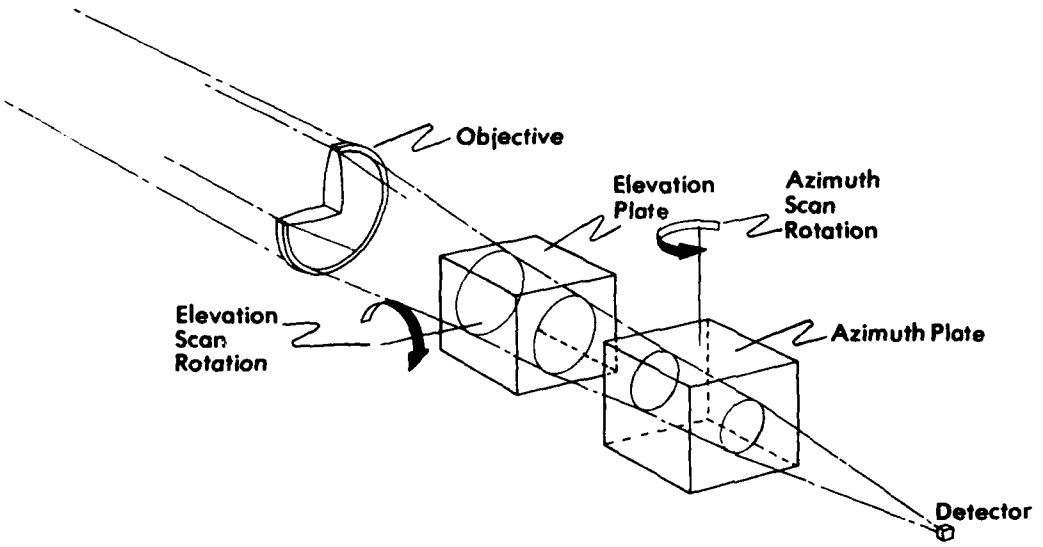

FIGURE 1-37. SCAN MECHANISM USING TWO PARALLEL PLATE SCAN ELEMENTS

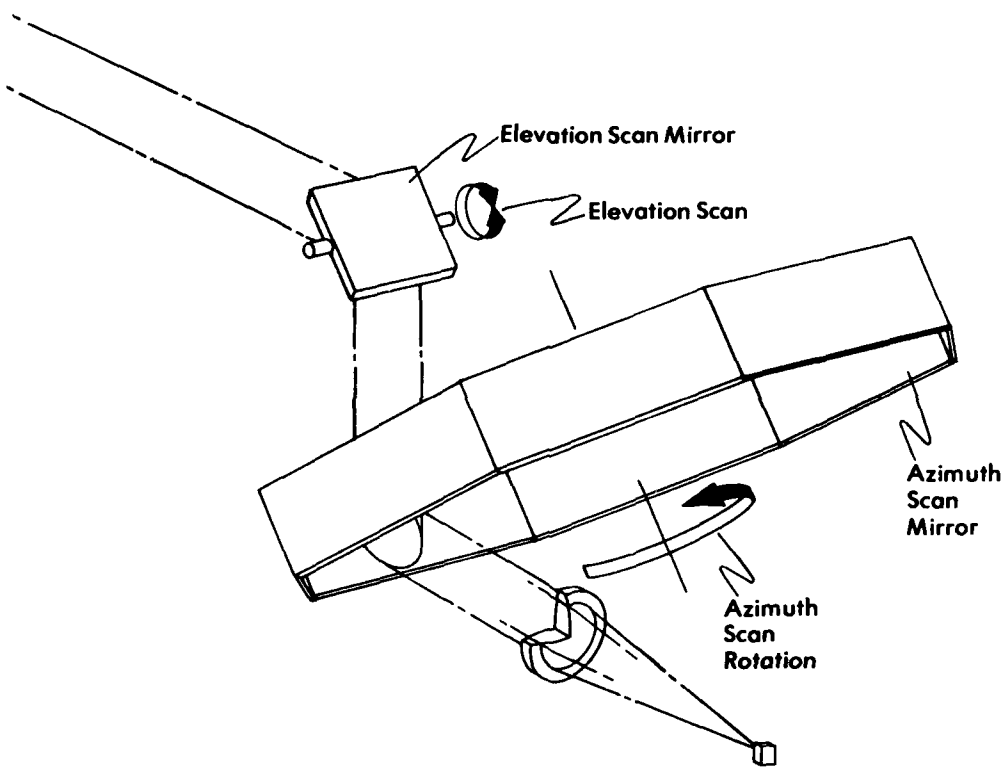

FIGURE 1-38. CAROUSEL SCANNER

This type of mechanism has a relatively high scan efficiency and is free of scan line distortion.

A method of improving the effective dwell time of a detector without increasing the scan rate is to use an array of detectors arranged in the direction of scan as illustrated in Figure 1-39. If the signal from each detector is delayed in time by an amount equal to the distance between the centers of the elements divided by the scan rate and mixed with the signal from the following detector, then the combined output of the array has an improved signal-to-noise ratio over that a single element detector. (See Reference [1-2], p.10-8.) This is referred to as serial scanning. Another method of accomplishing this is illustrated in Figure 1-40. Here the signal is delayed by an amount of time equal to the time taken for two scan cycles. This is called parallel scanning. A combination of approaches can be used as illustrated in Figure 1-41.

Another method of improving the detector dwell time is through the use of overscanning as illustrated in Figure 1-42. If the overlap ratio (in this case 0.5) is r_o, then the effective dwell time, τ_d', is

$$\tau_d' = \frac{\tau_d}{1-r_o} \tag{1-48}$$

where τ_d is the dwell time without overlap. This is accomplished at the expense of scan efficiency. Additionally, the display image can appear banded for $r_o < 0.5$.

Unidirectional scanners, with appropriate delay circuits and synchronization, can be made TV compatible. But in some applications this may not be necessary. Some systems use a display where an array of LEDs corresponding to the detector array is simultaneously scanned with the detectors to provide a visible image. This type of display can be viewed by a vidicon camera to provide TV compatibility without the need for synchronization or electronic multiplexing of the detector output.

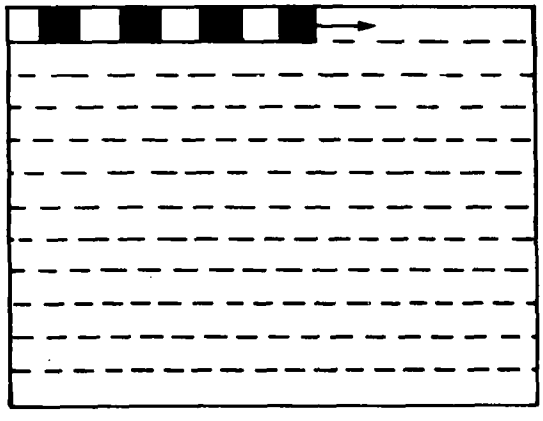

FIGURE 1-39. SERIAL SCANNING

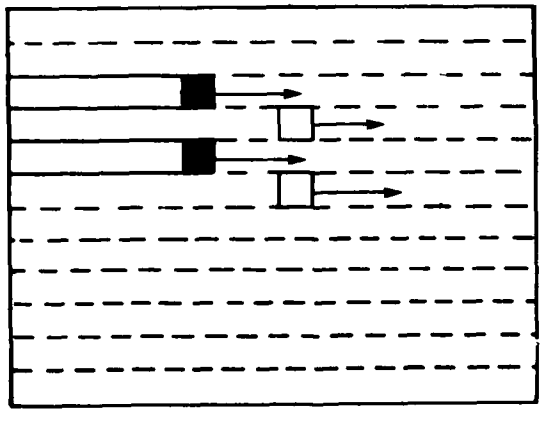

FIGURE 1-40. PARALLEL SCANNING

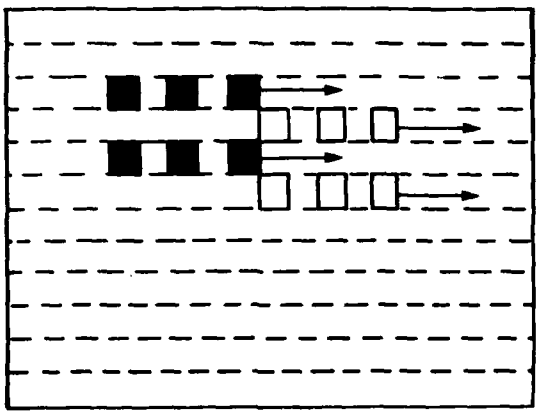

FIGURE 1-41. SERIAL-PARALLEL SCANNING

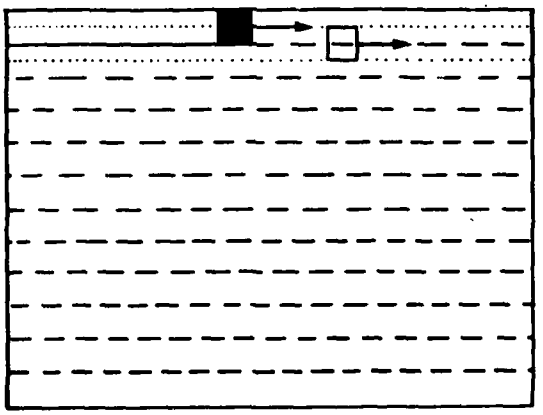

FIGURE 1-42. OVERSCANNING ($r_o = 0.5$ EXAMPLE)

Because of this, the scan pattern need not be restricted to unidirectional scanning.

Another type of scanning is bidirectional scanning. This is illustrated in Figures 1-43 and 1-44. Azimuth scanning is often produced by use of a planar mirror oscillating sinusoidally. Only the quasi-linear velocity portions of the scan motion are used. Interlace is accomplished by use of a second scan mirror as in Figure 1-45 or by rotating the azimuth scan mirror itself as in Figure 1-46. The latter method results in a scan distortion (tilted scan lines). This is usually tolerable for low interlace ratios.

One need not be restricted to use of a rectangular frame. A circular scan pattern is illustrated in Figure 1-47 and a spiral scan in Figure 1-48. In Figure 47, the detector array interlaces itself on each scan cycle. Two alternative methods of accomplishing this pattern are to rotate the detector itself or to use a rotating V-mirror as in Figure 1-49. The V-mirror design is simpler in that it eliminates electrical contact and cooler problems associated with rotating the detector. The V-mirror also has the advantage of rotating the scan pattern twice per mirror revolution. In Figure 48, a smaller number of detectors is used. Interlacing is accomplished by use of a radial scan mirror as illustrated in Figure 1-50.

One other scan pattern is the sector scan. This is pictured in Figure 1-51. It is produced by the so-called "soupbowl" scanner illustrated in Figure 1-52. Interlace is caused by minor adjustments in the scan mirror facet set angles.

1.5 DETECTORS

The term "detector" in the context of this writing means a transducer which converts infrared or visible radiation into a useable electrical

FIGURE 1-43. BIDIRECTIONAL SCANNING

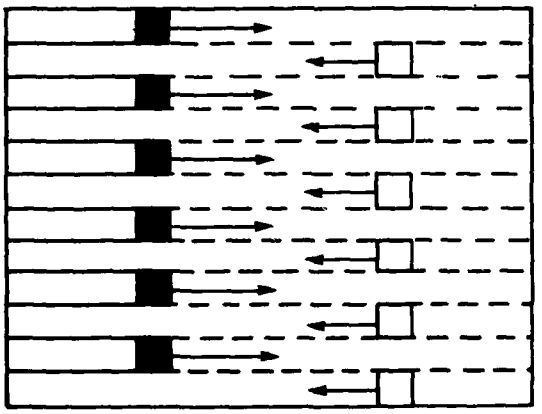

FIGURE 1-44. BIDIRECTIONAL SCANNING WITH 2:1 INTERLACE

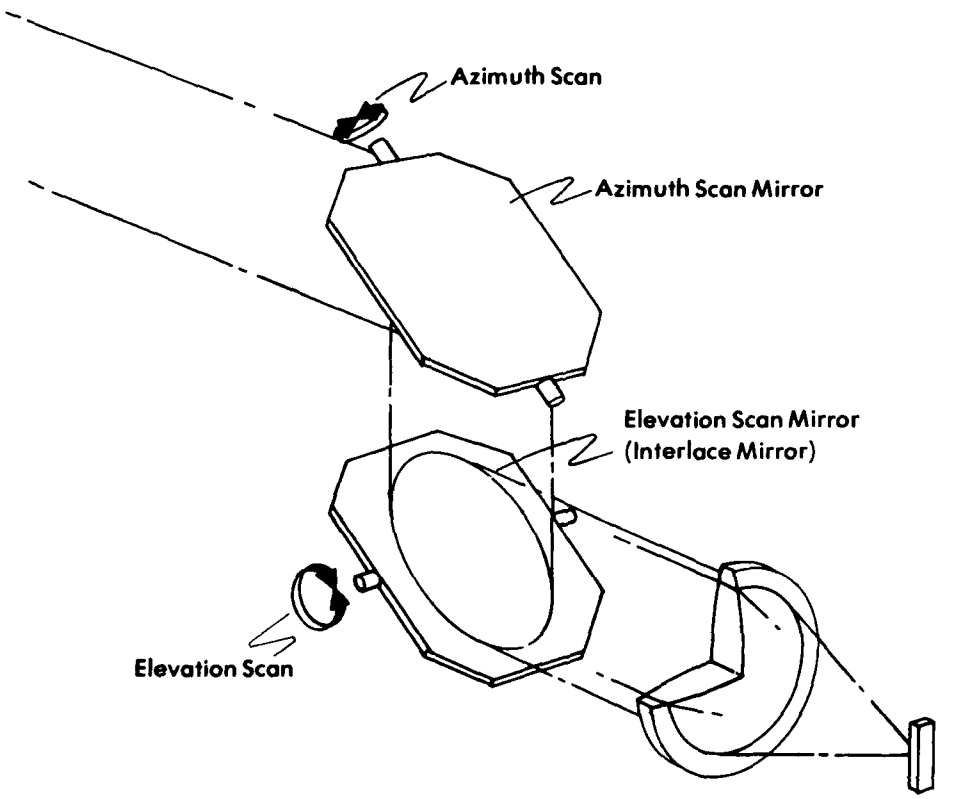

FIGURE 1-45. BIDIRECTIONAL SCANNER WITH TWO SCAN MIRRORS

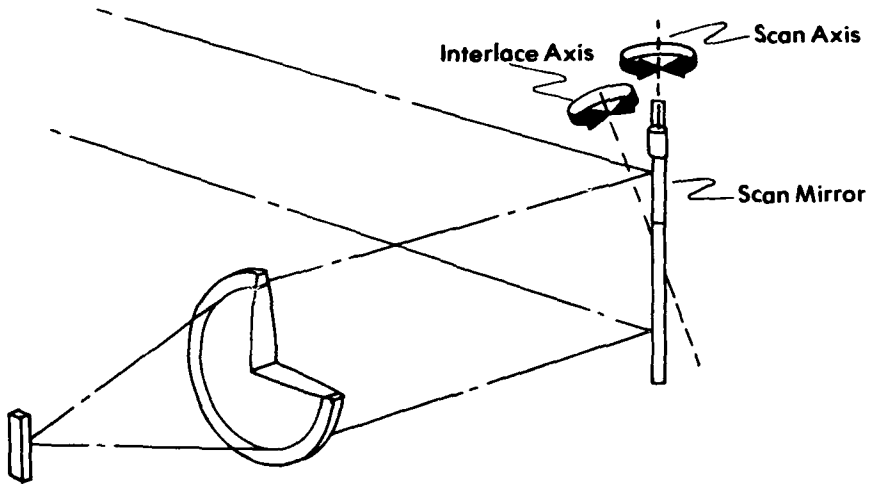

FIGURE 1-46. BIDIRECTIONAL SCANNER (SCAN MIRROR GIMBALLED TO OBTAIN INTERLACE AXIS)

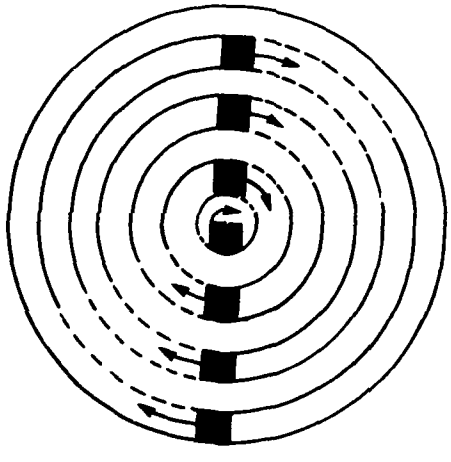

FIGURE 1-47. CIRCULAR SCAN WITH 2:1 INTERLACE

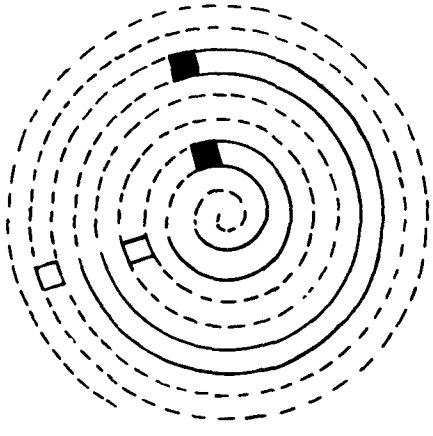

FIGURE 1-48. SPIRAL SCAN PATTERN

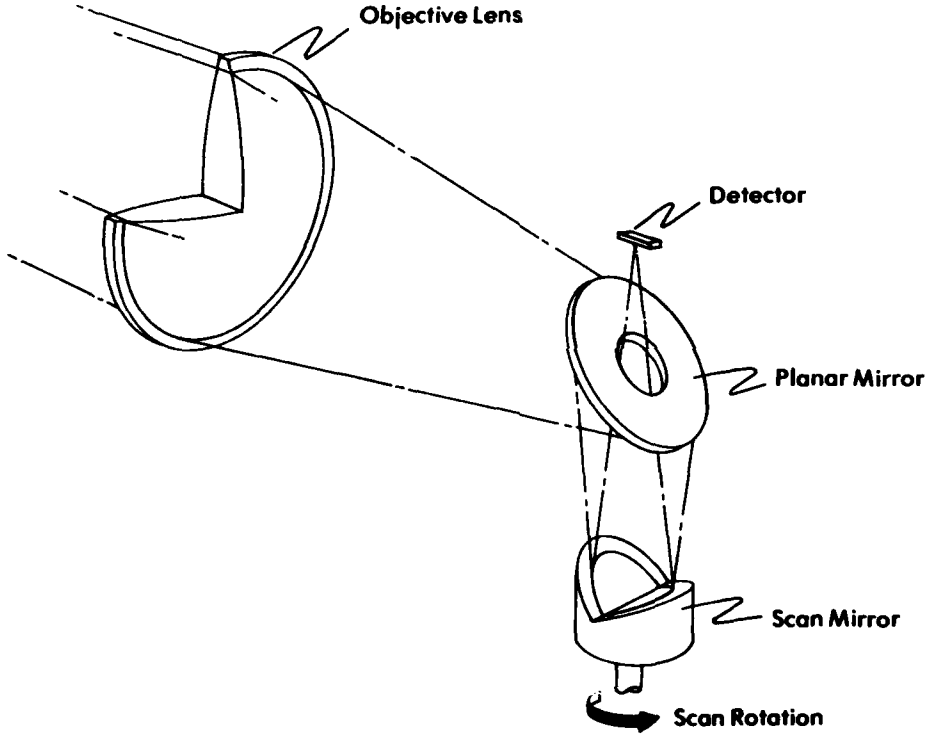

FIGURE 1-49. V-MIRROR SCANNING SYSTEM

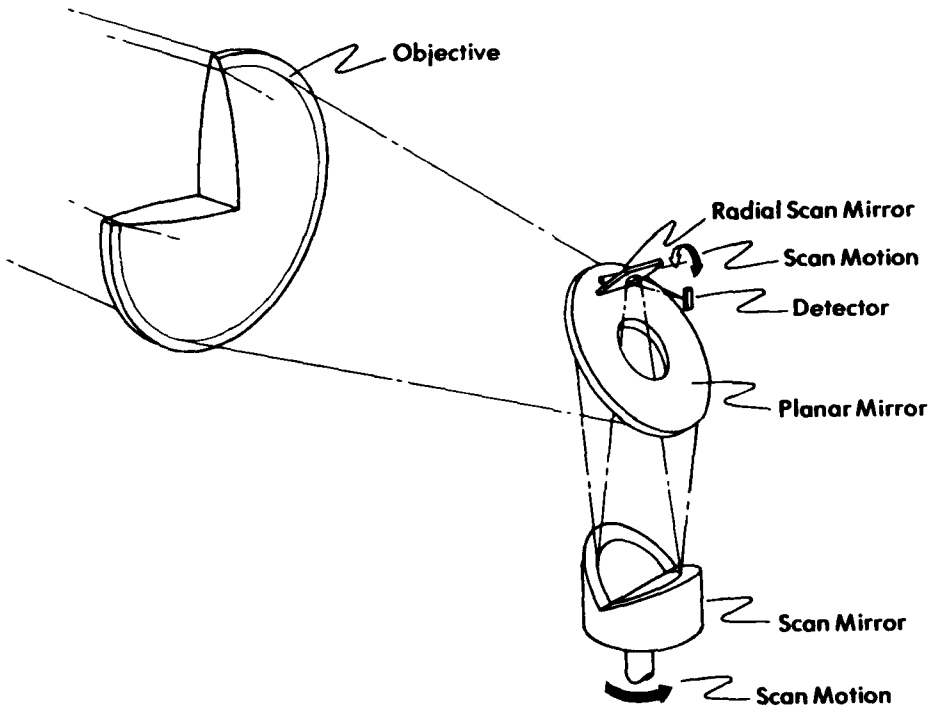

FIGURE 1-50. SPIRAL SCANNER (V-MIRROR SCANNER WITH A RADIAL SCAN MIRROR)

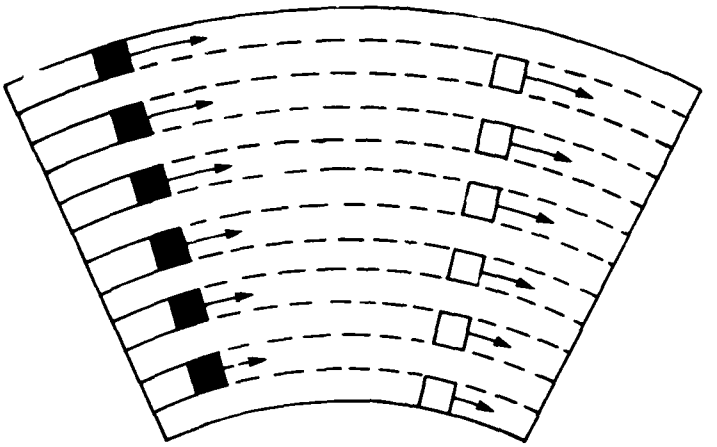

FIGURE 1-51. SECTOR SCAN WITH 2:1 INTERLACE

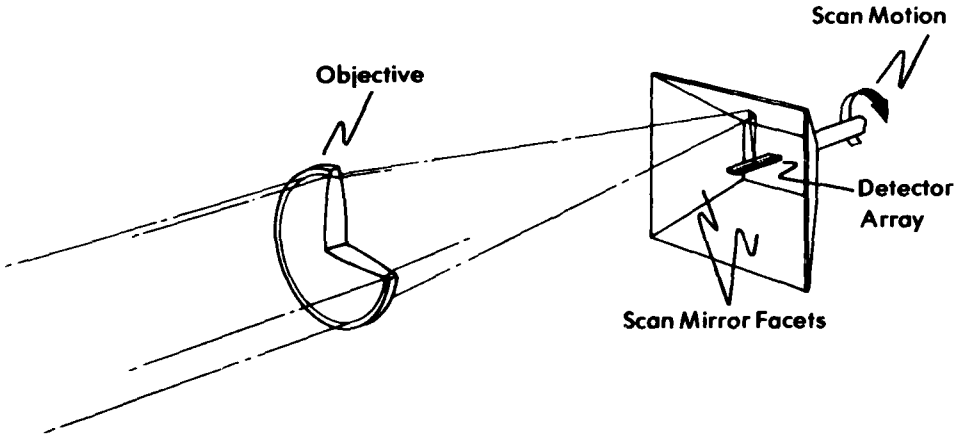

FIGURE 1-52. "SOUPBOWL" SCANNER

signal. In addition, the detectors discussed here are "point" detectors -- or detectors that are sensitive to an area much smaller than the image from an optical system to be scanned. This is not meant to imply the detector itself must be small. The detector's sensitive area can be limited by the use of a field stop as is often the case for photomultiplier tubes.

Much has been written about the field of infrared and visible detectors. The works of Limperis and Mudar (Reference [1-2], Chapter 11), Hudson (Reference [1-3], Chapter 7), and Yariv (Reference [1-14]), give a well-rounded introduction to a wide variety of detection mechanisms, detector types and performance evaluation. Since the emphasis here is on the use of detectors for optical-mechanically scanning imaging systems, the detectors are presented in view of their relative advantages and disadvantages in an imaging system.

1.5.1 Detector Performance

In the past, there was little agreement in the terminology used to describe the performance of a detector. The terms "sensitivity" and "response" were often used ambiguously or interchanged. At times, the word sensitivity meant the signal from the detector, sometimes the signal-to-noise ratio. The terminology which has since become widely used was devised by R. Clark Jones (Reference [1-15]) in a deliberate break from the previous terms.

[1-14] A. Yariv, Introduction to Optical Electronics, Holt, Rinehart, and Winston, New York, NY, 1976.

[1-15] R. C. Jones, D. Goodwin, and G. Pullan, "Standard Procedure for Testing Infrared Detectors and for Describing Their Performance," AD 257 597, Office of the Director of Defense Research and Engineering, Washington, DC, 12 September 1960.

One basic description of detector performance is its gain or responsivity -- that is, the detector output per unit input. The output quantity of interest in this discussion is open-circuit voltage. Since most detectors are ac-coupled to associated preamplifiers because of bias circuitry, the output signal voltage is an alternating quantity. Most detector measurements are made with a constant source of radiation and a chopper to alternate the input flux -- thus producing an alternating output. A useful measure of the output is the rms amplitude of the fundamental component of the signal. For consistency, the incident power on the detector is also measured in terms of the rms value of its fundamental component. Since the output of the detector is dependent on the total incident power, the responsivity is

$$R = \frac{V_s}{\Phi_i} = \frac{V_s}{E_i A_d} \qquad (V\ W^{-1}) \qquad (1\text{-}49)$$

where V_s = the rms value of the fundamental component of the signal voltage

Φ = the rms value of the fundamental component of the incident power on the detector

E = the rms value of the fundamental component of the irradiance on the detector

A_d = the sensitive area of the detector

Although responsivity is a useful parameter for the gain of a detector, it gives no indication of the minimum amount of radiant power that can be detected. As the signal radiation diminishes, the amount of noise in the output from the detector ultimately obscures the signal. The signal can be considered completely obscured when the output signal is equal to the output noise. Of interest in this situation is the amount of incident power on the detector when the signal-to-noise ratio is one. This is known as the noise equivalent power (NEP). Since it is

impractical to determine NEP when the signal is equal to the noise, measurements are typically made at a high signal level and the NEP is calculated from

$$V_n = R(NEP) \tag{1-50}$$

or

$$NEP = \frac{E_i A_d V_n}{V_s} \quad (W) \tag{1-51}$$

where V_n is the rms value of the noise voltage at the output of the detector. This assumes that the responsivity of the detector is a linear function, which is almost always valid for signal-to-noise ratios of less than 1,000. When a group of detectors is considered for use in a sensor, it is usually the minimum change in radiant power that can be detected that is of interest because this determines the contrast presented to the observer in the context of an imaging scanner. Thus the "best" detector is considered to be the one with the lowest NEP.

Many people dislike a situation where an improvement in quality results in a lower figure of merit. To remedy this situation, Jones [1-15] suggested that the reciprocal of the NEP be used. This figure of merit, which he called detectivity, is defined as

$$D = \frac{1}{NEP} \quad \left(W^{-1}\right) \tag{1-52}$$

In general, detectivity varies as a function of: (1) the wavelength of the incident radiation; (2) the temperature of the detector; (3) the bias applied to the detector; (4) the frequency of the alternating input radiation; (5) the area of the detector; and (6) the amount of noise accepted by the sensor electronics bandwidth. The relations between detectivity and incident radiation wavelength or detector temperature are dependent on detector type, material, and specific construction, and are thus deferred to discussions of detector types. It is customary to select the value of bias so as to maximize detectivity or to specify the bias

used. The response of a detector to alternating input radiation can be characterized by its time constant, usually specified as the time that the detector output takes to reach 63% of its final value after a sudden change in input power. For many detectors, the response to chopped input radiation can be characterized by

$$R(f_c) = \frac{R_o}{\left(1 + 4\pi^2 f_c^2 \tau^2\right)^{1/2}} \tag{1-53}$$

where $R(f_c)$ = the responsivity at the chopping frequency f_c

τ = the detector time constant

R_o = the dc (or very low frequency) response

Based on the empirically obtained result that detectivity usually varies inversely with the square-root of the detector area and the electrical bandwidth of the circuit used to measure noise voltage, Jones introduced the quantity D* to normalize detectivity with respect to detector area, A_d, and noise bandwidth, Δf:

$$D^* = D\left(A_d \Delta f\right)^{1/2} = \frac{\left(A_d \Delta f\right)^{1/2}}{NEP} \qquad \left(\text{cm Hz}^{1/2}\ \text{W}^{-1}\right) \tag{1-54}$$

The significance of D* is that it is the signal-to-noise ratio for a detector when 1 W of power is incident on a detector having 1 cm^2 of sensitive area and whose noise is measured with a circuit having an equivalent noise bandwidth of 1 Hz. Thus D* is particularly convenient for comparing detectors of the same type, but which have different areas and are used in circuits having different bandwidths.

Up to this point, little has been said about the radiant source used to measure detector parameters. If a blackbody is used as the source, it is customary to write the D* followed by three numbers in parentheses. The D* $(T, f_c, \Delta f)$ indicate that value of D* with a blackbody temperature, T, a chopping frequency, f_c, and a circuit noise bandwidth of Δf. (The

specification of Δf is redundant as this is taken into account by the definition of D*.) Since the response of most detectors varies with wavelength, it is also of interest to measure D* at specific wavelengths. This measurement can be specified by indicating the wavelength at which the measurement was taken, i.e., $D^*(\lambda, f_c, \Delta f)$. When the wavelength is that at which maximum detectivity occurs, it is indicated as $D^*_{\lambda p}(\lambda_p, f_c, \Delta f)$.

1.5.2 Detector Types

There are a wide variety of detector types, each with different spectral and electrical characteristics. A given detector may be useful in some applications but have inadequate performance in others. Thus it is of interest to explore some distinctions between detectors.

Detectors useful to the type of systems discussed here can be grouped into two classes that differ by the physical mechanism involved. Thermal detectors are detectors in which a temperature change in the material causes a change in its electrical properties. Detectors which operate by a quantum mechanical interaction between incident photons and electrons in the detector material are called photon or quantum detectors.

Thermal detectors typically do not require cooling and theoretically respond equally at all wavelengths. In practice, the spectral response of these detectors is determined by the blackening material used to coat the temperature sensitive element. Additionally, thermal detectors typically have time constants of a few milliseconds or longer. This limits their use to low scan rate imaging systems.

Because of the direct interaction between incident photons and electrons in photon detectors, the response times of these detectors are very short. Additionally, most photon detectors have a detectivity that is one or two orders of magnitude greater than that of thermal detectors. Because of the above reasons, photon detectors have found almost universal application to optical-mechanical imaging systems. As thermal detectors

have limited use in scanning systems today, they will not be discussed here. The detectivity values for a number of commercially available detectors are shown in Figure 1-53.

Photoelectric Detectors

If the incident photons onto a detector material transfer their energies to electrons, then the electrons may have sufficient energy to escape from the surface of the material. This is called the photoelectric or photoemissive effect. To use this phenomenon for electronic detection of radiation, one uses a photoemissive cathode and a plate electrode to collect emitted electrons. In practice, intervening grids called dynodes are used to cause secondary emission of electrons to amplify the electron stream received from the cathode. This can be performed in an evacuated tube known as a photomultipler tube (PMT).

The potential barrier at the surface will retain the electron unless it has sufficient energy to penetrate the barrier. The energy required to penetrate the barrier is a characteristic of the material and is called the work function, ψ. The kinetic energy of the electron as it leaves the surface of the material is the difference between the energy gained from the photon and the energy used to overcome the work function:

$$E = \frac{MV^2}{2} = \frac{hc}{\lambda} - \psi \qquad (1\text{-}55)$$

where M is the mass of the electron and V is its velocity.

Since the electrons in metals are already free of the lattice structure of the material, metals have relatively low work functions. The lowest work functions are found among the alkali metals. Cesium has a work function of 1.9 eV and has a cutoff wavelength of 0.65 μm. The cutoff wavelength is the maximum wavelength where emission will take place; i.e.,

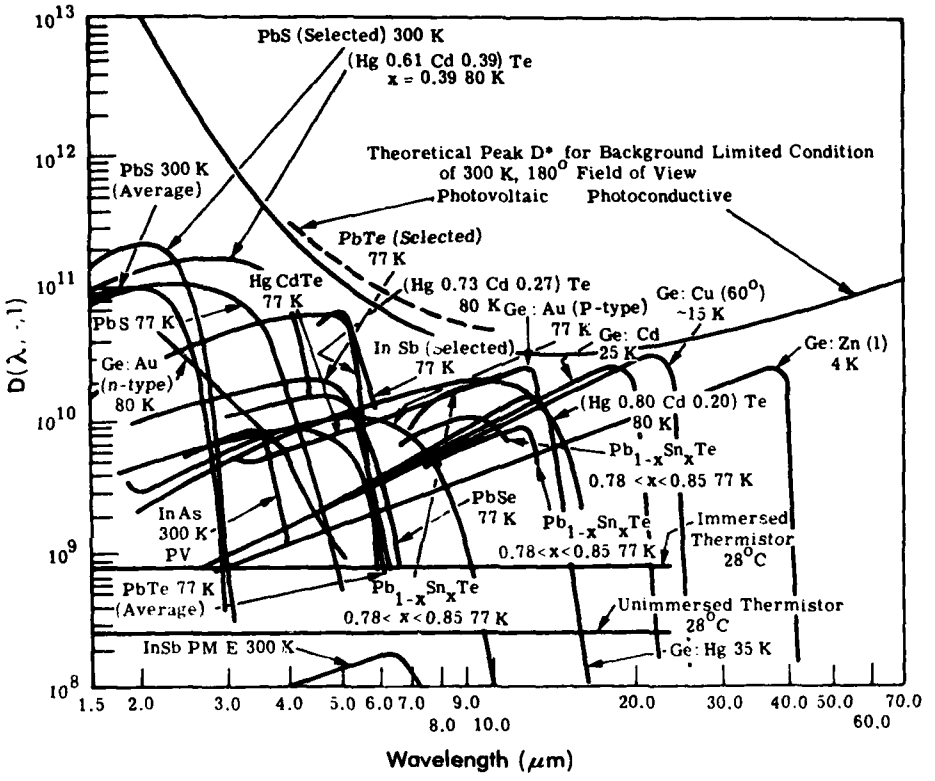

FIGURE 1-53. SPECTRAL D* FOR A NUMBER OF COMMERCIALLY AVAILABLE DETECTORS (Reference [1-2], p. 11-87)

$$\lambda_c = \frac{hc}{\psi} = \frac{1.245}{\psi} \qquad (1\text{-}56)$$

where λ_c is the cutoff wavelength in μm. Lower work functions can be obtained by compounding more than one material. For example, a value of 0.98 eV is obtained with a silver-oxygen-cesium surface, commonly called an S-I surface.

Photoconductive (PC) Detectors

When atoms are brought within close proximity as they are in solids, the discrete energy levels of the individual atoms broaden into nearly continuous bands of energy levels. Although these bands are actually made up of a number of discrete energy levels, they can be thought of as continuous because the differences between the various levels contained in the band are very small ($\sim 10^{-14}$ eV). The highest energy band which is completely filled with charge carriers when the material is at absolute zero temperature is called the valence band. When an electron acquires thermal energy or absorbs the energy from an incident photon, then the electron may have sufficient energy to reach the conduction band as in Figure 1-54. In metals, the conduction and valence bands are extremely close; thus conduction occurs even at extremely low temperatures. Insulators, on the other hand, have an extremely large band gap between the conduction and valence band. A semiconductor lies somewhere in between and the forbidden energy band is relatively narrow. Even at room temperature, some of the valence electrons in a semiconductor can acquire sufficient energy to jump across the forbidden band to the conduction band. This allows conduction of current through the material. The vacancy of an electron site in the valence band is called an electron hole and is capable of conduction in the direction opposite to the electron current.

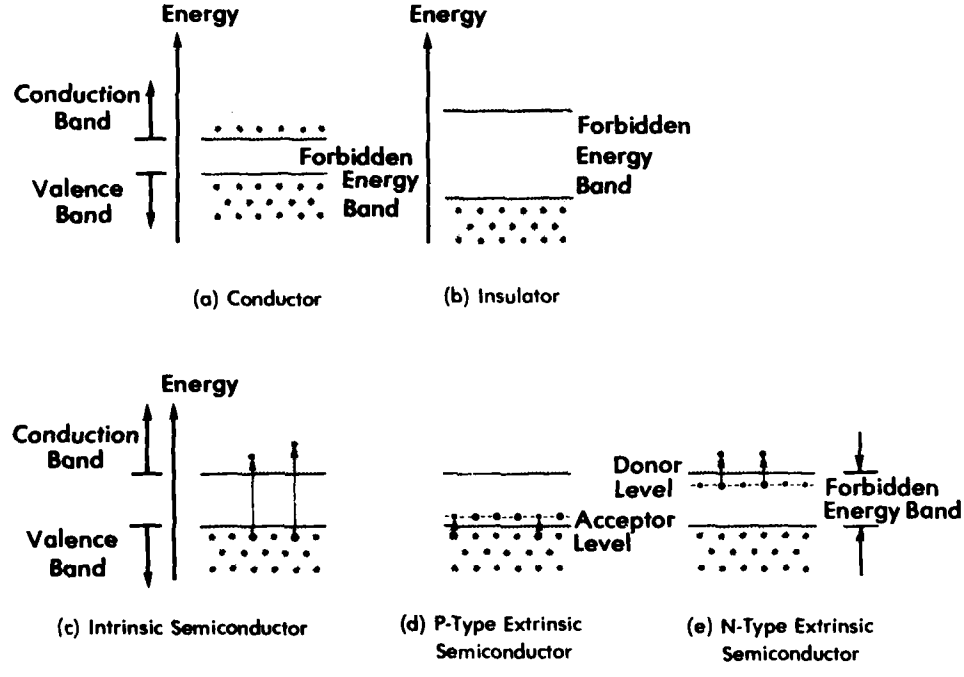

FIGURE 1-54. ENERGY BANDS IN ROOM TEMPERATURE SOLIDS

Electrons can acquire sufficient energy to cross the band gap from incident photons. A photon has sufficient energy to raise an electron to conduction when

$$\frac{hc}{\lambda} > E_g \tag{1-57}$$

where E_g is the energy required for the electron to cross the band gap. The cutoff wavelength, or wavelength of a photon with just sufficient energy to cross the gap is

$$\lambda_c = \frac{hc}{E_g} \tag{1-58}$$

In a semiconductor sample when there are no incident photons, the conductance can be written as

$$\sigma = q(N\ \mu_n + P\ \mu_p) \tag{1-59}$$

where σ = the conductance

N and P = the numbers of thermally generated conduction electrons and valence holes respectively

μ_n and μ_p = the free electron and hole mobilities

When photons impinge on the material, excess free carriers are generated. The change in conduction is

$$\Delta\sigma = q(\delta N\ \mu_n + \delta P\ \mu_p) \tag{1-60}$$

where δN and δP are the numbers of excess electrons and holes generated by incident photons. To use this effect to detect radiation, a bias is applied to the detector material. The conductivity change due to incident photons then, in turn, results in a change in current through the detector which can be measured.

Photovoltaic (PV) Detectors

A photovoltaic (PV) detector consists of a p-n junction formed in a semiconductor. The junction is formed at the boundary between a semiconductor layer having an excess of electrons (n-type) and another

layer having an excess number of holes (p-type). Incident photons produce electron hole pairs as in a photoconductor. These pairs are, in turn, separated by the electric field at the junction so as to generate a photovoltage. These devices are also referred to as photodiodes.

A typical voltage-current characteristic curve of a photovoltaic detector is shown in Figure 1-55. When there is no incident radiation, the I-V characteristics are identical with those of a circuit diode. In a photovoltaic detector, however, incident radiation causes the curve to shift downward as illustrated. The change in radiation may be detected by observing open-circuit voltage or short-circuit current, or by back-biasing the diode and observing the changes in current. In general, photovoltaic detectors exhibit the highest detectivity when operated in the short-circuit mode. An additional advantage of doing this is that the changes in current are relatively linear with changes in incident radiation.

1.6 SIGNAL PROCESSING AND DISPLAYS

The term signal processor here means the electronic circuit or circuits needed to receive the low level signals from the detector and produce a signal useable to the desired display device in order to construct a visible image of the scanned scene. One of the main elements of the signal processor is the amplifier circuitry needed to increase the signal level to a useful magnitude. Since space around the detector is usually limited, the amplifier chain is often divided. A small preamplifier circuit, located near the detector, amplifies the signal sufficiently to allow it to pass through the transmission lines to the main body of the amplifier.

A major consideration in amplifier design is the dynamic range that may be encountered in scene radiance. Signal levels may well change in some instances by 120 dB. In order to compensate, automatic gain control

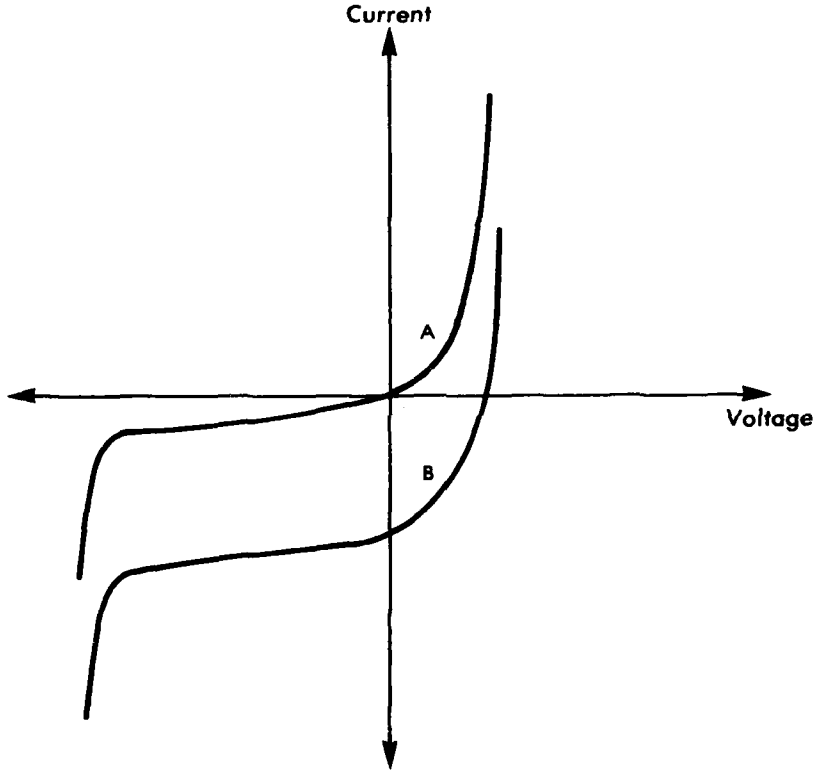

FIGURE 1-55. THE CURRENT - VOLTAGE CHARACTERISTICS OF A PHOTOVOLTAIC DETECTOR. Curve A is the characteristic with no incident radiation; curve B is with incident radiation.

(AGC) can be used on the amplifier or preamplifier. If an extremely large dynamic range is needed, a logrithmic amplifier can be used.

Another major consideration in signal design is bandwidth. Assuming that the noise accepted by the signal processor increases linearly with bandwidth, there is an optimum bandwidth for a given dwell time where the signal-to-noise ratio is maximized. This is given by

$$(BW)\ \tau_d \simeq \frac{1}{2} \tag{1-61}$$

where (BW) is the 3 dB bandwidth of the signal processor. (See Reference [1-3], p.408.) In practice, the constant of proportionality in the above equation may fall between 0.25 and 0.75. The variation in shape and amplitude of a rectangular pulse for a group of constants is shown in Figure 1-56.

The bandwidth discussed above is the voltage bandwidth. This is different from the noise equivalent bandwidth used in the calculation of detector parameters. The noise equivalent noise bandwidth is defined as

$$\Delta f = \frac{1}{G(f_o)} \int_0^\infty G(f)df \tag{1-62}$$

where G(f) is the power gain at an electrical frequency, f, and $G(f_o)$ is the maximum value of the power gain. In effect, Δf replaces the actual power bandpass of a circuit with an equivalent rectangular bandpass that is equal to the power bandpass of that circuit. The difference between Δf and (BW) depends on the shape of the response curve of the particular circuit used. If a perfectly rectangular bandpass were realizable, the voltage bandwidth and power bandwidth would be identical.

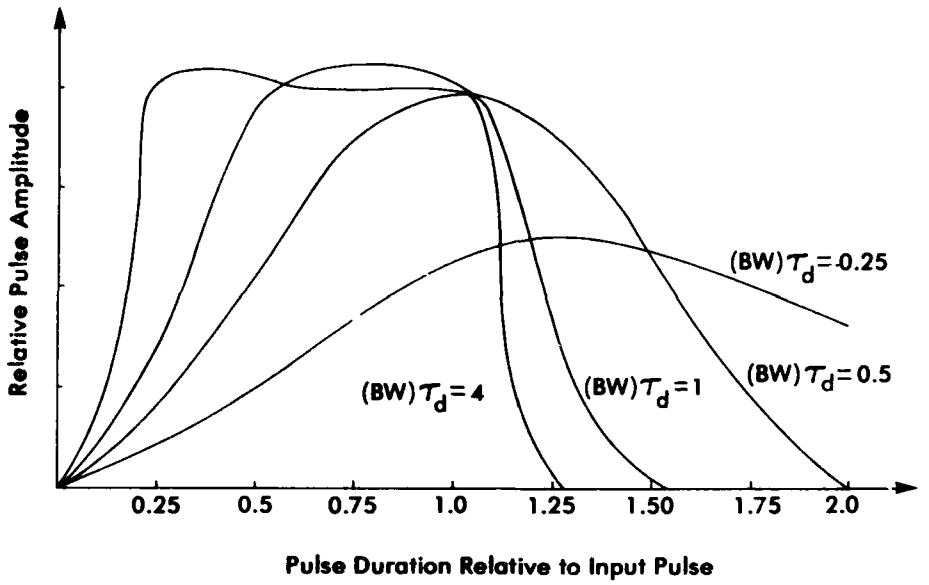

FIGURE 1-56. VARIATION IN THE SHAPE AND AMPLITUDE OF A RECTANGULAR PULSE AFTER PASSING THROUGH A NETWORK (Reference [1-16], Section 8.6)

AD-A120 044 INFRARED INFORMATION AND ANALYSIS CENTER ANN ARBOR MI F/G 17/5
IRIA STATE-OF-THE-ART REPORT: OPTICAL-MECHANICAL, ACTIVE/PASSIV--ETC(U)
MAY 82 C T DUE, L M PETERSON N00014-77-C-0125
UNCLASSIFIED IRIA-153200-2-T-1 SBI-AD-E750 695 NL

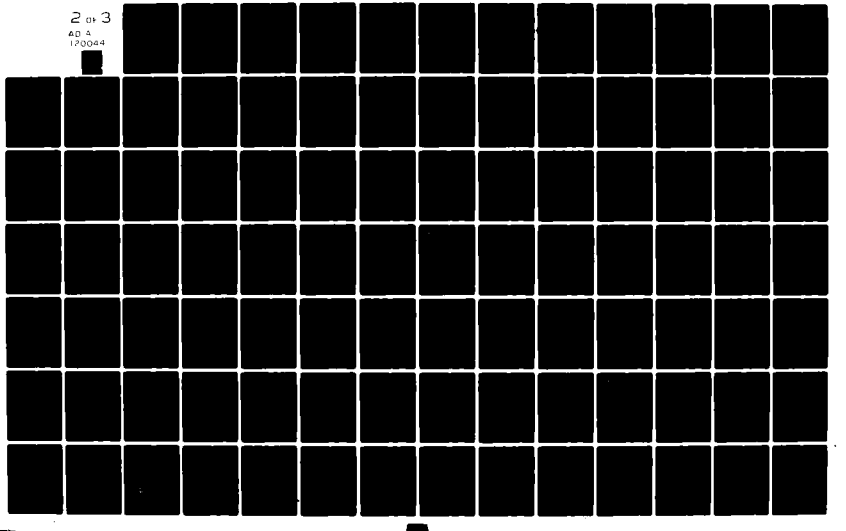

To describe the effectiveness of a signal processor in separating signals from noise, Genoud (Reference [1-17], p.1581)introduced the pulse visibility factor where

$$\nu = \left(\frac{V_p}{V_{ss}}\right) \frac{1}{\tau_d \Delta f} \tag{1-63}$$

The term V_p is the peak amplitude of a pulse at the output of the processor and V_{ss} is the peak amplitude that would be observed if the pulse suffered no loss in the processor. If one assumes optimum processing (i.e., $V_p/V_{SS} \approx 1$) in a linear signal processor and that the shape of the amplifier passband is such that the noise equivalent bandwidth, Δf, is equal to the 3 dB bandwidth, then from Equation (1-61) $\tau_d \Delta f \approx 0.5$ and $\nu \approx 2$. In practice, however, the value of ν is likely to be in the range of 0.25 to 0.75.

1.6.1 Synchronization

In many imaging systems, it is necessary to synchronize the mechanical scanning with electronic or mechanical scanning used in the display system in order to construct a meaningful image. In some display systems (e.g., TV monitors) the information rates that are acceptable to the display are standardized. In this case, mechanical scanning can be synchronized with a master clock circuit whose rate is compatible with the display.

Synchronization is accomplished by use of electronic or optical scan mechanism position encoding devices. The signal obtained from these devices are electronically compared with the master clock to obtain an error signal. This signal is, in turn, used to correct the scan rate and

---

[1-17] R. H. Genoud, "Infrared Search-System Range Performance," Proceedings of the IRE, Institute of Radio Engineers, New York, NY, Volume 47, No.9, 1959.

scan mechanism position through the use of servo-loop control of scan motor rotation rate.

1.6.2 dc Restoration and Calibration

The electronic circuits in most scanners are ac-coupled for ease of signal handling and separation of bias circuits. As a result, the average signal level at the output of the processor is zero, and the instantaneous signal is known only with respect to this average. In a scanning imaging system, this average signal level is dependent on the average level of radiation received by the scanner. This means the average brightness at the display is dependent on the average amount of radiation received.

This problem can be readily corrected by use of dc restoration. This is often accomplished by first placing a radiative source in a position such that it is viewed by the scanner during dead-time portions of the scan cycle. Then, since the position of the source in the video signal is known, the output of the signal processor can be clamped to a preset level while the scanner views the radiation source.

While dc restoration can make the tone of objects observed in the display independent of the average values of the neighboring pixels, the gray scale of the tone is not quantitative unless the system response is constant and known. If the response of the system is linear, then the response of the system can be calibrated by use of a second radiative source. Since the output of many systems are nonlinear, it is often desirable to use two or more calibration sources to specify completely the instantaneous response.

1.7 NOISE SOURCES

There are many potential sources of noise in an optical-mechanical scanner. The noise generated by each of these sources contributes to the

total noise presented to the observer via the image display device. Since it is the noise which ultimately obscures low signal level variations, it is of interest to examine some of these potential noise sources.

The total noise at the display can consist of noise components originating within the detector, electronic assemblies and display devices, as well as those generated externally (e.g., power supply hum). It is assumed here that the noise contributions from each source excepting the detector can be eliminated by proper design and that the noise output of the detector alone determines the limit to system performance. In addition, it is assumed here that the noise output of the detector does not contain noise components due to improper detector design, defects, or microphonics.

The noise in the detector output is due to random variations in carrier motion in the detector, or to fluctuations in the arrival rate of photons incident on the detector. The carrier-associated noise of a detector is controllable to some degree. However, even if one were able to eliminate successfully electron or hole noise, the system would still be limited by the photon noise.

Since the noise voltages due to these fluctuations are random, one must use statistical methods to characterize them. A useful characterization is to find the mean-square value of the voltage fluctuations over a time interval much greater than the time taken by the fluctuations. This can be stated

$$\overline{v^2} = \frac{1}{T}\int_0^T \left(v - V_{avg}\right)^2 dt \qquad (1\text{-}64)$$

where v = the noise voltage at time t
T = the time duration over which the average is taken
V_{avg} = the average noise voltage during the time period T
v^2 = the mean square voltage. Its square-root is the root mean square (rms) noise voltage.

If the noise voltages are generated by independent sources, the mean-square noise voltage in the detector output can be found by summing the mean-square noise voltage from each noise source:

$$\overline{v^2}_{total} = \overline{v^2}_{source\ 1} + \overline{v^2}_{source\ 2} + \overline{v^2}_{source\ 3} + \cdots \qquad (1\text{-}65)$$

1.7.1 Carrier Noise

Charge carriers in a solid are in constant motion, even at thermal and electrical equilibrium. The thermal motion of an electron may be visualized as random scattering from the atoms in the material. Since the movement is random, there is no net drift of a group of electrons in the material over large periods of time. At any given instant in time, however, the motion of electrons may result in a net current resulting in noise current. Since the mean-square velocity of electrons is proportional to absolute temperature, the noise current generated by this electron motion is also proportional to absolute temperature. This is Johnson or thermal noise.

Experimentally it has been shown (See Reference [1-3], p.306.) that a resistor has a mean-square voltage of

$$\overline{v_J^2} = 4\ k\ T\ R\ \Delta f \qquad (1\text{-}66)$$

where R = the resistance
T = the temperature of the resistor
Δf = the noise equivalent bandwidth

A derivation based on quantum mechanics (See Reference [1-18].) shows that the noise voltage frequency spectrum is

$$\overline{v_J^2}(f) = 4\ R\ \Delta f\ \frac{hf}{e^{hf/kT}-1} \qquad (1\text{-}67)$$

where f is frequency. If hf/kT is small compared with unity, the exponential can be replaced by 1 + hf/kT and Equation (1-67) reduces to Equation (1-66).

Electrons in solids obey Fermi-Dirac statistics. The Fermi-Dirac distribution function gives the distribution of electrons over a range of allowed energy levels at thermal equilibrium. This can be stated

$$f(E) = \frac{1}{1 + e^{(E-E_F)/kT}} \qquad (1\text{-}68)$$

where f(E) is the probability that an electron will occupy energy state E at absolute temperature T, and E_F is the Fermi level, the energy level that has a 50% probability of being occupied by an electron.

In the case of a semiconductor, the average number of electrons in the conduction band is proportional to the Fermi-Dirac distribution function evaluated at the edge of the conduction band. Additionally, the number of holes in the valence band are proportional to Fermi-Dirac function evaluated at the edge of the valence band. The sum of the number of electrons and holes gives the total number of charge carriers free to conduct. Obviously, these carriers recombine frequently. More carriers are, in turn, generated to compensate for the recombination and maintain the Fermi-Dirac distribution. The average time taken by a carrier to recombine is called the carrier lifetime.

[1-18] P. W. Kruse, L. D. McGlauchlin, and R. B. McQuistan, Elements of Infrared Technology, John Wiley and Sons, New York, NY, 1962.

The random generation and recombination of charge carriers causes instantaneous noise currents. This is generation-recombination (G-R) noise. The G-R noise voltage spectrum can be given by

$$v^2(f) = R^2 I^2 \left[\frac{2\tau \Delta f}{\bar{N}\left(1 + 4\pi^2 f^2 \tau^2\right)} \right] \tag{1-69}$$

where $\bar{N}$ = the total number of free carriers with lifetime τ

R = the resistance of the sample

I = the dc current flowing through the sample

Another form of electron associated noise is shot noise. This term was originally associated with the random rate of arrival of electrons on the plate of a vacuum tube. It has since come to be associated as well with the randomness of free electrons and holes passing p-n junctions in semiconductors.

The passage of charge carriers across the junction results in discrete current pulses which appear as a random noise current in the output. The mean-square noise can be given by

$$v_s = R(2\ q\ I\ \Delta f) \tag{1-70}$$

where q is the charge of an electron.

Yet another current-associated noise is 1/f noise. This is also known as modulation or current noise. The physical mechanism causing this form of noise is not completely understood. In general, the mean-square noise voltage can be characterized empirically by

$$v_{1/f}^2 \propto \frac{c\ I^a}{f^b} \tag{1-71}$$

where a, b and c are characteristic of a particular device.

1.7.2 Photon Noise

The fluctuation in the rate that photons arrive at the detector surface results in a random noise voltage in the detector. Photons obey Bose-Einstein statistics. The mean-square fluctuations in the number of photons arriving at a surface over a small wavelength interval, $\Delta\lambda$, is given by

$$\overline{\left(\Delta\Phi_{q,\lambda}(\lambda)\Delta\lambda\right)^2} = \Phi_{q,\lambda}(\lambda)\Delta\lambda\left[1 + \gamma\left(e^{hc/k\lambda T} - 1\right)^{-1}\right] \qquad (1\text{-}72)$$

where $\Phi_{q,\lambda}(\lambda)\Delta\lambda$ is the total photon flux per unit wavelength, including signal radiation and radiation from the detector's surroundings, and γ is the coherence factor between the photons arriving at the surface.

A generalized diagram of the noise voltage spectrum of a photoconductive detector is illustrated in Figure 1-57. Since a photoconductive detector does not have a p-n junction, shot noise is not present. The 1/f noise varies inversely with frequency and becomes appreciable only at low frequencies. By using amplifier pass bands above these frequencies, 1/f noise is diminished and noise due to generation and recombination of charge carriers dominates. In the absence of signal photons, this noise is due to thermal generation. By cooling the detector, one can minimize the number of thermally generated carriers. As can be seen from Equation (1-66), Johnson noise is also reduced by cooling.

Under these conditions, the noise is dominated by that which is due to the random arrival rate of photons. In passive sensors, the contribution to the noise from background photons (i.e., all non-signal photons) is dominant over the noise contribution from signal photons. When a system is limited by noise associated with background photons, it is referred to as a background limited system. Photon detectors in which the limiting

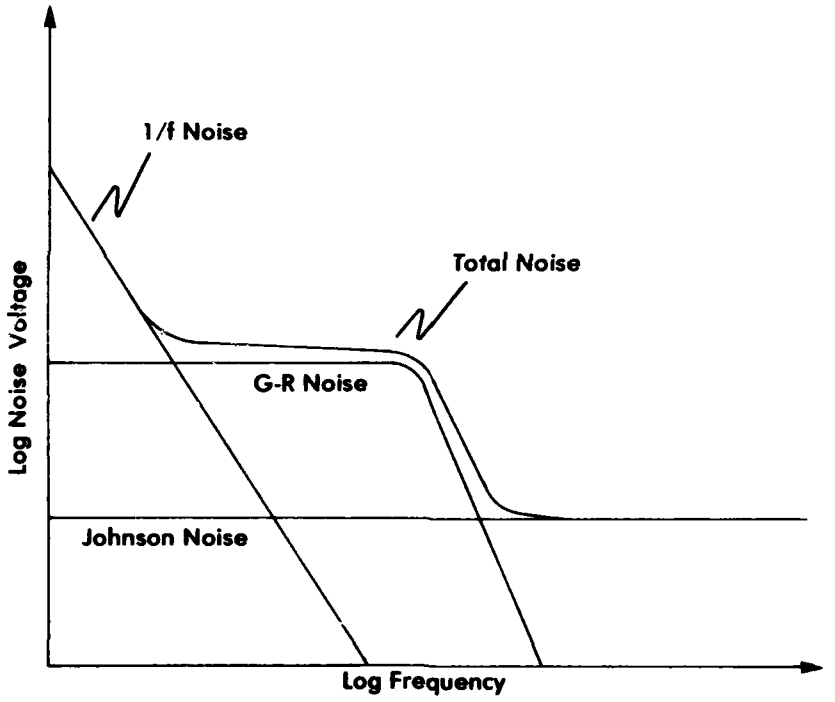

FIGURE 1-57. DETECTOR NOISE FREQUENCY SPECTRUM

noise is from background photons, are referred to as background-limited photodetectors (BLIP).

Since background noise imposes the ultimate limit of detection of low signal variation levels, it is of interest to compare the D* of an actual detector with the D* of a BLIP-limited (ideal) detector. The background-limited D* of a photoconductive detector is given by

$$D_\lambda(\lambda)_{BLIP} = \frac{\lambda}{2hc}\left(\frac{\eta}{M_{q,b}}\right)^{1/2} \quad \left(\text{cm Hz}^{1/2}\ \text{W}^{-1}\ \mu\text{m}^{-1}\right) \tag{1-73}$$

where η is the quantum efficiency of the detector and $M_{q,b}$ is the background photon flux density. The charge carriers generated in a photodiode are swept across the junction before they recombine. Because of this, photodiodes have generation noise only, and roughly 1/2 the mean-square noise of a photoconductor. Thus the D^*_{BLIP} of a photodiode is the $\sqrt{2}$ times that of a photoconductor:

$$D_\lambda(\lambda)_{BLIP} = \frac{\lambda}{\sqrt{2}\ hc}\left(\frac{\eta}{M_{q,b}}\right)^{1/2} \tag{1-74}$$

The term $M_{q,b}$ includes all of the background photons from zero wavelength up to the cutoff wavelength of the photodetector. If one assumes that the background is a blackbody emitting at some average temperature, then $M_{q,b}$ can be calculated by use of blackbody functions. The total radiant photon exitance from a hemispheric background from zero wavelength to the specified wavelength can be found from Figure 1-58. An ideal photodetector would have a quantum efficiency, η, of one. Typical values, however, range from 0.1 to 0.6. Figure 1-59 shows the D^*_{BLIP} for an ideal background-limited detector for a number of background temperatures.

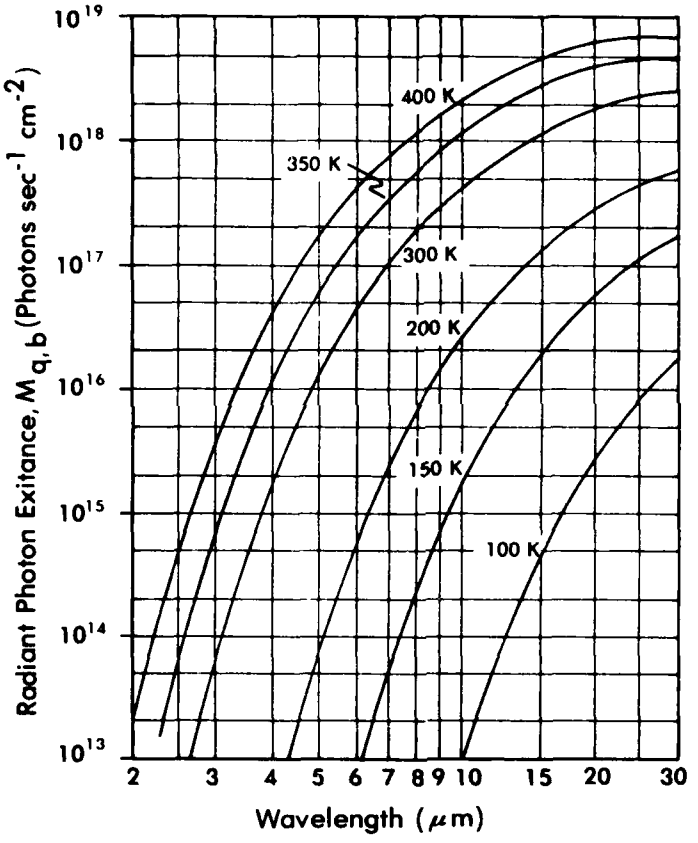

FIGURE 1-58. TOTAL PHOTON EXITANCE FROM A HEMISPHERIC BACKGROUND (Reference [1-3], p. 350)

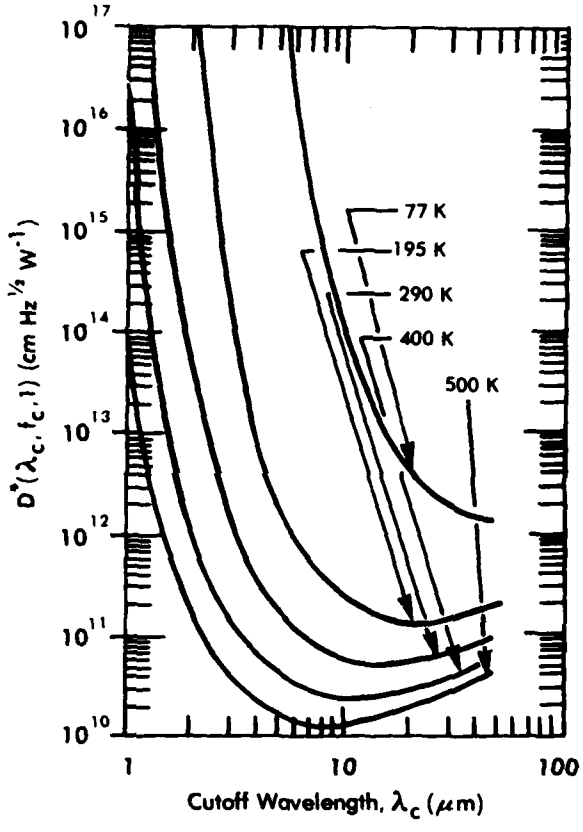

FIGURE 1-59. PHOTON NOISE LIMITED D*, AT CUTOFF WAVELENGTH, FOR VARIOUS BACKGROUND TEMPERATURES
(Reference [1-18] , p. 360)

1.8 PERFORMANCE CHARACTERISTICS

There are many characteristics to be considered when evaluating the performance of a system. For instance, a near-infrared imager which is thermally sensitive to objects with elevated temperatures would not be suitable for room temperature scenes. In addition, size, weight, and power consumption affect the performance of a system in a particular application, particularly in aircraft and spacecraft where space, power, and weight capacity are limited. Here we treat only a small portion of the parameters used to characterize an imaging system since a complete treatment is beyond the scope of this report. Excellent treatments of many of these parameters are given by Lloyd (Reference [1-19]) and Ratches (References [1-20 - 1-22]).

The type of performance considered here is how well an imaging system transfers the radiance distribution of objects of interest in the scene to the display. In addition to this, some performance models also include the transfer function of the eye to provide a measure of how well the observer is able to use the final display image.

In general, the transfer of spatial modulation of radiation through an imaging system is dependent on:

[1-19] J. M. Lloyd, Thermal Imaging Systems, Plenum Press, New York, NY, 1975.

[1-20] J. A. Ratches, "Static Performance Model for Thermal Imaging Systems," Optical Engineering, Society of Photographic Instrumentation Engineers, Palos Verde Estates, CA, Volume 15, No.6, November/December 1976.

[1-21] J. A. Ratches, W. R. Lawson, L. P. Obert, R. J. Bergman, T. W. Cassidy, and J. M. Swenson, "Night Vision Laboratory Static Performance Model for Thermal Viewing Systems," US Army Electronics Command Report 7043, AD A011 212, Night Vision Laboratory, Ft. Belvoir, NJ, April 1975.

[1-22] J. A. Ratches, "Comparison of NVL and Four Contractor Models for Minimum Resolvable Temperature," US Army Electronics Command Report 7050, Night Vision Laboratory, Ft. Belvoir, NJ, April 1976.

1. The spatial frequency of the modulation.
2. The position of the spatial modulation in the FOV.
3. The level of masking noise generated by the system.
4. The orientation of the spatial frequency.

The oldest and most widely used performance characteristics are based on scene modulation that produces a signal-to-noise ratio of one. More complete specifications of system performance may be obtained by specifying the noise equivalent scene modulation as a function of the above four parameters.

1.8.1 One-Number Characteristics

One-number performance characteristics are based on the change in irradiance at the aperture of the system as the IFOV scans the scene that produces a change in signal level equal to the noise generated by the system. The signal-to-noise ratio in the output of the detector is

$$\frac{V_s}{V_n} = \frac{1}{\sqrt{A_d \Delta f}} \int_0^\infty \Phi_{d,\lambda}(\lambda) D^*(\lambda) d\lambda \qquad (1\text{-}75)$$

where $\Phi_{d,\lambda}(\lambda)$ = the spectral power incident on the detector with spectral detectivity $D^*(\lambda)$

A_d = detector area

Δf = the equivalent noise bandwidth of the signal processor and display

Losses of signal within the processor and display can be accounted for by introducing the term V_p/V_{ss} as defined in Section 1.6:

$$\frac{V_s}{V_n} = \frac{V_p}{V_{ss}\sqrt{A_d \Delta f}} \int_0^\infty \Phi_{d,\lambda}(\lambda) D^*(\lambda) d\lambda \qquad (1\text{-}76)$$

The instantaneous power incident on the detector is a function of the radiance, L, available at the aperture of the sensor. If the solid angle of the IFOV is ω, then

$$\Phi_{d,\lambda} = \omega A_o \tau_o(\lambda) L_\lambda(\lambda) \tag{1-77}$$

where $\tau_o(\lambda)$ is the transmittance of the optical system with aperture area A_o. Combining Equations (1-76) and (1-77) one gets

$$\frac{V_s}{V_n} = \frac{V_p \omega A_o}{V_{ss}\sqrt{A_d \Delta f}} \int_0^\infty \tau_o(\lambda) D^*(\lambda) L_\lambda(\lambda) d\lambda \tag{1-78}$$

Since most imaging systems are ac-coupled and thus the concern is the modulation of radiance, the interest here is the change in signal, δV_s, corresponding to a change in radiance, δL, i.e.,

$$\frac{\delta V_s}{V_n} = \frac{V_p \omega A_o}{V_{ss}\sqrt{A_d \Delta f}} \int_0^\infty \tau_o(\lambda) D^*(\lambda) \delta L_\lambda(\lambda) d\lambda \tag{1-79}$$

The noise equivalent radiance difference (NEΔL) can be found by setting V_s/V_n equal to one and solving for the NEΔL value of δL. This can be simplified by assuming an average transmittance for the optical system and an average $D^*(\lambda)$ over the spectral region of the system:

$$\frac{V_s}{V_n} = 1 = \frac{V_p \omega A_d}{V_{ss}\sqrt{A_d \Delta f}} \tau_o D^*(NE\Delta L) \tag{1-80}$$

or

$$NE\Delta L = \frac{V_{ss}\sqrt{A_d \Delta f}}{V_p \omega A_o \tau_o D^*} \tag{1-81}$$

Making use of Genoud's visibility factor as defined by Equation (1-63), Equation (1-81) becomes

$$NE\Delta L = \frac{\sqrt{A_d \tau_d}}{v\omega A_o \tau_o D^*} \qquad (1\text{-}82)$$

where v is the visibility factor and τ_d is the detector dwell time.

This is a convenient measure of the limiting contrast in radiance that can be detected by a sensor. Another such measure is the noise equivalent irradiance (NEΔE) -- the irradiance at the aperture of the sensor that will produce a signal-to-noise ratio of one. This can be found from

$$NE\Delta E = \omega(NE\Delta L) \qquad (1\text{-}83)$$

where NEΔL is the noise equivalent radiance. One convenience in using these measures is that the result is independent of atmospheric transmission. It is, however, more informative to find the minimum change in a scene characteristic that can be observed such as a change in temperature, emissivity or reflectance. Recall from Sections 1.1 and 1.2 that the change in radiance due to a unit change in temperature, emissivity, or reflectance is of the form $\partial L/\partial X$ where X may be reflectance, temperature or emissivity.

The noise equivalent temperature difference (NEΔT) is defined as the equivalent blackbody temperature difference that will produce a system signal-to-noise ratio of one. This can be found by dividing NEΔL by the first partial derivative of the spectral radiance of the scene with respect to temperature as transmitted by the atmosphere (if one assumes $\varepsilon = 1$, $\Delta\varepsilon = 0$, and the IFOV is filled as in Section 1.2). If one assumes a spectrally averaged transmittance over the path to the sensor, τ_a, then

$$NE\Delta T = \frac{NE\Delta L}{\tau_a \left(\frac{\partial L}{\partial T}\right)\Big|_{T_{avg}}} \quad (^oC) \qquad (1\text{-}84)$$

Note that because $\partial L/\partial T$ is dependent on the average scene temperature, T_{avg}, the NEΔT is also dependent on T_{avg}. From the same reasoning, a noise equivalent emissivity difference (NEΔε) and noise equivalent reflectance difference (NEΔρ) can be defined:

$$NE\Delta\varepsilon = \frac{NE\Delta L}{\tau_a \left(\frac{\partial L}{\partial \varepsilon}\right)\Big|_{T_{avg}}} \tag{1-85}$$

$$NE\Delta\rho = \frac{NE\Delta L}{\tau_a \left(\frac{\partial L}{\partial \rho}\right)\Big|_{E_i}} \tag{1-86}$$

Note here that the $NE\Delta\varepsilon$ is also dependent on average scene temperature, and that the $NE\Delta\rho$ is dependent on the irradiance incident on the surface being imaged, E_i.

There is an obvious impossibility in distinguishing between signal and noise when signal levels approach the noise level in a system. In addition to this, these equations hold only for low spatial frequencies in the scene because of optical and electronic MTFs.

$NE\Delta T$ is often used to evaluate the performance of 3 to 5 and 8 to 12 μm imaging systems. Before 8 to 12 μm systems were developed, $NE\Delta T$ was used to evaluate (relatively) the performance of 3 to 5 μm systems. These systems were often used to detect the presence of objects with elevated temperatures, such as campfires. Here, $NE\Delta T$ provided a good measure in that 3 to 5 μm imaging systems were much more sensitive to the elevated temperatures than they were to changes in the emissivity in the scene. With the advent of 8 to 12 μm imaging systems, $NE\Delta T$ was extended to those systems as a measure of performance. In this spectral region, however, imaging systems are much more sensitive to room temperature objects. Along with this, sensitivity to emissivity changes are much greater. Because of this, $NE\Delta T$ is less accurate in describing the performance of these systems.

1.8.2 Minimum Resolvable Temperature Difference (MRTD)

The minimum resolvable temperature difference is defined as the minimum temperature difference above 300 K required by the observer

viewing the display of a thermal imaging system to resolve a vertical four bar pattern having bars with a 7:1 aspect ratio. (See Reference [1-20], p.527.) MRTD increases as a function of the spatial frequency of the bar target and has a limiting asymptote at the reciprocal of the angular IFOV of the scanner.

This provides a more complete description of the performance of the sensor in that it takes into account the spatial frequency of the radiation distribution in the scene. It also accounts for the inability to distinguish signal from noise when the signal level approaches the noise level in a system. An equation for MRTD as a function of spatial frequency has been derived by Ratches (Reference [1-20]) based on the experimental result that there is a threshold signal-to-noise ratio required in order for the observer to resolve the bar. Note that there is no attempt here to account for the effect of emissivity changes.

As previously mentioned, the above parameters are only a small portion of the parameters used to characterize the performance of an imaging system. For a more complete discussion of these and other parameters, consult the work of Lloyd (Reference [1-19]) and Ratches (References [1-20 - 1-22]).

REFERENCES

Volume I, Section 1

[1-1] R. G. Reeves, A. Anson and D. Landen, Manual of Remote Sensing, American Society of Photogrammetry, Falls Church, VA, Volume I, 1975.

[1-2] W. L. Wolfe and G. J. Zissis, The Infrared Handbook, Office of Naval Research, Arlington, VA, 1978. Available from Order Department, Environmental Research Institute of Michigan, Ann Arbor, MI.

[1-3] R. D. Hudson, Jr., Infrared Systems Engineering, John Wiley and Sons, New York, NY, 1969.

[1-4] J. A. Sanderson, "Emission, Transmission, and Detection of the Infrared," A. S. Locke (ed.), Guidance, Princeton, NJ, 1955.

[1-5] F. E. Nicodemus, J. C. Richmond, J. J. Hsia, I. W. Ginsberg and T. Limperis, "Geometrical Considerations and Nomenclature for Reflectance," NBS Monograph 160, National Bureau of Standards, Washington, DC, October 1977.

[1-6] D. M. Gates, "Spectral Distribution of Solar Radiation at the Earth's Surface," Science, American Association for the Advancement of Science, Washington, DC, Volume 151, 1966.

[1-7] H. W. Yates and J. H. Taylor, "Infrared Transmission of the Atmosphere," NRL Report 5453, U.S. Naval Research Laboratory, Washington, DC, 1960. Data are as presented by Santa Barbara Research Center Staff, "The SBRC Brochure," Santa Barbara Research Center, Goleta, CA 1979.

[1-8] Daedalus Staff, "Daedalus Scanner Applications Worldwide 1980," Daedalus Enterprises, Inc., Ann Arbor, MI 1980.

[1-9] W. J. Smith, Modern Optical Engineering: The Design of Optical Systems, McGraw-Hill, New York, NY, 1966.

[1-10] "Unique Optical Company," Unique Optical Company, Farmingdale, NY, December 1975.

[1-11] F. A. Jenkins and H. E. White, Fundamentals of Optics, McGraw-Hill, New York, NY, 3rd edition, 1957.

[1-12] R. R. Shannon and J. C. Wyant, Applied Optics and Optical Engineering, Academic Press, New York, NY, Vol. VIII, 1980.

[1-13] J. W. Goodman, Introduction to Fourier Optics, McGraw-Hill, New York, NY, 1968.

[1-14] A. Yariv, Introduction to Optical Electronics, Holt, Rinehart, and Winston, New York, NY, 2nd edition, 1976.

[1-15] R. C. Jones, D. Goodwin, and G. Pullan, "Standard Procedure for Testing Infrared Detectors and for Describing Their Performance," AD 257 597, Office of the Director of Defense Research and Engineering, Washington, DC, 12 September 1960.

[1-16] J. L. Lawson and G. E. Uhlenbeck, Threshold Signals, McGraw-Hill, New York, NY, 1950.

[1-17] R. H. Genoud, "Infrared Search-System Range Performance," Proceedings of the IRE, Institute of Radio Engineers, New York, NY, Volume 47, No.9, 1959.

[1-18] P. W. Kruse, L. D. McGlauchlin, and R. B. McQuistan, Elements of Infrared Technology, John Wiley and Sons, New York, NY, 1962.

[1-19] J. M. Lloyd, Thermal Imaging Systems, Plenum Press, New York, NY, 1975.

[1-20] J. A. Ratches, "Static Performance Model for Thermal Imaging Systems," Optical Engineering, Society of Photographic and Instrumentation Engineers, Palos Verde Estates, CA, Volume 15, No.6, November/December 1976.

[1-21] J. A. Ratches, W. R. Lawson, L. P. Obert, R. J. Bergman, T. W. Cassidy, and J. M. Swenson, "Night Vision Laboratory Static Performance Model for Thermal Viewing Systems," US Army Electronics Command Report 7043, AD A011 212, Night Vision Laboratory, Ft. Belvoir, NJ, April 1975.

[1-22] J. A. Ratches, "Comparison of NVL and Four Contractor Models for Minimum Resolvable Temperature," US Army Electronics Command Report 7050, Night Vision Laboratory, Ft. Belvoir, NJ, April 1976.

BIBLIOGRAPHY

Volume I, Section 1

Daedalus Staff, "Daedalus Scanner Applications Worldwide 1980," Daedalus Enterprises, Inc., Ann Arbor, MI 1980.

Gates, D. M., "Spectral Distribution of Solar Radiation at the Earth's Surface," Science, American Association for the Advancement of Science, Washington, DC, Volume 151, 1966.

Genoud, R. H., "Infrared Search-System Range Performance," Proceedings of the IRE, Institute of Radio Engineers, New York, NY, Volume 47, No.9, 1959.

Goodman, J. W., Introduction to Fourier Optics, McGraw-Hill, New York, NY, 1968.

Holter, M. R., S. Nudelman, G. H. Suits, W. L. Woble, and G. J. Zissis, Fundamentals of Infrared Technology, The Macmillan Company, New York, NY, 1963.

Hudson, Jr., R. D., Infrared Systems Engineering, John Wiley and Sons, New York, NY, 1969.

Kruse, P. W., L. D. McGlauchlin and R. B. McQuistan, Elements of Infrared Technology, John Wiley and Sons, New York, NY, 1962.

Jenkins, F. A. and H. E. White, Fundamentals of Optics, McGraw-Hill, New York, NY, 3rd edition, 1957.

Jones,, R. C., D. Goodwin and G. Pullan, "Standard Procedure for Testing Infrared Detectors and for Describing Their Performance," AD 257 597, Office of the Director of Defense Research and Engineering, Washington, DC, 12 September 1960.

Lawson, J. L. and G. E. Uhlenbeck, Threshold Signals, McGraw-Hill, New York, NY, 1950.

Lloyd, J. M., Thermal Imaging Systems, Plenum Press, New York, NY, 1975.

Nicodemus, F. E., J. C. Richmond, J. J. Hsia, I. W. Ginsberg and T. Limperis, "Geometrical Considerations and Nomenclature for Reflectance," NBS Monograph 160, National Bureau of Standards, Washington, DC, October 1977.

Ratches, J. A., "Comparison of NVL and Four Contractor Models for Minimum Resolvable Temperature," US Army Electronics Command Report 7050, Night Vision Laboratory, Ft. Belvoir, NJ, April 1976.

Ratches, J. A., "Static Performance Model for Thermal Imaging Systems," Optical Engineering, Society of Photographic and Instrumentation Engineers, Palos Verde Estates, CA, Volume 15, No.6, November/December 1976.

Ratches, J. A., W. R. Lawson, L. P. Obert, R. J. Bergman, T. W. Cassidy, and J. M. Swenson, "Night Vision Laboratory Static Performance Model for Thermal Viewing Systems," US Army Electronics Command Report 7043, AD A011 212, Night Vision Laboratory, Ft. Belvoir, NJ, April 1975.

Reeves, R. G., A. Anson and D. Landen, Manual of Remote Sensing, American Society of Photogrammetry, Falls Church, VA, Volume I, 1975.

Sanderson, J. A., "Emission, Transmission, and Detection of the Infrared," A. S. Locke (ed.), Guidance, Princeton, NJ, 1955.

Shannon, R. R. and J. C. Wyant, Applied Optics and Optical Engineering, Academic Press, New York, NY, Vol. VIII, 1980.

Smith, W. J., Modern Optical Engineering: The Design of Optical Systems, McGraw-Hill, New York, NY, 1966.

Unique Optical Company, "Unique Optical Company," Farmingdale, NY, December 1975.

Wolfe, W. L. and G. J. Zissis, The Infrared Handbook, Office of Naval Research, Arlington, VA, 1978. Available from Order Department, Environmental Research Institute of Michigan, Ann Arbor, MI.

Yariv, A., Introduction to Optical Electronics, Holt, Rinehart, and Winston, New York, NY, 2nd edition, 1976.

Yariv, A., Quantum Electronics, John Wiley and Sons, New York, NY, 1967, 2nd edition.

Yates, H. W. and J. H. Taylor, "Infrared Transmission of the Atmosphere," NRL Report 5453, U.S. Naval Research Laboratory, Washington, DC, 1960. Data are as presented by Santa Barbara Research Center Staff, "The SBRC Brochure," Santa Barbara Research Center, Goleta, CA 1979.

SECTION 2.0
ACTIVE OPTICAL-MECHANICAL IMAGING SENSORS

2.1 BACKGROUND

Prior to the advent of the laser in 1960, almost all remote sensing devices relied upon natural solar illumination or self-emission by objects in the scene. The laser, however, with its high output power, and more importantly its collimated beam, allowed the sensor to carry its own radiation source along with its receiver. Unlike incoherent sources, each watt of laser output power can be directed hundreds of meters to illuminate a small, diffraction-limited spot on a target. For an imaging sensor, this illuminated spot, in conjunction with the instantaneous field-of-view of the receiver, defines the spatial resolution element (reselm) or picture element (pixel) size.

For a laser to be used as a source of radiation for generating imagery from an airborne platform, the laser must:

(1) Possess high average output power to overcome the $1/R^2$ loss after reflection from a diffusely reflecting target.

(2) Be physically realistic in terms of:
   (a) input prime power.
   (b) size.
   (c) weight.
   (d) cooling.

These requirements place the laser in the realm of commercially available continuous wave (cw) or quasi-cw (high-rate repetitively pulsed) lasers with output powers typically of from 0.1 to 100 W. This includes gas, liquid, solid, and semiconductor lasers.

2.1.1 Visible (Overt) Active Sensors

The first cw laser to satisfy these requirements was flown in 1963 by Perkin-Elmer as an airborne laser line scanner (See Reference [2-1], pp.116-119.) using the familiar helium-neon gas laser. However, with only tens of milliwatts of output power available, the He-Ne laser was soon replaced by the more powerful (1 to 10 W) argon-ion laser. The He-Ne laser with visible output at 0.6328 μm, and the argon-ion laser with its strongest output at 0.4880 and 0.5145 μm are gas discharge lasers and are inherently inefficient (< 0.1%). In order to obtain 10 W of laser output, more than 10 kW of prime power must be provided.

The argon-ion laser line scanners made by Perkin-Elmer (See Reference [2-1].), Hughes, and Laser Sciences, Inc., beginning in 1964, were intended for nighttime reconnaissance and target acquisition with a daytime capability and were flown in helicopter gunships in Viet Nam. A major drawback of the sensor was its overt nature. The high intensity visible laser beam was like a beacon in the night, originating from the helicopter.

2.1.2 Infrared (Covert) Active Sensors

Improvements in the efficiency, power output, dependability, and durability of the infrared carbon dioxide laser made it an excellent candidate as a radiation source for a covert line-scan sensor. Its inherent good efficiency made it a source of several tens of watts of laser output with prime power requirements on the order of a kilowatt. Rooftop imaging systems using the CO_2 laser were built and operated by Honeywell and Electro-Optical Systems in 1970. In 1971, the

---

[2-1] W. F. Matthews and R. F. Jung, "Laser Line Scanning Sensors", Optical Engineering, Society of Photographic and Instrumentation Engineers, Palos Verde Estates, CA, Volume 14, No.2, 1975.

Environmental Research Institute of Michigan (ERIM) modified an HRB Singer AN/AAS-6 passive thermal IR sensor to accommodate a CO_2 laser source. This system was flown in an aircraft, and strip-map imagery at 10.6 μm were generated (Reference [2-2]).

Passive imagery in the visible and near IR can provide bistatic reflectance information of the scene using the sun for illumination. Passive imagery in the thermal IR (e.g., 8 to 12 μm) can provide self-emission information of the scene. Active imaging systems, however, can provide monostatic reflectance information of the scene whether the source radiation is in the visible or the far-IR. Wavelength dependent target characteristics are directly related to how specularly reflecting or how diffusely reflecting an object is. This is discussed in Section 2.5.

Although the CO_2 laser imaging sensors used lasers which were efficient and which produced high average power, they possessed significant shortcomings. Since the radiation wavelength was long (10.6 μm), diffraction dictated that the transmitter beam be 20 times as large as an equivalent visible wavelength active sensor which had the same angular resolution. Also, since the wavelength was long, targets were smoother compared to the radiation wavelength such that the targets were more specular in their reflective characteristics rather than diffusely reflecting as found for the visible and near IR. Lastly, and most importantly, detectors at 10 μm had to be cryogenically cooled and were detector noise limited rather than photon-induced shot noise limited. The range capability of these active imaging sensors using conventional detection techniques was therefore limited to less than about 100 m.

[2-2] M. E. Bair, Environmental Research Institute of Michigan, Ann Arbor, MI, Private Communication, 1981.

The Nd:YAG (neodymium:yttrium aluminum garnet) laser, like the CO_2 laser, is an industrially viable laser and saw much commercial development in the late 1960s. Its output wavelength is 1.064 μm and is therefore covert, but it is near enough to the visible spectral region that imagery generated with such a laser has characteristics similar to those observed by the eye, i.e., most objects are diffuse reflectors and only smooth shiny objects have specular lobes. Nearly photon-noise-limited operation and therefore long range imagery can be obtained with red-enhanced photomultiplier tubes and with silicon photo-detectors and silicon avalanche photodiodes (Si:APD).

The Nd:YAG laser is more powerful and efficient than the He-Ne and Ar lasers and is comparable in power output but less efficient than the CO_2 laser. The laser head for a Nd:YAG laser is, however, considerably smaller than that of a comparable power conventional CO_2 laser. Unlike the gas discharge lasers, the ND:YAG laser possesses a YAG crystal host rod about the size of a cigarette and is doped with a small percentage of neodymium, the active ion. Optical pumping from adjacent high intensity lamps provides the excitation for laser action. The multimode output of a single Nd:YAG laser oscillator is about 100 W cw and requires about 10 kW of prime power.

Active airborne imagery using an Nd:YAG laser and an Si:APD detector were first generated by ERIM in 1973. In order to assess the advantages and disadvantages of active and passive sensing in the near- and thermal-IR regions, ERIM modified an HRB Singer Reconofax®X scanner possessing three separate receiver ports. Passive near-IR and thermal-IR imagery, and active Nd:YAG laser and CO_2 laser imagery were generated simultaneously and compared (Reference [2-2]).

Developments in the cw operation of semiconductor lasers have led to compact active line scanners for the near-IR. In 1972, Perkin-Elmer built and flew a 1 W GaAs laser in conjunction with a Kennedy-type line

scanner. (See Reference [2-1].) The laser emits at 0.85 μm with an efficiency of about 15% and requires cooling to 77 K using liquid nitrogen. Since the laser radiation originates from a semiconductor junction, the radiation is highly divergent with a rectangular cross section and requires cylindrical optics to obtain a symmetrical diffraction-limited beam of low divergence. In addition to being compact, the semiconductor laser has an advantage of being conveniently amplitude modulated for use as a three-dimensional (3D) imager. (See Section 2.7.) Since the laser is current pumped, modulation of the drive current results in amplitude modulation of the laser output.

2.1.3 "All-Weather" Active Sensors

All of the active sensors discussed to this point have essentially been clear-weather devices. Since visible and near-IR radiation are heavily attenuated by haze, fog, and smoke, these sensors are severely limited by adverse weather conditions. The CO_2 laser sensor has the ability to penetrate through these scattering media well, but if conventional direct detection is employed, sensor range capability is limited regardless of weather conditions.

Photon-induced shot-noise-limited operation of a CO_2 laser sensor can be accomplished using heterodyne detection techniques. (See Section 2.6.) Orders of magnitude increases in sensitivity or range capability can be realized but at the expense of increased system complexity and increased speckle noise due to the coherent detection process. (See Section 2.5.2.) In addition to increased sensitivity, a heterodyne sensor can also provide Doppler information on targets or moving target indication (MTI). Such a heterodyne sensor is able to penetrate (with only moderate loss) most haze, fog, and smoke which would shut down a visible or near IR sensor. Cloud cover, large particle fogs or certain

smokes, however, severely attenuate even the 10 μm radiation making it less than "all weather".

Since much of the interest in imaging sensors is for military purposes of reconnaissance, surveillance, target acquisition and weapon delivery, the "all-weather" capability is extremely important for a battlefield scene. Much of the recent DoD-funded research and development has been in this arena.

2.1.4 Three-Dimensional (3D) Imaging

In 1973, the Electro-Optical Systems (EOS) Division of the Xerox Corporation, under funding from the Air Force Avionics Laboratory, employed a mode-locked argon-ion laser to impart range information to line scan imagery (Reference [2-3]). The technique of ranging to targets using amplitude modulated laser radiation was not new (e.g., geodometer instruments); however, ranging to a target on a pixel by pixel basis was new and was used to generate the third dimension of a scene. This third dimension is of value in providing depth to a sensor-generated image, i.e., a three-dimensional image, but more importantly it provides additional information for identifying targets in a complex scene. For example, a target whose reflectance or emissive characteristics matched those of its surroundings would blend into a scene. A 3D sensor could be used to extract the target from its background by imparting a gray-scale to the scene based upon its relative range, height, or 3D relief.

In 1974, ERIM, also funded by the Air Force Avionics Laboratory, began developing and implementing this 3D technology using a

---

[2-3] L. D. Green, Electro-Optical Systems Division, Xerox Corporation, Pasadena, CA, Private Communication, 1981.

mode-locked Nd:YAG laser. A 3D sensor was fabricated and flight tested. Subsequent sensors employed amplitude-modulated Nd:YAG and CO_2 lasers (Reference [2-4]).

2.2 LASERS

Laser is an acronym for light amplification by stimulated emission of radiation. This stimulated emission results in the high spectral purity or monochromaticity of the laser output and also its high directionality or collimation. Numerous texts exist describing laser action in gases, liquids, solids, and semiconductors. (See References [2-5 through 2-12].) This section touches only briefly upon the basic features of laser action, principally those features which are of direct importance to active sensors.

2.2.1 Laser Action

In order to achieve dominance of stimulated emission in a material which exhibits (stimulated) absorption, there must be a greater number

[2-4] D. C. Carmer and M. E. Bair, Environmental Research Institute of Michigan, Ann Arbor, MI, Private Communication, 1981.
[2-5] A. Yariv, Optical Electronics, Holt, Rinehart, and Winston, New York, NY, 1976, 2nd edition; also, A. Yariv, Quantum Electronics, John Wiley and Sons, New York, NY, 1975, 2nd edition.
[2-6] A. E. Siegman, An Introduction to Lasers and Masers, McGraw Hill, New York, NY, 1971.
[2-7] B. A. Lengyel, Introduction to Laser Physics, John Wiley and Sons, New York, NY, 1971, 2nd edition.
[2-8] O. Svelto, Principles of Lasers, Plenum Press, New York, NY, 1976.
[2-9] A. L. Bloom, Gas Lasers, John Wiley and Sons, New York, NY, 1968.
[2-10] D. C. Sinclair and W. E. Bell, Gas Laser Technology, Holt, Rinehart, and Winston, New York, NY, 1969.
[2-11] C. G. B. Garrett, Gas Lasers, McGraw-Hill, New York, NY, 1967.
[2-12] J. F. Ready, Industrial Applications of Lasers, Academic Press, New York, NY, 1978.

of atoms or molecules in the upper energy level than in the lower energy level. Since this is contrary to the usual Boltzmann distribution, it is referred to as a population inversion. In order to have a population inversion: (1) pumping to the upper state must be rapid and efficient, (2) the upper state must be long-lived, and (3) the lower state should be short-lived. A typical 4-level laser system is presented in Figure 2-1*. Pumping occurs from ground state (1) to excited state (2). Energy is rapidly and non-radiatively transferred to state (3) which is long-lived (i.e., metastable). If an atom is in state (3), the presence of a photon (wavy single arrow in the figure) whose energy ($E = h\nu$) is equal to the separation in energy of levels (3) and (4) can stimulate the atom to make a transition to lower-energy state (4). The energy lost in this transition appears as a photon of energy $h\nu$. The stimulated photon is identical in energy phase, polarization and direction as the photon which induced the transition. A long column containing a large number ($\sim 10^{17}$) of these atoms (or molecules), if adequately pumped, can result in a significant population in excited state (3). If one of these atoms spontaneously drops to level (4) and emits a photon down the length of the column, it is capable of stimulating the emission of another photon and these two in turn can stimulate the emission of more, etc. By placing mirrors at the ends of this column, as shown in Figure 2-2, the photons are able to oscillate back and forth inducing other excited atoms to radiate their energy. If one of these mirrors is partially transmitting, useful laser output is obtained.

Once started, this process of stimulated emission and oscillation continues (1) until equilibrium is established, such that the pump rate equals the cavity loss rate (loss predominately in the form of laser

*There may be numerous other states present in the energy level diagram of an atom or molecule, but we chose to draw only those participating in the laser process.

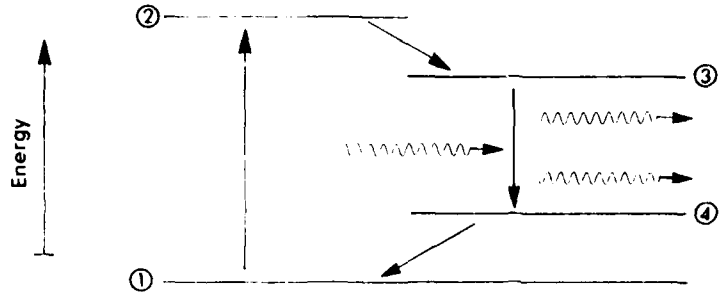

FIGURE 2-1. A 4-LEVEL LASER. Pumping from the ground state (1) to the upper laser level (3) establishes the population inversion. A single resonant photon can stimulate the transition from (3) to (4). Energy of the atom is used to create a new photon.

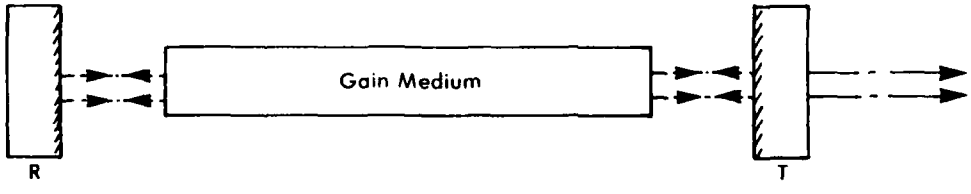

FIGURE 2-2. LASER OSCILLATOR. Mirrors placed around an excited medium provide necessary feedback of stimulated radiation such that oscillation may occur. A highly reflecting mirror, R, and a partially transmitting mirror, T, permit the output of a laser beam.

output), or (2) until the population inversion is depleted due to de-excitation (relaxation) of the upper state and/or build-up in population of the lower state such that laser action is terminated. The former condition in the presence of continuous pumping action results in a cw laser output while the latter results in a pulsed output (possibly repetitively pulsed).

Since the spectral width (in Hz) of the energy levels is equal to the reciprocal of the lifetime, a long-lived or metastable state is very narrow and results in stimulated emission which is spectrally very narrow, i.e., monochromatic. The resonant cavity formed by the mirrors leads to further narrowing making the laser a truly monochromatic radiation source. (See Section 2.2.3.)

2.2.2 Pumping Mechanisms

Input energy to achieve pumping of the excited laser state is of course important, and several mechanisms can be used to achieve this end. They include:

(1) optical pumping.
(2) electrical excitation.
(3) electron beam excitation.
(4) chemical reaction.

Most commercially available cw (or quasi-cw) lasers suitable for active imaging sensors are in the first two categories. Thus, the following discussion ignores the last two as well as pulsed pumping.

Optical pumping with cw lasers is usually achieved with a high intensity discharge lamp whose output characteristics best match the absorption bands of the pump levels for the active laser atom. Tungsten filament lamps initially used to pump the cw Nd:YAG laser have been replaced by high pressure Krypton dc arc lamps. Typically, one or two lamps are oriented parallel to the Nd:YAG laser rod within a

reflecting pump cavity of elliptical cross section as shown in Figure 2-3. Efficient pumping is achieved by placing the lamp(s) and rod at respective foci of the ellipse.

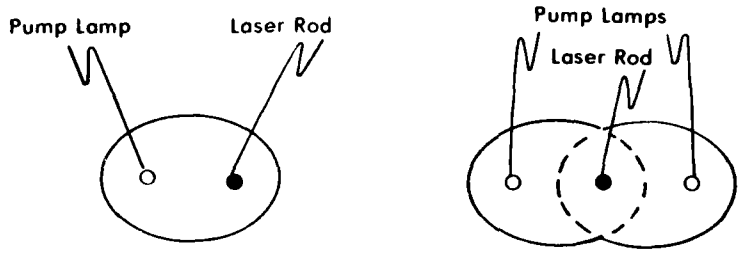

FIGURE 2-3. ELLIPTICAL CAVITIES USED FOR OPTICAL PUMPING.
The pump cavity is viewed in cross section. Radiation emitted in all directions by the linear lamp is reflected by the elliptical mirror to form a line focus at the laser rod to provide optical pumping.

Electrical excitation is utilized for gas lasers in order to pump the laser transition. An arc discharge is used to create a plasma of high velocity electrons and ions. Collisions with the laser molecule can lead to excitation and population inversion or collisions with a buffer gas can result in excitation of the buffer molecule followed by subsequent energy transfer to the laser molecule provided that a close match in energy levels exists. The He-Ne laser, for example, acquires excitation of the helium atoms through collisions and this excitation energy is effectively transferred to the neon atom via a resonant collision. Lasing action can occur between the resulting excited energy level of the neon atom and one of its lower energy levels. Another example is the CO_2 molecular laser. Nitrogen in the gas discharge is excited through collisions and its energy is transferred to the CO_2 molecule's 00^01 vibrational level due to a close match between that level and the first vibrational state of nitrogen. Laser action in the excited CO_2 molecule results from a vibration-rotation

transition and can result in a build-up of the population of the lower laser energy level. Efficient operation is achieved by adding a third gas, helium, to the N_2:CO_2 mixture. The light weight, high velocity helium atom is effective in depopulating the lower energy level thereby improving the performance of the CO_2 laser.

Although chemical lasers, most notably the HF and DF lasers, with outputs around 2.9 and 3.8 μm respectively, have been in use for about a decade and can be obtained commercially with high cw output power, they have not been used as radiation sources for active scanners. This has been partly due to the corrosive nature of the participating gases and the need to exhaust the combustion products, and also due to the failure to establish an advantage for operating in the spectral region around 3 μm, rather than at 1 or 10 μm (the Nd:YAG and CO_2 laser wavelengths).

It is worth mentioning that optical pumping may be achieved using pump lasers rather than pump lamps. Overall efficiency and net laser power output are usually a problem, however. Green lasers (argon-ion or frequency-doubled Nd:YAG) are routinely used to pump organic dye lasers, providing tunable outputs of less than 1 W throughout the visible and near IR. CO_2 lasers are also used to pump far infrared molecular lasers (30 to 300 μm), but here also power output is limited to below 0.1 W thereby limiting their utility as remote sensing radiation sources.

2.2.3 Resonant Cavity

As discussed above, laser action occurs by establishing a population inversion in a medium. By itself, the inverted medium is an amplifier, but to achieve laser action or oscillation, feedback must be provided. Reflecting mirrors, perpendicular to the axis of the medium,

are typically used to establish a resonant cavity similar to a Fabry-Perot etalon, and thereby produce the desired optical feedback.

Longitudinal Modes

Since the circulating electromagnetic wave of the radiation field within a laser cavity interferes with itself, a low loss condition exists when an integer number of half-wavelengths can fit within the cavity. (See Figure 2-4.) The wavelengths which satisfy the resonant condition are called longitudinal or temporal modes. Since L, the optical length*, is generally large (except for semiconductor lasers), and λ is small, the number of waves (or mode number m) which fit in the cavity is large. For a 0.5 m cavity, and a laser wavelength of 1 μm,

$$m \approx \frac{L}{\lambda/2} = 10^6 \qquad (2\text{-}1)$$

An increase or decrease in wavelength of only one part in 10^6 (10^{-6} μm for our example) will result in the laser operating in the next adjacent mode. A convenient means of determining the intermode separation, $\delta\nu$, in Hz is

$$\delta\nu = \frac{\nu_o}{m} = \frac{c}{2L} \qquad (2\text{-}2)$$

where c is the speed of light in vacuum, and ν_o is the frequency of the laser transition.

Since stimulated emission or laser gain occurs only over a narrow spectral region due to the narrowness of the participating energy levels (as discussed above), only a finite number of modes can lase. Figure 2-5 shows a bell-shaped laser gain profile of width, $\Delta\nu$, and a comb array of

*The optical length of the cavity includes the physical length and the refractive index.

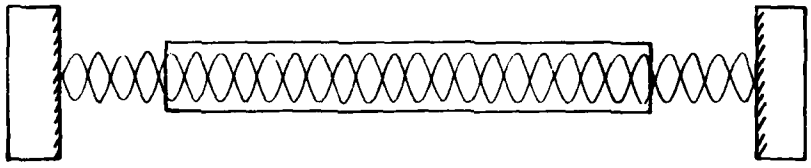

FIGURE 2-4. LASER RESONANT CAVITY. Only those wavelengths (modes) which precisely fit between the reflecting mirrors will oscillate with low loss, i.e., produce a standing wave resonance.

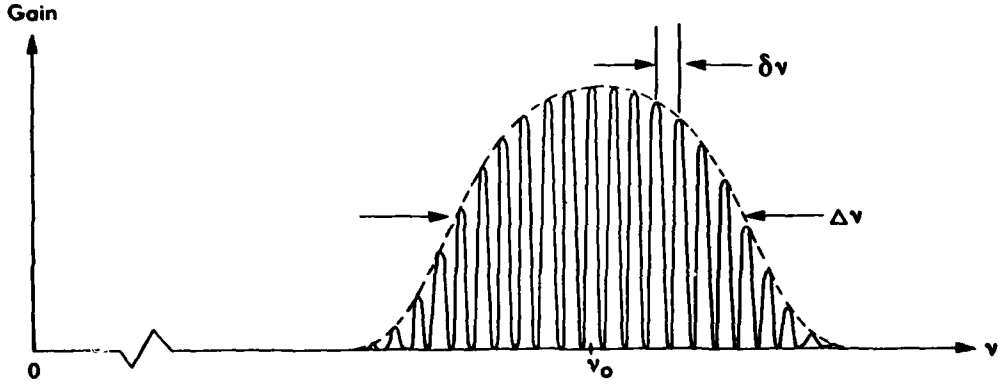

FIGURE 2-5. LASER GAIN PROFILE AND RESONANT MODES

allowed cavity resonances or modes. Since $\Delta\nu$ and $\delta\nu$ are several orders of magnitude less than ν_o (Table 2-1), the laser radiation from a single mode is highly (though not perfectly) monochromatic.

TABLE 2-1. SPECTRAL CHARACTERISTICS OF SELECTED LASERS

	λ_o (μm)	ν_o (Hz)	$\Delta\nu$ (Hz)	$\delta\nu$ (Hz)
GaAs	0.85	3.5×10^{14}	10^{11}	$\sim 10^{11}$
Nd:YAG	1.064	2.82×10^{14}	1.9×10^{11}	10^{8}
CO_2	10.6	0.28×10^{14}	0.50×10^{8}	10^{8}

The array of allowed modes within the laser gain profile would better be likened to an accordion than to a comb. If the laser cavity optical length is changed due to acoustic, thermal or mechanical perturbations which change the physical length or refractive index by only a small amount, the modes will shift position within the gain profile. If the optical length is decreased (increased) by one half wavelength, each mode is shifted to the position of the next higher (lower) mode. These changes in the mode positions are usually of only minor consequence for active sensors which use the laser as a simple radiation source, possibly leading to slight fluctuations in laser output. These excursions in mode position, however, which occur primarily due to slow thermal drift (long term stability) can degrade or destroy the mode-locking process in a mode-locked laser. (See Section 2.7.) Small excursions in mode-position which occur on the time scale of microseconds (short term stability) can reduce the coherence length of the laser and can severely degrade the performance of a heterodyne system. (See Section 2.6.)

Transverse Modes

So far, the discussion has been limited to laser radiation which oscillates along the laser axis to set up a standing wave. If the mirrors and gain medium are wide enough, resonant conditions may also be established for slightly off-axis propagation. These off-axis modes are classified as transverse or spatial modes (See References [2-5 through 2-13].) because they result in spatially varying flux distributions which are transverse to the direction of propagation. The Fresnel number, N, is the parameter used to specify losses for higher order modes and is defined as

$$N = \frac{d^2}{\lambda L} \qquad (2\text{-}3)$$

where d is the limiting transverse dimension. If the lowest order TEM_{oo} mode (with a Gaussian transverse radiation profile) is desired, it is necessary to use a small enough Fresnel number such that higher order modes are suppressed but the TEM_{oo} is not. This may mean using an intracavity aperture to limit d, or lengthening the cavity, or both. Operating multimode may be desirable in order to use more of the active medium such that greater laser output is attained. In this case, large d, short L and therefore a large Fresnel number are desired. As N increases, the number of allowed transverse modes increases also.

High order transverse modes are usually undesirable due to the resulting spatial inhomogeneity of the beam and due to the larger divergence of the beam as a result of their off-axis propagation. Spatial inhomogeneity can result in undesirable fluctuations in the return signal

[2-13] H. Kogelnik and T. Li, "Laser Beams and Resonators," Applied Optics, Optical Society of America, Washington, DC, Volume 5, No.10, 1966, pp.1550-1567; also, R. J. Pressley (ed.), Handbook of Lasers, Chemical Rubber Company, Cleveland, OH, 1971.

for an active scanner. This temporal structure may be of little consequence since it will be high frequency and susceptible to filtering. Large divergence associated with higher order modes may be undesirable if it results in delivery of a wide beam to the target thereby compromising spatial resolution. However, if adequate up-collimation is achieved using beam expander optics, divergence, too, may be of little consequence. The higher power output of a multimode laser beam may indeed be worthwhile.

2.3 PROPAGATION CHARACTERISTICS

The high degree of directionality, or collimation, of laser beams allows one to efficiently deliver radiation energy to a distant point. In a properly designed system, the spread of this beam or its divergence is determined by diffraction effects. As such, the designer of an active system must use the disciplines of physical optics as well as those of geometrical optics.

The spread of a diffraction-limited beam (whether from a laser or non-laser source), is inversely proportional to the diameter of the limiting aperture stop. For example, a point source at infinity or at the focus of a lens results in plane wave propagation as shown in Figure 2-6(a). If these waves encounter a circular aperture of diameter D, the beam will retain its diameter for only a limited distance called the near-field or Fresnel region. (See References [2-14 through 2-16].) Beyond this distance the beam spreads significantly, eventually achieving a constant divergence angle, θ_o^A. This is called the far field or

---

[2-14] F. A. Jenkins and H. E. White, Fundamentals of Optics, McGraw-Hill, New York, NY, 1957, 3rd edition.
[2-15] E. Hecht and A. Zajac, Optics, Addison-Wesley, Reading, MA, 1974.
[2-16] M. Born and E. Wolf, Principles of Optics, Pergamon Press, Elmsford, NY, 1975, 5th edition.

Fraunhofer region. A screen placed at a distance z from the aperture displays the familiar concentric rings of an Airy pattern and has an

$$E(r) = E_o \left[\frac{2J_1\left(\frac{\pi rD}{z}\right)}{\frac{rD}{z}} \right]^2 \qquad (2\text{-}4)$$

where E_o = peak irradiance (W m^{-2}), at the center of the pattern

r = axial radius

J_1 = the first order Bessel function

If the divergence angle, θ_o^A, is defined as the full angle between zero irradiance points, then the diameter of the first dark ring of the pattern is simply $z\,\theta_o^A$. The full angle divergence in the far field is directly proportional to optical wavelength, λ, and inversely proportional to the aperture diameter, D:

$$\theta_o^A = 2.44\,\frac{\lambda}{D} \quad \text{(rad)} \qquad (2\text{-}5)$$

If a physical aperture or stop were not present in Figure 2-6(a), D would represent the lens diameter itself.

Note that in the far field of a plane wave illuminated aperture, the beam behaves as though it originated from a point at the center of the aperture, i.e., the center of curvature of the wavefronts is at the aperture center. Also, if the aperture is not round but rectangular, say

*The International System of Units (SI) is used here where the radiometric quality of irradiance has units of W m^{-2}. Although the SI specifies intensity, I, as W sr^{-1}, one finds intensity I as W m^{-2} in common usage [2-5,2-10,2-14,2-16]. In most cases, W sr^{-1} may be simply divided by z^2 to obtain W m^{-2}.

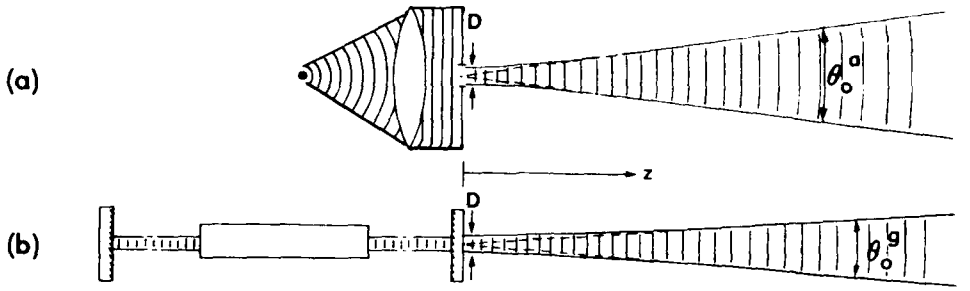

FIGURE 2-6. DIFFRACTION DUE TO (a) A HARD APERTURE AND (b) A GAUSSIAN LASER MODE

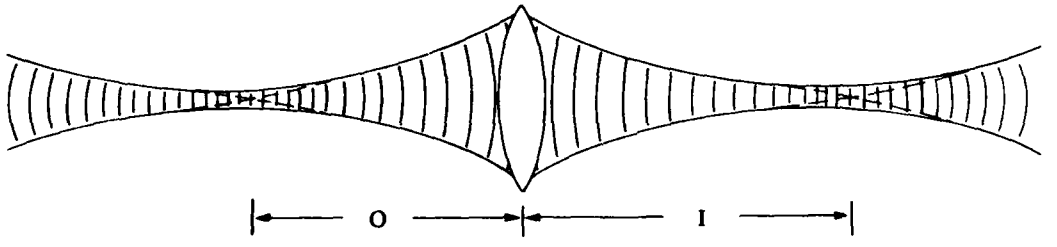

FIGURE 2-7. GAUSSIAN BEAM TRANSFORMATION BY A SIMPLE LENS

short and fat, the vertical divergence will exceed the horizontal divergence to yield a rectangular diffraction pattern which is tall and thin. The divergence of a beam of radiation is critical in delivering as much energy as possible into a small spot at the distant target under free propagation. If one is interested in focussing radiation to as small a point as possible, diffraction again is the limiting process.

A circular beam of radiation of diameter D may be focussed by a lens of focal length f to a spot of diameter S. If the diameter is of uniform irradiance, the irradiance at the focus will exhibit the Airy pattern where S, the diameter of the first dark Airy ring, is

$$S = 2.44 \frac{\lambda}{D} f \tag{2-6}$$

If f/D, the f-number, is on the order of unity, a focal spot approaching the wavelength of the radiation may be achieved. The next section shows that the smallest spot may be delivered to a remote target by first expanding the beam to as large a diameter as possible, then focusing the radiation using a long focal length lens (or lens pair in the form of a telescope) whose focal length is equal to the distance to the target.

2.3.1 Gaussian Beam Propagation

The output of a laser operating in its lowest order transverse mode, or TEM_{oo} mode, is called a Gaussian beam because its radial intensity distribution is Gaussian in shape both in the near field and in the far field:

$$I(r) = I_o e^{-2r^2/w^2} \tag{2-7}$$

where w is the beam radius, r, at the $1/e^2$ (=0.135) intensity point. If the mirrors are much larger than the laser beam, and the beam is otherwise unobstructed, the beam remains collimated in the near field but eventually

diverges at a constant rate when the far field is reached as shown in Figure 2-6(b). More precisely, the Gaussian beam profile is maintained while w increases with z as a hyperbolic function. (See References [2-5,2-6,2-9,and 2-13].)

$$w(z) = w_0 \sqrt{1 + \left(\frac{z}{z_c}\right)^2} \tag{2-8}$$

where w_0 is the beam radius at its narrowest point (i.e., the waist) and z_c is the confocal parameter

$$z_c = \frac{\pi w_0^2}{\lambda} = \frac{\pi w_0^2 n}{\lambda_0} \tag{2-9}$$

In Equation (2-9), n is the index of refraction and λ_0 the vacuum wavelength.

The waist, w_0, defined to be at z = 0, is often but not always found at the output mirror of the laser. It may be found outside the laser or within the laser cavity. As shown in Figure 2-6(b), the waist may be located by projecting the far field divergence back into the near field (dashed line in the figure) and locating the crossing point (i.e., the origin of the hyperbola). The wave fronts at the waist are plane (that is, the radius of curvature, $\tilde{R}$, of the wave fronts is infinite) and their curvature decreases as z increases, reaches a minimum at $z = z_c$ (where $\tilde{R} = 2z_c$), and then increases with z, eventually achieving wave front curvature $\tilde{R}$ equal to z, which is (by definition) the far field. $\tilde{R}$ may be expressed analytically as

$$\tilde{R}(z) = z\left(1 + \frac{z_c^2}{z^2}\right) \tag{2-10}$$

Given the waist location and its radius, w_0, the beam size, w, and radius of curvature, R, of the wave fronts can be determined for any

position of z under conditions of free propagation using Equations (2-8) and (2-10). If obstructions are encountered, complex computations are required using the Fresnel-Kirchoff integral (See References [2-16 and 2-17]. Also, see "Beam Truncation", below.) to determine the modified, non-Gaussian, diffraction pattern. If optical elements such as lenses or mirrors are encountered, the wavefront radius of curvature is modified by the focal length of the elements. Given a point or waist at distance O from a lens of focal length f (Figure 2-7), an image or new waist is located at a distance, I, from the lens with the familiar

$$\frac{1}{f} = \frac{1}{O} + \frac{1}{I} \tag{2-11}$$

If the lens is in the far field of this waist, then $\tilde{R}_1 = O$ before the lens and $R_2 = -I$ after the lens such that

$$\frac{1}{\tilde{R}_2} = \frac{1}{\tilde{R}_1} - \frac{1}{f} \tag{2-12}$$

Even if one is not in the far field, the radius of curvature, $\tilde{R}_2$, is determined by Equation (2-12).

Conversely, if the size of a beam, w, at a particular point along the propagation path and the radius of curvature, $\tilde{R}$, of its wave fronts are known, then the position of the waist and its size can be determined (See References [2-9 and 2-10].) using

$$z = \frac{\tilde{R}}{1 + \left(\lambda R/\pi w^2\right)^2} \tag{2-13}$$

and

$$w_o = \frac{w}{\sqrt{1 + \left(\pi w^2/\lambda \tilde{R}\right)^2}} \tag{2-14}$$

[2-17] J. W. Goodman, Introduction to Fourier Optics, McGraw-Hill, New York, NY, 1968

Near and Far Fields

Just as beam divergence for a uniformly illuminated hard aperture is proportional to the radiation wavelength and inversely proportional to the aperture dimensions, the divergence of a Gaussian beam is similarly determined. (See Figure 2-6.) Since the transverse beam dimension is not uniquely determined as for a hard aperture, an arbitrary dimension based upon amplitude or intensity must be chosen. Conventionally, this is either the $1/e^2$ intensity (equal to the 1/e amplitude) point or the one-half (3 dB) intensity point. The full angle beam divergence of a Gaussian beam, defined by its $1/e^2$ intensity points, is

$$\theta_e^G = \frac{4}{\pi} \frac{\lambda}{(2w_0)} = 1.27 \frac{\lambda}{(2w_0)} \tag{2-15}$$

where $2w_0$ is the beam diameter at its narrowest point, i.e., its waist.

The near field of a Gaussian beam is that region near the waist where the beam spread with z is minimal. The near field is defined by Equation (2-9), the confocal parameter z_c, and is often referred to as the Rayleigh range

$$R_R = z_c = \frac{\pi w_0^2}{\lambda} \tag{2-16}$$

Hypothetical rays originating from a "point" and geometrically diverging at a full angle of $\theta = (4/\pi)(\lambda/2w_0)$ will have a diameter of $2w_0$ at the Rayleigh range. (See the dashed lines in Figure 2-6.) Also, at the Rayleigh range, the Gaussian beam radius has diverged to a value $w = 2\ w_0$. (See Equation (2-8).)

In the near field where $z < R_R$, the beam is well collimated with nearly plane waves and may be treated as a point source near infinity. A lens placed in the near field beam will produce a waist close to the focal position of the lens. (Note that the focal volume, V, is determined by

the new waist radius, w_o', and confocal parameter, z_c, such that $V = 2 w_o'^2 z_c$.) A telescope of magnification M, focussed for infinity and placed in the near field beam, produces a collimated beam which is M times (MX) larger or smaller than the input beam. This is referred to as up-collimation or down-collimation and results in low divergence or high divergence, respectively, according to Equation (2-5). The waist location for a properly adjusted collimating telescope is at its output.

A simple MX Galilean telescope may be used as an up-collimator as shown in Figure 2-8. If the input lens is in the near field and the telescope is focussed for infinity (i.e., the lens separation is $f_2 - f_1$), as in Figure 2-8(a), then the output beam is M times larger ($D_2 = MD_1$) and the beam divergence is decreased by a factor of M ($\theta_2 = \theta_1/M$). It is important to note that the beam will propagate as a Gaussian only if the beam is unobstructed out to several beam radii (i.e., ~3 w). This is often difficult to accommodate in a real system and results in non-Gaussian propagation and increased divergence even if only a small amount of the beam is intercepted by the exit aperture. This is discussed in "Beam Truncation", below.

The far field of a Gaussian beam is that region significantly beyond the Rayleigh range whereby the beam divergence is constant, and the beam may be treated as though it originated from a point source located at the waist position. (The radiation emanating from this point source must have a Gaussian spatial distribution.) Up-collimation of the laser presented in Figure 2-8(b) can be achieved with an MX telescope placed in the far field which is adjusted not for infinity but to behave as a long focal length lens. If the beam waist is located at the focal point of this "compound lens", the output beam will be properly collimated. (This condition is most often encountered with the increasingly popular CO_2 waveguide laser. Since the wavelength is long and the beam size small, the beam divergence is large and it is difficult if not impossible to place the telescope in the near field.) The exact beam size should be

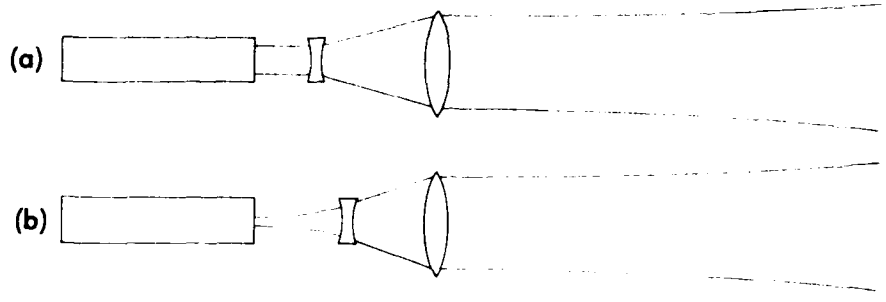

FIGURE 2-8. BEAM EXPANSION (a) IN THE NEAR FIELD OF THE LASER BEAM AND (b) BEYOND THE NEAR FIELD

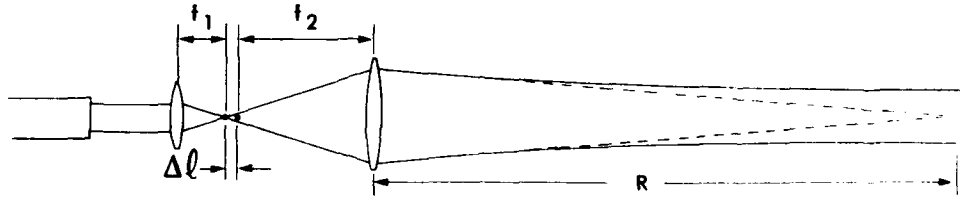

FIGURE 2-9. BEAM EXPANDING TELESCOPE ADJUSTED FOR A MINIMUM SPOT AT RANGE R

determined by calculation or ray trace but a good estimate of the output beam size may be determined by simply multiplying the beam size at the input of the telescope (eyepiece lens) by the magnification of the telescope. If the telescope is properly adjusted, the output beam is collimated with its waist located at the exit optic and the divergence is determined by the beam size there. The telescope used in the far-field laser beam of Figure 2-8(b) requires that the lenses be slightly farther apart to accommodate the diverging input beam.

If the telescope input is located neither in the near nor the far field of the laser beam, the focusing of the telescope must be calculated using Equations (2-8) through (2-14). References [2-5 and 2-13] deal with such calculations thoroughly.

Beam Expansion

As mentioned in the previous section, up-collimating or beam expansion telescopes may be used to increase the Gaussian beam diameter thereby reducing the beam divergence by the ratio of the input to output beam diameter ratio. (If the beam is truncated at its edges, or if the expander contains a central obscuration as do most reflective telescopes, then the beam divergence will be larger than expected. (See "Beam Truncation" below.) A maximally collimated beam is desired if one wishes to deliver the smallest possible spot to a target in the far field. If, however, the target is not in the far field, a condition often found even for long ranges, one does not use a collimated beam but a beam which is focused. Instead of setting the up-collimating telescope for perfect collimation, the telescope is adjusted such that the beam is focused at the target. In effect, the telescope optics are increased slightly in separation to behave like a long focal length positive lens and, since the focus of a lens corresponds to the far field, achieve the smallest possible spot at the target. With the help of Figure 2-9, one may

calculate the increase in separation, $\Delta\ell$, between the optics of a telescope such that the beam is focused at distance R. Using Equation (2-11) applied to the objective lens of focal length f_2, one may determine $\Delta\ell$, where the object distance is $f_2 + \Delta\ell$, such that an image is formed at distance R:

$$\frac{1}{f_2} = \frac{1}{f_2 + \Delta\ell} + \frac{1}{R} \tag{2-17}$$

Rearranging, one gets

$$\frac{\Delta\ell}{f_2(f_s + \Delta\ell)} = \frac{1}{R} \tag{2-18}$$

and, since

$$\Delta\ell \ll f_2 \tag{2-19}$$

$$\Delta\ell = \frac{f_2^2}{R}$$

If f_2 is 20 cm and one wishes to focus at a range of 0.3 km, then $\Delta\ell$ is only 120 μm.

Sample Computation

An example which entails everything discussed above may be valuable. Consider a neodymium laser with an output wavelength of 1.06 μm which has been up-collimated to a Gaussian beam 50 mm in diameter. From Equation (2-15), the $1/e^2$ divergence is

$$\theta_e^G = \frac{4}{\pi} \frac{1.06 \times 10^{-6}\,m}{50 \times 10^{-3}\,m} \tag{2-20}$$

$$= 27\ \mu rad$$

If one is interested in illuminating a target at 0.3 km, one may multiply θ_e^G by that range to get 8 mm. Since this is less than the beam size of 50

mm started with, it is still in the near field. (See the dashed lines in Figure 2-6(b).) To be sure, calculate the Rayleigh range from Equation (2-16) to get R_R = 7.4 km. The value of 0.3 km is well within the Rayleigh range and the target is in the near field of the collimated laser beam.

One can place the target in the far field by focusing the beam using the collimating telescope. If the telescope objective has a 20 cm focal length, then (from Equation (2-19)) by moving it by only 120 μm from its eyepiece, the telescope changes from a focus at infinity to a focus at 0.3 km. The spot size at the target is then f θ_e^G where f is 0.3 km. One can see that the fine tuning on the telescope is critical. Longitudinal motion of the objective lens of less than 1/8 millimeter can result in the spot size at 0.3 km to change from about 50 mm to 8 mm, assuming diffraction-limited optics.

If a CO_2 laser with a wavelength of 10.6 μm were chosen, θ_e^G would have been 270 μrad. Since R_R would be 0.19 km, the 0.3 km target would be neither in the near nor the far field. Focusing by the same 120 μm would result in only a slightly improved spot diameter (80 mm) at 0.3 km. At 1 km range, clearly in the far field, focusing would achieve no improvement, but at 0.1 km focusing could cut the spot diameter by about one-half.

The above examples assume diffraction-limited optics and no truncation of the beam, and the numbers and equations are approximate. If more precision is desired, detailed calculations based upon Equations (2-8) through (2-16) or References [2-5,2-6,and 2-13] are required. A pronounced effect occurs if the Gaussian beam is truncated at the $1/e^2$ diameter as is often encountered. If such is the case, the divergence and spot sizes increase such that the numbers computed above closely correspond to half power values rather than $1/e^2$ values for an untruncated Gaussian. This is discussed below.

Beam Truncation

Throughout this section on Gaussian beam propagation it is assumed that the beam is unobstructed as it propagates such that it maintains a Gaussian radial distribution from the near field, through the optics and all the way out to the far field. In a real optical system, the wings of the beam will be truncated to a greater or lesser degree by the optical mounts or system structure, and will result in diffraction effects which can perturb the spatial irradiance profile of the propagating beam. The most drastic effect occurs if a telescope possessing a central obscuration is used. (See Reference [2-18], pp.2397-2401 and 2762.)

The problem of truncated and obscured beams is generally soluble using the Fresnel-Kirchhoff formulation of Huygen's principle. (See References [2-16 through 2-18].) When a propagating beam encounters an obscuration, the beam may be treated as broken down into infinitesimal areas which are considered as point sources with particular amplitudes and phases compared to other points in the beam. Radiation propagates along different paths from each of these point sources to a particular point in the observation or target plane (Figure 2-10) where the individual (Huygen's) wavelets are superimposed to provide a resultant amplitude and phase. Each and every point in the observation plane (U-V) requires integration over the entire source plane (X-Y). If the source plane is a circular aperture with uniform, plane wave illumination, the observation plane corresponds to an Airy distribution (provided $z > d^2/\lambda$ where d is the diameter of the aperture). Generally, the source plane is not that simple. It may have a more complicated aperture, a nonuniform irradiance distribution, and/or non-plane wave illumination.

[2-18] J. J. Degnan and B. J. Klein, "Optical Antenna Gain 2: Receiving Antennas", Applied Optics, Optical Society of America, Washington, DC, Volume 13, 1974.

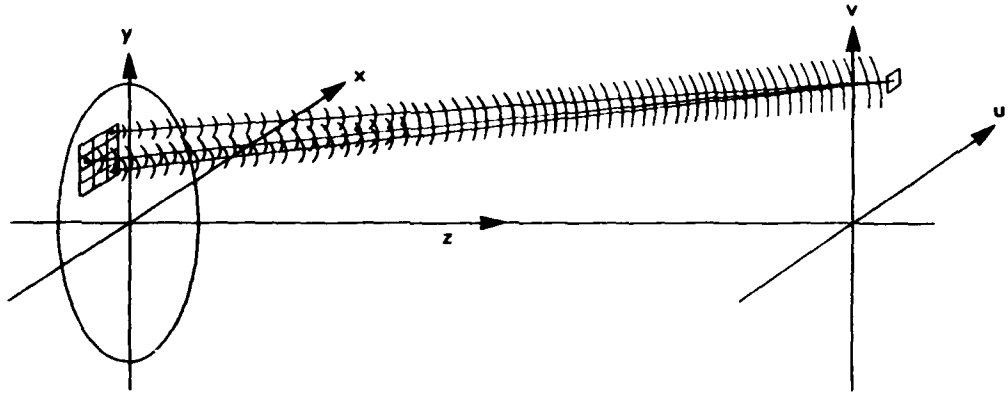

FIGURE 2-10. DIFFRACTION EFFECTS MAY BE TREATED USING THE SUPERPOSITION OF HUYGEN'S WAVELETS

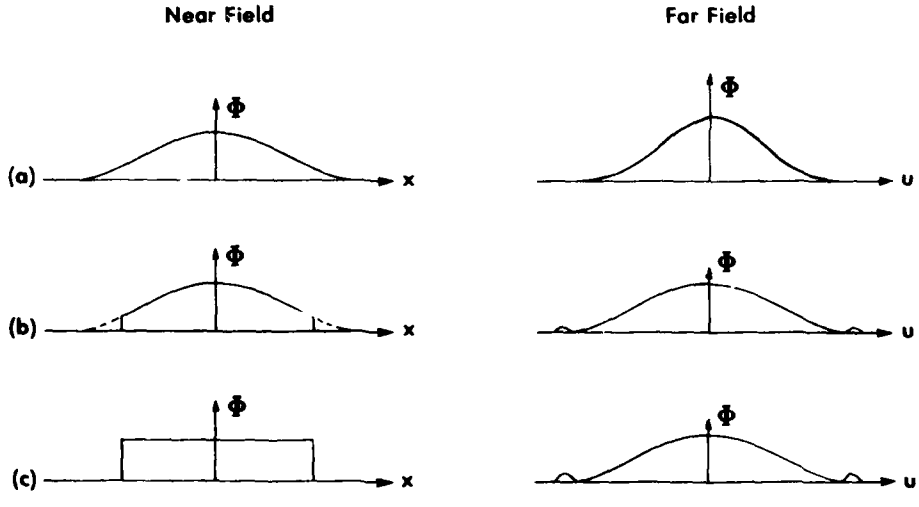

FIGURE 2-11. APERTURE FLUX PATTERNS AND CORRESPONDING FAR FIELD DIFFRACTION PATTERNS

Truncation of a circular Gaussian beam by the circular aperture of an optic is probably the most common type of perturbation to free propagation. If the aperture diameter is three or more times as large as the $1/e^2$ diameter of the Gaussian beam, then the beam is only intercepted at its 10^{-8} power points and the beam propagates as a true Gaussian. If the aperture diameter is only twice as large as the $1/e^2$ diameter of the beam, although the value of the Gaussian is only 3×10^{-4} as much as the central peak, the diffraction effects are such that the resulting beam deviates somewhat from that of a true Gaussian. If the aperture diameter is equal to the $1/e^2$ diameter, the Gaussian value is only 13.5% of the central peak yet the far field pattern resembles an Airy pattern more than it does a Gaussian pattern. Secondary rings (i.e., side-lobes) are found although they are weaker than those of a true Airy pattern. Most importantly, the beam size (or equivalently the beam divergence) at the first null or at the half power points are approximately that of the Airy pattern. In fact, the half power width is roughly 50% wider than that of an unobscured Gaussian under the same conditions. Although only 13.5% of the beam's energy is stopped by the aperture, the beam divergence is significantly increased.

Figure 2-11 presents far field diffraction patterns corresponding to an aperture illuminated with (b) Gaussian distribution and (c) uniform distribution. Figure 2-11(a) is the pattern expected for a Gaussian beam with no limiting aperture.

2.3.2 Multimode Beam Propagation

The discussions above have been limited to the most commonly encountered laser output, the Gaussian or TEM_{00} transverse mode. Laser cavities may also oscillate on higher order transverse TEM_{mn} modes. The laser power output may be increased by using these higher order modes and this may be desirable if the resulting increase in beam divergence,

spatial nonuniformity, and loss of spatial coherence are of no consequence.

The transverse intensity distribution of high order modes are discussed in numerous texts. (See References [2-5 through 2-13].) Suffice it to say that the distributions may be expressed in closed analytical form as Hermite-Gaussian functions, for lasers with rectangular geometry, and as Laguerre-Gaussian functions, for cylindrical geometry.

A scaling parameter, ζ_m, may be obtained for each of the higher order modes, with $\zeta_o = 1$ for the TEM_{oo} mode. If one rearranges Equation (2-15) and defines $2w_o = D_o$, one gets for a TEM_{oo} beam

$$1 = \frac{\pi D_o \theta_e^G}{4\lambda} \tag{2-21}$$

Replacing D_o by D_m, and θ_e^G by θ_m defines the right hand side to be ζ_m^2, that is

$$\zeta_m = \sqrt{\frac{\pi D_m \theta_m}{4\lambda}} \tag{2-22}$$

One finds that

$$D_m = \zeta_m \; D_o \tag{2-23}$$

and

$$\theta_m = \zeta_m^2 \left(\frac{4\lambda}{\pi D_m}\right) \tag{2-24}$$

The rules of thumb determined in the previous sections for a Gaussian, TEM_{oo} beam may be similarly employed for a multimode beam using the proper

scaling parameter. If the laser cavity has rectangular symmetry* and m = n, then two scaling parameters must be used for the X and Y coordinates.

2.3.3 Atmospheric Effects

Absorption and scattering are the principal mechanisms of the atmosphere which adversely affect the ability to efficiently deliver laser radiation to a remote target and gather its reflected return. Atmospheric windows in the visible and near infrared, the middle infrared from 3 to 5 μm, and the thermal infrared from 8 to 14 μm are chosen to minimize absorption. Any laser whose output falls in one of these windows is a candidate for an active sensor. Lasers such as the CO_2 laser at 10.6 μm are preferred to minimize attenuation due to scattering by aerosols in haze, fog and smoke, since scattering decreases with increasing wavelength. However, longer wavelength results in greater beam divergence and therefore degraded resolution for an imaging sensor.

Absorption of laser radiation, like other forms of radiation, follows Beer's law:**

$$L_\nu(z) = L_{\nu,o} e^{-\beta_\nu z} \tag{2-25}$$

where β_ν is the extinction coefficient usually expressed in km^{-1}. The absorption coefficient, β_ν', may also be expressed in decibels (dB) as

---

*It is worth noting that a cylindrical laser tube or rod with circular mirrors has rectangular symmetry if the mirrors are not parallel to each other.

**If the propagation path is not homogeneous, Equation (2-25) must be expanded to

$$L_\nu(z) = L_{\nu,o} \exp\left[-\int_o^z k_\nu \rho(s) ds\right]$$

where k_ν is the mass spectral extinction coefficient and is composed of absorption and scattering terms

$$k_\nu = k_{\nu,A} + k_{\nu,S}$$

$$I(z) = I_0 \, 10^{-\frac{\beta' z}{10}} \qquad (2\text{-}26)$$

where β'_ν is 4.343 β_ν.

The absorption coefficient is in general a function of wavelength. In order to describe the transmission of broadband nonlaser sources, spectrally averaged values of β are often used. Laser radiation is very narrowband, however, and the absorption coefficient for a single laser line may be greater or less than the spectral average depending upon whether or not the laser line falls on or near an absorption line for a molecular constituent of the atmosphere. A knowledge of the fine structure in the spectral transmittance of the atmosphere is therefore needed. This fine structure is well documented in the Air Force Geophysics Laboratory Atmospheric Absorption Line Parameters Compilation (See Reference [2-19]; also [2-20], pp.791-795.) and has been used to compute atmospheric attenuation coefficients for numerous HF, DF, CO, and CO_2 laser lines. (See References [2-21 and 2-22].) It is worth noting that an airborne imaging sensor might encounter increased or decreased attenuation due to motion of the sensor in the direction of laser beam propagation, since this motion can result in a Doppler shift which can

---

[2-19] R. A. McClatchey, et al., "Atmospheric Absorption Line Parameters Compilation," Report No. AFCRL-TR-73-0096, Air Force Systems Command, Andrews Air For Base, Washington, DC, 1973.

[2-20] L. S. Rothman, "AFGL Atmospheric Absorption Line Parameters Compilation: 1980 Version", Applied Optics, Optical Society of America, Washington, DC, Volume 20, No.5, 1981.

[2-21] W. L. Wolfe and G. J. Zissis (eds.), The Infrared Handbook, Office of Naval Research, Arlington, VA, 1978. Available from Order Department Environmental Research Institute of Michigan, Ann Arbor, MI; also, W. L. Wolfe (ed.), Handbook of Military Infrared Technology, United States Government Printing Office, Washington, DC, 1965.

[2-22] R. A. McClatchey and J.E.A. Selby, "Atmospheric Attenuation of Laser Radiation from 0.76 to 31.25 μm," Report No. AFCRL-TR-74-0003, Air Force Cambridge Research Laboratories, Bedford, MA, January 1974.

move the laser line closer to or further from the absorption line center. A sensor moving at Mach 1. for example, would produce a Doppler shift of about 0.02 cm^{-1} roughly one-third of the half-width at half-height of an atmospheric pressure broadened absorption line. The resulting change in absorption may not be dramatic, but still may be significant.

Scattering of laser radiation out of the collimated beam by molecules and aerosols can also lead to reduced transmission of laser radiation through the atmosphere. In fact, this may be the dominant loss mechanism for laser radiation falling in an atmospheric window where molecular absorption is low. The aerosols are in greatest abundance near the earth's surface in the form of smoke, dust, moisture droplets, or airborne chemicals. Scattering by individual molecules or particles much smaller than the radiation wavelength (Rayleigh scattering) is significant in the visible spectrum but falls off rapidly as λ^{-4}, making it of little significance in the infrared. Mie scattering, however, where the particle size is on the order of or greater than the radiation wavelength, can be quite significant in the infrared. In particular, theory and experiment show (See References [2-16,2-21]; also [2-23], pp.181-189.) that for particle diameter, d, less than $\pi\lambda$, scattering is weak, while for $d > \pi\lambda$ scattering becomes appreciable. This is shown dramatically in Figure 2-12 as nearly two orders of magnitude greater transmission of radiation through haze in the thermal infrared than in the visible or near IR. Similar advantages can be found for propagation in light fogs, but for heavy fogs where aerosol droplet sizes are larger, even the thermal IR is heavily attenuated. This is shown in Figure 2-13. Although the

[2-23] H. G. Hougton and W. R. Chalker, "The Scattering Cross Section of Water Drops in Air For Visible Light," Journal of the Optical Society of America, Optical Society of America, Washington, DC, Volume 39, 1949, p. 955; also, P. W. Kruse, L. D. McGlauchlin, and R. B. McQuistan, Elements of Infrared Technology, John Wiley and Sons, New York, NY, 1962.

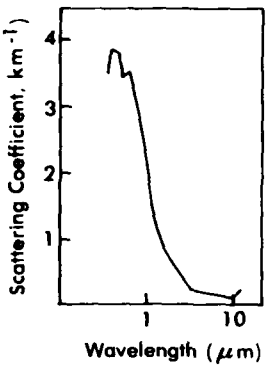

FIGURE 2-12. SCATTERING COEFFICIENT FOR A HAZE [2-24]

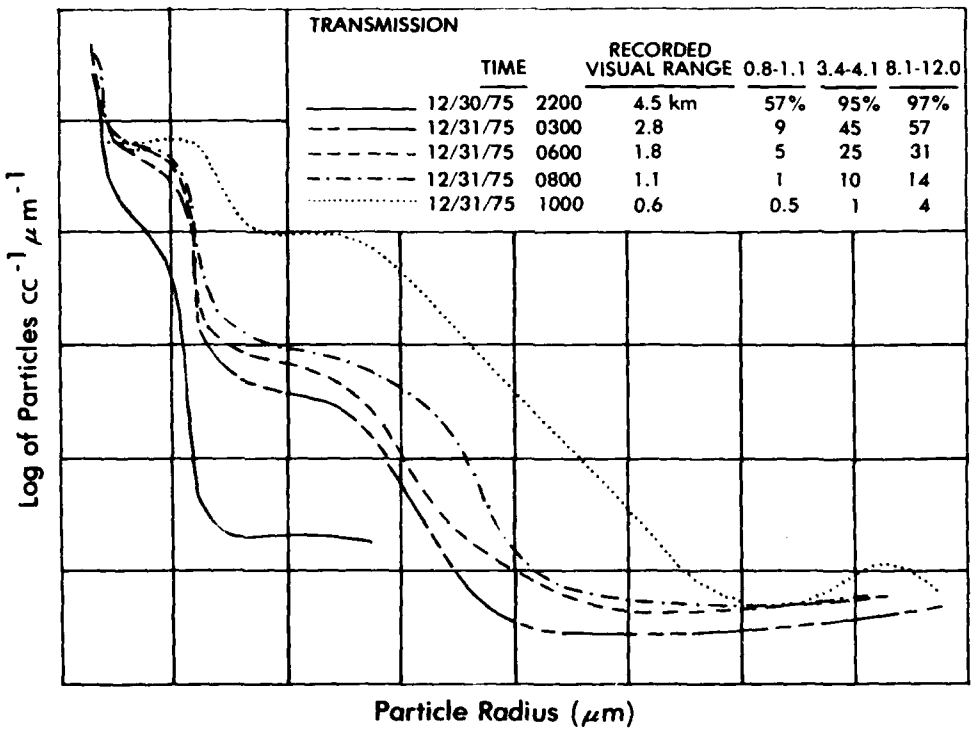

FIGURE 2-13. CHANGE IN AEROSOL DROPLET SIZE AS FOG BUILDS, DECEMBER 30-31, 1975, AT GRAFENWÖHR [2-25]

measurements for this figure are spectrally broadband, they should be applicable to narrowband laser radiation since scattering has little or no fine spectral structure.

Imagery from an active or passive sensor is degraded due to loss of signal resulting from the scattering of radiation out of the line of sight. The imagery may be additionally compromised due to scattering into the line of sight. For a passive, solar-illuminated sensor, this results in unwanted background radiation getting into the receiver IFOV. For an active sensor, the contributer of unwanted radiation is laser backscatter. In most active systems the transmitter and receiver are separated spatially, temporally or spectrally in order to keep the backscatter to a minimum.

2.4 SCANNING OPTICS

The scanning optics for laser-illuminated imaging sensors are similar to those described in Section 1.4.3 for passive imaging sensors. The passive sensor is simpler in that the entire scene is illuminated by the sun or the entire scene is self-emissive. A passive image is generated by simply imaging a point from the scene onto the detector element (thereby establishing the instantaneous field of view, or IFOV) and providing the necessary scan mechanism to cover the total field of view. An active imaging sensor may use a similar scan mechanism and similar optics, but is necessarily more complex since the sensor carries its own source and usually does not have the luxury of flooding the whole scene with radiation. Instead, the active sensor must project a small beam of radiation to a point in the scene which corresponds to the IFOV of the detector. Although the speed of light is very fast, time of flight to the target and back must be considered for a high speed scanner such that the laser beam must lead the receiver beam in order to achieve registration with the detector IFOV.

For a sensor with a resolution of 1 mrad, the transmitter and receiver beams must be aligned to a fraction of a milliradian. This alignment must be maintained not just for a single point in the scene but for the entire scan line. The alignment tolerance is often relaxed slightly by using a detector IFOV at the target which is larger than the laser illuminated spot. This is usually acceptable so long as the background radiation gathered from this larger IFOV is not deleterious to the imagery. The resolution element for a passive sensor is established by the IFOV of the detector, but for an active sensor, it is usually established by the laser beam size at the target.

An active sensor using a laser as the illuminator is able to efficiently deliver almost all of its energy to the target in a collimated beam. Diffuse reflection by the target scatters this radiation in all directions such that the signal radiation delivered to the detector is proportional to the solid angle, Ω, of the receiver aperture of area A_r at a range R (i.e., $\Omega = A_r/R^2$). This is referred to as $1/R^2$ loss. Since A_r is on the order of meters squared or less and R is on the order of kilometers, the $1/R^2$ loss is on the order of 10^{-6}. Therefore, it is necessary to have as powerful a laser as is practical in order to have a good signal-to-noise ratio and a good range capability for the active sensor.

2.4.1 Stray Radiation

The presence of a powerful laser with an output of several watts adjacent to a sensitive receiver which is able to detect powers on the order of nanowatts means that stray radiation is a potential problem. Most active sensors address this problem by spatially separating the transmitter and receiver beams, and by using baffling to eliminate stray radiation.

The ERIM M-8 active/passive sensor (See Reference [2-26].) employs two 45 deg mirrors which rotate on opposite ends of the drive motor shaft. One mirror serves as the laser transmitter mirror (and also as the passive receiver mirror) and the other, a distance of two feet away, serves as the active receiver mirror. The ERIM modified Reconofax® X scanner and modified AVD-4 scanner, and the Perkin Elmer KA-98 scanner [2-1] employ Kennedy-type scan optics (See Section 1.4.3.) where one end of the rotating polygon mirror is used to transmit the laser radiation and the rest of the mirror is used to receive the radiation.

United Technology Research Center (UTRC) (See Reference [2-27].) and Raytheon (See Reference [2-28], pp.1600-1604.) use frequency multiplexing to prevent backscattered radiation from getting into the receiver channel. Since these scanners are CO_2 laser heterodyne sensors, motion of the sensor along the line of sight imparts a Doppler frequency shift to the radiation which returns from the target. Transmitted laser radiation which is scattered into the receiver by the optics is not frequency shifted and therefore is easily rejected by electronic filtering. It is thus possible to share the optics for both the transmitter beam and the receiver beam (provided stray reflections do not saturate the detector). In particular, UTRC and Raytheon use a

---

[2-26] P. Hasell, L. Peterson, F. Thomson, E. Work and F. Kriegler, "Active and Passive Multispectral Scanner for Earth Resources Applications: AAFE," Report No. 115800-49-F, Environmental Research Institute of Michigan, Ann Arbor, MI, June 1977.

[2-27] R. J. Mongeon, W. J. Green, and H. H. Naidich, "Laser Obstacle Terrain Avoidance Warning Systems (LOTAWS)," AD B034 319L, United Technology Research Center, Hartford, CT, November 1978.

[2-28] C. M. Sonnenschein and F. A. Horrigan, "Signal-to-Noise Relationships for Coaxial Systems that Heterodyne Backscatter from the Atmosphere," Applied Optics, Optical Society of America, Washington, DC, Volume 10, 1971.

common rotating wedge(s) and telescope to achieve the desired scan for their CO_2 laser heterodyne systems.

It would also be possible to use time gating to allow the use of shared optics. If a high repetition rate pulsed laser ($\gtrsim 10^5$ pps, so that at least one pulse would illuminate each pixel or reselm) were used as a source, the receiver could be gated off while the pulse was being transmitted and while stray radiation was reaching the detector. Use of shared optics offers the advantage of reduced sensor size and weight. It also has the advantage of no parallax but still suffers from time-of-flight effects for rapid scanning systems.

2.4.2 Parallax

If the transmitter and receiver optics are physically separated in the sensor in order to reduce stray radiation, registration of the illuminating beam and the detector IFOV occurs at only one point in space (i.e., the intersection of two lines) as shown in Figure 2-14 for range R_1. At ranges less than or greater than R_1, registration is less than ideal. It is worth noting that for decreased ranges, the loss of signal due to poor registration is usually more than compensated for by the increase in signal due to the $1/R^2$ effect. For increased range, however, loss of registration further compounds the loss of signal due to the $1/R^2$ effect. It is obvious from Figure 2-14 that the transmitter and receiver should be as close together as possible to minimize parallax, although the receiver aperture should be as large as possible to maximize the amount of radiation which can be collected.

For a downward-looking line-scan active sensor, the airborne platform can be maintained at a fairly constant altitude such that ranges at nadir (immediately below) change only slightly. However, the range to the scene at nadir is significantly less than it is when the sensor look-angle is significantly off-nadir as shown in Figure 2-15.

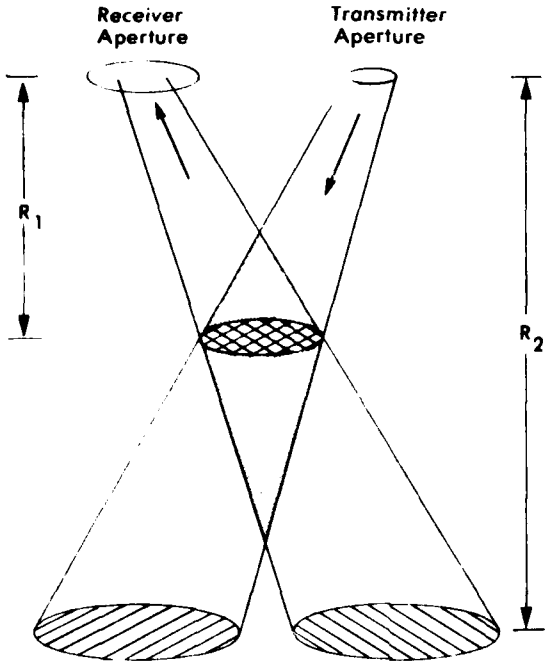

FIGURE 2-14. PARALLAX IS THE RESULT OF A SPATIALLY SEPARATED TRANSMITTER AND APERTURE

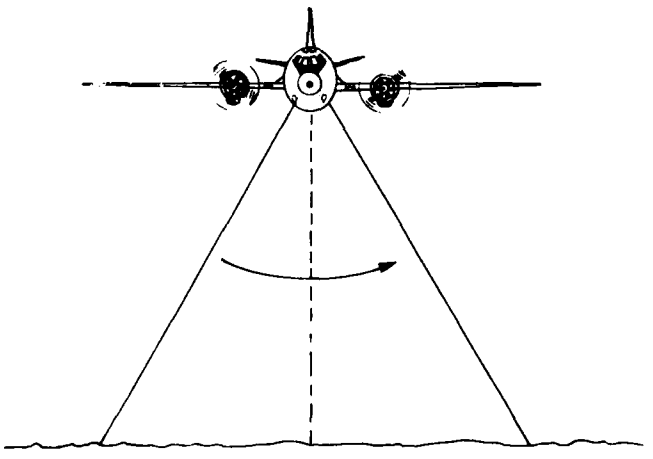

FIGURE 2-15. THE RANGE-TO-TARGET CHANGES WITH SCAN ANGLE

At large scan angles, the illuminated spot is larger (and therefore has coarser resolution, possibly overlapping with previous scan lines), and the registration is different than for nadir. Since the signal-to-noise ratio is greatest for the shortest range, performance throughout the scanner's total field of view may be optimized by adjusting the alignment for best registration close to the maximum scan angle where the $1/R^2$ loss is greatest.

If the laser transmitter beam or the receiver beam (defined by the detector position in the sensor and the location of the receiver optics) are (1) both perpendicular to the axis of rotation for the scan mirror in a Kennedy scanner, or (2) in-line with the axis of a rotating 45 deg scan mirror, then the scanned beam defines a plane in space. The intersection of this scan plane and the plane of the earth is a straight line. In both instances, the transmitter scan plane and the receiver scan plane are parallel such that their line scans in the scene cannot have overlapping fields of view.

For the active Kennedy scanner, the fields of view can be made to overlap by adjusting the transmitter and/or receiver beam to be non-perpendicular to the axis of rotation, i.e., slightly off-normal to the mirror surface, as shown in Figure 2-16. The rotating scan beam therefore describes a cone rather than a plane. Assuming the earth to be a plane which is parallel to the scan mirror's axis of rotation, the intersection of a cone and such a plane is a hyperbola so that the scan pattern in the scene is that of a hyperbola and not a straight line. Since the cones of the transmitter beam and the receiver beam are oppositely directed, their hyperbolas are of opposite curvature as shown in Figure 2-17. If the two beams are in registration at nadir, they gradually lose registration as they move off-nadir. This is the same effect noted in Figures 2-14 and 2-15.

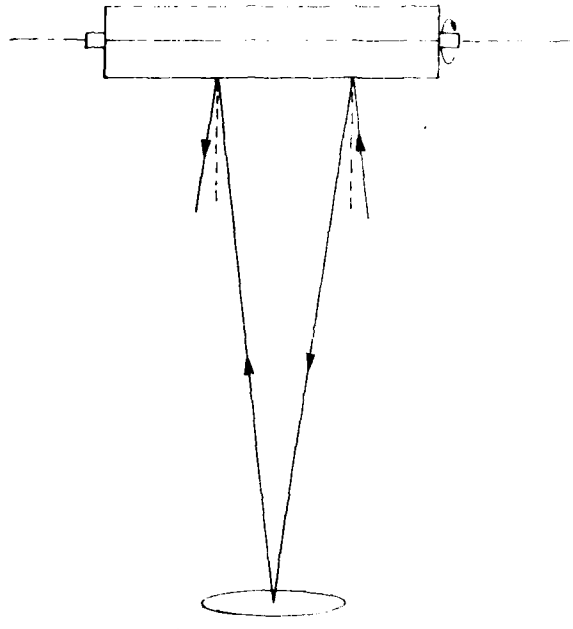

FIGURE 2-16. TRANSMITTER AND RECEIVER BEAM GEOMETRY FOR THE ROTATING POLYGON MIRROR OF A KENNEDY SCANNER

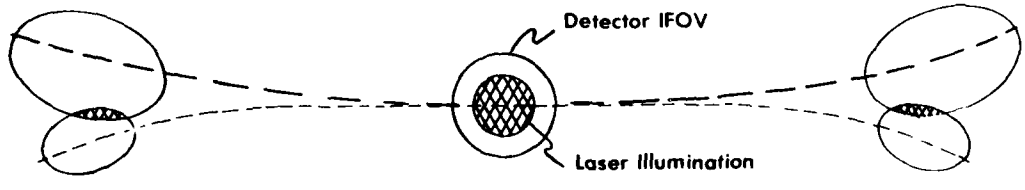

FIGURE 2-17. LOSS OF TRANSMITTER/RECEIVER REGISTRATION WITH INCREASING SCAN ANGLE

Consider, as an example, an active Kennedy scanner with transmitter and receiver beams separated by 1 ft at their centers and operating at a range of 1000 ft. To be in registration, one of the beams must be off-normal by 1 mrad ($1/1000 = 10^{-3}$ rad) or they must both be off-normal by 0.5 mrad. If the altitude of the sensor is 1000 ft, the beams are in registration at nadir, and if the scan field of view is 45 deg, then the maximum range is 1414 ft and the separation between IFOVs on the ground is 1.4 ft at their centers. If the resolution of the sensor is 1 mrad, they are less than one-half overlapping; if the resolution is 0.5 mrad, there is almost complete loss of registration.

The transmitter and receiver beams for a rotating 45 deg scan mirror, such as the ERIM M-8 scanner, can be put into registration using two methods. The first would require coincidence of the transmitter and receiver axes with the scan mirror axis of rotation, but the mirrors would be oriented slightly greater than 45 deg (45 deg plus 0.25 mrad for the conditions in the example above). By so doing, hyperbolic scan lines result as for the Kennedy scanner, with corresponding loss of registration with scan angle. (See Figure 2-17.) The second method employs the two scan mirrors at precisely 45 deg (tolerances of a small fraction of a milliradian are required) with the beams slightly off-axis (0.5 mrad each in our example) as shown in Figure 2-18. Examination of the figure shows that tilted beam planes rather than cones are generated such that a straight line scan through the scene is achieved. Critical alignment is required so that the transmitter and receiver axes must lie in the plane of the figure within a small fraction of a milliradian. Time of flight effects, discussed in the next section, require the transmitted beam to lead the receiver beam. This should be done by leading with the transmitter scan mirror by an amount (~mrad) which is range and scan rate dependent, rather than by leading with the transmitter optic axis.

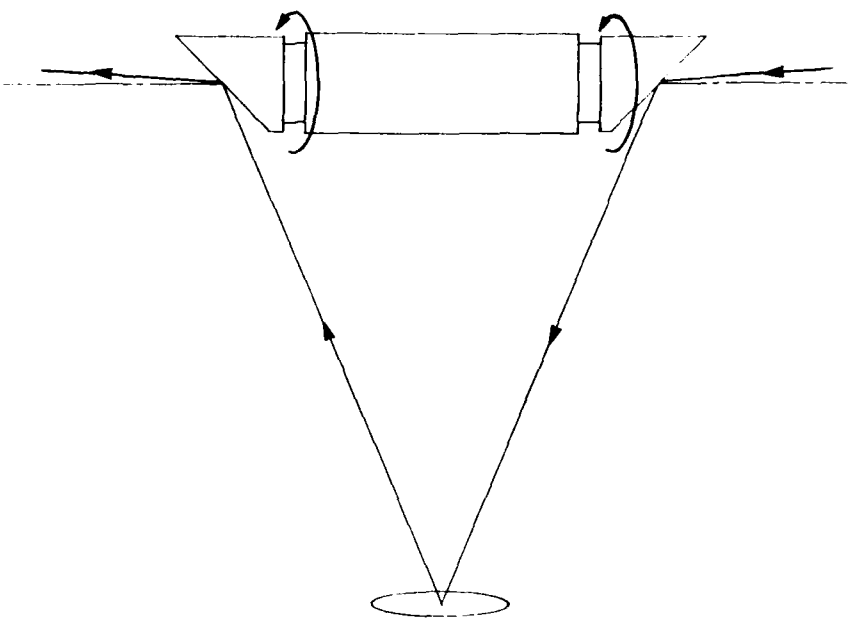

FIGURE 2-18. RANGE DEPENDENT ALIGNMENT FOR A 45 deg MIRROR ACTIVE SCANNER

For a forward-looking rather than downward-looking sensor, range changes can be quite significant due to aircraft pitch and terrain variations, especially at low depression angles. Parallax may be particularly degrading to sensor performance and should be carefully evaluated.

2.4.3 Time of Flight

Just as parallax is a range-dependent parameter, so also is the time of flight of the radiation to the target and back to the receiver. Since light travels in air at rate of approximately 1 ft in 1 nsec, a range of 1000 ft takes 2 μsec round trip. For a rapid scanning Kennedy sensor with a 1 mrad IFOV and spinning at 1000 rpm, the dwell time for a pixel or reselm is only 0.5 μsec. At a range of 1000 ft, the laser beam must lead the receiver beam by 4 reselms or 4 mrad.

The proper lead angle may be achieved for 45 deg mirror scanners by having the rotation of the transmitter mirror lead slightly the rotation of the receiver mirror as mentioned in the previous section. Unfortunately, this usually fixes the lead angle for a single range and lacks flexibility. Lead angle may also be achieved by changing the optic axis of, for example, the laser transmitter with respect to the scan mirror surface. For a Kennedy scanner, this is an effective and flexible method to provide the proper lead. For a rotating 45 deg mirror scanner, this method is also used, but provides an undesirable tilting of the transmitter scan line in the scene compared to the receiver scan line.

For a constant range, the time of flight may be compensated for by a single lead angle. The problem arises when the range changes due to scan angle, as for a downward-looking sensor, or due to geometry, as mentioned in the previous section for a forward-looking sensor. Range changes of approximately 250 ft in the above example result in total

loss of registration. Careful evaluation of this effect is required for any practical sensor. The choice of 1000 rpm as an example of scan rate is appropriate for a downward-looking sensor which provides contiguous line scans with a single detector. Use of multiple detectors allows a reduction of the scan rate and therefore the dwell time, but requires a fan-shaped laser spot at the target to cover the IFOVs of the multiple detectors. For a forward-looking sensor, 1000 rpm is high for low depression angles unless one wishes to overscan the scene. Slower scan rates and/or multiple detector elements may aid in reducing the time of flight effects which are very pronounced for low depression angles.

To date, all active imaging sensors fall in the category of flying spot scanners using a single element detector. The logical next step is the use of a linear detector array and fan-shaped laser illumination to cover the IFOV, or possibly a two-dimensional array with time delay and integration (TDI). TDI may not, however, be used for smoothing speckle noise since the correlation time for a single speckle (See Section 2.5.4.) is much longer than a few dwell times.

2.5 TARGET CHARACTERISTICS

Passive sensors in the visible and near IR rely upon diffusely reflected (or scattered) solar radiation to obtain target signatures, just as the human eye obtains images of a scene. Since most objects have surfaces which are rough compared to visible and near IR wavelengths, they diffusely reflect the radiation into all angles making them "visible" from all angles. Detail or contrast is a result of spatial variations in reflectivity within the scene, or within the target itself. Needless to say, if the sun is not shining, no imagery are obtained. Also, changes in cloud cover, shading or time of day can affect an image.

Passive sensors in the thermal IR rely upon self emission from the scene. Detail or contrast is a result of spatial variations in temperature and emissivity within the scene or within the target itself. Since temperature can be a function of time of day and thermal inertia of an object, signatures may change with time.

Active sensors rely upon reflected radiation whether the laser wavelength is visible, near IR or far IR. Reflected solar radiation or radiation emitted by the scene which reaches the detector along with the reflected laser radiation constitutes the background. Background radiation is usually undesirable and is often rejected by a narrowband spectral filter placed in front of the detector. Background radiation may, nonetheless, be of significance compared to the laser return signal. In the visible and near IR, this may be of little consequence since the reflected solar radiation should correlate well with the reflected laser radiation. In the far IR, however, a good emitting material which provides strong background radiation is also a good absorbing material for the probing laser radiation and vice-versa for a poor emitter. Consequently, the low reflectivity portion of a target may produce a weak signal (reflected return) while an adjacent, highly reflecting area may produce a strong return thereby providing good contrast. However, since the emitted (background) return for these same two adjacent areas may be high and low, respectively, the contrast could tend to be washed out.

2.5.1 Rough Surfaces

Quantitatively, a surface may be classified as being rough or smooth based upon the Rayleigh criterion. (See Reference [2-29].)

[2-29] P. Beckman and A. Spizzichino, The Scattering of Electromagnetic Waves from Rough Surfaces, Macmillan Company, New York, NY, 1963.

Rays reflected by surface irregularities arrive at an observation point with a phase change dependent upon the difference in path lengths between the rays as shown in Figure 2-19(a). Two rays have a path length difference

$$\Delta\ell = 2h \cos \theta \tag{2-27}$$

if h is the height of a single irregularity and θ is the angle of incidence. If $\Delta\ell$ is much less than the radiation wavelength, λ, then the two rays are in phase with each other and they interfere constructively. If, however, $\Delta\ell$ equals $\lambda/2$, the rays interfere destructively to cancel each other and their energy appears elsewhere in space, that is, the radiation is scattered. A measure of surface roughness (essentially the phase difference between the two beams) is

$$\xi = \frac{4\pi h}{\lambda} \cos \theta \tag{2-28}$$

In a real material surface, single steps are rarely encountered, but random distributions of hills and valleys are usually found, as shown in Figure 2-19(b). Since h is not a fixed quantity but varies statistically over a surface, and since the incident angle, θ_i, does not always equal the observation angle, θ_s, one gets, in general,

$$\xi = \frac{4\pi\sigma}{\lambda}\left(\cos \theta_i + \cos \theta_s\right) \tag{2-29}$$

where σ is the variance in the height distribution. For $\xi < 1$, the surface may be considered smooth, and for $\xi > 1$ rough, with gradations in each category. This is the Rayleigh criterion for roughness. Whether a surface is rough or smooth therefore depends not only on the surface structure (i.e., σ), but also upon the angles and wavelength involved. For grazing angle ($\theta << 90$ deg) a "rough" surface may appear smooth.

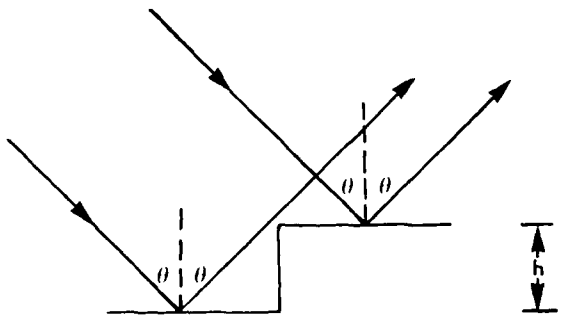

(a)

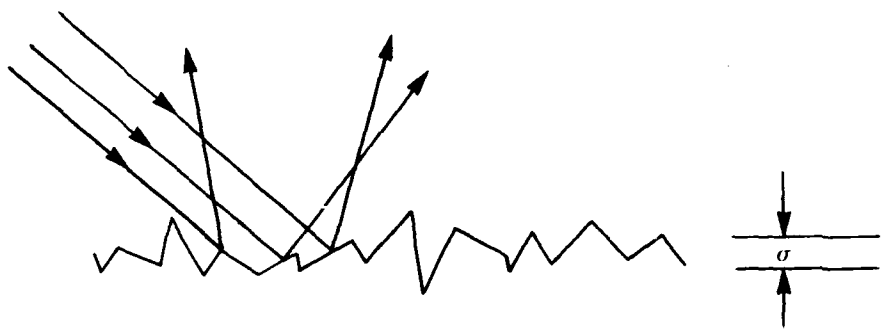

(b)

FIGURE 2-19. DIFFUSE REFLECTION. A simple step reflector in (a) and a complex reflector in (b).

2.5.2 Diffuse Reflection -- Near IR

When one observes a scene visually, the eye collects radiation from a source (sun or light) which has been diffusely reflected by objects in the scene. Occasionally, one may encounter smooth surfaces which partially reflect and partially scatter radiation. These smooth surfaces may lead to reflected images or glare, especially if the radiation path is at a glancing angle with respect to the surface. Smooth surfaces are usually man-made or cultural objects with a high degree of polish. Natural objects (except for liquids) are usually rough and therefore diffusely scatter* rather than specularly reflect* visible and near IR radiation.

In spite of the significant reflected components, most smooth objects still possess a significant scattered component such that structure or contrast entailed in the object is discernible. This diffusely scattered radiation which reaches the eyes is what allows one to "see" smooth as well as rough objects. Only in the case of highly polished glasses and metals is the material devoid of the scattered components.

Passive and active sensors in the visible and near IR generate images which closely match those seen visually. Active sensors are different primarily in four areas: (1) the illumination is monochromatic, (2) the image may contain speckle, (3) there are no shadows(for the usual monostatic case, as discussed below), and (4) operation in day or night is usually equivalent. The monochromatic or single wavelength character of a laser has little effect upon the

*To avoid confusion, note that scattered radiation is that radiation which is diffusely reflected in all direction according to Lambert's Law (See Reference [2-21].) and specular radiation is that radiation which is reflected by a surface such that the angle of incidence equals the angle of reflection, and the reflected rays lie in the plane of incidence.

reflective characteristics of a target. A passively illuminated scene viewed with a sensor having a spectral filter will have imagery which are almost identical to a similar but active sensor at the same wavelength. The image generated by an active sensor may possess a granularity, or spatial intensity variation, not present in the passive image. This is a consequence of the coherent nature of laser radiation and is termed speckle (clutter in radar terminology). Speckle is discussed in Section 2.5.4. Since the source of illumination for a passive sensor is in general at a random position in space, shadows are cast by objects with vertical relief. This situation of source and receiver at grossly different angular positions is classified as bistatic. For an active sensor, however, since the position of the source is in proximity with that of the receiver, no shadow can be seen. This is classified as monostatic reflection.

If the radiation source and the receiver are separated as for a passive sensor, the bistatic reflectance characteristics of a target vary in a complex manner depending upon the position of the source and the receiver with respect to the object, and upon the orientation of the object surface itself (See Reference [2-30].) as shown in Figure 2-20(a). If the target normal, $\hat{n}$ (defined as a line which is perpendicular to the surface element), is in the plane of incidence and bisects the angle between the source and the receiver, the conditions of specular reflection are satisfied and glint off the target may be observed. If the target is truly Lambertian, the source radiation is diffusely scattered in all directions equally, and no glint is observed at the specular angle. The other extreme is that of a highly polished smooth surface whereby no source radiation reaches the receiver via the target element except when the specular condition is precisely satisfied. Generally speaking, natural objects fall in the Lambertian category and cultural objects fall somewhere between the Lambertian and specular extremes. In the latter case, one finds that the specular

peak or glint increases with increasing bistatic angle between the incident beam and the receiver beam.

Monostatic reflection found for active sensors (See Figure 2-20(b).) is simpler to describe since the object orientation with respect to the line-of-sight may be described by a single angle, β. Specular reflection or glint is therefore only obtained at normal incidence and increased glint for grazing angles does not apply.

Figure 2-21 presents reflectance measurements of natural objects for radiation wavelengths in the visible and near-IR as a function of the angle θ_R between the object normal and the receiver line-of-sight. (See Reference [2-30].) In Figure 2-21(a), the transmitter is within 2 deg, β, of the receiver and moves with the receiver as θ_R changes (monostatic). In Figure 2-15(b) and (c), the transmitter is oriented normal to the target (θ_i = 0 deg) and the receiver angle θ_R is changed from -90 to +90 deg (bistatic conditions).

The symbols used in the figure correspond to the polarization vector of the transmitted laser beam and the receiver sensitivity:

| : parallel to the plane of incidence
⊥ : perpendicular to the plane of incidence
| |: Xmtr and Rcvr are ||
⊥ ⊥: Xmtr and Rcvr are ⊥ ⊥
| ⊥: Xmtr is | and Rcvr is ⊥
⊥ |: Xmtr is ⊥ and Rcvr is |
U T: Unpolarized

[2-30] IST Staff, "Target Signature Analysis Center: Data Compilation," Willow Run Laboratories of the Institute of Science and Technology, Report No. IST 3221-41-B, AD 904 999L (I), AD 905 000L (II), The University of Michigan, Ann Arbor, MI, Volumes I and II, October 1972.

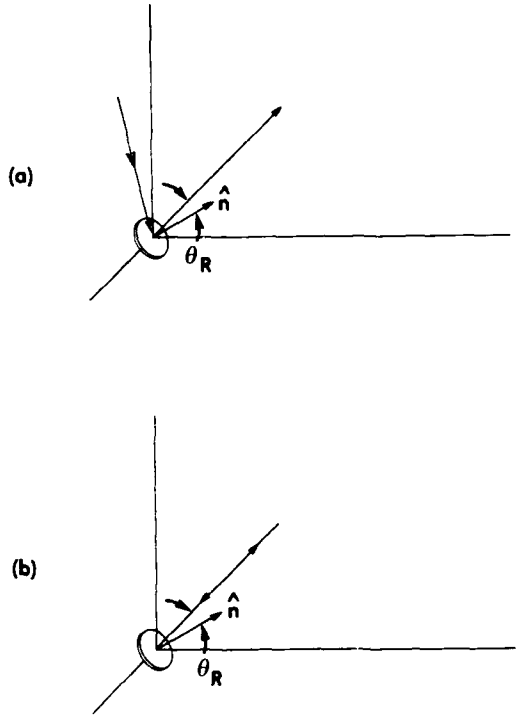

FIGURE 2-20. BIDIRECTIONAL REFLECTANCE. Bistatic condition in (a) where the source and receiver are at different positions. Monostatic condition in (b) with the source and receiver together.

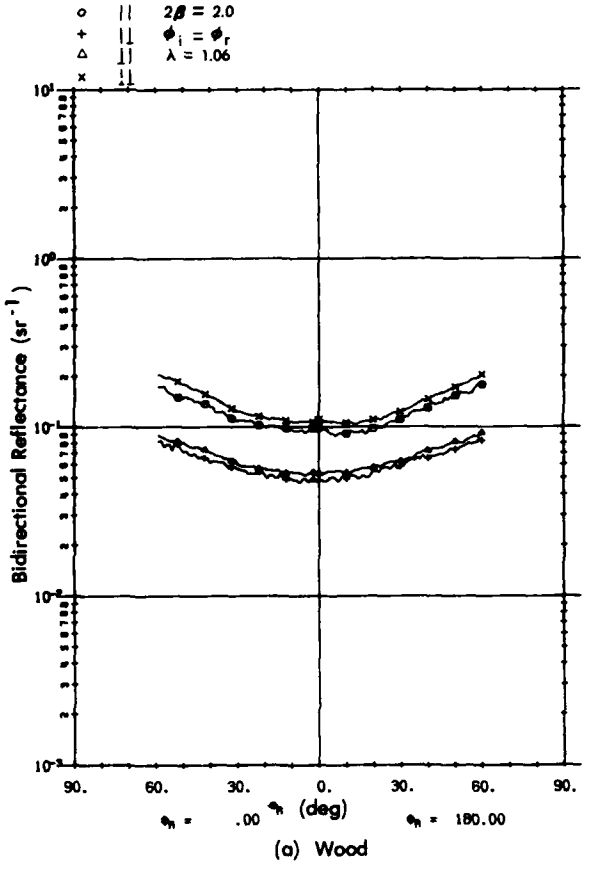

FIGURE 2-21. DIRECTIONAL REFLECTANCE MEASUREMENTS OF NATURAL OBJECTS IN THE VISIBLE AND NEAR-IR. Part (a) is a monostatic measurement; parts (b) and (c) are bistatic [2-30]

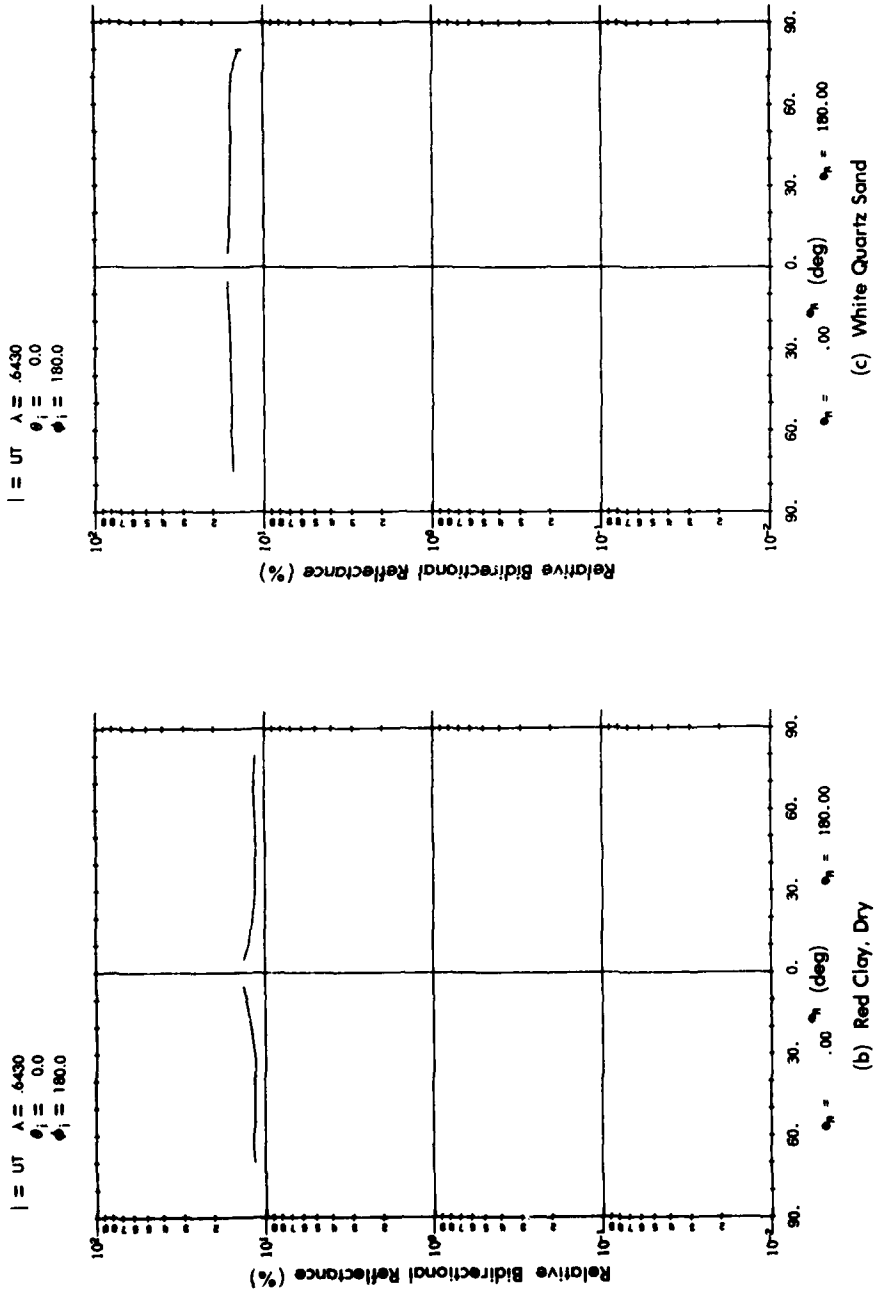

FIGURE 2-21. DIRECTIONAL REFLECTANCE MEASUREMENTS OF NATURAL OBJECTS IN THE VISIBLE AND NEAR-IR (Continued) [2-30]

The reflectivity of natural objects is almost constant with θ_R and is very close to that for a true Lambertian reflector. A nonabsorbing Lambertian reflector (ρ = 100%) would have a directional reflectance, ρ', of $1/\pi$ sr^{-1} for all θ_R, i.e., $\rho' = \rho/\pi$. (See References [2-21 and 2-30].) The reflectance of wood can be seen from Figure 2-21(a) to be about 50% for polarization matched transmitter and receiver beams, and the average is about 0.15 sr^{-1} (ρ' at θ_R = 0 deg is 0.10 sr^{-1}, and at large θ_R is 0.20 sr^{-2}). The diffusely reflected radiation is highly depolarized, although not completely so. If there were no depolarizing effects, then the $\parallel\perp$ and $\perp\parallel$ data would be zero in the figure. If the reflected radiation were completely depolarized, the $\parallel\perp$ and $\perp\parallel$ data would fall upon the $\parallel\parallel$ and $\perp\perp$ data. Depolarization is a consequence of multiple reflections from the rough surface. (See Reference [2-29].)

The monostatic bidirectional reflectances for some man-made objects are presented in Figure 2-22 for a wavelength of 1.06 μm. The canvas can be seen to be nearly Lambertian, as might be expected from its roughness, compared to the radiation wavelength. The painted steel and metals possess pronounced polarized specular peaks at $\theta_R \sim 0$ deg. The depolarized ($\parallel\perp$ and $\perp\parallel$) component is weaker by roughly an order of magnitude at off-specular angles and the specular peak is weak or absent.

2.5.3 Specular Reflection -- Far IR

In previous sections, diffuse and specular reflection were discussed as they relate to surface roughness. Since the specular component increases as the target surface becomes smoother compared to the wavelength of incident radiation, targets are an order of magnitude smoother for CO_2 laser radiation at 10.6 μm than for Nd:YAG laser radiation at 1.06 μm. As discussed above, the eye relies upon diffusely reflected radiation to obtain shape, contrast or detail

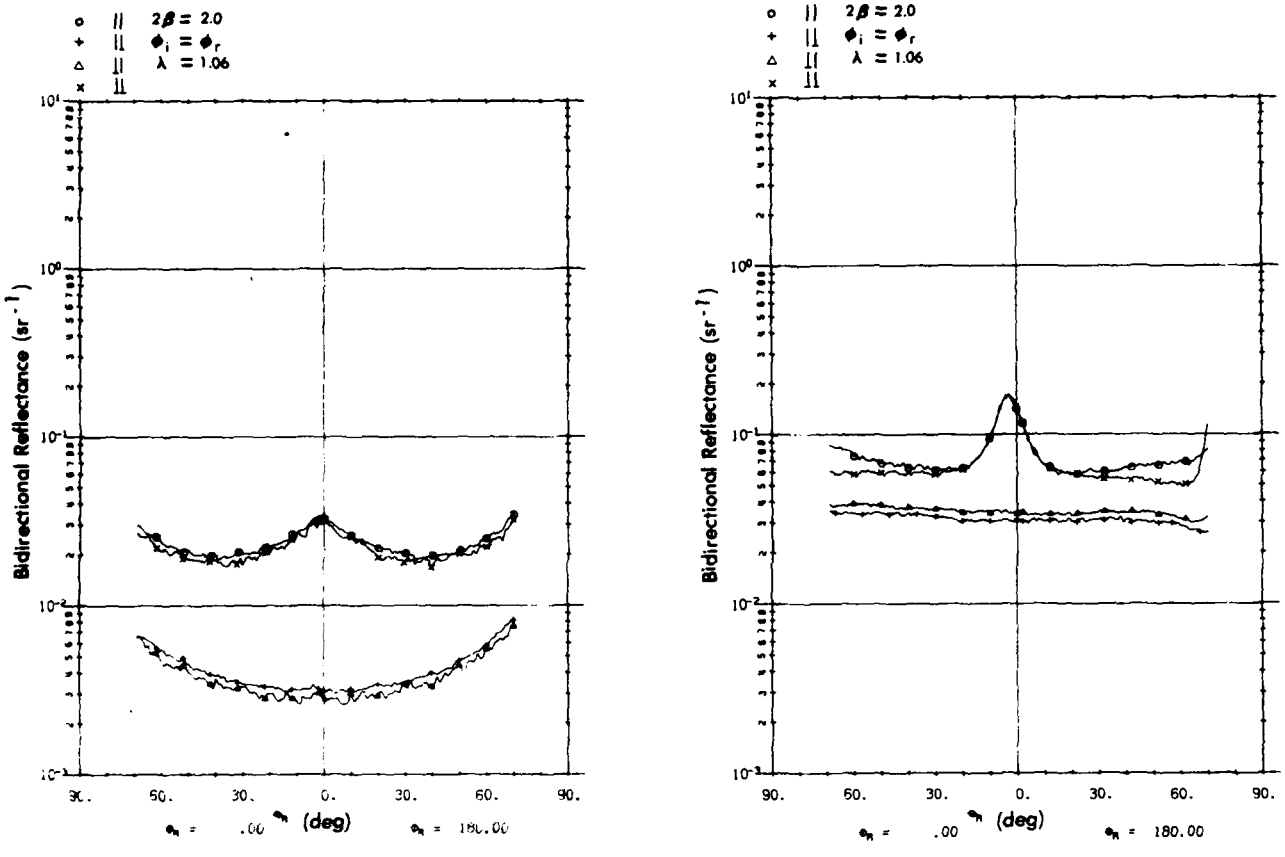

(a) Olive Drab Paint on Steel

(b) Camouflage Paint on Metal

FIGURE 2-22. MONOSTATIC DIRECTIONAL REFLECTANCE, ρ', MEASUREMENTS OF CULTURAL OR MAN-MADE OBJECTS [2-30]

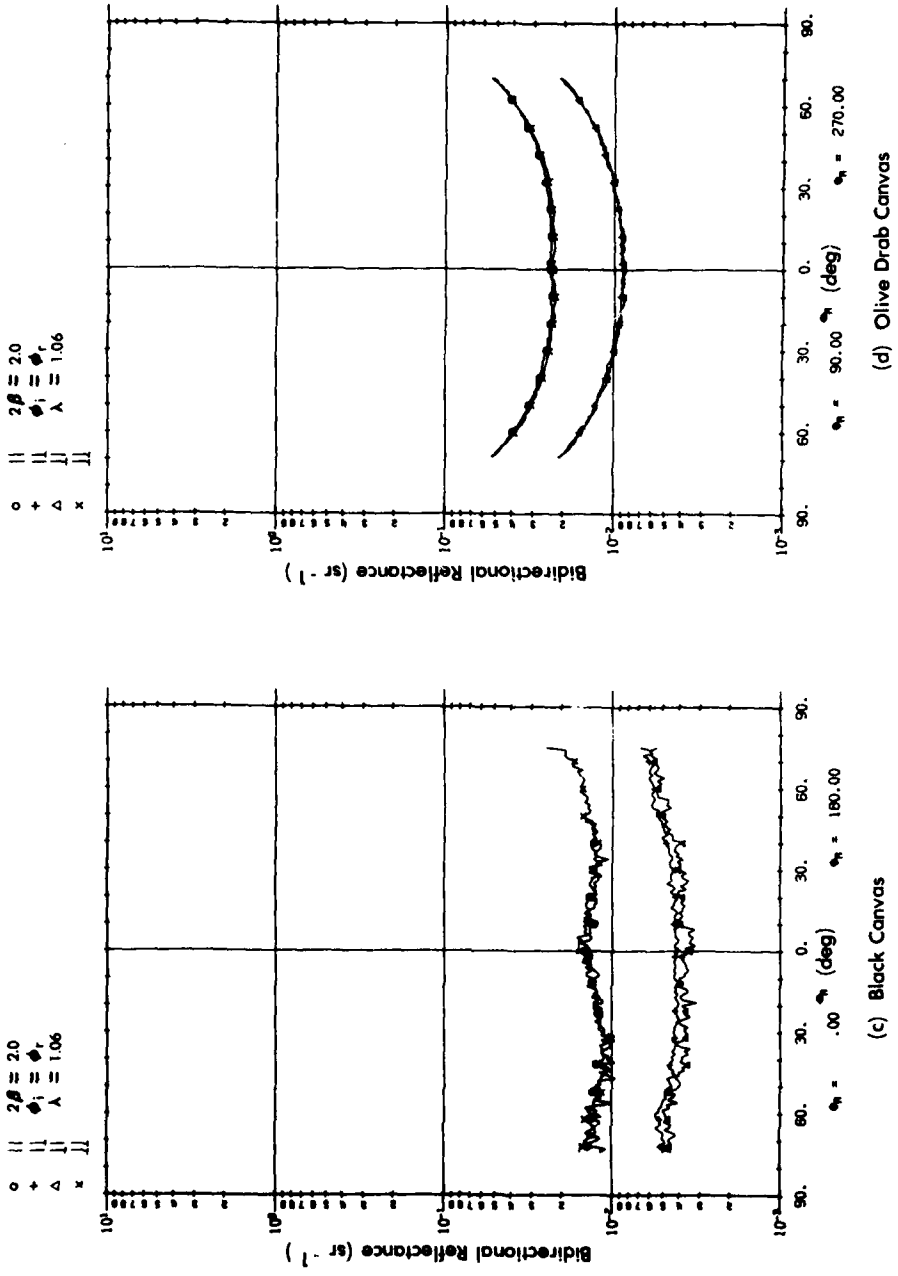

FIGURE 2-22. MONOSTATIC DIRECTIONAL REFLECTANCE, ρ', MEASUREMENTS OF CULTURAL OR MAN-MADE OBJECTS (Continued) [2-30]

information about a target. That is, a significant return on a pixel-by-pixel basis from a target is needed in order to generate an image of an object in the usual sense. If, however, the object is highly specularly reflecting, most of the radiation directed to a target may be specularly reflected in a direction other than that of the receiver. On a pixel-by-pixel basis for an active imaging sensor (monostatic), facets of the target which are not normal to the radiation beam may provide very weak or absent returns, while those rarer facets or pixels which are near normal may provide strong (possibly saturating) returns. Similarly, 90 deg dihedrals (inside corners) may provide strong returns because of multiple reflection. Images of highly specular targets (for example, radar images) look considerably different than those images familiar to the human observer who relies upon diffusely reflecting targets and their corresponding signatures. Each specular target has its own characteristic signature and it may be the job of machine processors to identify these unique signatures for target cueing applications.

It is worth noting that viewing a specular target with a passive sensor may be quite different than viewing it with an active sensor. If a passive sensor has its line-of-sight located upon a specularly reflecting facet of an object, it may receive reflected radiation from another part of the scene or from the sky, i.e., the facet behaves like a mirror. In an active sensor, laser radiation may be reflected from a specular facet to another part of the scene, but the instantaneous field of view of the active receiver is not in registration with the laser-illuminated part of the scene unless that part of the scene is close to the target such that time of flight and parallax conditions are satisfied. (See Section 2.4.) All pixels which specularly reflect radiation to provide no return to the receiver constitute a portion of the target which has complete absence of signal.

Figure 2-23 presents reflectance measurements of natural backgrounds illuminated with 10.6 μm radiation. Surprisingly, the sand shows a weak depolarized component and a slight specular peak. Figure 2-24 presents measurements of cultural targets. Most notable is the pronounced specular peaks, especially for the painted metals. Figure 2-24(b) presents bistatic measurements showing polarization/depolarization effects for an angle of incidence, θ_i, equal to 30 deg. Both a depolarized and a polarized specular peak are found when $\theta_R = \theta_i$.

It should be noted that the bidirectional reflectance ρ' can exceed 1 sr^{-1} for specular reflectance. This is possible since almost all of the incident energy can be found in the specular beam or lobe. Since this lobe is much less than 1 sr of solid angle, ρ' can be greater than unity. (An upper limit might be estimated by considering a diffraction-limited beam 10 mm in diameter, D, reflected by a polished mirror. The reflected radiation is contained in a diffraction-limited lobe of solid angle $\sim(\lambda/D)^2$. If λ is 10 μm, the lobe has a solid angle of 10^{-6} sr, and if λ is 1 μm, 10^{-8} sr. The ρ' for the specular angle is therefore 10^6 and 10^8 sr^{-1}, respectively, and essentially zero elsewhere. Note that if the target is composed of 1 mm facets, the 10 mm beam is broken down into 100 smaller beams, each having a lobe of about 10^{-4} sr at 10 μm. Diffuse reflection results when the facet dimensions are less than the wavelength of the radiation, such that the specular lobe from each facet is greater than 2π sr.)

2.5.4 Speckle

Illumination of a diffusely reflecting surface by a beam of incoherent radiation results in radiation being spread uniformly in all directions according to Lambert's cosine distribution as shown in Figure 2-25(a). If the illuminating beam of radiation is coherent, as

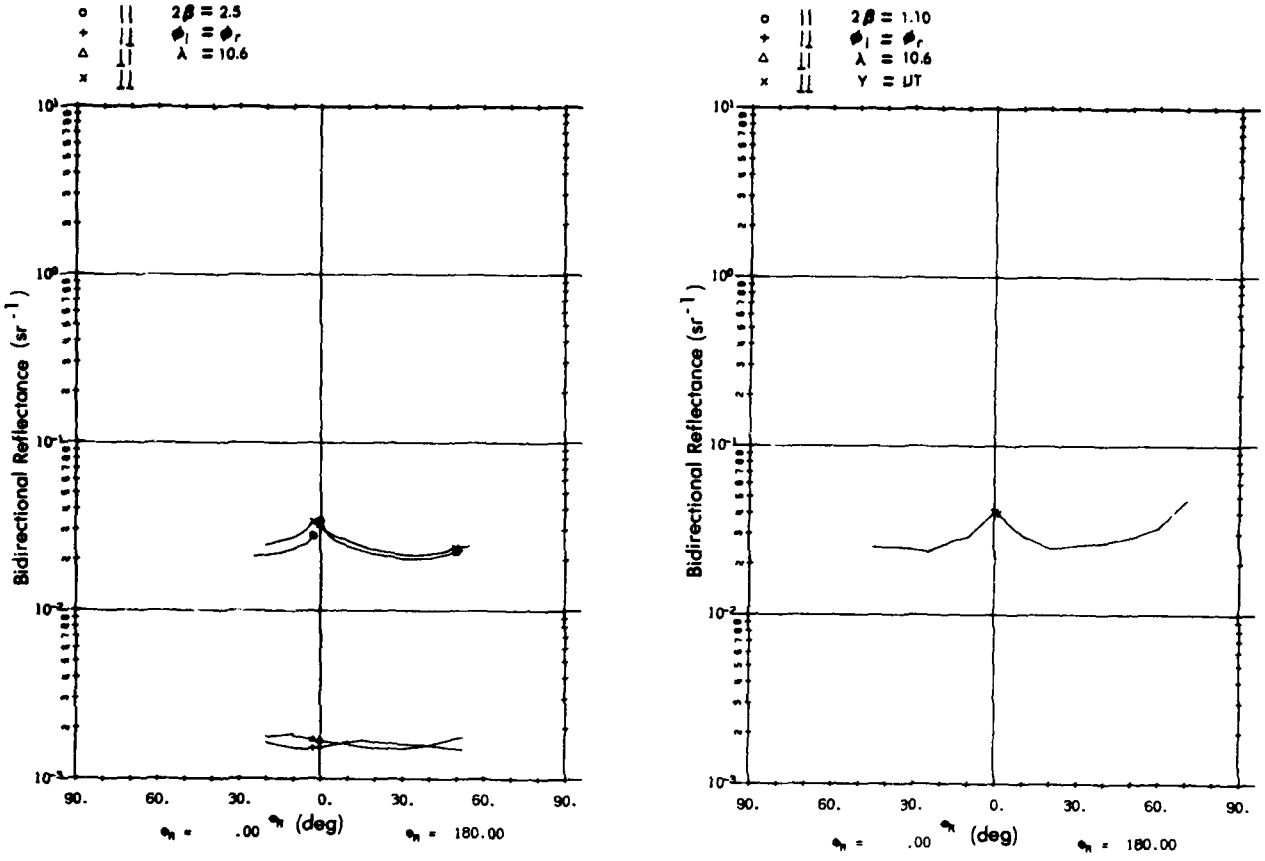

(a) Sand with Other Particles in it from California

(b) Tree Bark

FIGURE 2-23. MONOSTATIC BIDIRECTIONAL REFLECTANCE OF BACKGROUNDS [2-30]

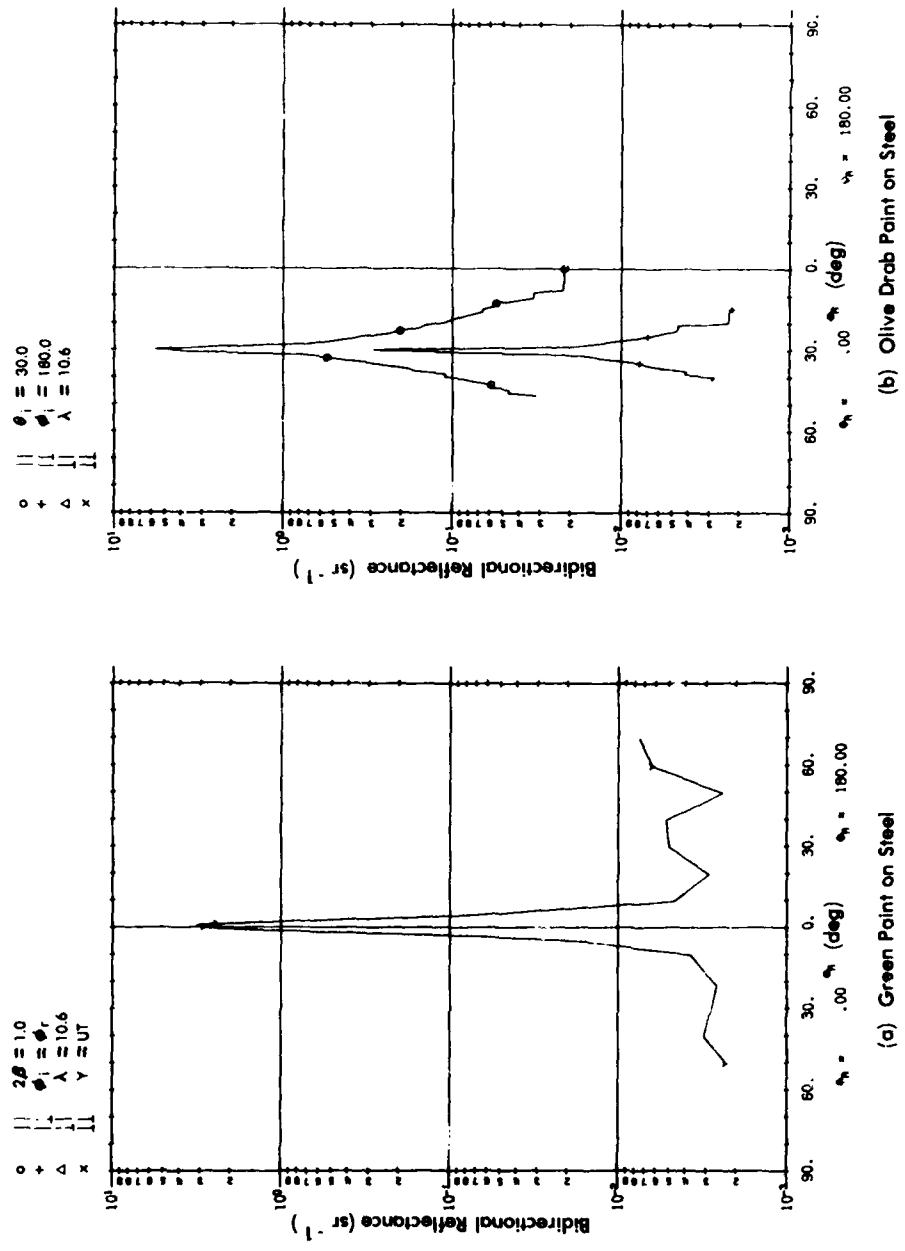

FIGURE 2-24. DIRECTIONAL REFLECTANCE FOR CULTURAL OBJECTS.
Parts (a), (c), and (d) are monostatic; (b) is bistatic with $\theta_i = 30$ deg [2-30]

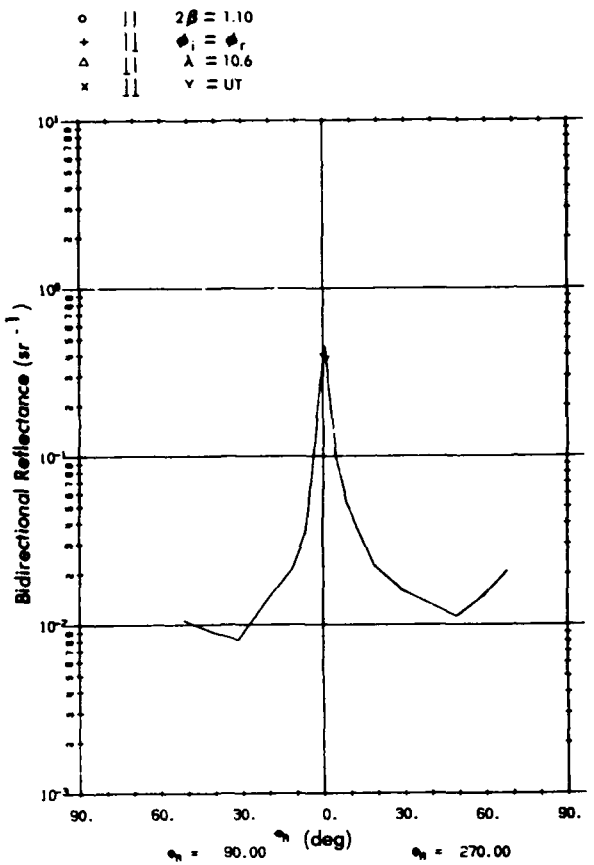

(c) California White Oak Block

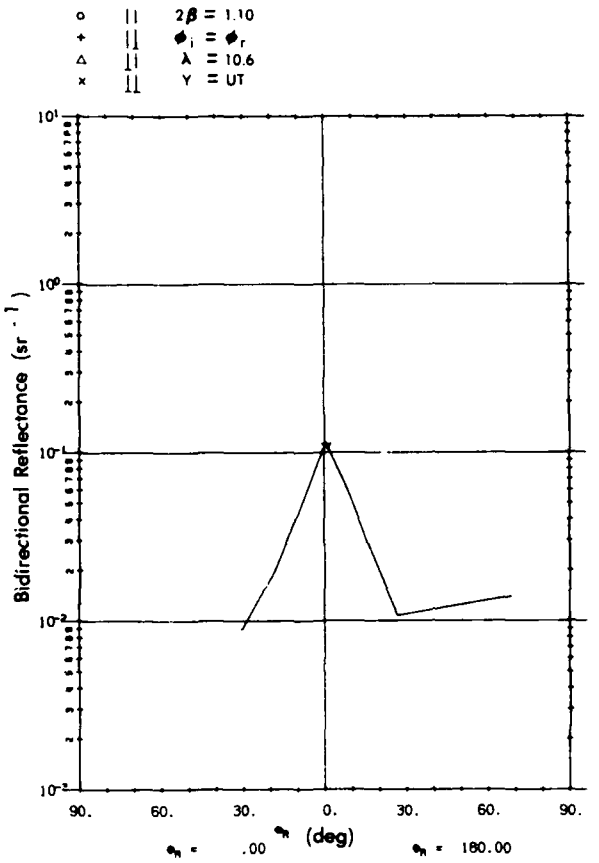

(d) Olive Drab Paint on Aluminum

FIGURE 2-24. DIRECTIONAL REFLECTANCE FOR CULTURAL OBJECTS (Continued) [2-30]

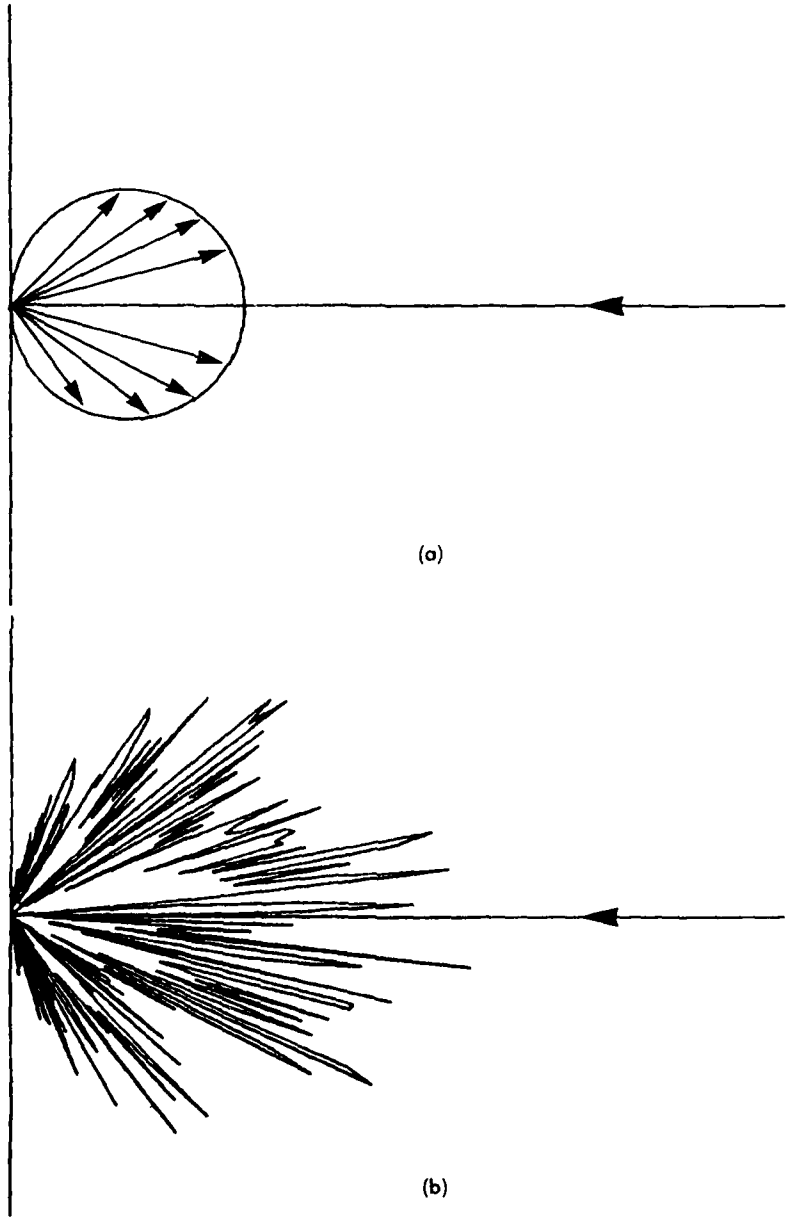

FIGURE 2-25. SCATTERED INTENSITY PATTERN OF A ROUGH SURFACE ILLUMINATED WITH (a) INCOHERENT RADIATION AND (b) COHERENT RADIATION

from a laser, the scattered rays are similarly spread in all directions but possess random phases and interfere with each other in a statistical way. If the total scattered radiation reaching a particular point in space interferes in a predominantly constructive manner, then a high intensity is exhibited at that point. If the individual rays interfere to produce a net cancellation of energy, then a low intensity is exhibited. Figure 2-25(b) shows the spatially distributed intensity variations for a laser-illuminated rough surface. A screen placed so as to intercept the scattered radiation would exhibit a granular or speckled pattern of irradiance. The spatially averaged intensity follows the cosine law; the intensity variations follow Rayleigh statistics; and the highest spatial frequency is determined by the size of the illuminating beam. (See Reference [2-31].)

The rough surface may be considered to be a random reflection grating. Fourier decomposition of this grating results in sinusoidal phase gratings with line spacings at the molecular level all the way up to a maximum Fourier component corresponding to the maximum dimension of the illuminated spot, i.e., the lowest spatial frequency. The amplitude of the continuum of spatial Fourier components is random down to the low spatial frequency cutoff. The superposition of the corresponding diffracted orders results in the random (Rayleigh) intensity distribution, classified as speckle. The highest spatial frequency in the speckle pattern is determined by the lowest frequency grating. The speckle frequency spectrum is therefore flat up to a cutoff frequency equal to $S/\lambda R$ where S is the diameter of the illuminating beam and R is the distance from the point of observation to the illuminated diffuse reflector. A "single speckle" or

---

[2-31] J. C. Dainty (ed.), Laser Speckle and Related Phenomena, Springer-Verlag, New York, NY 1975.

correlation cell therefore has a size of $\lambda R/S$, that is, inversely proportional to the diameter of the illuminated spot.

This speckle effect can degrade the imagery generated by an active sensor by imparting this granularity to the images on a pixel-by-pixel basis. If the receiver aperture is smaller than a speckle or correlation cell, then a diffusely reflecting target having a uniform reflectivity yields an image where the intensity for each pixel varies in a random manner but with a mean value which is proportional to the target's reflectivity. Comparing pixels, one can say that the speckle-signal-to-noise ratio is equal to one. If the receiver aperture area is N times larger than a correlation cell, then N correlation cells appear in the image plane and a detector element gathering all of these speckles spatially averages the radiant power. The pixel-to-pixel variation is therefore smoothed and the speckle-signal-to-noise ratio is equal to $\sqrt{N}$. This aperture averaging is valid for direct detection active systems but is not appropriate for heterodyne detection systems. Since the heterodyne process detects the electric field, E, of the signal radiation rather than its intensity or power, and since the phase of the E-field varies in a random manner from speckle to speckle, the net E-field also varies in a random manner when several speckles are added. The net result is that the speckle-signal-to-noise for a heterodyne sensor is equal to one, independent of the aperture or detector sizes.

2.6 DETECTION

The receiver for an active sensor (See References [2-32 and 2-33].) is in many ways identical to a passive sensor. Both gather radiation originating from the scene using reflective or refractive optics and focus it down on a single detector element or an array of elements. Registration between the detector IFOV and the laser-illuminated spot in the scene is, of course, critical for an active sensor, but does not apply to a passive one. Narrow bandpass filters centered at the laser wavelength are usually placed in front of the detector of an active sensor such that laser scattered radiation is detected and background radiation is rejected. The background radiation is undesirable not only because a target signature may be different for the passive radiation but also because it can contribute to the shot noise.

Detectors of laser radiation in the visible, NIR or thermal IR are essentially the same as for passive sensors. Table 2-2 presents some of the common lasers, their wavelengths of operation, and corresponding detectors.

[2-32] M. Ross, Laser Receivers, John Wiley and Sons, New York, NY, 1966.

[2-33] C. G. Bachman, Laser Radar Systems and Techniques, Artech House, Dedham, MA, 1979.

TABLE 2-2. CANDIDATE LASERS AND DETECTORS FOR ACTIVE IMAGING SENSORS

Lasers	Wavelength (μm)	Detectors	
HeCd		PM Tube*	Si
Kr			
Dye	0.4 - 0.7		
Ar*	0.4880 0.5145		
Double YAG	0.532		
HeNe*	0.6328		Si/APD*
GaAs*	0.85	Red enhanced PM Tubes	
Nd:YAG*	1.06		
Ho:YLF	2.0	InAs	
HF	2.6 - 3.1		
DF	3.5 - 3.8	InSb	
CO	5		
CO_2*	9 - 11	HgCdTe* PbSnTe	

*Used in active imaging systems which have been built to date.

Detector response time requirements for conventional sensors are dictated by the dwell time on a pixel or reselm just as for a passive sensor. For an active imaging sensor employing a single detector element, the dwell time may be on the order of 0.5 μsec requiring a detector with a bandwidth in excess of 1 MHz, a requirement easily achieved by all of the detectors in the table.

More complex heterodyne and 3D imaging systems have more stringent requirements on detector speed. For heterodyne systems (Section 2.6.2), the detector behaves like a mixer and must respond to an IF from tens to hundreds of megahertz. Similarly, for a 3D system (Section 2.7), the detector must be fast enough to respond efficiently to the modulation frequency of the laser radiation. This modulation may range from a few hundred kilohertz to as high as several hundred megahertz.

2.6.1 Direct Detection

Figure 2-26 presents a schematic diagram of an active laser sensor with appropriate parameters indicated. Laser radiation with average output power, P_L, propagates through the transmitter optics and is directed to the scene by the scan mechanism (object plane scanning as presented in the figure). Radiation which reaches the target is reflected by the scene either diffusely, specularly, or a mixture of the two. For the particular type of material being illuminated, and for its orientation with respect to the line-of-sight, a monostatic

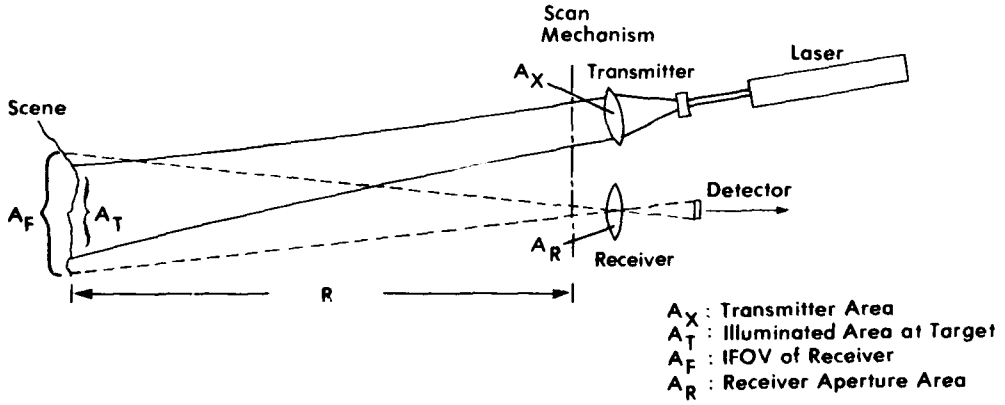

FIGURE 2-26. SENSOR GEOMETRY

bidirectional reflectance, ρ', is defined. (For example, a 30% diffuse reflector has a ρ' of 0.1 sr^{-1}, where $\rho' = \rho/\pi$. If it is not completely diffuse but has a specular lobe, $\rho' > 0.1\ sr^{-1}$ near normal incidence and $\rho' < 0.1\ sr^{-1}$ for more grazing angles.)

Laser radiation reaching the target scene contains radiant power equal to

$$\Phi_T = \Phi_L \tau_X \tau_A \tag{2-30}$$

where τ_X and τ_A are the transmissions of the transmitter optics and atmospheric path, respectively. This power is concentrated in a spot of area A_T*.

Scattered radiation which is gathered by the receiver aperture of area A_R is

$$\Phi_S = \Phi_L \tau_X \tau_A^2 \rho' \frac{A_R}{R^2} \tau_R \eta_B \tag{2-31}$$

where R = the range to the target (R^2 has the same units as A_R such that A_R/R^2 is the solid angle Ω_R (sr) of the receiver aperture with respect to the scene element)

---

*As discussed in "Beam Truncation", under Section 2.3.1, a circular Gaussian beam which is even slightly truncated by the transmitter optics has an illumination pattern at the target which resembles an Airy pattern. The diameter of the spot should be based upon the Airy distribution rather than the Gaussian one. For example, a Gaussian beam which is truncated at its $1/e^2$ intensity points by the transmitter telescope of diameter D_x has a half-irradiance diameter of (λ/D_x) R at the target, and <u>not</u> 0.75 (λ/D_x) R as would be obtained with no truncation. Loss of only 13% of the beam power at the telescope results in a roughly 2X reduction of the power density at the scene.

τ_R = the transmission of the receiver optics including the scan mechanism and any spectral filter

η_B = transmitter/receiver beam overlap factor

If the area of the laser spot at the target, A_T, is less than the IFOV of the detector, A_F, then $\eta_B = 1$; if not, $\eta_B = A_F/A_T$.*

The signal radiation is converted to signal current, i_S, by the detector a

$$i_S = \Phi_S R \tag{2-32}$$

where R is the detector current responsivity in A W^{-1}.

The performance of an active sensor depends not only upon an adequate signal level but also upon low noise. The various noise mechanisms were discussed in Section 1.0 and include:

(1) photon-induced shot noise due to signal radiation and background radiation (and local oscillator radiation in the case of heterodyne detection).

(2) Johnson (also called Nyquist) or thermal noise.

(3) current noise or 1/f noise (also called excess noise, contact noise modulation noise or flicker noise).

(4) generation-recombination noise in photoconductors noise in photoconductors.

*More precisely,

$$\eta_B = \frac{\int_{A_F} E_T da}{\int_{\infty} E_T da} = \frac{\int_{A_F} E_T da}{P_T}$$

where E_T is the irradiance or laser power density distribution at the target in W m^{-2}, and where uniformity of response over the detector area is assumed.

(5) shot noise in junction devices (photovoltaic detectors, i.e., photodiodes) or photoemissive devices (photomultiplier tubes).

For a photovoltaic detector, the mean-square noise current can be expressed as

$$\langle i_n \rangle^2_{PV} = 2eI\Delta f + 4kT\Delta fG \qquad (2\text{-}33)$$

where e = charge on an electron
Δf = information bandwidth
T = temperature of the detector
G = the conductance of the detector
I = total diode current (including photocurrent due to signal radiation, Φ_S, and background radiation, Φ_B, incident upon the detector, as well as dark current, I_D,)

$$I = (\Phi_S + \Phi_B)R + I_D \qquad (2\text{-}34)$$

The first term in Equation (2-33) is often referred to as the shot noise and is a combination of photon-induced shot noise and electronic shot noise. The second term is the Johnson thermal noise term. The T is often replaced by an effective temperature, T_e, to include the noise introduced by the detector's preamplifier. If the preamplifier has a noise figure of F (expressed in dB), then

$$T_e = T + 290\left(10^{F/10}-1\right) \qquad (2\text{-}35)$$

where all temperatures are expressed in K.

The mean-square noise current for a photoconductive detector is

$$\langle i_n \rangle^2_{PC} = 2e\Delta f\left(\Phi_S+\Phi_B\right)R + \frac{2\tau\Delta f\ I^2}{N\left(1+\omega^2\tau^2\right)} + 4kT\Delta fG \qquad (2\text{-}36)$$

where the first noise term is photon noise and the second noise term is due to generation-recombination noise (discussed in Section 1). At equilibrium in a photoconductor, the total noise power of both photon and generation-recombination noise (the first two terms of Equation (2-36)) can be no less than twice the photon noise power. That is, at best,

$$\langle i_n \rangle_{PC}^2 = 4e\Delta f\left(\Phi_S+\Phi_B\right)R + 4kT\Delta fG \qquad (2\text{-}37)$$

Infrared detector performance is often characterized by D* expressed in cm $Hz^{1/2}$ W^{-1} as

$$D^* = \frac{\sqrt{A_d\Delta f}}{NEP} \qquad (2\text{-}38)$$

where A_d is the detector element area (cm^2) and NEP is the noise equivalent power of the detector (W) and entails the blackbody photon noise and Johnson noise. The mean-square noise current for a photovoltaic or a photoconductive detector is, therefore,

$$\langle i_n \rangle^2 = 2\ e\Delta f\Phi_S R + \frac{A_d\Delta f}{D^{*2}} R^2 \qquad (2\text{-}39)$$

The second term is found to dominate for detectors in the thermal IR. The signal photon noise becomes of significance in the intermediate IR and can be the dominant noise mechanism in the near IR. In the intermediate and thermal IR spectral regions, blackbody emission from the detector surroundings and from the scene are the dominant sources of background photons, and the resulting photon noise is included in the D* value. In the near IR and visible, however, one must additionally be concerned with background photon noise due to reflected or scattered solar radiation. The Φ_S in Equation (2-39) should, where applicable, be replaced by $\Phi_S + \Phi_B'$, the signal power plus solar

background power reaching the detector, to account for this additional background noise component.

The power signal-to-noise ratio for the sensor equals the ratio of mean-square signal and noise currents as

$$\left(\frac{S}{N}\right)_{power} = \frac{\Phi_S^2 R^2}{\frac{A_d \Delta f}{D^{*2}} R^2 + 2e\Delta f\left(\Phi_S + \Phi_B\right) R} \tag{2-40}$$

The rms signal-to-noise ratio is the square root of this,

$$\left(\frac{S}{N}\right)_{rms} = \sqrt{\left(\frac{S}{N}\right)_{power}} \tag{2-41}$$

The term $(S/N)_{rms}$ is often used as a performance parameter for visible and near IR sensors. The term $(S/N)_{power}$ is often used for heterodyne sensors due to their similarity to microwave and RF radars where decibels (dB) are common units. Confusion can result when power or rms is not explicitly specified.

In the visible and near IR, shot noise often dominates the detection process. If adequate spectral filtering or nighttime operation can suppress the background radiation at the detector to a value significantly below the signal radiation, the familiar shot noise or quantum-noise-limited expression results:

$$\left(\frac{S}{N}\right)_{rms} = \frac{\Phi_S R}{2e\Delta f} \tag{2-42}$$

Current responsivity may be expressed as

$$R = \eta \frac{e}{h\nu} = \eta \frac{e\lambda}{hc} \tag{2-43}$$

where η = the quantum efficienty of the detector
h = Planck's constant (6.626×10^{-34} J sec)
ν and λ = the frequency and wavelength, respectively, of the received radiation

Responsivity (A W^{-1}) is the efficiency with which photons, $h\nu$, are converted to electrons, e. Shot-noise-limited operation is readily achieved with photomultiplier tubes by virtue of the low dark current and noiseless amplification inherent in the electron multiplication process.

If Equation (2-43) is substituted into Equation (2-42),

$$\left(\frac{S}{N}\right)_{rms} = \eta \frac{\Phi_S}{h\nu\Delta f} \tag{2-44}$$

Since $\Phi_S/h\nu$ is the number of photons per second reaching the detector and $\eta\Phi_S/h\nu$ is the number of photoelectrons generated per second, shot-noise-limited operation means that the signal-to-noise ratio equals the number of photoelectrons generated per unit frequency interval.

As one goes deeper into the IR, detector noise usually dominates over photon-induced shot noise such that Equation (2-40) becomes

$$\left(\frac{S}{N}\right)_{power} = \frac{\Phi_S^2}{\left(A_d \Delta f / D^{*2}\right)} \tag{2-45}$$

or

$$\left(\frac{S}{N}\right)_{rms} = \frac{\Phi_S}{NEP} \tag{2-46}$$

Since photon-induced shot-noise-limited operation is quantum limited, it provides the highest S/N for a given return signal. In an active IR sensor which is detector noise limited, one is able to

AD-A120 044 INFRARED INFORMATION AND ANALYSIS CENTER ANN ARBOR MI F/G 17/5
IRIA STATE-OF-THE-ART REPORT: OPTICAL-MECHANICAL, ACTIVE/PASSIV--ETC(U)
MAY 82 C T DUE, L M PETERSON N00014-77-C-0125
UNCLASSIFIED IRIA-153200-2-T-1 SBI-AD-E750 695 NL

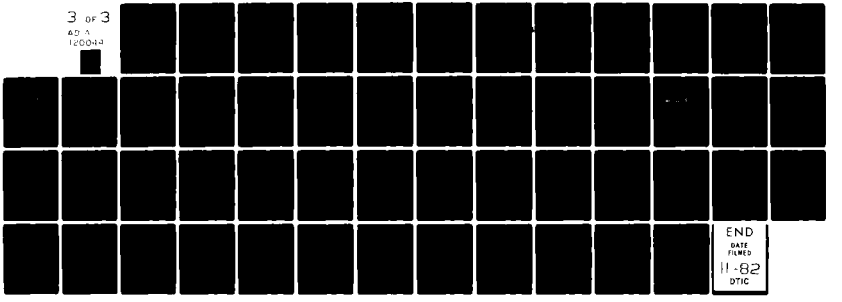

utilize the coherence of the laser radiation to suppress the detector noise in order to achieve quantum limited operation. This is called coherent or heterodyne detection. Since the energy, $h\nu$, of a far IR photon may be an order of magnitude smaller than a near IR photon, Equation (2-44) shows that the $(S/N)_{power}$ can be two orders of magnitude larger for the far IR.

2.6.2 Heterodyne Detection

Heterodyne detection, sometimes called coherent detection, is analogous to superheterodyne receiver systems found in electronics. (See References [2-34]; also [2-35], pp.252-263, and [2-36].) Signal radiation is mixed with local oscillator radiation and the difference frequency becomes the carrier of the information. If the local oscillator is sufficiently intense, detector noise can be suppressed and photon-induced shot noise in the local oscillator radiation predominates. In radio frequency systems, the radiation is truely coherent and the wavelength is long. In optical systems, however, the radiation can be made coherent and frequency stable with some effort, and the physically short wavelengths lead to stringent phase front alignment requirements.

[2-34] D. Fink, "Coherent Detection Signal-to-Noise," Applied Optics, Optical Society of America, Washington, DC, Volume 14, March 1975, pp. 689-690.

[2-35] B. J. Peyton, A. J. DiNardo, G. M. Kanischak, F. R. Arams, R. A. Lange, and E. W. Sard, "High-Sensitivity Receiver for Infrared Laser Communications," IEEE Journal of Quantum Electronics, Institute of Electrical and Electronics Engineers, New York, NY, Volume QE-8, No.2, 1972.

[2-36] J. F. Shanley, "n-p(Hg,Cd)Te Photodiodes for Infrared Heterodyne Applications," Status Report, Honeywell Radiation Center, Lexington, MA, 1980.

where η = the quantum efficienty of the detector
h = Planck's constant (6.626×10^{-34} J sec)
ν and λ = the frequency and wavelength, respectively, of the received radiation

Responsivity (A W^{-1}) is the efficiency with which photons, $h\nu$, are converted to electrons, e. Shot-noise-limited operation is readily achieved with photomultiplier tubes by virtue of the low dark current and noiseless amplification inherent in the electron multiplication process.

If Equation (2-43) is substituted into Equation (2-42),

$$\left(\frac{S}{N}\right)_{rms} = \eta \frac{\Phi_S}{h\nu\Delta f} \tag{2-44}$$

Since $\Phi_S/h\nu$ is the number of photons per second reaching the detector and $\eta\Phi_S/h\nu$ is the number of photoelectrons generated per second, shot-noise-limited operation means that the signal-to-noise ratio equals the number of photoelectrons generated per unit frequency interval.

As one goes deeper into the IR, detector noise usually dominates over photon-induced shot noise such that Equation (2-40) becomes

$$\left(\frac{S}{N}\right)_{power} = \frac{\Phi_S^2}{\left(A_d \Delta f / D^{*2}\right)} \tag{2-45}$$

or

$$\left(\frac{S}{N}\right)_{rms} = \frac{\Phi_S}{NEP} \tag{2-46}$$

Since photon-induced shot-noise-limited operation is quantum limited, it provides the highest S/N for a given return signal. In an active IR sensor which is detector noise limited, one is able to

Heterodyne Systems

The schematic of a typical optical heterodyne detection system is shown in Figure 2-27. Laser radiation is directed toward the target which reflects some of the radiation back to the receiver. This weak signal radiation is collected by the receiver objective and is focussed onto the detector. Local oscillator (LO) radiation is also directed to the detector where it can mix with the signal. The LO radiation may originate from a second laser which is frequency locked to the transmitter laser (See Figure 2-27(a).) such that a constant offset frequency, $\Delta\omega$, is maintained. Or, as shown in Figure 2-27(b), part of the transmitter radiation may be sampled by beam splitter, BS, and frequency shifted (up or down), usually by a traveling wave acousto-optic modulator, M, although electro-optical modulators and moving reflector Doppler shifters have been used. Whichever LO technique is chosen, the LO and signal radiation are combined using a partially reflecting mirror (typically a few percent), or beam combiner, BC, as shown in the figures.

If there is relative motion along the line-of-sight between the scene and the sensor, the Doppler shift due to this motion may be used to provide the desired offset frequency for heterodyne detection. If the sensor and scene are moving toward each other, the signal radiation is up-shifted by an amount

$$\Delta\nu = \frac{\Delta\omega}{2\pi} = 2\,\frac{v_{||}}{c} = 2\,\frac{v_{||}}{\lambda} \qquad (2\text{-}47)$$

where $v_{||}$ is the component of velocity parallel to the line-of-sight and c is the speed of light in air. For a sensor traveling at the speed of sound, $v_{||} = 346\ \text{m sec}^{-1}$, and $\Delta\nu$ is about 70 MHz for a radiation wavelength of 10.6 μm.

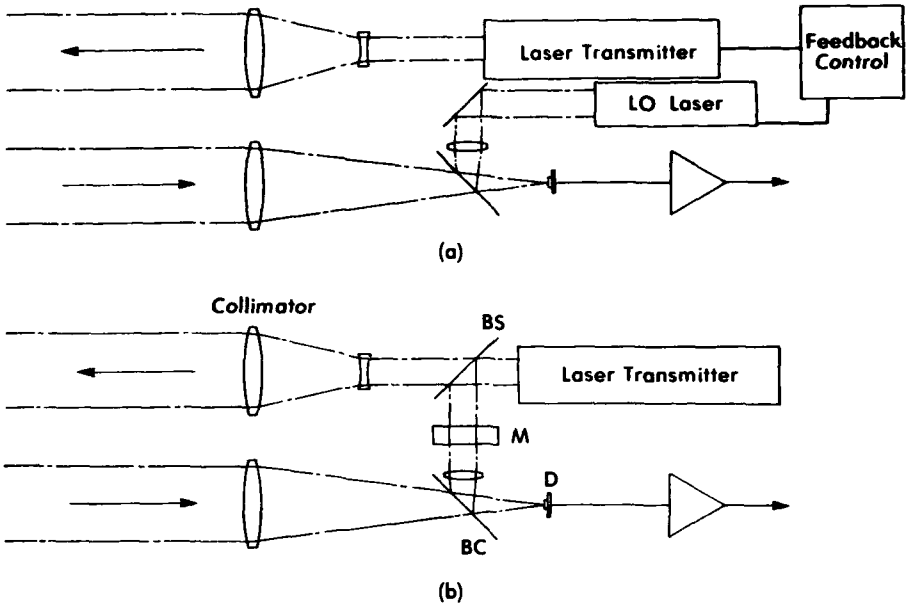

FIGURE 2-27. OPTICAL HETERODYNE DETECTION USING A SINGLE LASER AND A FREQUENCY SHIFTER IN (a) AND USING A SEPARATE LOCAL OSCILLATOR LASER IN (b)

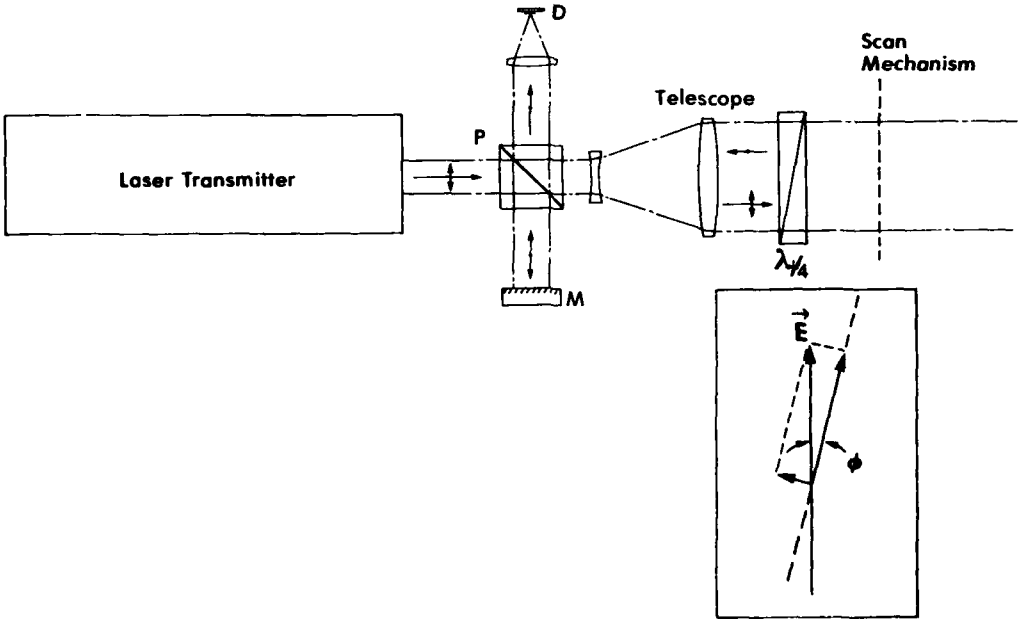

FIGURE 2-28. A COMMON APERTURE HETERODYNE SENSOR

Common Aperture Sensor

Transmit/receive multiplexing to utilize a common optical aperture is also possible using frequency and polarization division as presented schematically in Figure 2-28. If the polarizing element, P, is slightly detuned by an angle, ϕ, such that the linearly polarized laser radiation is resolved into orthogonal components (See figure inset.) with, for example, a 97:3 intensity ratio, the local oscillator radiation is provided by the 3% component which is directed to mirror M and the remaining 97% of the radiation is propagated to the target scene by the scan mechanism. For a 10 W laser, 300 mW of LO is directed to M and back again to the polarization element. If that element has an extinction of 99:1, only 3 mW will pass through to the detector. Since local oscillator power on the order of milliwatts provides the desired shot-noise-limited operation, and since tens of milliwatts can saturate or destroy the detector, this is an appropriate LO power. The presence of the quarter wave plate, $\lambda/4$ in Figure 2-28, results in circularly polarized radiation propagating to the target. If the radiation is not depolarized during its interaction with the target, it returns as circularly polarized radiation but of opposite rotation (See References [2-14 and 2-16].) such that radiation passing back through the quarterwave plate is of a polarization orthogonal to the transmitted polarization. The polarization element, which was highly transmitting for the laser radiation, is now highly reflecting for the signal radiation and directs all but about 4% of the return signal to the detector. If radiation is depolarized by the scattering process, it passes on to the laser and almost none reaches the detector. (The quarter wave plate may be removed from the sensor making it sensitive only to the depolarized component of the scattered signal radiation. In this case, strong glints may be suppressed but the diffuse return may be extremely weak.)

Theory

The electromagnetic waves of the signal and LO beams interact or interfere such that the total E-field, E_T, at the detector is

$$E_T = E_S \cos \omega_S t + E_L \cos \omega_L t \tag{2-48}$$

where S and L refer to signal and LO respectively, and where radial frequency $\omega = 2\pi\nu$. Since the detector current, i, is proportional to the total intensity of the radiation

$$\begin{aligned} i = \kappa E_T^2 &= \kappa\left[E_S^2 \cos^2 \omega_S t + E_L \cos^2 \omega_L t + 2 E_S E_L \cos\omega_S t \cos\omega_L t\right] \\ &= \kappa \left[E_S^2 \cos^2 \omega_S t + E_L \cos^2 \omega_L t + E_S E_L \cos \left(\omega_S+\omega_L\right)t \right. \\ &\quad \left. + E_S E_L \cos(\omega_S-\omega_L)t\right] \end{aligned} \tag{2-49}$$

where κ is the proportionality constant. Since the detector cannot respond to optical frequencies, the first three terms are averaged to dc currents and the last term oscillates at the intermediate frequency, $\Delta\omega$, such that

$$\begin{aligned} i &= \kappa \left[\frac{1}{2} E_S^2 + \frac{1}{2} E_L^2 + 0 + E_S E_L \cos \Delta\omega t\right] \\ &= i_{dc} + i_{IF} \end{aligned} \tag{2-50}$$

Or, rewriting

$$i = i_{dc}\left[1 + \frac{2 E_S E_L \cos \Delta\omega t}{E_S^2 + E_L^2}\right] \tag{2-51}$$

Since the LO is much stronger than the signal radiation, $E_L >> E_S$, and

$$i \doteq i_{dc}\left[1 + 2 \frac{E_S}{E_L} \cos \omega\Delta t\right] \tag{2-52}$$

the rms current is therefore

$$\langle i_{IF}^2 \rangle^{1/2} = \frac{\sqrt{2}}{2} \quad 2\left(\frac{E_S}{E_L} i_{dc}\right)$$

$$= \sqrt{2}\sqrt{\frac{\Phi_S}{\Phi_L}}\, i_{dc} \tag{2-53}$$

where Φ_S and Φ_L are optical powers (W). Knowing the current responsivity, $R(A\ W^{-1})$, of the detector, one gets

$$i_{dc} \doteq R \quad \Phi_L \tag{2-54}$$

such that the mean square current is

$$\langle i_{IF}^2 \rangle = 2\, \frac{\Phi_S}{\Phi_L} \left(R\, \Phi_L\right)^2$$

$$= 2\, \Phi_S \Phi_L\, R^2 \tag{2-55}$$

Note that the IF signal current can be increased by increasing the LO power Φ_L.

Most heterodyne systems employ photovoltaic rather than photoconductive detectors due to their high frequency response. The noise current as discussed in Section 2.6.1 is, therefore, due to photon noise, Johnson or thermal noise, and amplifier noise:

$$\langle i_n^2 \rangle = 2\, e \left(\Phi_L + \Phi_S\right) R\Delta f + 2\, e\, \Delta f\, I_{dark} + 4\, k\, T_e\, \Delta f\, G \tag{2-56}$$

where Δf is the system bandwidth ($\Delta f = 1/2\ \tau$ where τ is the dwell time in scanning systems or pulse duration in pulsed systems), and T_e is the effective temperature of the detector and takes into account the noise figure of the IF amplifier. The conductance of the detector, G, is in general frequency dependent. (See Reference [2-36].) At low and moderate frequencies, G is equal to the reciprocal of the detector shunt impedance, R_D, but at high frequencies (large $\Delta\omega$), G rolls off as $1 + (\Delta\omega)^2 C^2 R_S R_D$ where C and R_S are the junction capacitance and series

resistance respectively of the photovoltaic detector. (See Reference [2-36].)

The power signal-to-noise ratio is, therefore,

$$\left(\frac{S}{N}\right)_{power} = \frac{2\Phi_S \Phi_L R^2}{2e \Phi_L R \Delta f + 2e \Delta f I_{dark} + 4 k T_e \Delta f G} \qquad (2\text{-}57)$$

where, again, $\Phi_L >> \Phi_S$. It can be seen that the effects of detector noise can be eliminated entirely by increasing the local oscillator power such that the signal level increases and therefore S/N increases also, up to the point where local oscillator shot noise dominates over detector noise. When

$$\Phi_L >> \frac{2 k T_e G}{e R} + \frac{I_{dark}}{R} \qquad (2\text{-}58)$$

(Φ_L is on the order of milliwatts), Equation (2-57) simplifies to

$$\left(\frac{S}{N}\right)_{power} = \frac{\Phi_S R}{e \Delta f} = \frac{\Phi_S}{h\nu \Delta f} \qquad (2\text{-}59)$$

where the current responsivity is

$$R = \frac{\eta e}{h\nu} \qquad (2\text{-}60)$$

and η = the quantum efficiency of the detector

$\nu = \omega/2\pi$ = the radiation frequency

h = Planck's constant

By setting S/N = 1 and solving for Φ_S, one can see that this is a quantum-limited detection system, i.e.,

$$\Phi_S^{min} = \frac{h\nu}{\eta} \Delta f \qquad (2\text{-}61)$$

It should be noted that although milliwatts of LO power are desirable to optimize the S/N, the power density on a small detector element is

about 1 W cm^{-2} and is near the saturation or damage level for many detectors*.

2.6.3 Heterodyne versus Nonheterodyne Performance

A comparison of the performance equations for heterodyne detection and those for direct detection shows that the former provides orders of magnitude improvement. Examining Equation (2-40), one sees that for large enough signal radiation, Φ_S, the photon-induced shot noise due to the signal dominates. In this limit, Equations (2-40) and (2-59) are identical and no advantage in signal-to-noise ratio is achieved for the heterodyne system. (In fact, the complexity of a heterodyne system and the difficulty in approaching the theoretical S/N makes heterodyning less desirable.) As signal level drops, the signal-to-noise ratio for both systems falls linearly with Φ_S. For direct detection, however, a point is reached where the detector noise or background photon-induced shot noise dominates over the signal photon-induced shot noise. From this point on, the signal-to-noise ratio falls as Φ_S^2 for direct detection, but it falls only as Φ_S for heterodyne detection. Figure 2-29 shows this effect for a detector with a D* of 2×10^{10} cm Hz W^{-1}, an area, A_d, of 4×10^{-4} cm^2 and a system with a 1 MHz bandwidth. Whether the detector is background limited or thermal noise limited will affect the break-point in the figure, but not its general form. Signal photon-induced shot-noise-limited operation has a slope of one and detector-noise-limited operation has a slope of two. The minimum detectable power for a heterodyne detector having a quantum efficiency of 20% is

*The damage threshold for photovoltaic HgCdTe detectors is approximately 5 W cm^2. (See Reference [2-36].)

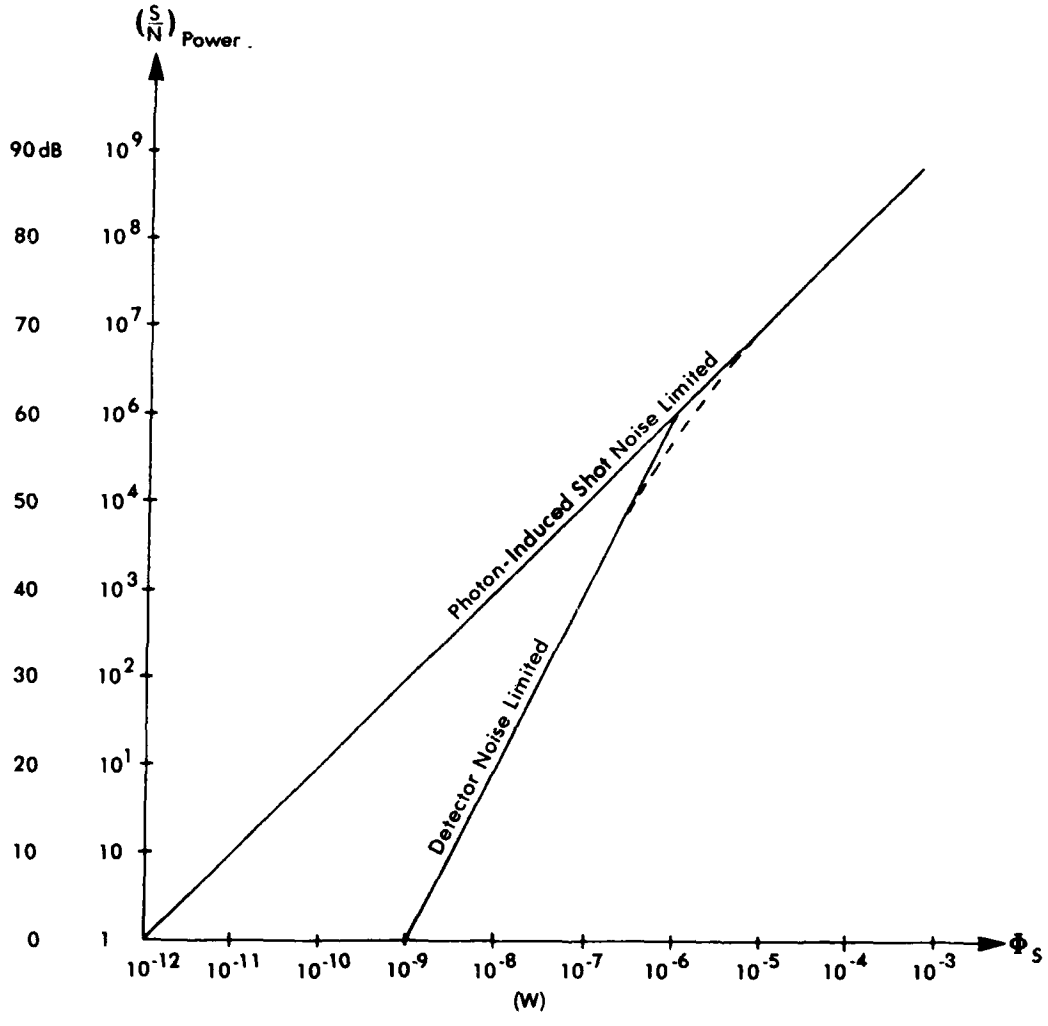

FIGURE 2-29. SIGNAL -TO-NOISE RATIO AS A FUNCTION OF RECEIVED SIGNAL POWER FOR HETERODYNE AND NONHETERODYNE RECEIVERS

$$\left(\Phi_S^{min}\right)_{het} = \frac{h\nu\,\Delta f}{\eta} = (NEP)_{het} = 10^{-13} \quad (W) \tag{2-62}$$

and, for detector-noise-limited direct detection, is

$$\left(\Phi_S^{min}\right)_{direct} = \frac{\sqrt{A_d \Delta f}}{D^*} = (NEP)_{direct} = 10^{-9} \quad (W) \tag{2-63}$$

The theoretically achievable improvement in sensitivity is therefore 4 orders of magnitude (i.e., 40 dB). Since Φ_S^{min} varies linearly as the bandwidth for a heterodyne system and as the square root of bandwidth for a direct detection system, the improvement is less pronounced for a higher bandwidth system and more pronounced if the bandwidth is lower. The theoretical limit has been demonstrated experimentally in the laboratory, but achieving this in practice is difficult due to several practical limitations inherent in the detection process. These are discussed below.

Practical Constraints

The heterodyne detection system is a very sensitive system. With sufficient LO power, the signal IF current from the detectors can be made high and the signal-to-noise ratios can be made several orders of magntiude larger than for a similar nonheterodyne system. In addition, background radiation is virtually eliminated without the need of an optical (IR) filter. Only radiation which lies within $\pm \frac{1}{2} \Delta f$ of $(\nu_L \pm \Delta\nu)$ beats with the LO such that the detected signal current is passed by the IF amplifier and IF filter. Background radiation is therefore suppressed as though an optical filter of width $2\,\Delta f$ ($\sim 10^6$ Hz $\sim 10^{-2}$ Å at 10 μm) were placed in front of the detector.

Unfortunately, the heterodyne detection system is not only sensitive to low level signals which carry information of interest, it is also very sensitive to:

(1) signal and LO beam alignment.
(2) frequency stability of the LO with respect to the received signal.
(3) stray radiation (usually due to scattered transmitter radiation).
(4) speckle noise.

Phase Front Alignment

Equation (2-48), describing the superposition of the signal and local oscillator radiation fields, was obtained with the assumption that the wave fronts were perfectly aligned. That is, their respective propagation vectors, $\vec{k}_S$ and $\vec{k}_L$, (where $\vec{k}_i$ is perpendicular to the wavefront and $|\vec{k}_i| = 2\pi/\lambda_i$) were assumed parallel such that at any particular time their waves interfered to create a single fringe. If the wave fronts are at an angle, θ, with respect to each other, so are their k-vectors, and interference fringes are generated in space. Each of these interference fringes possesses a beat frequency, $\Delta\nu$, but adjacent bright and dark fringes are 180 deg out of phase with each other in time. If a fringe is much larger than the detector dimension, the beat signal from the detector has maximum amplitude. However, as

the fringe size and detector size become comparable, the beat amplitude (which produces the heterodyne IF current) decreases and becomes equal to zero when one complete fringe cycle is found on the detector.

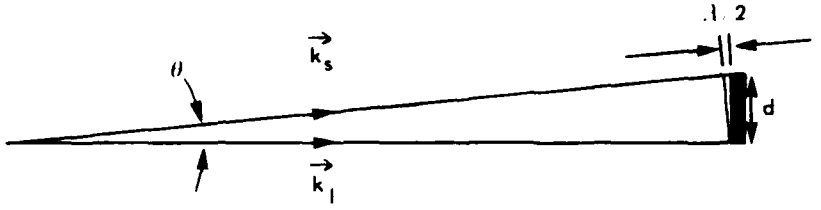

FIGURE 2-30. SIGNAL AND LOCAL OSCILLATOR BEAMS ARE MISALIGNED BY AN ANGLE, θ

With the aid of Figure 2-30, which depicts a misalignment corresponding to one-half of a fringe cycle, θ is

$$\theta \triangleq \sin \theta = \frac{\lambda}{2d} \tag{2-64}$$

where θ is expressed in radians. This is about the maximum misalignment which the heterodyne system can tolerate. If the misalignment is double this value, no signal is obtained; and, of course, alignment which is better than this value is desirable. For most purposes, the above is adequate to establish tolerances or to estimate performance. As an example, if λ = 10 μm and d = 0.2 mm then the wave fronts must be aligned to better than about 50 mrad or 3 deg. (In the visible the tolerance is only 3 mrad or 1/7 deg.) More precisely, an alignment efficiency factor, η_a, which has the familiar Airy distribution for a circular detector, is

$$\eta_a = \left[\frac{2\, J_1(\pi\, \theta\, d/\lambda)}{\pi\, \theta\, d/\lambda}\right]^2 \tag{2-65}$$

where J_1 is the first order Bessel function and the first zero is at $\theta = 1.22\ \lambda/d$.

The above discussion assumes that both the signal and LO radiation exist as plane wave fronts at the detector. Since the wave fronts at the waist (of a lens for example) are plane parallel, a detector placed at the waist of both the LO beam and the signal beam allow the two sets of waves to interfere as described. In fact, if the f-numbers of the two beams are the same such that their wavefronts are matched at the waist and elsewhere, the detector may be placed where the wavefronts are even curved, and the interference will be the same giving good heterodyne performance.

Frequency Stability

The heterodyne detection system is in effect a long path-length-difference Michelson interferometer where a beat frequency is established such that the interference fringes change in time at the IF frequency. However, since relative phase between transmitted and received radiation is unimportant for the heterodyne system, the coherence requirement is relaxed considerably. The coherence length of the laser does not have to exceed twice the range distance as it must in holography or for a true Michelson interferometer.

The requirement which must be met is that the frequency of the optical (IR) radiation cannot change appreciably in the round-trip time of flight of the photons such that the difference frequency moves out of the electronic IF bandpass. Since the radiation frequencies are on the order of 10^{14} Hz and the bandpass is on the order of 10^6 Hz, this is better than a 1 part in 10^8 stability requirement on a time scale of the order of microseconds.*

*A useful rule-of-thumb is that light travels 1 ft in free space in about 1 nsec, or 1 kft (round trip) in 1 μsec.

Stray Radiation

Since the laser transmitter may be operating at tens of watts of output or greater, and since the heterodyne receiver is sensitive to radiation on the order of picowatts and less, any stray radiation (due to scattering or diffraction) which gets into the receiver can generate noise or even obscure the signal entirely. If the sensor is stationary such that the signal radiation and laser output are the same frequency, then radiation scattered from the transmitter optics may enter the receiver or, more importantly for a system utilizing acousto-optical (A-O) shifters for LO radiation, unshifted scattered radiation may "ride along" with the LO beam. Proper baffling to separate the transmitter and receiver optics, and the use of two A-O shifters in series can eliminate the respective problems. The problem of stray radiation is obviated for a moving heterodyne sensor since the return signal differs in frequency from the intense transmitted laser radiation by the Doppler shift. (See "Common Aperture Sensor" in Section 2.6.2.)

Speckle Phenomena

Speckle noise can degrade performance in any system which uses coherent radiation as a source. (See Reference [2-31]; also [2-37], pp.1479-1489.) In a heterodyne receiver, it is even a greater problem because it can limit the signal current level and is not subject to aperture smoothing or averaging. As calculated above, the system

---

[2-37] L. H. Enloe, "Noise-Like Structure in the Image of Diffusely Reflecting Objects in Coherent Illumination," Bell System Technical Journal, American Telephone and Telegraph, Holmdel, NJ, September 1967.

signal-to-noise ratio can be greater for a heterodyne system than for a direct detection system but the degradation in image quality due to the speckle granularity can also be greater for a heterodyne system. On a pixel-by-pixel basis, the ratio of rms fluctuations to mean intensity is one for a heterodyne system.

Since a direct detection sensor detects average intensity impinging on the detector element, the presence of several speckles results in spatial smoothing or averaging of the speckle noise such that the ratio of rms fluctuations to mean intensity is greater than one (numerically equal to the square root of the "number of speckles"). Equation (2-51) shows that a heterodyne detector responds to the signal E-field, E_s, not to its intensity. The presence of several speckles (or correlation cells) on the detector signifies the presence of several independent radiation modes, only one of which can have wave fronts which satisfy Equation (2-64). Therefore, no smoothing results. Although the other modes can mix with the LO, they do so inefficiently. (They correspond to the wings of the Airy distribution, Equation (2-65).) Siegmen (See Reference [2-38], pp.1350-1356.) treats this subject as an antenna problem where the detector is considered as a diffraction-limited transmitting antenna by implementing reciprocity. The antenna lobe of the detector thereby defines that part of the receiver optics which are effective.

To appreciate this more fully, consider a laser transmitter of diameter D_x. Although this beam may have a nearly Gaussian distributon, it will likely be truncated such that the beam propagates to the far field as an Airy pattern (See "Beam Truncation" in Section 2.3.1.) with a full angle divergence of $\theta = 2.44\ \lambda/D_x$. At a range of R

[2-38] A. E. Siegman, "The Antenna Properties of Optical Heterodyne Receivers," Proceedings of the IEEE, Institute of Electrical and Electronics Engineers, New York, NY, Volume 54, No.10, October 1966.

(assumed to be the far field), the spot size at the zeros of the Airy pattern are $S = 2.44\ \lambda R/D_x$. The diffusely scattered radiation from the illuminated spot has speckle correlation cells at the receiver with dimensions of

$$D_s \doteq 2.44\ \frac{\lambda}{S}\ R \qquad (2\text{-}66)$$

$$= D_x$$

Therefore, for a diffraction-limited system, the speckle size is equal to the transmitter dimension*. (This would also be true if other than a circular transmitting aperture had been chosen.) A receiver aperture of diameter D_x is spoken of as a matched aperture.

Rigorous computations based upon the Fresnel-Kirchhoff integral equation (Reference [2-39]) show that increasing the receiver aperture beyond the matched aperture results in a nearly constant heterodyne signal which increases only slowly toward an asymtotic 2X improvement (over that for a matched aperture) as the aperture approaches infinite size. If A_r is the physical area of the receiver aperture, and A_x is the matched aperture size for a diffraction limited system, then the receiver area efficiency, η_A, or relative heterodyne signal, is

$$\eta_A = \frac{1}{1 + \frac{A_x}{A_r}} \qquad (2\text{-}67)$$

which is plotted in Figure 2-31. The effective area, A_e, which should be used in a signal-to-noise computation is, therefore,

---

*Note that the presence of significant aberrations in the optics or turbulence in the propagtion path will decrease the correlation cell or speckle size to a value less than D_x. Turbulence is usually of no consequence at ranges which are typical for imaging sensors.

[2-39] C. Buczek, Consultant, Private Communication, 1981.

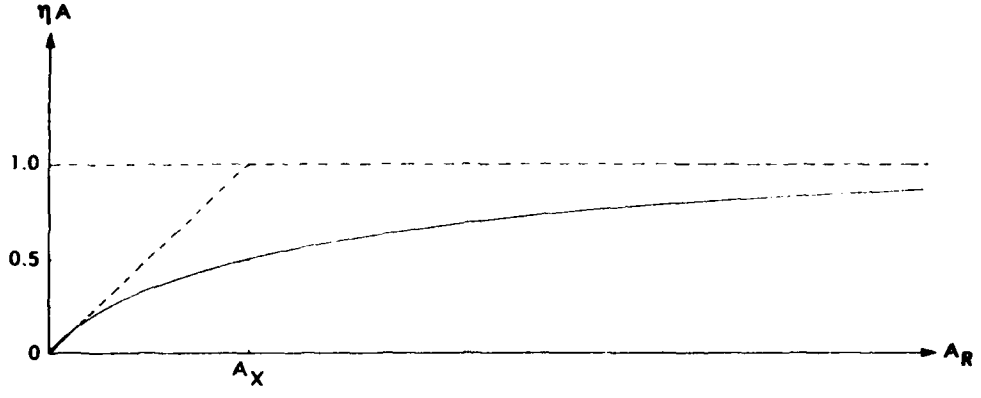

FIGURE 2-31. HETERODYNE RECEIVER APERTURE EFFICIENCY AS A FUNCTION OF PHYSICAL APERTURE AREA

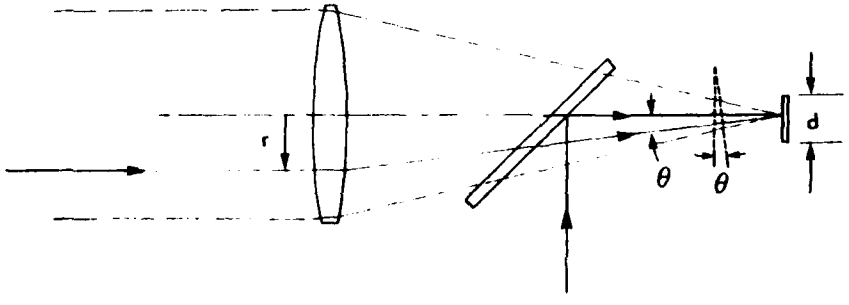

FIGURE 2-32. HETERODYNE RECEIVER GEOMETRY

$$A_e = \eta_A A_x = \frac{A_x}{1 + \frac{A_x}{A_r}} \qquad (2\text{-}68)$$

If $A_r << A_x$, then $A_e = A_r$; if $A_r = A_x$, then $A_e = 1/2\ A_x$; and, if $A_r >> A_x$, then $A_e \ll A_x$.

One can see this intuitively with the aid of Figure 2-32. Consider radiation from a target being gathered by the receiver optics and focused onto the detector. Consider within this bundle of rays, a single ray which is a distance, r, from the optic axis. Consider also a single ray of local oscillator radiation which is combined with the signal using a partially reflecting mirror. This LO ray may be on-axis such that it is at an angle, , with respect to the single signal ray under consideration and such that their wave fronts are also at angle with respect to each other at the detector. Per Figure 2-30 and Equation (2-64), in order for these waves to interfere effectively, must be on the order of $\lambda/2d$ or less, i.e.,

$$\theta \leq \frac{\lambda}{2d} \qquad (2\text{-}69)$$

From Figure 2-31,

$$\theta \doteq \tan\theta = \frac{r}{f} \qquad (2\text{-}70)$$

where r is assumed to be much less than the focal length, f (i.e., a large f-number lens). Combining these two equations,

$$\frac{r}{f} < \frac{\lambda}{2d} \qquad (2\text{-}71)$$

As the receiver aperture diameter is increased from zero to a value of f/d, the heterodyne signal increases almost linearly with aperture area. Beyond a diameter $D = \lambda f/d$, however, the signal level increases only slowly due to poor interference resulting from the additional marginal rays. In such a case the effective receiver aperture

diameter* is approximately

$$D_{eff} \doteq \frac{\lambda f}{d} \tag{2-72}$$

This same effective receiver diameter is obtained by Siegman [2-38] by considering the detector of diameter d as a radiating antenna. Its antenna lobe has an angle (in radians) of

$$\theta_{antenna} \doteq \frac{\lambda}{d} \tag{2-73}$$

Propagating a distance, f, to the receiver optics, the antenna pattern has a diameter of $\lambda f/d$. This defines the effective receiver diameter and is identical to Equation (2-72). Equation (2-73) is the one-dimensional analog to the two-dimensional radar antenna formula

$$\Omega A \leq \lambda^2 \tag{2-74}$$

where Ω = *the solid angle of the antenna lobe*
A = the antenna area
λ = the radar radiation wavelength

For a diffraction-limited sensor, if the IFOV of the detector element matches the illuminated spot at the target, then D_{eff} is equal to D_x, the matched receiver aperture. To summarize, if a heterodyne sensor possesses a diffraction-limited transmitter and receiver, and if the IFOV of the detector matches the illuminated spot at the target, then a correlation cell or speckle at the receiver aperture is equal to the effective receiver aperture. If the actual receiver aperture is larger than the effective receiver aperture, more radiation is gathered. However, the radiation is in the form of several uncorrelated speckles and the signal improvement will not be proportional. In fact, with an infinite receiving aperture, the heterodyne signal only improves by a

*The above description is over-simplified but provides an intuitive description of the effective aperture.

factor of two over that obtained with an aperture size equal to a single correlation cell.

2.7 3D IMAGING SENSORS

The principle behind the Michelson interferometer is the basis for one application of laser technology which has found its way from the laboratory to the industrial shop. This is interferometric metrology using instrumentation based upon the Michelson interferometer with a movable mirror. If the mirror is part of a shop work-piece,that piece may be moved in a straight line and interference fringes may be counted such that the relative positions of the piece can be known to an accuracy of a fraction of a micrometer (each fringe corresponds to motion of one-half the wavelength of the laser radiation).

A similar use of the principle is the basis for the commercially available geodometers or electronic distance meters used to accurately measure distances on a greater scale. A laser is used as the measuring probe, but since its radiation wavelength, λ, is too fine a measuring unit, the laser is amplitude modulated at a frequency, f, to create a new wavelength, $\Lambda = c/f$, where c is the speed of light. If a mirror, retroreflector, or even diffuse reflector at a distant range, R, returns the modulated radiation to the instrument, then the phase of the return compared to that of the transmitted radiation provides a measure of R. In particular, if f is chosen such that $R = \Lambda/2$, then the total round trip path is $2R = \Lambda$ and the return is in-phase with the transmitted radiation as shown in Figure 2-33. If $R = \Lambda/4$, then they are out of phase. In general,

$$\phi = 2\pi \frac{R}{\Lambda/2} \qquad (2\text{-}75)$$

where ϕ is the measured phase angle between the transmitted modulated

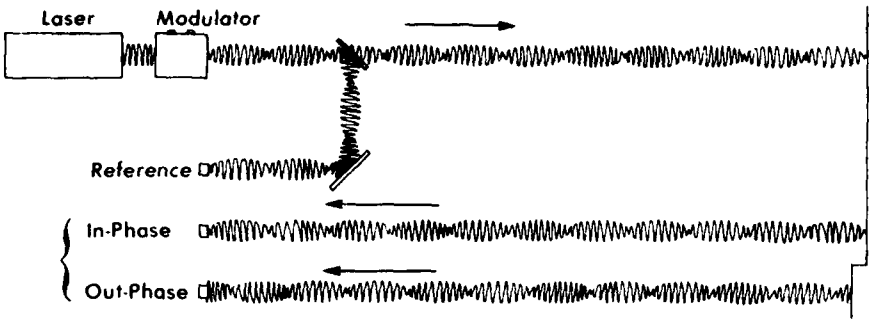

FIGURE 2-33. RANGE MEASURING DEVICE

radiation and the received modulated radiation. If R is less than $\Lambda/2$, and Λ is known, measuring ϕ provides an unambiguous measurement of R.

The phase, ϕ, can realistically be measured with only finite accuracy which affects the accuracy with which R is determined. If Λ is decreased by increasing the modulation frequency, the accuracy by which R can be measured correspondingly improves; but since R is now greater than $\Lambda/2$, more than one value of R can produce the same phase measurement ϕ, i.e.,

$$\phi = m\, 2\pi\, \frac{R}{\Lambda/2} \qquad (2\text{-}76)$$

where m is an integer. This is referred to as range ambiguity.

Selection of more than one frequency of operation allows unambiguous determination of range as well as improved accuracy. For example, if one is interested in measuring ranges up to 5 km and the instrument is capable of measuring phase with an accuracy of 3%, one might select the following modulation frequencies

$$f = 0.03,\ 0.3,\ 3,\ 30,\ \text{and}\ 300\ \text{MHz}$$

with corresponding modulation wavelengths of

$$= 10^4,\ 10^3,\ 10^2,\ 10\ \text{and}\ 1\ \text{m}.$$

With such a system, one could measure R to an accuracy of 3 cm providing that the signal-to-noise ratio is adequate. At such long ranges, it would be necessary to use a retroreflector rather than a diffuse reflecting target within the scene, or to require long integration times to improve the signal-to-noise ratio.

2.7.1 Relative Range Imaging

By integrating such a phase measuring instrument with a scan mechanism, one can measure the range on a point-by-point basis. If the scan mechanism maps out the X and Y directions then the measurement of phase or range can provide Z to yield a 3D image. (See Reference [2-40], p.206; also [2-41], p.259.) Since the dwell time on a particular point or pixel must necessarily be short for a practical system, a powerful laser and a sensitive receiver are required.

If absolute range is not necessary, single frequency operation such that Λ is on the order of the dimension of the objects in the scene is desirable. If the sensor is downward looking, it becomes a height measuring device presenting a scene with vertical relief. If the sensor is forward looking, it can present a scene with depth or shape along the line of sight. If f is chosen such that Λ is much less than the maximum dimension of an object, then strips (or fringes) will appear over the object. If Λ is greater than the maximum dimension, changes in range or phase will correspond to changes in grey scale within the image.

[2-40] D. Nitzan, A. E. Brain, R. O. Duda, "The Measurement and Use of Registered Reflectance and Range Data in Scene Analysis," Proceedings of the IEEE, Institute of Electrical and Electronics Engineers, New York, NY, Volume 65, No.2, 1977.

[2-41] R. O. Duda, D. Nitzan, P. Barrett, "Use of Range and Reflectance Data to Find Planar Surface Regions," IEEE Transactions on Pattern Analysis and Machine Intelligence, Institute of Electrical and Electronics Engineers, New York, NY, Volume PAMI-1, No.3, July 1979.

Figure 2-34 shows how some simple geometrical figures would appear to a 3D sensor if illuminated from above. The fringes in practice do not necessarily have sharp edges as drawn, but have an intensity distribution which varies from zero to a maximum.

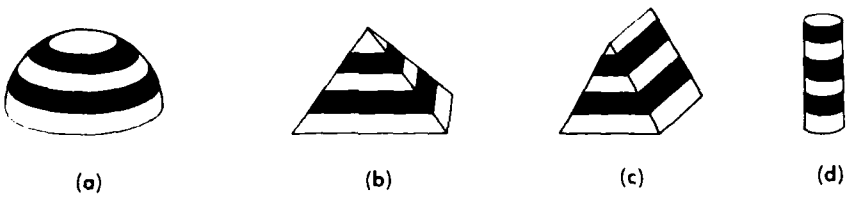

FIGURE 2-34. ISORANGE CONTOURS OR FRINGES ON SIMPLE GEOMETRICAL SHAPES

2.7.2 Laser Modulation

Modulation of the laser source is an important factor in a 3D sensor. (See Reference [2-42], p.3176.) The modulation should be done efficiently to maintain average laser power and to provide the maximum amplitude of modulation at the desired frequency. The most straight-forward method is loss modulation of the radiation after it exits the laser. More difficult but more efficient methods operate within the laser cavity, i.e., intracavity mode-locking, cavity dumping and high repetition rate Q-switching. Achieving modulation rates on the order of 0.1 to 100 MHz precludes the use of optical-mechanical chopping. Acousto-optical (A-O) and electro-optical (E-O) techniques are better suited for these frequencies.

[2-42] S. R. Robinson and R. C. Chapuran, "Modulation Techniques for an Airborne Laser Scanner," Applied Optics, Optical Society of America, Washington, DC, Volume 18, 15 September 1979.

Placement of a voltage-driven E-O crystal and a polarization analyzer in the output beam of a laser as shown in Figure 2-35(a) provides a means of controlling the intensity of that beam. (See Reference [2-5 through 2-7].) If no voltage is applied, the polarized laser radiation is passed by the polarization analyzer. As the voltage in increased, it rotates the polarization of the radiation such that part of the energy is rejected by the polarization analyzer. If the voltage applied to the E-O device is amplitude modulated, then the laser beam is amplitude modulated at the same frequency. Since the transfer characteristics for E-O devices are nonlinear, weak side bands or harmonics are generated in addition to the fundamental frequency.

E-O modulators can be used from dc up to several hundred MHz. However, practical problems develop at higher frequencies, especially when high average laser powers are needed. Since the voltages required to achieve good modulation depths are in the kilovolt range, RF heating can induce refractive index changes in the E-O crystal to degrade performance. This may be further compounded by absorptive heating if high average power laser radiation is being modulated. Practical considerations associated with heating, external cooling, and RFI must be addressed by the 3D system designer.

The A-O device is an attractive alternative to E-O modulation. Figure 2-35(b) presents a typical traveling wave A-O modulator. Amplitude modulation of the laser radiation is achieved by amplitude modulating the RF driver to the device. A typical RF drive frequency of 50 MHz produces a 50 MHz acoustic wave in the device via the acoustic transducer bonded to the acoustic cell. This acoustic wave behaves as a moving phase grating such that radiation is diffracted out of the laser beam. If the acoustic wave has the proper strength (See Reference [2-5].), nearly 100% of the radiation can be deflected out of the primary beam. If the 50 MHz carrier is amplitude modulated (AM) at frequency f, the transmitted laser radiation is modulated at the same frequency. Just as for the E-O device,

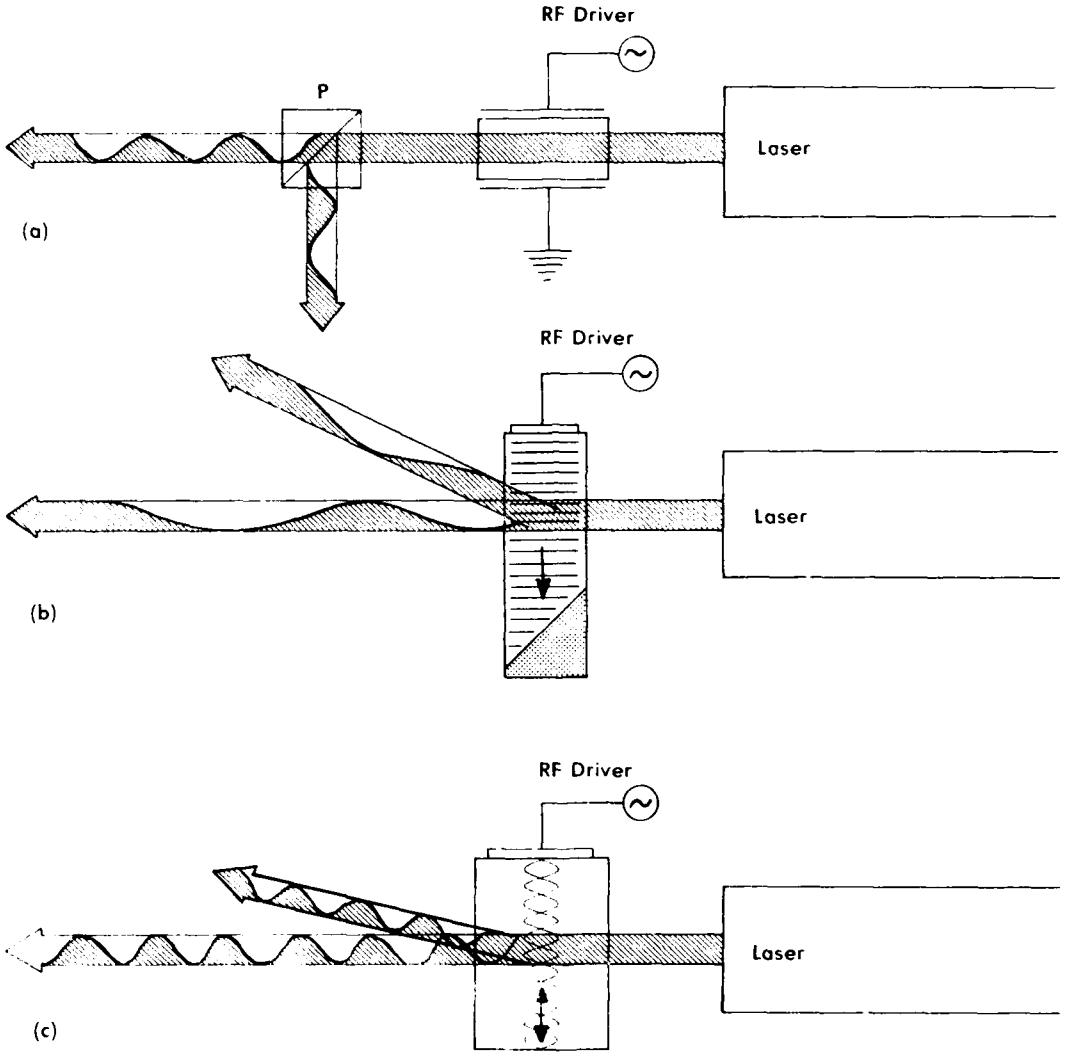

FIGURE 2-35. AMPLITUDE MODULATION OF LASER RADIATION USING (a) E-O, (b) TRAVELING WAVE A-O, AND (c) STANDING WAVE A-O TECHNIQUES

the nonlinear transfer characteristics of an A-O device mean that a sinusoidal AM produces modulated laser radiation which deviates somewhat from a pure sinusoid.

Traveling wave A-O modulators also have practical considerations which can limit the maximum achievable modulation frequencies. Since the acoustic wave has a finite propagation velocity, the acoustic transit time across the laser beam is the limiting factor. Since the upper frequency limit is equal to the sound velocity in the cell divided by the laser beam width, one simply needs to focus the beam to a smaller size such that the modulation frequency is increased. This may be done with low power laser radiation until diffraction effects dominate; but with high average power lasers, cell damage limits the amount of allowable focusing. In fact, for the powers required for active sensors, beam expansion rather than focusing is usually required. If focusing is allowed, the upper frequency limit is about 100 MHz, and if beam expansion is required, it is less than 1 MHz. The latter frequency limit is too low for many 3D sensors and the traveling wave A-O device may not be applicable.

A less conventional A-O device is the standing wave A-O modulator. As shown in Figure 2-35(c), the acoustic wave which is launched from the transducer is allowed to reflect back upon itself to set up an acoustic standing wave. Unlike the traveling wave device which has an AM carrier, the standing wave device has a constant amplitude carrier. Interference between the downward and the upward going acoustic waves results in the collapsing (i.e., destructive interference) of the acoustic wave twice per RF cycle. When the acoustic wave collapses, the transmission of the A-O cell is nearly 100%. When the acoustic wave is finite, radiation is deflected out of the laser beam. The laser radiation is nearly sinusoidally modulated (again due to the nonlinear transfer characteristics) at a frequency which is twice that of the RF drive frequency.

The standing wave A-O modulator is a resonant device and therefore has advantages and disadvantages. Since the acoustic wave is reflected back and forth within the cell, the acoustic wave becomes strong such that only modest RF drive power is required to achieve efficient modulation compared to a similar traveling wave device. However, this strong superposition of acoustic waves is only possible for selected acoustic wavelengths, or modes, which are resonant with the dimensions of the cell (i.e., $L = m \Lambda/2$ where L is the length of the acoustic cell, m is an integer, and Λ is the acoustic wavelength). Unlike the traveling wave device which is continuously tunable from dc to its upper frequency cutoff, the standing wave device is limited to the frequency band of the acoustic transducer and only those frequencies within that band which are resonant with the cell dimensions. In essence, it is a single frequency device well suited for 3D sensor applications but of limited use elsewhere.

Laser intracavity modulation has the potential for providing efficient and frequency diverse laser output for 3D sensing. Q-switching, mode-locking, cavity dumping and pulse transmission mode fall into this category. Since the key to high signal-to-noise ratio is high average power, these intracavity techniques should be performed without loss of overall laser efficiency. In addition, the pulsed output can be resolved into (Fourier) frequency components which are multiples of the pulse repetition frequency to aid in removing the ambiguity problem. Also, the power spectrum associated with a laser pulse train can be as much as a factor of four greater than a sine-wave-modulated laser beam possessing the same average power. Given a particular cw laser, if extracavity loss modulation is employed, the average power will at best drop by a factor of two. If, however, that same laser were intracavity modulated to produce a repetitively pulsed output whose average power remained the same, not only would the signal-to-noise ratio be greater by a factor of 2 than the extracavity system, but the power spectral component S(f) would also be greater by as much as a factor of four. The potential improvement, in the

rms signal-to-noise ratio can be 8X for an intracavity pulse-modulated 3D sensor over an extracavity loss-modulated one.

Preservation of the average laser output has been demonstrated using mode-locking of the Nd:YAG laser (See Reference [2-43], pp.650-653.) and high repetition rate Q-switching of the CO_2 laser. (See Reference [2-44], pp.4910-4912.) Cavity dumping of the CO_2 laser is presently being pursued although overall efficiency remains a problem. (See Reference [2-45].) In order for cavity-dumping and Q-switching to be of value for a 3D imaging sensor, the pulse repetition rate must be equal to or greater than the pixel rate. Also, in order for the m^{th} harmonic to be useful for phase/range detection, the pulse width should be on the order of or less than the reciprocal of the desired Fourier component. For example, if a 15 m ambiguity interval is desired, one would choose a modulation frequency, f, of 10 MHz. If the desired pixel rate is 10^6 sec^{-1}, then a Q-switched laser with repetition rate in excess of 10^6 pps and with pulses of duration less than 0.1 μsec would be appropriate. With such a laser, absolute (unambiguous) range could be determined by pulse time-of-flight or by phase detection at both 1 and 10 MHz.

2.7.3 Phase Detection

Determination of the relative range to a particular pixel in the target can be accomplished by measuring the relative phase between the

---

[2-43] L. M. Peterson and D. C. Carmer, "A Highly Stable 30 Watt Average Power Mode-Locked Nd:YAG Laser," IEEE Journal of Quantum Electronics, Institute of Electrical and Electronics Engineers, New York, NY, Volume QE-16, No.6, June 1980.

[2-44] S. Marcus and J. W. Caunt, "Compact CO_2 Laser for Infrared Heterodyne Radar," Review of Scientific Instruments, American Institute of Physics, New York, NY, Volume 49, No.10, 1978.

[2-45] L. A. Newman, L. M. Laughman, P. P. Chenausky, N. N. Hoffman and R. A. Hart, "Coherent Modulated Source Development Program," Technical Report Number AFWAL-TR-R81-924406, Air Force Wright Aeronautical Laboratories, Wright Patterson AFB, OH, 1981.

transmitted radiation and the return signal radiation. (See Reference [2-46], p.775.) Since the modulation frequency may be as high as 100 MHz, fast response detection is required. A reference wave may be obtained by sampling some of the outgoing radiation and directing it to a fast detector, or the reference wave may be derived directly from the modulator driver. In the case of a standing acoustic wave modulator or for mode-locking, the RF drive frequency must be doubled in order to provide a reference voltage wave of equal frequency to that of the signal wave. Received signal radiation is converted to an electrical wave with a high speed detector and compared to the reference wave using an electronic phase detector.

The accurate transformation of phase into third dimension or range information requires linearity of response and rapid transition from 2 to zero (snap-back) as shown in Figure 2-36. It also requires that the phase detection process be signal-level independent such that a high reflectivity target and a low reflectivity one at the same range provide the exact same phase output. These aspects of phase linearity, phase snap-back and amplitude-phase cross-talk (or conversion) are important considerations in the design of a 3D imaging sensor.

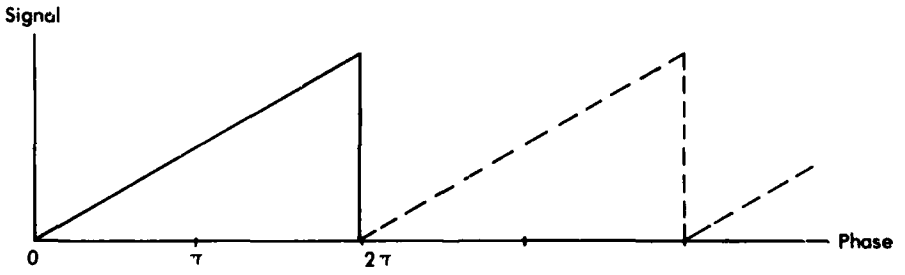

FIGURE 2-36. 3D IMAGERY SIGNAL AS A FUNCTION OF RANGE OR PHASE

[2-46] S. R. Robinson and W. D. Strautman, "Spatial Filtering Design Considerations for a Line Scanning Sensor," Applied Optics, Optical Society of America, Washington, DC, Volume 18, 15 March 1979.

The amplitude-phase conversion is particularly problematic for a far IR 3D system. Due to the spectular nature of targets in the far IR, targets which are near normal have extremely strong returns, and those that are significantly off-normal have extremely weak returns. This large dynamic range of return signals emphasizes the importance of minimizing the amplitude-phase conversion in the detection process. The presence of a diffusely reflecting object reduces the effects of specular returns, but leads to intensity variations due to speckle. Although the dynamic range may not be as large as for specular targets, intensity variations due to speckle are random and occur on a pixel-by-pixel basis making intensity variations the rule rather than the exception.

2.7.4 Signal-to-Noise Ratio

The signal-to-noise ratio for an active 3D system is basically the same as presented in Section 2.6 but modified to account for the modulation/demodulation in the phase detection process. Modifying Equation (2-40), one has

$$\left(\frac{S}{N}\right)_{power} = \frac{\langle i_S \rangle^2}{\langle i_n \rangle^2} = \frac{\Phi_S^2 R^2 \, 2S(f)}{2e\Delta f\left(\Phi_S + \Phi_b\right) R + NEP^2 R^2} \qquad (2\text{-}77)$$

where S(f) is the power spectrum component at modulation frequency f and the 2 accounts for the double-sided (i.e., positive and negative frequencies) spectrum. In calculating the return signal radiation, Φ_S, from Equation (2-32), average modulated laser power should be used for Φ_L. For example, if a 10 W laser is sinusoidally loss modulated with 100% efficiency, the average power, Φ_L, is about 5 W and 2S(f) is 0.5. If the laser is efficiently mode-locked (or cavity-dumped or Q-switched) to produce a train of short pulses with a time-averaged power output of 10 W, Φ_L is 10 W and 2S(f) is slightly less than 2 at the fundamental frequency (i.e., the pulse repetition rate). If higher harmonics of the mode-locked train are used, 2S(f) decreases with increasing frequency.

For a 3D system which employs photon-induced shot-noise-limited heterodyne detection, Equation (2-59) is similarly modified to

$$\left(\frac{S}{N}\right)_{power} = \frac{\langle i_S \rangle^2}{\langle i_n \rangle^2} = \frac{\Phi_S R}{e\Delta f} 2S(f) \tag{2-78}$$

In this case, the electronic detection is additionally complex. After heterodyne detection, the phase information rides on the modulation or carrier frequency which in turn rides on the heterodyne beat frequency or IF.

The accuracy with which the range is measured is determined by the accuracy with which the phase is measured. The range error, σ_R (standard deviation), also referred to as the noise-equivalent range change or NEΔR, is

$$\sigma_R = \frac{c}{2\omega} \frac{1}{\sqrt{2(S/N)_{power}}} \tag{2-79}$$

where ω is the modulation frequency in rad sec^{-1} and c is the speed of light. Rewriting,

$$\sigma_R = \frac{\Lambda}{(4\pi\sqrt{2})(S/N)_{rms}} = 0.11 \frac{\Lambda/2}{(S/N)_{rms}} \tag{2-80}$$

where $\Lambda/2$ is the ambiguity interval. These equations for σ_R should be accurate for $(S/N)_{rms}$ in excess of 6.

REFERENCES

Volume I, Section 2

[2-1] W. F. Matthews and R. F. Jung, "Laser Line Scanning Sensors", Optical Engineering, Society of Photographic and Instrumentation Engineers, Palos Verde Estates, CA, Volume 14, No.2, 1975, pp. 116-119.

[2-2] M. E. Bair, Environmental Research Institute of Michigan, Ann Arbor, MI, Private Communication, 1981.

[2-3] L. D. Green, Electro-Optical Systems Division, Xerox Corporation, Pasadena, CA, Private Communication, 1981.

[2-4] D. C. Carmer and M. E. Bair, Environmental Research Institute of Michigan, Ann Arbor, MI, Private Communication, 1981.

[2-5] A. Yariv, Optical Electronics, Holt, Rinehart, and Winston, New York, NY, 1976, 2nd edition; also, A. Yariv, Quantum Electronics, John Wiley and Sons, New York, NY, 1975, 2nd edition.

[2-6] A. E. Siegman, An Introduction to Lasers and Masers, McGraw-Hill, New York, NY, 1971.

[2-7] B. A. Lengyel, Introduction to Laser Physics, John Wiley and Sons, New York, NY, 1971, 2nd edition.

[2-8] O. Svelto, Principles of Lasers, Plenum Press, New York, NY, 1976.

[2-9] A. L. Bloom, Gas Lasers, John Wiley and Sons, New York, NY, 1968.

[2-10] D. C. Sinclair and W. E. Bell, Gas Laser Technology, Holt, Rinehart, and Winston, New York, NY, 1969.

[2-11] C. G. B. Garrett, Gas Lasers, McGraw-Hill, New York, NY, 1967.

[2-12] J. F. Ready, Industrial Applications of Lasers, Academic Press, New York, NY, 1978.

[2-13] H. Kogelnik and T. Li, "Laser Beams and Resonators," Applied Optics, Optical Society of America, Washington, DC, Volume 5, No.10, 1966, pp. 1550-1567; also, R. J. Pressley (ed.), Handbook of Lasers, Chemical Rubber Company, Cleveland, OH, 1971.

[2-14] F. A. Jenkins and H. E. White, Fundamentals of Optics, McGraw-Hill, New York, NY, 1957, 3rd edition.

[2-15] E. Hecht and A. Zajac, Optics, Addison-Wesley, Reading, MA, 1974.

[2-16] M. Born and E. Wolf, Principles of Optics, Pergamon Press, Elmsford, NY, 1975, 5th edition.

[2-17] J. W. Goodman, Introduction to Fourier Optics, McGraw-Hill, New York, NY, 1968.

[2-18] J. J. Degnan and B. J. Klein, "Optical Antenna Gain 2: Receiving Antennas", Applied Optics, Optical Society of America, Washington, DC, Volume 13, 1974, pp. 2397-2401 and 2762.

[2-19] R. A. McClatchey, et al., "Atmospheric Absorption Line Parameters Compilation," Report No. AFCRL-TR-73-0096, Air Force Systems Command, Andrews Air Force Base, Washington, DC, 1973.

[2-20] L. S. Rothman, "AFGL Atmospheric Absorption Line Parameters Compilation: 1980 Version", Applied Optics, Optical Society of America, Washington, DC, Volume 20, No.5, 1981, pp. 791-795.

[2-21] W. L. Wolfe and G. J. Zissis (eds.), The Infrared Handbook, Office of Naval Research, Arlington, VA, 1978. Available from Order Department, Environmental Research Institute of Michigan, Ann Arbor, MI; also, W. L. Wolfe (ed.), Handbook of Military Infrared Technology, United States Government Printing Office, Washington, DC, 1965.

[2-22] R. A. McClatchey and J. E. A. Selby, "Atmospheric Attenuation of Laser Radiation from 0.76 to 31.25 μm," Report No. AFCRL-TR-74-0003, Air Force Cambridge Research Laboratories, Bedford, MA, January 1974.

[2-23] H. G. Hougton and W. R. Chalker, "The Scattering Cross Section of Water Drops in Air for Visible Light," Journal of the Optical Society of America, Optical Society of America, Washington, DC, Volume 39, 1949, p. 955; also, P. W. Kruse, L. D. McGlauchlin, and R. B. McQuistan, Elements of Infrared Technology, John Wiley and Sons, New York, NY, 1962, pp. 181-189.

[2-24] A. J. Arnulf, J. Bricard, E. Cure and C. Veret, "Transmissions by Haze and Fog in the Spectral Region 0.35 to 10 Microns," Journal of the Optical Society of America, Optical Society of America, Washington, DC, Volume 47, 1957, p. 491.

[2-25] F. Rosell and G. Harvey (eds.), "The Fundamentals of Thermal Imaging Systems", Report 8311, EOTP No.46, Naval Research Laboratory, Arlington, VA, May 1979.

[2-26] P. Hasell, L. Peterson, F. Thomson, E. Work and F. Kriegler, "Active and Passive Multispectral Scanner for Earth Resources Applications: AAFE," Report No. 115800-49-F, Environmental Research Institute of Michigan, Ann Arbor, MI, June 1977.

[2-27] R. J. Mongeon, W. J. Green, and H. H. Naidich, "Laser Obstacle Terrain Avoidance Warning System (LOTAWS)," AD B034 319L, United Technology Research Center, Hartford, CT, November 1978.

[2-28] C. M. Sonnenschein and F. A. Horrigan, "Signal-to-Noise Relationships for Coaxial Systems that Heterodyne Backscatter from the Atmosphere," Applied Optics, Optical Society of America, Washington, DC, Volume 10, 1971, pp. 1600-1604.

[2-29] P. Beckman and A. Spizzichino, The Scattering of Electromagnetic Waves from Rough Surfaces, Macmillan Company, New York, NY, 1963.

[2-30] IST Staff, "Target Signature Analysis Center: Data Compilation," Willow Run Laboratories of the Institute of Science and Technology, Report No. IST 3221-41-B, AD 904 999L (I), AD 905 000L (II), The University of Michigan, Ann Arbor, MI, Volumes I and II, October 1972.

[2-31] J. C. Dainty (ed.), Laser Speckle and Related Phenomena, Springer-Verlag, New York, NY, 1975.

[2-32] M. Ross, Laser Receivers, John Wiley and Sons, New York, NY, 1966.

[2-33] C. G. Bachman, Laser Radar Systems and Techniques, Artech House, Dedham, MA, 1979.

[2-34] D. Fink, "Coherent Detection Signal-to-Noise," Applied Optics, Optical Society of America, Washington, DC, Volume 14, March 1975, pp. 689-690.

[2-35] B. J. Peyton, A. J. DiNardo, G. M. Kanischak, F. R. Arams, R. A. Lange, and E. W. Sard, "High-Sensitivity Receiver for Infrared Laser Communications," IEEE Journal of Quantum Electronics, Institute of Electrical and Electronics Engineers, New York, NY, Volume QE-8, No.2, 1972, pp.252-263.

[2-36] C. T. Flanagan and J. F. Shanley, "Heterodyne Photodiode Array Development and Characterization," Report No. 8012-8, AD B055 927L, Honeywell Electro-Optics Operations, Lexington, MA, December 1980.

[2-37] L. H. Enloe, "Noise-Like Structure in the Image of Diffusely Reflecting Objects in Coherent Illumination," Bell System Technical Journal, American Telephone and Telegraph, Holmdel, NJ, September 1967, pp. 1479-1489.

[2-38] A. E. Siegman, "The Antenna Properties of Optical Heterodyne Receivers," Proceedings of the IEEE, Institute of Electrical and Electronics Engineers, New York, NY, Volume 54, No.10, October 1966, pp. 1350-1356.

[2-39] C. Buczek, Consultant, Private Communication, 1981.

[2-40] D. Nitzan, A. E. Brain and R. O. Duda, "The Measurement and Use of Registered Reflectance and Range Data in Scene Analysis," Proceedings of the IEEE, Institute of Electrical and Electronics Engineers, New York, NY, Volume 65, No.2, 1977, p. 206.

[2-41] R. O. Duda, D. Nitzan and P. Barrett, "Use of Range and Reflectance Data to Find Planar Surface Regions," IEEE Transactions on Pattern Analysis and Machine Intelligence, Institute of Electrical and Electronics Engineers, New York, NY, Volume PAMI-1, No.3, July 1979, p. 259.

[2-42] S. R. Robinson and R. C. Chapuran, "Modulation Techniques for an Airborne Laser Scanner," Applied Optics, Optical Society of America, Washington, DC, Volume 18, 15 September 1979, p. 3176.

[2-43] L. M. Peterson and D. C. Carmer, "A Highly Stable 30 Watt Average Power Mode-Locked Nd:YAG Laser," IEEE Journal of Quantum Electronics, Institute of Electrical and Electronics Engineers, New York, NY, Volume QE-16, No.6, June 1980, pp. 650-653.

[2-44] S. Marcus and J. W. Caunt, "Compact CO_2 Laser for Infrared Heterodyne Radar," Review of Scientific Instruments, American Institute of Physics, New York, NY, Volume 49, No.10, 1978, pp. 4910-4912.

[2-45] L. A. Newman, L. M. Laughman, P. P. Chenausky, N. N. Hoffman, and R. A. Hart, "Coherent Modulated Source Development Program," Technical Report Number AFWAL-TR-R81-924406, Air Force Wright Aeronautical Laboratories, Wright-Patterson AFB, OH, 1981.

[2-46] S. R. Robinson and W. D. Strautman, "Spatial Filtering Design Considerations for a Line Scanning Sensor," Applied Optics, Optical Society of America, Washington, DC, Volume 18, 15 March 1979, p. 775.

BIBLIOGRAPHY

Volume I, Section 2

Arnulf, A. J., J. Bricard, E. Cure and C. Veret, "Transmissions by Haze and Fog in the Spectral Region 0.35 to 10 Microns," Journal of the Optical Society of America, Optical Society of America, Washington, DC, Volume 47, 1957, p. 491.

Bachman, C. G., Laser Radar Systems and Techniques, Artech House, Dedham, MA, 1979.

Bair, M. E., Environmental Research Institute of Michigan, Ann Arbor, MI, Private Communication, 1981.

Beckman, P. and A. Spizzichino, The Scattering of Electromagnetic Waves from Rough Surfaces, Macmillan Company, New York, NY, 1963.

Bloom, A. L., Gas Lasers, John Wiley and Sons, New York, NY, 1968.

Born, M. and E. Wolf, Principles of Optics, Pergamon Press, Elmsford, NY, 1975, 5th edition.

Buczek, C., Consultant, Private Communication, 1981.

Carmer, D. C. and M. E. Bair, Environmental Research Institute of Michigan, Ann Arbor, MI, Private Communication, 1981.

Dainty, J. C. (ed.), Laser Speckle and Related Phenomena, Springer-Verlag, New York, NY, 1975.

Degnan J,. J. and B. J. Klein, "Optical Antenna Gain 2: Receiving Antennas", Applied Optics, Optical Society of America, Washington, DC, Volume 13, 1974, pp.2397-2401 and 2762.

Duda, R. O., D. Nitzan and P. Barrett, "Use of Range and Reflectance Data to Find Planar Surface Regions," IEEE Transactions on Pattern Analysis and Machine Intelligence, Institute of Electrical and Electronics Engineers, New York, NY, Volume PAMI-1, No.3, July 1979, p. 259.

Enloe, L. H., "Noise-Like Structure in the Image of Diffusely Reflecting Objects in Coherent Illumination," Bell System Technical Journal, American Telephone and Telegraph, Holmdel, NJ, September 1967, pp. 1479-1489.

Fink, D., "Coherent Detection Signal-to-Noise," Applied Optics, Optical Society of America, Washington, DC, Volume 14, March 1975, pp. 689-690.

Flanagan, C. T. and J. F. Shanley, "Heterodyne Photodiode Array Development and Characterization," Report No. 8012-8, AD B055 927L, Honeywell Electro-Optics Operations, Lexington, MA, December 1980.

Garrett, C. G. B., Gas Lasers, McGraw-Hill, New York, NY, 1967.

Goodman, J. W., Introduction to Fourier Optics, McGraw-Hill, New York, NY, 1968.

Green, L. D., Electro-Optical Systems Division, Xerox Corporation, Pasadena, CA, Private Communication, 1981.

Hasell, P., L. Peterson, F. Thomson, E. Work and F. Kriegler, "Active and Passive Multispectral Scanner for Earth Resources Applications: AAFE," Report No. 115800-49-F, Environmental Research Institute of Michigan, Ann Arbor, MI, June 1977.

Hecht, E. and A. Zajac, Optics, Addison-Wesley, Reading, MA, 1974.

Hougton, H. G. and W. R. Chalker, "The Scattering Cross Section of Water Drops in Air for Visible Light," Journal of the Optical Society of America, Optical Society of America, Washington, DC, Volume 39, 1949, p. 955; also, P. W. Kruse, L. D. McGlauchlin, and R. B. McQuistan, Elements of Infrared Technology, John Wiley and Sons, New York, NY, 1962, pp. 181-189.

IST Staff, "Target Signature Analysis Center: Data Compilation," Willow Run Laboratories of the Institute of Science and Technology, Report No. IST 3221-41-B, AD 904 999L (I), AD 905 000L (II), The University of Michigan, Ann Arbor, MI, Volumes I and II, October 1972.

Jenkins, F. A. and H. E. White, Fundamentals of Optics, McGraw-Hill, New York, NY, 1957, 3rd edition.

Kogelnik, H. and T. Li, "Laser Beams and Resonators," Applied Optics, Optical Society of America, Washington, DC, Volume 5, No.10, 1966, pp. 1550-1567; also, R. J. Pressley (ed.), Handbook of Lasers, Chemical Rubber Company, Cleveland, OH, 1971.

Lengyel, B. A., Introduction to Laser Physics, John Wiley and Sons, New York, NY, 1971, 2nd edition.

Marcus, S. and J. W. Caunt, "Compact CO_2 Laser for Infrared Heterodyne Radar," Review of Scientific Instruments, American Institute of Physics, New York, NY, Volume 49, No.10, 1978, pp. 4910-4912.

Matthews, W. F. and R. F. Jung, "Laser Line Scanning Sensors", Optical Engineering, Society of Photographic and Instrumentation Engineers, Palos Verde Estates, CA, Volume 14, No.2, 1975, pp. 116-119.

McClatchey, R. A., et al., "Atmospheric Absorption Line Parameters Compilation," Report No. AFCRL-TR-73-0096, Air Force Systems Command, Andrews Air Force Base, Washington, DC, 1973.

McClatchey, R. A. and J. E. A. Selby, "Atmospheric Attenuation of Laser Radiation from 0.76 to 31.25 μm," Report No. AFCRL-TR-74-0003, Air Force Cambridge Research Laboratories, Bedford, MA, January 1974

Mongeon, R. J., W. J. Green and H. H. Naidich, "Laser Obstacle Terrain Avoidance Warning System (LOTAWS)," AD B034 319L, United Technology Research Center, Hartford, CT, November 1978.

Newman, L. A., L. M. Laughman, P. P. Chenausky, N. N. Hoffman, and R. A. Hart, "Coherent Modulated Source Development Program," Technical Report AFWAL-TR-R81-924406, Air Force Wright Aeronautical Laboratories, Wright-Patterson AFB, OH, 1981.

Nitzan, D., A. E. Brain and R. O. Duda, "The Measurement and Use of Registered Reflectance and Range Data in Scene Analysis," Proceedings of the IEEE, Institute of Electrical and Electronics Engineers, New York, NY, Volume 65, No.2, 1977, p. 206.

Peterson, L. M. and D. C. Carmer, "A Highly Stable 30 Watt Average Power Mode-Locked Nd:YAG Laser," IEEE Journal of Quantum Electronics, Institute of Electrical and Electronics Engineers, New York, NY, Volume QE-16, No.6, June 1980, pp. 650-653.

Peyton, B. J., A. J. DiNardo, G. M. Kanischak, F. R. Arams, R. A. Lange, and E. W. Sard, "High-Sensitivity Receiver for Infrared Laser Communications," IEEE Journal of Quantum Electronics, Institute of Electrical and Electronics Engineers, New York, NY, Volume QE-8, No.2, 1972, pp. 252-263.

Ready, J. F., Industrial Applications of Lasers, Academic Press, New York, NY, 1978.

Robinson, S. R. and R. C. Chapuran, "Modulation Techniques for an Airborne Laser Scanner," Applied Optics, Optical Society of America, Washington, DC, Volume 18, 15 September 1979, p. 3176.

Robinson, S. R. and W. D. Strautman, "Spatial Filtering Design Considerations for a Line Scanning Sensor," Applied Optics, Optical Society of America, Washington, DC, Volume 18, 15 March 1979, p. 775.

Rosell, F. and G. Harvey (eds.), "The Fundamentals of Thermal Imaging Systems", Report 8?11, EOTP No.46, Naval Research Laboratory, Arlington, VA, May 1979.

Ross, M., Laser Receivers, John Wiley and Sons, New York, NY, 1966.

Rothman, L. S., "AFGL Atmospheric Absorption Line Parameters Compilation: 1980 Version", Applied Optics, Optical Society of America, Washington, DC, Volume 20, No.5, 1981, pp. 791-795.

Shanley, J. F., "n-p(Hg,Cd)Te Photodiodes for Infrared Heterodyne Applications", Status Report, Honeywell Radiation Center, Lexington, MA, 1980.

Siegman, A. E., An Introduction to Lasers and Masers, McGraw-Hill, New York, NY, 1971.

Siegman, A. E., "The Antenna Properties of Optical Heterodyne Receivers," Proceedings of the IEEE, Institute of Electrical and Electronics Engineers, New York, NY, Volume 54, No.10, October 1966, pp. 1350-1356.

Sinclair, D. C. and W. E. Bell, Gas Laser Technology, Holt, Rinehart, and Winston, New York, NY, 1969.

Sonnenschein, C. M. and F. A. Horrigan, "Signal-to-Noise Relationships for Coaxial Systems that Heterodyne Backscatter from the Atmosphere," Applied Optics, Optical Society of America, Washington, DC, Volume 10, 1971, pp. 1600-1604.

Svelto, O., Principles of Lasers, Plenum Press, New York, NY, 1976.

W. L. Wolfe (ed.), Handbook of Military Infrared Technology, United States Government Printing Office, Washington, DC, 1965.

Wolfe, W. L. and G. J. Zissis (eds.), The Infrared Handbook, Office of Naval Research, Arlington, VA, 1978. Available from Order Department, Environmental Research Institute of Michigan, Ann Arbor, MI;

Yariv, A., Optical Electronics, Holt, Rinehart, and Winston, New York, NY, 1976, 2nd edition; also, A. Yariv, Quantum Electronics, John Wiley and Sons, New York, NY, 1975, 2nd edition.

APPENDIX A
GLOSSARY OF TERMS

The nomenclature and definitions used to describe optical-mechanical scanners have varied over time and by individual or group. In addition, relatively simple, objectively determinable parameters such as weight can be ambiguous unless there is a list of the equipment included. Noise equivalent temperature difference is now precisely defined in terms of measurement procedure. Yet, for any given system in this report it is not always clear whether the value stated was measured or calculated nor which method of measurement or calculation was used. The following is what the author considers the most widely accepted terminology and definitions, together with applicable symbols, units, and equations.

ABSORPTANCE: The ratio of the power absorbed by a surface to the total radiative power incident on the surface.

ACTIVE SCANNER: One which employs its own source (usually a laser) of illumination radiation.

AFOCAL: An optical system (telescope) which images infinitely distant object points at a minus infinity. The performance of an afocal optical system is specified in terms of its angular magnification.

ALIASING: Spurious signals introduced by electronic sampling of the signal voltage (or current).

APERTURE DIAMETER: The diameter of the bundle of radiation allowed to enter a unobscured circular optical system.

APERTURE STOP: A baffle located in an optical system to physically limit the amount of radiation from the scene passing through the system.

ASPECT RATIO: The ratio of frame width to frame height in a framing imaging system (such as a TV).

AUTOMATIC GAIN CONTROL (AGC): The gain of a video channel or group of channels is automatically adjusted at regular intervals such that the channels will yield the same output for a given input at all times.

BANDWIDTH (Δf): See Equivalent Noise Bandwidth.

CALIBRATION: A process in which the detector is exposed to radiation from a group of sources whose output is known to provide a correlation between the detector output and the level of radiation.

CARBON DIOXIDE LASER: An efficient, high power gas laser whose output can be at several lines in the 9 to 11 μm region. The strongest is the P(20) line at 10.6 μm.

COHERENCE: The property of a laser output whereby the electromagnetic waves of the photons oscillate in phase with each other; leads to interference effects.

COLD SHIELD: A cryogenically cooled shield used in far infrared imaging systems to prevent extraneous radiation from reaching the infrared detectors.

COLD SHIELD EFFICIENCY: The ratio of detectivity obtained with an actual cold shield to the detectivity which would be obtained with an ideal cold shield.

COLLIMATION: Property of low divergence in a beam of radiation. (See Diffraction Limit.)

dc RESTORATION: In an ac-coupled amplifier circuit, signal voltage fluctuations revolve about the average signal level. dc restoration is a process in which the dc level of the ac coupling is reset to absolute voltage while the detector is exposed to a radiative source whose output is constant.

DETECTIVITY (D): Detectivity is defined as the inverse of Noise Equivalent Power (NEP), i.e.,:

$$D = \frac{1}{NEP}$$

DETECTOR: A small piece of material located in the focal plane of the device's optical system which produces an electrical signal when exposed to radiation.

DETECTOR MATERIAL: The radiation sensitive material consituting the detector.

DETECTOR OPERATING TEMPERATURE: The temperature, in Kelvin, at which the detector is operated.

DETECTOR SIZE: The physical dimensions of the photo-sensitive surface area of a detector element.

DETECTOR TYPE: The physical mechanism used by the detector to detect radiation (i.e., photoconductive, photovoltaic, photoemissive, or thermal).

DIFFRACTION LIMIT: (1) the minimum beam divergence which is allowed by the laws of physical optics; (2) the minimum spot size which an ideal lens may focus radiation based upon laws of physical optics.

DIFFUSE REFLECTION: Reflection of radiation by a rough (compared to the wavelength of the radiation) surface whereby reflected rays propagate in all directions according to Lambert's Law.

DISPLAY: Any device or mechanism which converts the video signal from the detector into visible images for interpretation by the observer.

DISTORTION: *Irregularities in the displayed image owing to variations in* the optical system field of view, scan rate changes and other system anomalies.

DIVERGENCE: The angular spreading (increase in transverse dimension) of a beam with propagation distance.

DOPPLER SHIFT: Slight change or shift in the radiation frequency due to relative motion along the line-of-sight between the source and the observer (or reflecting target).

DWELL TIME (τ_d): The length of time required for the image of an infinitely distant point source to be scanned across the detector.

DYNAMIC RANGE: The range of input signal levels that can be accepted by a device without unacceptable saturation or noise in the display.

EFFECTIVE APERTURE AREA (A_o): The geometrical area of the aperture opening that actually permits radiation to pass into the optical system.

EFFECTIVE f/no.: For unobscured circular optics the f/no. is the effective focal length divided by the diameter of the effective aperture area. For obscured optics, the effective f/number can be found from

$$\text{Effective f/no.} = \frac{EFL}{2}\sqrt{\frac{\pi}{A_o}}$$

EFFECTIVE FOCAL LENGTH (EFL): The distance between the last principal plane of an optical system to the focal plane of the system.

ELECTRICAL (INFORMATION) BANDWIDTH (BW): The range of electrical frequencies where the output of an electrical circuit (such as an amplifier) is at least 50% of the maximum output. This is specified by the 50% point (3 dB) frequencies.

EMISSIVITY (ε): The ratio of the amount of radiation emitted by a surface to the amount of radiation emitted by a blackbody with equivalent surface area.

EQUIVALENT NOISE BANDWIDTH (Δf): The equivalent noise bandwidth of a circuit is defined as

$$\Delta f = \frac{1}{G(f_o)}\int_0^\infty G(f)df$$

where $G(f)$ is the power gain at an electrical frequency, f, and $G(f_o)$ is the maximum value of the power gain.

EXTINCTION: Loss of propagating radiation due to the combined effects of absorption and scattering.

FAR FIELD: (1) the region beyond the collimation range of a laser beam where the beam diameter increases linearly with propagation distance, i.e., where wavefronts are spherical; (2) the focus of a lens or mirror.

FAR INFRARED: The spectral region from 6 to 100 μm.

FIELD: Any one of two or more parts into which an image frame is divided in interlaced scanning with a detector array.

FIELD OF VIEW (FOV): For frame-scanning systems, the field of view is the total angular frame imaged, expressed in degrees of elevation and azimuth. For strip mappers, the field of view is the angular width of the strip image (more frequently referred to as the swathwidth).

FIELD RATE: The number of fields scanned per second by the detector array.

FRAME: A single complete picture scanned by the detector.

FRAME RATE: The number of frames scanned per second by the detector array.

GAUSSIAN BEAM: A beam whose transverse intensity distribution is Gaussian. See TEM_{oo} mode.

GALLIUM-ARSENIDE LASER: Semiconductor junction laser whose output is in the 0.8 to 0.9 μm region.

HELIUM-NEON LASER: Common, low power laser at 0.6328 μm.

HETERODYNE DETECTION: Detection where weak signal radiation is beaten against strong local oscillator radiation to achieve amplification and noise suppression.

INSTANTANEOUS FIELD OF VIEW (IFOV): The instantaneous field of view is the field of view of the detector photosensitive region in the object plane. In most cases this is synonymous with spatial resolution and can be found by geometrical optics. The angular IFOV can be found by dividing the detector dimensions by the effective focal length. The solid angular IFOV (ω) is found by dividing the detector sensitive area by the effective focal length squared.

INTERMEDIATE (MID) INFRARED: The spectral region from 3 to 6 μm.

INTERLACE RATIO: The number of scan fields in a frame.

INTERLACE SCANNING: A scanning process in which the distance from center to center of simultaneously scanned lines is greater than two times the nominal line width. Gaps left in the imagery are filled by succeeding scan fields to yield a complete frame.

LASER (Light Amplification by Stimulated Emission of Radiation): A source of UV, visible or IR radiation which is collimated, coherent and monochromatic.

MAGNIFICATION (ANGULAR): The ratio of the apparent angular extent of an image presented to an observer to the angular extent of the corresponding object viewed by the unaided eye.

MICROPHONISM: Generation of electrical noise by vibration of a component or system.

MINIMUM RESOLVABLE TEMPERATURE: A combined measure of resolution and sensitivity in a far infrared imaging system. The smallest temperature difference in a standard periodic test pattern of a given spatial frequency that is resolvable to an observer over an unlimited viewing time.

MULTIPLEXING: The reduction of the multiple outputs of a number of parallel processed detector elements to a single video channel.

NEAR FIELD: The region over which a beam of radiation has little or no divergence and where the wavefronts are parallel (or nearly so).

NEAR INFRARED: The spectral region from 0.7 to 3 μm.

NEODYMIUM YAG LASER: Laser composed of a YAG host crystal (cigarette size) with active neodymium ions. Lasing at 1.064 and 1.34 μm is achieved by optical pumping.

NOISE: Unwanted electrical disturbances superimposed on a useful electrical signal that, in part, obscures the signal.

NORMALIZED DETECTIVITY (D*): Detectivity normalized with respect to detector area and equivalent noise bandwidth:

$$D^* = \frac{D}{\sqrt{A_d \Delta f}}$$

OPTICAL EFFICIENCY: The fraction of incident irradiance in a spectral region of interest that is transmitted through an optical system after suffering losses by absorption, reflection, etc.

OVERSCAN: Points in the scene image are scanned more than once per frame due to overlapping of scan lines.

PIXEL: Picture element for electro-optic generated imagery. (See Reselm.)

RADIOMETRIC SYMBOLS AND UNITS:

TABLE A-1. RADIOMETRIC SYMBOLS AND UNITS

TERM	SYMBOL	DEFINING EQUATION	UNITS
Radiant Energy	Q	--	J
Radiant Density	w	$w = \frac{\partial Q}{\partial V}$	J cm^{-3}
Radiant Flux or Power	Φ	$\Phi = \frac{\partial Q}{\partial t}$	W
Radiant Exitance (radiant flux density emitted by a surface)	M	$M = \frac{\partial \Phi}{\partial A}$	W cm^{-2}
Irradiance (radiant flux density impinging on a surface)	E	$E = \frac{\partial \Phi}{\partial A}$	W cm^{-2}
Radiant Intensity	I	$I = \frac{\partial \Phi}{\partial \omega}$	W sr^{-1}
Fluence	ψ	$\psi = \frac{\partial Q}{\partial A}$	J cm^{-2}
Radiance	L	$L = \frac{\partial \Phi}{\partial \omega \, \partial A \cos\theta}$	W sr^{-1} cm^{-2}

TABLE A-1. RADIOMETRIC SYMBOLS AND UNITS (Continued)

TERM	SYMBOL	DEFINING EQUATION	UNITS
Emissivity	ε	$\varepsilon = \frac{M(T)}{M(T)_{Blackbody}}$	--
Absorptance	α	$\alpha = \Phi_{absorbed}/\Phi_{incident}$	--
Reflectance	ρ	$\rho = \Phi_{reflected}/\Phi_{incident}$	--
Transmittance	τ	$\tau = \Phi_{transmitted}/\Phi_{incident}$	--

where
- T = temperature — K
- V = volume — cm^3
- A = area — cm^2
- ω = solid angle — sr
- θ = angle between line of sight and normal to surface — rad

RAYLEIGH RANGE: Range or distance comprised of the near field.

REGISTRATION: Overlap of the radiation beam which illuminates a target and the IFOV of the receiver in an active sensor.

RESELM: Resolution element for electro-optic generated imagery.

RESPONSIVITY: The ratio of the electrical signal output (voltage or current) from an infrared detector to the radiant power input over a specified wavelength interval.

SCAN CONVERSION: A process by which video information available in one format is converted to video information in some other scan format.

SCAN FIELD OF VIEW: The total scan angle or swathwidth for line scanners. For raster scanners, it is the frame size (given in azimuth and elevation).

SCAN EFFICIENCY: The ratio of active scan time to total operating time.

SIGNAL-NOISE-RATIO: The ratio of the desired signal to unwanted masking noise.

SPATIAL RESOLUTION: In almost all cases, spatial resolution is synonymous with angular, instantaneous field of view; it may be calculated by dividing the linear dimension of the detector by the effective focal length of the optical system. The cross section of the instantaneous field of view is usually square.

SPECKLE: The granular appearance of a rough (compared to the radiation wavelength) object when illuminated by coherent radiation.

SPECTRAL: Relating to wavelength or frequency dependent properties.

SPECTRAL BANDWIDTH: See Wavelength Interval.

SPECULAR REFLECTION: Mirror-like reflection of a ray of radiation whereby the angle of incidence equals the angle of reflection, and the reflected ray lies in the plane of incidence.

TEM_{oo} MODE (TRANSVERSE ELECTRO-MAGNETIC): The lowest order transverse mode for a laser cavity. (See Gaussian Beam.)

THREE-DIMENSIONAL (3D) IMAGE: Imagery which not only contains cross range spatial resolution (2D) but also contains relative range information; e.g., vertical relief or height information for a downward-looking 3D sensor.

TIME DELAY AND INTEGRATION (TDI): Signals generated by successive detectors in an array as an image is scanned parallel with the array are sequentially delayed and summed. An increase in signal-to-noise ratio equal to the square root of the number of detectors in the series is obtained.

TRUNCATION: The blocking or intercepting of part of a beam of radiation.

V/h (V = aircraft velocity; h = aircraft height above the ground): V/h (maximum) is the maximum velocity-to-height ratio for contiguous scanning (i.e., for no overlap or underlap of successive scans of the instantaneous field of view as it is projected onto the object scene at the center of the scan field of view).

WAVELENGTH INTERVAL: The range of wavelengths of infrared radiation to which a device is sensitive. (There is little consistency in how this interval is specified, ranging from simply identifying the atmospheric transmission band within which the device's peak sensitivity occurs to giving specific values of wavelength between which, say, 90% of the device's integrated response occurs or at which its response drops to, say, 10% of its peak value.)

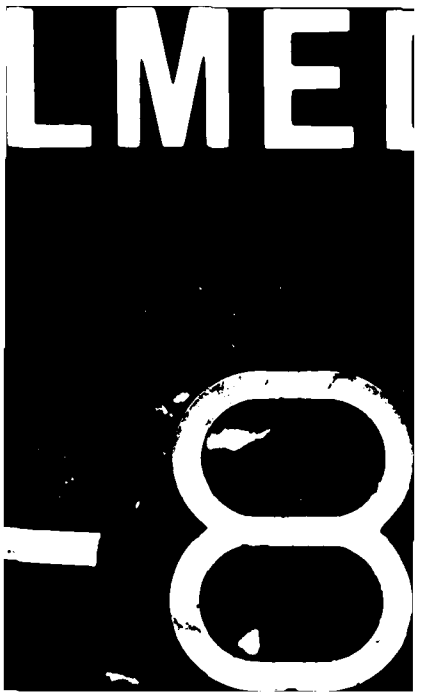
LME
8